frontiers | Research Topics

Clinical trials in drug metabolism and transport

2022

Edited by
Yurong Lai, Stanislav Yanev and Zhihao Liu

Published in
Frontiers in Pharmacology

ISSN 1664-8714
ISBN 978-2-8325-3797-8
DOI 10.3389/978-2-8325-3797-8

About Frontiers

Frontiers is more than just an open access publisher of scholarly articles: it is a pioneering approach to the world of academia, radically improving the way scholarly research is managed. The grand vision of Frontiers is a world where all people have an equal opportunity to seek, share and generate knowledge. Frontiers provides immediate and permanent online open access to all its publications, but this alone is not enough to realize our grand goals.

Frontiers journal series

The Frontiers journal series is a multi-tier and interdisciplinary set of open-access, online journals, promising a paradigm shift from the current review, selection and dissemination processes in academic publishing. All Frontiers journals are driven by researchers for researchers; therefore, they constitute a service to the scholarly community. At the same time, the *Frontiers journal series* operates on a revolutionary invention, the tiered publishing system, initially addressing specific communities of scholars, and gradually climbing up to broader public understanding, thus serving the interests of the lay society, too.

Dedication to quality

Each Frontiers article is a landmark of the highest quality, thanks to genuinely collaborative interactions between authors and review editors, who include some of the world's best academicians. Research must be certified by peers before entering a stream of knowledge that may eventually reach the public - and shape society; therefore, Frontiers only applies the most rigorous and unbiased reviews. Frontiers revolutionizes research publishing by freely delivering the most outstanding research, evaluated with no bias from both the academic and social point of view. By applying the most advanced information technologies, Frontiers is catapulting scholarly publishing into a new generation.

What are Frontiers Research Topics?

Frontiers Research Topics are very popular trademarks of the *Frontiers journals series*: they are collections of at least ten articles, all centered on a particular subject. With their unique mix of varied contributions from Original Research to Review Articles, Frontiers Research Topics unify the most influential researchers, the latest key findings and historical advances in a hot research area.

Find out more on how to host your own Frontiers Research Topic or contribute to one as an author by contacting the Frontiers editorial office: frontiersin.org/about/contact

Clinical trials in drug metabolism and transport: 2022

Topic editors

Yurong Lai — Gilead, United States

Stanislav Yanev — Institute of Neurobiology, Bulgarian Academy of Sciences (BAS), Bulgaria

Zhihao Liu — University of Maryland, College Park, United States

Citation

Lai, Y., Yanev, S., Liu, Z., eds. (2023). *Clinical trials in drug metabolism and transport: 2022*. Lausanne: Frontiers Media SA. doi: 10.3389/978-2-8325-3797-8

Table of contents

frontiers | Frontiers in Pharmacology

TYPE Editorial
PUBLISHED 13 June 2023
DOI 10.3389/fphar.2023.1223428

OPEN ACCESS

EDITED AND REVIEWED BY
Jaime Kapitulnik,
Hebrew University of Jerusalem, Israel

*CORRESPONDENCE
Yurong Lai,
laiyurong@gmail.com
Stanislav Yanev,
stanislav_yanev@yahoo.com
Zhihao Liu,
liuzhihao12399@126.com

RECEIVED 16 May 2023
ACCEPTED 06 June 2023
PUBLISHED 13 June 2023

CITATION
Lai Y, Yanev S and Liu Z (2023), Editorial: Clinical trials in drug metabolism and transport: 2022.
Front. Pharmacol. 14:1223428.
doi: 10.3389/fphar.2023.1223428

Editorial: Clinical trials in drug metabolism and transport: 2022

Yurong Lai[1]*, Stanislav Yanev[2]* and Zhihao Liu[3]*

[1]Gilead Sciences Inc., Foster City, CA, United States, [2]Institute of Neurobiology, Bulgarian Academy of Sciences (BAS), Sofia, Bulgaria, [3]Department of Clinical Pharmacology, College of Pharmacy, Dalian Medical University, Dalian, China

KEYWORDS

clinical trials, pharmacoknietics, metabolism, transport, physiologically based pharmacokinetic (PBPK)

Editorial on the Research Topic
Clinical trials in drug metabolism and transport: 2022

Investigational drugs that have been demonstrated reasonably safe and efficacious for disease therapy can be tested in humans to elucidate the pharmacokinetic (PK) behavior, pharmacodynamics (PD), safety, tolerance, and efficacy in healthy volunteers and subjects suffering from diseases (Mauri et al., 2018). Human clinical trials are an essential component of the drug development process, as they provide critical information about a new drug's safety, efficacy, and mechanism of action. The practices are irreplaceable for obtaining valuable insights into specific questions. They serve as an essential educational resource for further studies and comparisons. The processes must be included, as the PK data are necessary for determining appropriate dosing regimens, informing the drug interactions, and establishing the relationship between PK and efficacy and safety.

High-quality data obtained in clinical trials can be used in understanding how the body processes a drug, including how it is absorbed, distributed, metabolized, and excreted (ADME). Publishing these high-quality original data can significantly advance the field and provide a basis for developing new drugs or improving existing ones (Li et al., 2019). In addition, it is known that metabolism and transport are two crucial components of PK. As expected, clinical trials in PK are critical in advancing our understanding of how drugs are metabolized and transported in the body and developing safe and effective patient medications.

Conventional scientific journals typically prioritize the publication of research demonstrating significant positive outcomes or insights into the mechanisms underlying a drug's effects. However, clinical trial data sometimes need more positive results and mechanism insights, making publishing the findings in a scientific journal challenging. When clinical trial data fails to meet these criteria, it may be rejected for publication or remain unpublished, leaving the results inaccessible to the scientific community and the public. In some cases, these negative or inconclusive clinical trial results may become available to the public through other means, such as public registries or reports fields with regulatory agencies. However, with the context and analysis provided by peer-reviewed scientific publications, it can be easier for individuals outside the scientific community to fully interpret and understand these results.

In recent years, there has also been a growing push for greater transparency and access to clinical trial data, regardless of the outcomes. Many researchers and organizations advocate for the publication of all clinical trial results, regardless of whether they demonstrate positive

outcomes or insights, to ensure that the scientific community and the public have access to the full range of information about a drug's effects and potential risks.

The current Research Topic accepts traditional aspects of drug-metabolizing enzymes, drug transporters, and complementary facets critical for a clear understanding of the current field and upcoming challenges. Finally, a total of 12 original articles were published on this Research Topic, covering several aspects related to this field, including the bioequivalence trials, phase I clinical trials in healthy subjects, population PK analysis in patients, physiologically based pharmacokinetic (PBPK) modeling and simulation study, and drug-drug/food interaction evaluation.

Understanding the PK and tolerability of drugs in healthy volunteers is a critical step in drug development, which can provide valuable information on drug pharmacokinetics and ADME behaviors. After confirming that a new investigational drug is reasonably safe to dose in humans, Phase I clinical trials can be followed for the human safety, tolerability, PK and PD of a new investigational drug in a small number of healthy volunteers or patients with the disease of interest. The maximum tolerated dose MTD or efficacious phase II exposure of the investigational drugs can be determined in subsequent efficacy and safety studies. Phase I trials may also provide preliminary data on the drug's efficacy, optimal dosing regimen, and potential biomarkers for monitoring the drug's activity. On the other hand, human bioequivalence studies administer two drug products to healthy volunteers or patients in a randomized crossover design to determine whether the test product meets the regulatory criteria for bioequivalence. The data usually expressed in terms of confidence intervals for vital pharmacokinetic parameters such as the area under the curve (AUC) and maximum concentration (Cmax) are critical for regulatory authorities in approving and regulating generic drugs. Qu et al. and others conducted a phase I bioequivalence trials to compare cefaclor granule and cefaclor suspension were bioequivalent in healthy Chinese subjects in fasting and postprandial states. The authors found that both Cefaclor granule and Cefaclor suspension are bioequivalent with similar PK profiles, and food effects are observed for both formulations.

To assess the PK, safety, and tolerability profiles of a potential selective JAK1 inhibitor, WXFL10203614, Huang et al. and others conducted a randomized, open-label, crossover study in 14 healthy subjects receiving single and multiple oral doses of WXFL10203614. The authors found that WXFL10203614 showed good tolerability and favorable PK and safety profiles in healthy Chinese subjects, which supports further clinical development in patients with rheumatoid arthritis. A follow-up trial conducted by Huang et al. investigated the food effects on the PK of the drug candidate WXFL10203614. The authors found that WXFL10203614 is rapidly absorbed in fasted conditions. The high-fat and high-calorie diet intake can lower its absorption rate; however, the PK changes are not clinically relevant.

101BHG-D01 is a selective muscarinic receptor antagonist with stable physical-chemical properties and is developing for treating chronic obstructive pulmonary disease. Gao et al. conducted a randomized, double-blind, placebo-controlled dose-ranging finding study of 101BHG-D01 inhalation aerosol to evaluate its pharmacokinetics, metabolite profiling, safety, and tolerability in healthy Chinese subjects. The authors observed no circulating metabolites at greater than 10% of total drug-related exposure. The results indicate that 101BHG-D01 can be a suitable candidate for further clinical development in subsequent studies in COPD patients.

SHR2285 is a selective human coagulation factor XIa inhibitor and is a potential anticoagulant. After completing three clinical phase I trials in healthy subjects, Ma et al. conducted a single-center, randomized, double-blind, placebo-controlled studies to assess its safety, tolerability, PK, and PD in combination with aspirin, clopidogrel or ticagrelor. The authors observed the dose-dependent inhibition of FXIa activity with SHR2285. In healthy subjects, co-administration of aspirin, clopidogrel, or ticagrelor with SHR2285 was well-tolerated, and no safety or tolerance concerns were identified. Meanwhile, these authors also published a randomized, double-blind, single-dose escalation, placebo-controlled phase I trials to evaluate the safety, tolerability, PK, and immunogenicity of an anti-nerve growth factor monoclonal antibody candidate for treating pain, DS002 injection, in healthy Chinese subjects. Based on the results, the authors concluded that DS002 demonstrated good safety profiles within the tested dose ranges and, through blocking nerve growth factor, it is expected to be a novel, safe and non-addictive treatment for pain.

Besides single-dose administration, clinical trial studies in PK may involve the administration of multiple doses of a drug to evaluate its behavior (Kasichayanula et al., 2018). In a 7-days repeating dosing study, Khan et al. investigated the comparative tolerability and metabolism of primaquine, an 8-aminoquinoline antimalarial, in normal glucose-6-phosphate dehydrogenase (G6PDn) and G6PD deficient subjects (G6PDd). Primaquine is a racemic drug, and the enantiomers have widely divergent metabolites and exposure to the parent drug. Both enantiomers and racemates consistently showed gradual increases in methemoglobin and bilirubin. However, in a single hemizygous G6PDd male, the bilirubin response was much more pronounced and required discontinuation of both enantiomers.

Population PK models are a branch of PK that aims to describe and quantify the variability in drug PK among individuals within a population (Klünder et al., 2018). It uses mathematical models to analyze data from large patient groups to understand better how drug concentrations in the body change over time. Li et al. and others built a nonlinear mixed-effect population PK model to analyze PK variables in patients with solid tumors of TQ-B3203, a novel topoisomerase I inhibitor currently developing for the treatment of advanced solid tumors. The authors found that direct bilirubin and body mass index (BMI) were the two most influential factors in clearance. The model can aid the design of future clinical trials by optimizing the dose regimen for TQ-B3203. Similarly, Luo et al. developed a non-linear mixed-effect population PK model for tigecycline, a new type of antibiotic, in critically ill patients. The model suggested that APACHEII score and age are two variables to impact the clearance and volume distribution of tigecycline, respectively. The standard dosing schedule of tigecycline may not be optimal for sound therapeutic effects for critically ill patients.

Physiologically based pharmacokinetic (PBPK) modeling is a mathematical modeling technique used to predict the pharmacokinetic behavior of drugs in the human body based on physiological and anatomical parameters. The model divides the human body into compartments representing different tissues or

organs and then uses mathematical equations to describe how the drug moves between these compartments. PBPK modeling has increased in recent years to evaluate the impact of factors such as age, sex, disease state, and drug-drug interactions on drug exposure. It can aid in predicting the optimal dosing regimen in various populations (Smits et al., 2019). In this Research Topic, Li et al. developed a PBPK model to predict the plasma concentration profiles of schaftoside, a significant ingredient of traditional Chinese medicine for treating urolithiasis. The model was first built using *in vivo* rat data following iv and oral administration of the total flavonoids and extrapolated to humans through incorporating *in vitro* human data. The PBPK model helps determine appropriate dosages of the total flavonoids of Desmodium styracifolium in various populations, representing a practical approach for evaluating the effectiveness and safety of herbal remedies.

A radioactive mass balance study is a type of clinical trial that involves administering a small amount of radiolabeled drug to humans and measuring the amount of radioactivity in various biological excreta over some time, to determine the fate of the drug in the body, including its ADME pathways. This type of study is beneficial for evaluating the ADME properties of new drugs or for comparing the ADME properties of different formulations of the same drug. Zhang et al. investigated the PK, biotransformation pathway, and mass balance of [14C]SHR6390, a selective and effective cyclin-dependent kinase 4/6 inhibitor, in humans. The results showed that 94.63% of the dose is recovered in the urine and feces after a single oral administration of [14C] SHR6390 and fecal elimination is a major route. Also included in this Research Topic, Guo et al. investigated the PK behavior in healthy beagles receiving single and multiple administrations of glutamine tablets developed for potential veterinary use to treat animal gastrointestinal diseases. The study characterized the ADME properties of glutamine tablets in dogs and discovered the PK parameters and dose linearity. The results provided a theoretical guide for pet clinical practice and formulation development.

Overall, the current research focuses on showcasing top-tier clinical trials published in Drug Metabolism and Transport, encompassing traditional aspects of drug-metabolizing enzymes and drug transporters and critical complementary facets contributing to a comprehensive understanding of the current landscape and future challenges. It provides a valuable platform for publishing high-quality clinical trials and promoting discoveries in the field. Drug hunters can use the data published to develop safer and more effective patient medications by advancing our understanding of these critical areas.

Author contributions

All authors listed have made a substantial, direct, and intellectual contribution to the work and approved it for publication.

Acknowledgments

We want to thank all the authors for sharing their findings and opinions.

Conflict of interest

YL was empolyed by Gilead Sciences Inc.

The remaining authors declare that the research was conducted in the absence of any commercial or financial relationships that could be construed as a potential conflict of interest.

Publisher's note

References

Kasichayanula, S., Grover, A., Emery, M. G., Gibbs, M. A., Somaratne, R., Wasserman, S. M., et al. (2018). Clinical pharmacokinetics and pharmacodynamics of evolocumab, a PCSK9 inhibitor. *Clin. Pharmacokinet.* 57 (7), 769–779. doi:10.1007/s40262-017-0620-7

Klünder, S., Mohamed, M. F., and Othman, A. A. (2018). Population pharmacokinetics of upadacitinib in healthy subjects and subjects with rheumatoid arthritis: analyses of phase I and II clinical trials. *Clin. Pharmacokinet.* 57 (8), 977–988. doi:10.1007/s40262-017-0605-6

Li, Y., Meng, Q., Yang, M., Liu, D., Hou, X., Tang, L., et al. (2019). Current trends in drug metabolism and pharmacokinetics. *Acta Pharm. Sin. B* 9, 1113–1144. doi:10.1016/j.apsb.2019.10.001

Mauri, M. C., Paletta, S., Di Pace, C., Reggiori, A., Cirnigliaro, G., Valli, I., et al. (2018). Clinical pharmacokinetics of atypical antipsychotics: An update. *Clin. Pharmacokinet.* 57, 1493–1528. doi:10.1007/s40262-018-0664-3

Smits, A., De Cock, P., Vermeulen, A., and Allegaert, K. (2019). Physiologically based pharmacokinetic (PBPK) modeling and simulation in neonatal drug development: How clinicians can contribute. *Expert Opin. Drug Metab. Toxicol.* 15, 25–34. doi:10.1080/17425255.2019.1558205

frontiers | Frontiers in Pharmacology

TYPE Original Research
PUBLISHED 30 September 2022
DOI 10.3389/fphar.2022.1014474

OPEN ACCESS

EDITED BY
Stanislav Yanev,
Bulgarian Academy of Sciences (BAS), Bulgaria

REVIEWED BY
Yi Tao,
Zhejiang University of Technology, China
Anusak Kijtawornrat,
Chulalongkorn University, Thailand
Xiangjun Qiu,
Henan University of Science and Technology, China

*CORRESPONDENCE
Zugong Yu,
yuzugong@njau.edu.cn

†These authors share first authorship

SPECIALTY SECTION
This article was submitted to Drug Metabolism and Transport, a section of the journal Frontiers in Pharmacology

RECEIVED 08 August 2022
ACCEPTED 12 September 2022
PUBLISHED 30 September 2022

CITATION
Guo F, Liu D, Zhou Y, Yu Y, Xu Y, Zou Y, Li C, Zhang F and Yu Z (2022), Pharmacokinetic study of single and multiple oral administration of glutamine in healthy Beagles. *Front. Pharmacol.* 13:1014474. doi: 10.3389/fphar.2022.1014474

Pharmacokinetic study of single and multiple oral administration of glutamine in healthy Beagles

Fanxi Guo†, Dongying Liu†, Yuqing Zhou, Yuanqian Yu, Yidan Xu, Yuanpeng Zou, Chongyang Li, Fengyichi Zhang and Zugong Yu*

Laboratory of Veterinary Pharmacology and Toxicology, College of Veterinary Medicine, Nanjing Agricultural University, Nanjing, China

Glutamine is an amino acid that is mainly used for the treatment of gastrointestinal diseases in clinic, but there is a lack of such medicine in veterinary clinic, and its research in dogs has never been seen. This study aimed to investigate the pharmacokinetics of single and multiple administration of glutamine (Gln) tablets in Beagles. Twenty-four healthy Beagles were randomly selected for the pharmacokinetic study of a single dose of low (120 mg/kg), medium (240 mg/kg), and high (360 mg/kg) Gln tablets. After 7 days of washout period, six Beagles in the medium group were selected for a multiple-dose pharmacokinetic study, 240 mg/kg twice a day for 7 days. The Gln concentration in plasma was determined by a validated UPLC-MS/MS method. The results of single oral administration of different doses of Gln tablets showed that C_{max}, $AUC_{0\to t}$, $AUC_{0\to\infty}$ had a certain linear relationship with the dosage. T-tests were performed for single and multiple administration of T_{max}, C_{max}, $t_{1/2\lambda z}$, $AUC_{0\to t}$, and $AUC_{0\to\infty}$, and the results showed no significant differences ($p > 0.05$). Therefore, Gln tablets were absorbed quickly by oral administration, and there was no accumulation in Beagles after 7 days of administration.

KEYWORDS

glutamine tablets, pharmacokinetics, multiple administration, single administration, Beagles

1 Introduction

Gastrointestinal mucosal barrier injury is closely related to gastrointestinal diseases (Turner 2009; Camilleri et al., 2012), and increasing evidence shows that the increase of intestinal permeability plays a major pathogenic role in some intestinal diseases (Zuckerman et al., 1993; Spiller et al., 2000; Marshall et al., 2004; Dunlop et al., 2006). Vomiting and diarrhea caused by gastrointestinal mucosa injury are common in pets (Niu et al., 2021), but the lack of medicine that can effectively repair the intestinal mucosa leads to slow recovery, which affects the health and quality of life of pets. Therefore, medicines that can nourish and repair intestinal mucosal cells are urgently needed in veterinary clinic.

Glutamine (Gln) is an amino acid whose main function is to provide nutrition to gastrointestinal cells and immune cells and maintain the integrity of gastrointestinal mucosa (Ardawi and Newsholme 1983; Burke et al., 1989; Jiang and Fang 2009; Wang and Liu 2009). Therefore, Gln is also suitable for the treatment of diseases related to gastrointestinal mucosal injury in pets. Gln has been widely used in human clinical medicine in a variety of dosage forms, mainly for the treatment of gastritis, gastric ulcer and duodenal ulcer (Griffiths et al., 2000; Anderson and Lalla 2020). A large number of clinical controlled studies have proved the good efficacy of Gln on gastrointestinal diseases (Mochiki et al., 2011; Dai and Meng 2015; Zuo 2015; Yao et al., 2016; Zhou et al., 2019).

Pharmacokinetic studies of Gln in humans (Ziegler et al., 1990; Ward et al., 2003; Zhu et al., 2003; Berg et al., 2005; Tang et al., 2005; Yu et al., 2014; Du et al., 2015; Han et al., 2016; Morris et al., 2022) and rats (Wang et al., 2015) have been reported in some literatures and the results show that oral Gln was rapidly absorbed and metabolized *in vivo*. However, there was a lack of relevant studies in pets, so pharmacokinetic studies of Gln in dogs are necessary to introduce it into pet clinical practice.

The aim of this study was to clarify the absorption, distribution, metabolism and excretion of Gln tablets in dogs, provide theoretical basis for the introduction of Gln tablets into pet clinical practice, and provide reliable data for the formulation of clinical recommended drug administration program. The pharmacokinetic study of single and multiple oral administration of Gln tablets in dogs was conducted to study the correlation between main pharmacokinetic parameters and dosage, and to compare the similarities and differences between single and multiple administration to investigate the safety of multiple administration.

2 Materials and methods

2.1 Animals

Twenty-four healthy Beagles (half male and half female) aged from 15 to 17 months, weighing 7.0–10.9 kg, were purchased from Jiangsu Yadong Experimental Animal Research Center. The laboratory animal production license number: SCXK (Su) 2016-0009. All dogs were kept in individual cages and given a daily ration of drug-free feed to maintain proper weight and adequate water. Before each experiment, dogs were fasted for 12 h and water was forbidden for 1 h. In addition, 5 ml of water was fed with a syringe during drug administration, water was fed for 2 h and food for 4 h after drug administration. All animal experiments were conducted in accordance with the guidelines of the Animal Ethics Committee of Nanjing Agricultural University (Nanjing, China).

2.2 Drugs and reagents

Gln tablets were produced by Nanjing Jindun Animal Pharmaceutical Co., Ltd., and the production batch number was 20190501. The working standard of Gln and Penciclovir (Internal Standard) were obtained from China National Institutes for Drug Control. Acetonitrile and formic acid were HPLC grade, and ammonium formate was LC/MS grade.

2.3 Experimental design

2.3.1 Pharmacokinetic study design of single dose

Pharmacokinetics of low (120 mg/kg), medium (240 mg/kg) and high (360 mg/kg) doses of Gln tablets were studied in 24 healthy Beagles, including 6 in the low and high dose groups and 12 in the medium dose group. All animals were weighed and blank plasma samples were collected at −24, −18, −12, and 0 h before administration. The mean value of Gln concentration in blank plasma was used as baseline concentration for correction. Plasma samples were collected at 0.17, 0.33, 0.5, 0.67, 0.83, 1, 1.25, 1.5, 1.75, 2, 2.5, 3, 4, 6, 8, 10, 12, and 24 h after oral administration, and the Gln concentration in plasma was measured by UPLC-MS/MS. The concentration of drug-derived Gln was obtained by subtracting the baseline concentration before administration from the total Gln concentration in plasma.

2.3.2 Pharmacokinetic study design of multiple dosing

Six Beagles (half males and half females) from the medium-dose group were selected for a pharmacokinetic study of multiple doses (240 mg/kg) after a 1-week cleaning period following a single dose. Multiple oral pharmacokinetic studies were administered twice a day, with an interval of 12 h, for 7 consecutive days (13 times). Blank blood samples were collected at 24, 18, 12, and 0 h before the first dose. The mean glutamine concentration in blank blood samples collected at these times served as the baseline endogenous glutamine concentration. Blood samples were collected at the following time points after the start of dosing: before the 7th dosing (the morning of the 4th day of dosing), before the 9th dosing (the morning of the 5th day of dosing), before the 11th dosing (The morning of the 6th day of administration), 6 h after the 11th administration, before the 12th administration (the evening of the 6th day of administration), before the 13th administration (the morning of the 7th day of administration), and 10, 20, 30, 40, 50 min, 1, 1.25, 1.5, 1.75, 2, 2.5, 3, 4, 6, 8, 10, 12, 24 h after the 13th administration. The Gln concentration in plasma was measured by UPLC-MS/MS, and the concentration of drug-derived Gln was obtained by subtracting the baseline concentration before first administration from the total Gln concentration in plasma.

TABLE 1 The gradient elution.

Time, min	Acetonitrile, %	40 mmol/L ammonium formate mixture
0.0	80.0	20.0
0.5	80.0	20.0
3.0	70.0	30.0
4.0	70.0	30.0
4.1	80.0	20.0
5.5	80.0	20.0

2.3.3 Collection and storage of samples

About 3–3.5 ml of blood is collected from the dog's forelimb vein with a disposable vacuum blood collection tube using heparin (dry powder) anticoagulation. The blood samples were centrifuged at 2,152 ± 5 g for 10 min at 4°C, and the separated plasma was divided into 0.5 ml/part. All blood samples should be centrifuged and aliquoted within 60 min after collection, and the aliquoted plasma should be immediately stored in an ultra-low temperature refrigerator (−80 ± 10°C).

2.4 Analytical method

The measurement of plasma FFC levels was performed using a ultra performance liquid chromatography/tandem mass spectrometry (UPLC-MS/MS) device (Waters XEVO TQD, Waters Technologies Co. Ltd., United States) comprised a UPLC separation system and a triple quadrupole mass analyzer.

Separation was carried out using a Waters Acquity UPLC BEH Amide column (100 mm×2.0 mm, particle size 1.7 μm; Waters Technologies Co., Ltd., Milford United States). The injection volume was 5 μl. The temperature of the column and auto-sampler was set at 35 and 6°C, respectively. The mobile phase was composed of acetonitrile (mobile phase A) and 40 mmol/L ammonium formate mixture (pH = 3.0 with formic acid, mobile phase B) at a flow rate of 0.4 ml/min. The gradient elution was shown in Table 1. This resulted in an overall run time of 5.5 min.

Detection was performed using a TQD triple quadrupole mass spectrometer equipped with an electrospray ionization source in the electrospray positive ion mode (ESI +). Nitrogen was used as both drying and nebulizing gas. Product ions were detected using the multiple reaction-monitoring (MRM) mode, using argon as collision gas. The capillary voltage and source temperature were optimized at 3.0 kV and 150°C, respectively. The collision energy and cone voltage were optimized for each compound individually. The collision energy varied from 10 to 35 eV, and the cone voltage varied from 23 to 36 V. The MS/MS transition compounds for Gln were 147.2 > 84 and 147.2 > 130 at collision voltages of 10 and 18 eV, respectively. And for Penciclovir (Internal standards) were 254.1 > 135 and 254.1 > 152 at collision voltages of 35 and 18 eV (Liu et al., 2022). Data were collected and processed using the MassLynx software 4.1.

2.5 Sample preparation

The plasma pretreatment method was acetonitrile and ammonium formate solution for protein precipitation, and penciclovir was used as the internal standard. 100 μl of plasma samples were thawed at room temperature, added 20 μl of water, 200 μl of IS working solution, and 800 μl of initial mobile phase, then vortexed for 2 min and centrifuged at 4°C 14,462 g for 10 min. 780 μl initial mobile phase was added to 20 μl of supernatant liquid, then vortexed for 1 min. Ultimately, the samples were filtered through membrane filters (0.22 μm). The processed samples were injected into UPLC-MS/MS for analysis.

2.6 Pharmacokinetic and statistical analysis

Pharmacokinetic parameters were determined with Phoenix WinNonlin Professional software (Version 8.1) by using non-compartmental analysis. The area under the plasma concentration-time curve (AUC) was calculated by the linear trapezoidal linear interpolation method, and the pharmacokinetic parameters such as the terminal elimination half-life ($t_{1/2\lambda z}$), the maximum concentration of Gln in plasma (C_{max}), the time to reach C_{max} (T_{max}) were also obtained. All pharmacokinetic results were presented as mean ± SD.

3 Results

3.1 Results of a single oral glutamine tablets at different doses

After a single oral dose of low-dose (120 mg/kg), medium-dose (240 mg/kg), and high-dose (360 mg/kg) in

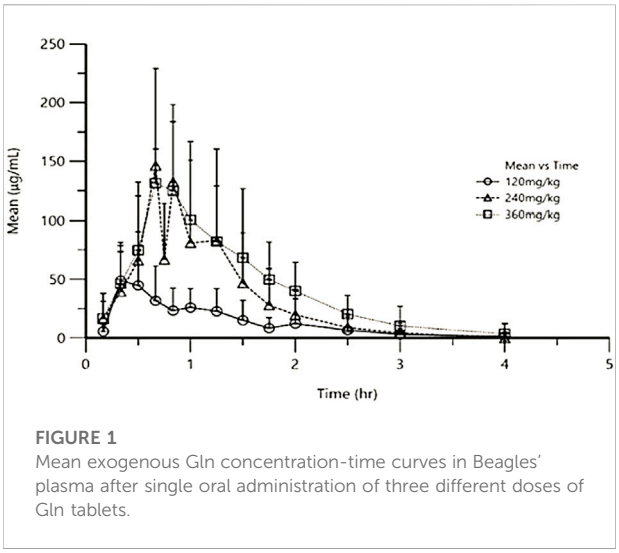

FIGURE 1
Mean exogenous Gln concentration-time curves in Beagles' plasma after single oral administration of three different doses of Gln tablets.

Beagles, the mean plasma concentration-time curve of exogenous Gln was shown in Figure 1 and the mean pharmacokinetic parameters (mean ± SD) were shown in Table 2.

TABLE 3 Results of ANOVA for the main pharmacokinetic parameters-dosage of three different dosage groups.

Parameter	Spearman's rank correlation coefficient r	*P*
C_{max}	0.5108	<0.05
$AUC_{0\rightarrow t}$	0.6725	<0.01
$AUC_{0\rightarrow \infty}$	0.7463	<0.01

3.2 Results of a dose-dependent analysis of a single oral dose of glutamine tablets

Taking the dose as the abscissa, and the C_{max}, $AUC_{0\rightarrow t}$ and $AUC_{0\rightarrow \infty}$ of each tested Beagle as the ordinate, the linear regression was performed. The results were shown in Figure 2. After Spearman rank correlation analysis, the results were shown in Table 3. The results showed that the correlation coefficient r of C_{max}-dose was 0.5108 ($p < 0.05$), the correlation coefficient r of $AUC_{0\rightarrow t}$-dose was 0.6725 ($p < 0.01$), and the correlation coefficient r of $AUC_{0\rightarrow \infty}$-dose was 0.7463($p<0.01$). It showed that C_{max}, $AUC_{0\rightarrow t}$, $AUC_{0\rightarrow \infty}$ were positively correlated with the dose, respectively.

TABLE 2 Mean pharmacokinetic parameters of exogenous Gln in Beagle' plasma after single oral administration of three different doses of Gln tablets. (mean ± SD).

Parameter	Units	120 mg/kg (n = 6)	240 mg/kg (n = 12)	360 mg/kg (n = 6)
λ_z	1/h	2.35 ± 1.98	2.38 ± 1.57	1.83 ± 0.89
$t_{1/2\lambda z}$	h	0.49 ± 0.33	0.42 ± 0.27	0.58 ± 0.56
T_{max}	h	0.93 ± 0.63	0.85 ± 0.29	1.00 ± 0.76
C_{max}	μg/mL	64.56 ± 28.67	136.11 ± 72.51	141.41 ± 60.65
$AUC_{0\rightarrow t}$	h·μg/mL	52.63 ± 19.85	116.30 ± 75.15	160.15 ± 51.84
$AUC_{0\rightarrow \infty}$	h·μg/mL	58.73 ± 20.20	138.76 ± 87.45	191.85 ± 30.37
MRT	h	1.13 ± 0.62	1.03 ± 0.33	1.33 ± 0.37

λ_z, terminal phase rate constant; $t_{1/2\lambda z}$, terminal elimination half-life; T_{max}, time needed to reach C_{max}; C_{max}, peak plasma concentration; AUC_{0-t}, the mean area under the concentration–time curve from 0 h to last time collected samples; $AUC_{0-\infty}$, the mean area under the concentration–time curve from 0 h to infinity; MRT, mean residence time.

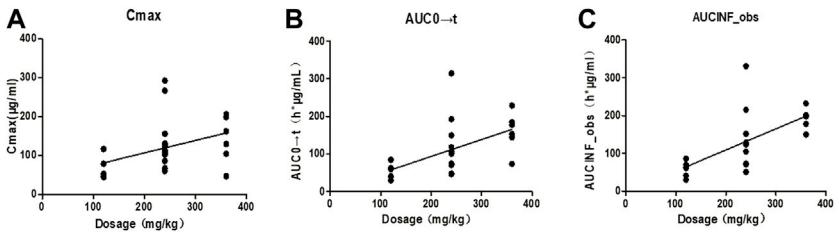

FIGURE 2
Correlation curves of pharmacokinetic parameters and dosage of each Beagle. Note: **(A)**. The correlation curve of Cmax/dose of each Beagle; **(B)**. The correlation curve of AUC0→t/dose of each Beagle; **(C)**. The correlation curve of AUC0→∞/dose of each Beagle.

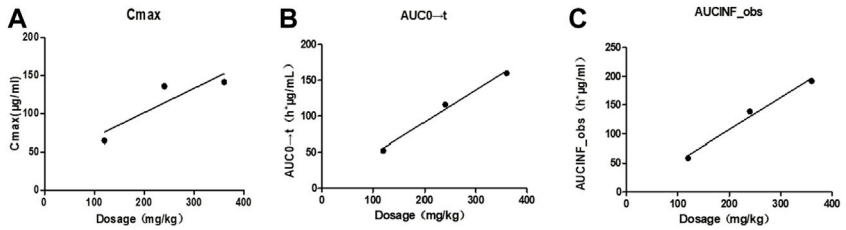

FIGURE 3
Correlation curves of mean pharmacokinetic parameters and dosage of Beagles. Note: **(A)**. The correlation curve of mean Cmax/dose of Beagles; **(B)**. The correlation curve of mean AUC0→t/dose of Beagles; **(C)**. The correlation curve of mean AUC0→∝/dose of Beagles.

TABLE 4 Linear regression results of the means of the main pharmacokinetic parameters for three dosage groups.

Parameter	Regression equation	r^2
C_{max}	$Y = 0.3202x + 37.1730$	0.8014
$AUC_{0→t}$	$Y = 0.4480x + 2.1700$	0.9888
$AUC_{0→\infty}$	$Y = 0.5547x - 3.3368$	0.9865

TABLE 5 Comparison of the mean pharmacokinetic parameters of exogenous Gln between single and multiple oral administration of 240 mg/kg Gln tablets in Beagls (mean ± SD, n = 6).

Parameter	Units	Single dose	Multiple doses
$t_{1/2\lambda z}$	h	0.51 ± 0.28	0.27 ± 0.15
T_{max}	h	0.81 ± 0.16	0.89 ± 0.36
C_{max}	μg/mL	176.21 ± 82.65	150.52 ± 66.88
$AUC_{0→t}$	h·μg/mL	155.36 ± 88.22	104.05 ± 35.66
$AUC_{0→\infty}$	h·μg/mL	167.40 ± 93.34	107.64 ± 32.62
MRT	h	1.26 ± 0.36	1.09 ± 0.40

Taking the dose as the abscissa and taking the mean of each C_{max}, $AUC_{0→t}$ and $AUC_{0→\infty}$ as the ordinate, the linear regression was performed. The results were shown in Figure 3, and the linear regression equation and determination coefficient r^2 were shown in Table 4.

3.3 Results of a comparative pharmacokinetic study of single and multiple oral glutamine tablets

The average pharmacokinetic parameters of 240 mg/kg Gln tablets after single or multiple oral administration of 6 Beagles were shown in Table 5, and the mean Gln concentration in plasma versus time curve was shown in Figure 4. SPSS software was used to conduct t-test on the pharmacokinetic parameters of single and multiple administrations. The results showed that there was no significant difference compared with single administration ($p > 0.05$).

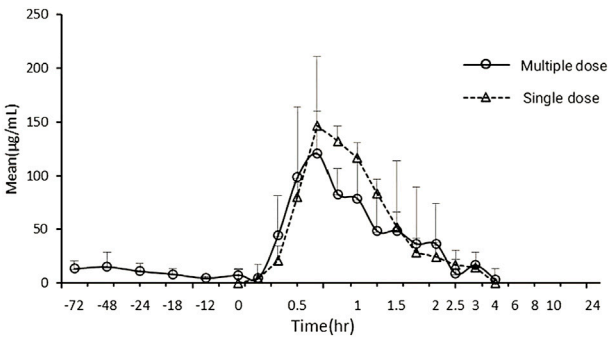

FIGURE 4
Mean exogenous Gln concentration–time curves in Beagles' plasma after single and multiple oral administration of 240 mg/kg Gln tablets (mean ± SD, n = 6).

4 Discussion

As an endogenous substance, the pharmacokinetics of glutamine may be affected by the level of endogenous substances, food, and rhythm changes compared with other drugs (Marzo et al., 1993; Dissanayake 2010; Zhang et al., 2011). This study optimized the experimental design by adjusting for baseline substance levels, administering supra-therapeutic doses, and standardizing dietary management. The methods reported in the literature for the base value subtraction of endogenous substances mainly include the mean value subtraction method (Wang et al., 2015) and the point-to-point subtraction method (Berg et al., 2005; Han et al., 2016). Previous studies by our group (Unpublished prior to submission of this article, but accepted.) showed that the concentration of

endogenous Gln in the plasma of Beagles remained basically constant within 48 h, with no circadian rhythm and periodic differences.

Based on the stable endogenous glutamine concentration of beagle dogs, and referring to the guiding principles for human bioavailability and bioequivalence test of pharmaceutical preparations (guiding principles 9,011, Part IV, Chinese Pharmacopoeia, 2020 Edition), blank blood samples were collected at four time points of 24, 18, 12, and 0 h before administration in this study, and the endogenous glutamine concentration was measured, and the average value was calculated as the baseline concentration. The exogenous glutamine concentration was obtained by subtracting the baseline concentration from the total glutamine concentration in blood after administration, and the pharmacokinetics was analyzed with the exogenous glutamine concentration.

In this study, the pharmacokinetics of Gln tablets were tested in dogs with a single oral administration of three dosages, and according to the analysis of exogenous Gln concentration in plasma it can be seen that: after oral administration of glutamine tablets, T_{max} was 30–60 min, C_{max} were 64.56 ± 28.67 μg/ml (120 mg/kg), 136.11 ± 72.51 μg/ml (240 mg/kg) and 141.41 ± 60.65 μg/ml (360 mg/kg), respectively, and then gradually decreased to the normal range within 90–120 min (120 mg/kg) or 120–240 min (240 mg/kg and 360 mg/kg). According to the report of Ziegler (Ziegler et al., 1990), after oral administration of glutamine 100 mg/kg and300 mg/kg in healthy people, the T_{max} was 30–45 min, and the C_{max} were 44.89 μg/ml (100 mg/kg) and 88.71 μg/ml (300 mg/kg). And then dropped steadily to the normal range within 90–120 min (100 mg/kg) or 180–240 min (300 mg/kg). From the above results, it can be seen that under the condition of oral low-dose glutamine, the pharmacokinetic behavior in dogs was more similar to that in humans, and the drug-induced C_{max} in dogs at high doses was higher than that in humans.

The mean values of C_{max} ($r^2 = 0.8014$), $AUC_{0\to t}$ ($r^2 = 0.9888$), $AU_{C0\to\infty}$ ($r^2 = 0.9865$) showed a certain linear relationship with the administered dose in this test. It was consistent with the results reported by Ziegler that the concentration of glutamine in blood increased in a dose-related after oral glutamine of low and high doses in healthy people (Ziegler et al., 1990).

When glutamine plays a clinical therapeutic role, it is usually administered multiple times (Rotovnik et al., 2017; Arutla et al., 2019; Chang et al., 2019; Zhou et al., 2019). Therefore, it is necessary to clarify the pharmacokinetic characteristics of Gln tablets when they are administered multiple times in dogs, and to investigate whether it will cause accumulated toxicity. The result of the multiple-dose study showed a mean Gln concentration of 8.97 μg/ml at steady state after administration (baseline correction), with an accumulation factor of 1.00. The pharmacokinetic parameters of six dogs who received both single and multiple doses were tested by *t* test. The results showed that there was no significant difference in T_{max}, C_{max}, $t_{1/2\lambda z}$, $AUC_{0\to t}$ and $AUC_{0\to\infty}$ for single and multiple administrations ($p > 0.05$). It showed that the absorption, distribution and metabolism of Gln tablets *in vivo* after repeated administration were similar to those of single administration, and there was no accumulation *in vivo*.

The results of this study showed that after oral administration of glutamine tablets in dogs, the plasma concentration generally reached a peak value at 30–60 min after administration, with an average peak concentration of 64.56 ± 28.67 μg ml^{-1} (120 mg kg^{-1}), 136.11 ± 72.51 μg ml^{-1} (240 mg kg^{-1}) and 141.41 ± 60.65 μg ml^{-1} (360 mg kg^{-1}), then gradually decreased to the normal range within 90–120 min (120 mg kg^{-1}) or 120–240 min (240 mg kg^{-1} and 360 mg kg^{-1}).

It has been reported that after oral administration of glutamine 0.1 g/kg (low dose) and 0.3 g/kg (high dose) in adults, the blood concentration of glutamine increases in proportion to the dose. The peak appeared at 30–45 min after the intake of glutamine, and then steadily decreased to the normal range within 90–120 min (low dose) or 180–240 min (high dose). After administration of 0.1 g kg^{-1} (low dose) and 0.3 g kg^{-1} (high dose) glutamine, the peak blood concentration of glutamine was 1,028 ± 97 μmol L^{-1} (150.24 μg ml^{-1}) and 1,328 ± 99 μmol L^{-1} (194.09 μg ml^{-1}) respectively. The above shows that the pharmacokinetic behavior of glutamine in dogs is similar to that in humans after oral administration.

The dosage regimen of glutamine in the treatment of human gastroenteritis and gastric ulcer is: oral, 0.5 g each time, 2–3 times a day. The body surface area calculation method could be used to convert the human dose to the dog dose, and the dog's dose was 30–60 mg/kg BW, treatment is repeated at 8 h or 12 h intervals.

Based on available pharmacokinetic data, we speculate that the human dose can be converted into the dog dose for further clinical trials. But the formulation of the final dosing regimen for dogs needs to be based on the results of further clinical trials.

5 Conclusion

The results of single dose showed that C_{max}, $AUC_{0\to t}$, $AUC_{0\to\infty}$ had a certain linear relationship with dosage. There were no significant differences in T_{max}, C_{max}, $t_{1/2\lambda z}$, $AUC_{0\to t}$ and $AUC_{0\to\infty}$ between multiple administration and single administration ($p > 0.05$), indicating no accumulation of oral Gln in the body.

Data availability statement

The raw data supporting the conclusion of this article will be made available by the authors, without undue reservation.

Ethics statement

The animal study was reviewed and approved by Animal Ethics Committee of Nanjing Agricultural University (Nanjing, China).

Author contributions

FG, DL, and ZY contributed significantly to the conception and design of this experimental protocol. DL, FG, YY, YZ, YX, YZ, CL, and FZ participated in the experiments of pharmacokinetics. DL, YY, and YZ contributed to plasma sample preparation. DL and FG contributed to analysis and interpretation of data for the work. DL, FG, and ZY, edited and reviewed the final version of the article.

Funding

This study was supported by the Priority Academic Program Development of Jiangsu Higher Education Institution (PAPD).

Conflict of interest

The authors declare that the research was conducted in the absence of any commercial or financial relationships that could be construed as a potential conflict of interest.

Publisher's note

All claims expressed in this article are solely those of the authors and do not necessarily represent those of their affiliated organizations, or those of the publisher, the editors and the reviewers. Any product that may be evaluated in this article, or claim that may be made by its manufacturer, is not guaranteed or endorsed by the publisher.

References

Anderson, P. M., and Lalla, R. V. (2020). Glutamine for amelioration of radiation and chemotherapy associated mucositis during cancer therapy. *Nutrients* 12, 1675. doi:10.3390/nu12061675

Ardawi, M. S., and Newsholme, E. A. (1983). Glutamine metabolism in lymphocytes of the rat. *Biochem. J.* 212 (3), 835–842. doi:10.1042/bj2120835

Arutla, M., Raghunath, M., Deepika, G., Jakkampudi, A., Murthy, H. V. V., Rao, G. V., et al. (2019). Efficacy of enteral glutamine supplementation in patients with severe and predicted severe acute pancreatitis- A randomized controlled trial. *Indian J. Gastroenterol.* 38, 338–347. doi:10.1007/s12664-019-00962-7

Berg, A., Rooyackers, O., and Norberg, A. (2005). Elimination kinetics of L-alanyl-L-glutamine in ICU patients. *Amino Acids* 29, 221–228. doi:10.1007/s00726-005-0230-9

Burke, D. J., Alverdy, J. C., Aoys, E., and Moss, G. S. (1989). Glutamine-supplemented total parenteral nutrition improves gut immune function. *Arch. Surg.* 124 (12), 1396–1399. doi:10.1001/archsurg.1989.01410120042009

Camilleri, M., Madsen, K., Spiller, R., Greenwood-Van Meerveld, B., Van Meerveld, B. G., and Verne, G. N. (2012). Intestinal barrier function in health and gastrointestinal disease. *Neurogastroenterol. Motil.* 24, 503–512. doi:10.1111/j.1365-2982.2012.01921.x

Chang, S. C., Lai, Y. C., Hung, J. C., and Chang, C. Y. (2019). Oral glutamine supplements reduce concurrent chemoradiotherapy-induced esophagitis in patients with advanced non-small cell lung cancer. *Med. Baltim.* 98 (8), e14463. doi:10.1097/MD.0000000000014463

Dai, H., and Meng, Q. H. (2015). Clinical effect of glutamine on traumatic stress gastrointestinal ulcers. *Chin. J. Clin. Pharmacol.* 31 (23), 2287–2289. doi:10.13699/j.cnki.1001-6821.2015.23.003

Dissanayake, S. (2010). Assessing the bioequivalence of analogues of endogenous substances ('endogenous drugs'): Considerations to optimize study design. *Br. J. Clin. Pharmacol.* 69, 238–244. doi:10.1111/j.1365-2125.2009.03585.x

Du, Q. Q., Wang, T., Wang, Z. J., Jiang, X., and Wang, L. (2015). Rapid determination of glutamine in human plasma by high-performance liquid chromatographic–tandem mass spectrometry and its application in pharmacokinetic studies. *J. Chromatogr. Sci.* 53 (01), 79–84. doi:10.1093/chromsci/bmu022

Dunlop, S. P., Hebden, J., Campbell, E., Naesdal, J., Olbe, L., Perkins, A. C., et al. (2006). Abnormal intestinal permeability in subgroups of diarrhea-predominant irritable bowel syndromes. *Am. J. Gastroenterol.* 101, 1288–1294. doi:10.1111/j.1572-0241.2006.00672.x

Griffiths, R. D., Jones, C., and Palmer, T. (2000). Six months outcome of critically ill patients given glutamine supplemented parenteral nutrition. *Nutrition* 2, 145–149. doi:10.1016/S0899-9007(97)00017-8

Han, Y. Z., Jiang, Y., and Lin, M., (2016). Determination of glutamine in human plasma by LC-MS/MS. *J. Shenyang Pharm. Univ.* 33 (07), 572–576+580. doi:10.14066/j.cnki.cn21-1349/r.2016.07.011

Jiang, X. F., and Fang, R. J. (2009). Advances in studies on nutritive and physiological functions of glutamine. *China feed.* 11, 31–36. doi:10.15906/j.cnki.cn11-2975/s.2009.11.007

Liu, D. Y., Guo, F. X., Yu, Y. Q., Zhou, Y., Xu, Y., Zou, Y., et al. (2022). A validated UPLC-MS/MS method for quantification of glutamine in plasma and pharmacokinetic study of oral glutamine tablets in healthy Beagles. *J. Vet. Pharmacol. Ther.* 45, 432–439. doi:10.1111/jvp.13075

Marshall, J. K., Thabane, M., Garg, A. X., Clark, W., Meddings, J., Collins, S. M., et al. (2004). Intestinal permeability in patients with irritable bowel syndrome after a waterborne outbreak of acute gastroenteritis in Walkerton, Ontario. *Aliment. Pharmacol. Ther.* 20, 1317–1322. doi:10.1111/j.1365-2036.2004.02284.x

Marzo, A., Rescigno, A., and Arrigoni, M. E. (1993). Some pharmacokinetic considerations about homeostatic equilibrium of endogenous substances. *Eur. J. Drug Metab. Pharmacokinet.* 18, 215–219. doi:10.1007/BF03188798

Mochiki, E., Ohno, T., Yanai, M., Toyomasu, Y., Andoh, H., and Kuwano, H. (2011). Effects of glutamine on gastrointestinal motor activity in patients following gastric surgery. *World J. Surg.* 35, 805–810. doi:10.1007/s00268-011-0962-5

Morris, C. R., Kuypers, F. A., Hagar, R., Larkin, S., Lavrisha, L., Saulys, A., et al. (2022). Implications for the metabolic fate of oral glutamine supplementation within plasma and erythrocytes of patients with sickle cell disease: A pharmacokinetics study. *Complement. Ther. Med.* 64, 102803. doi:10.1016/j.ctim.2022.102803

Niu, H. Y., Zhang, X. Y., and Ma, Q. B., (2021). Investigation and statistical analysis of 2 249 cases of feline diseases in a pet hospital in Nanjing from 2018 to 2019. *Animal Husb. Veterinary Med.* 53, 115–120.

Rotovnik, K. N., Kompan, L., Žagar, T., and Mrevlje, Z. (2017). Influence of enteral glutamine on inflammatory and hormonal response in patients with rectal cancer during preoperative radiochemotherapy. *Eur. J. Clin. Nutr.* 71, 671–673. doi:10.1038/ejcn.2017.11

Spiller, R. C., Jenkins, D., Thornley, J. P., Hebden, J. M., WrighT, T., SkinnerM., et al. (2000). Increased rectal mucosal enteroendocrine cells, T lymphocytes, and increased gut permeability following acute Campylobacter enteritis and in post-dysenteric irritable bowel syndrome. *Gut* 47, 804–811. doi:10.1136/gut.47.6.804

Tang, J. L., Zhou, S. W., and Ying, Y., (2005). Study on bioequivalence evaluation of compound glutamine granules in human body. *Chin. Pharmacol. Bull.* 12, 1509–1513. doi:10.11669/cpj.2015.03.015

Turner, J. R. (2009). Intestinal mucosal barrier function in health and disease. *Nat. Rev. Immunol.* 9, 799–809. doi:10.1038/nri2653

Wang, S. P., and Liu, J. H. (2009). Research progress in the physiological function and application of glutamine. *J. Anhui Agri* 37 (22), 10375–10377. doi:10.13989/j.cnki.0517-6611.2009.22.038

Wang, T., Jiang, X. H., and Wang, L. (2015). HPLC-MS/MS method for determination of glutamine in rat plasma and application to pharmacokinetic study. *Chin. Pharm. J.* 50 (03), 253–257. doi:10.11669/cpj.2015.03.015

Ward, E., Picton, S., Reid, U., Gardener, C., Smith, M., Henderson, M., et al. (2003). Oral glutamine in paediatric oncology patients: A dose finding study. *Eur. J. Clin. Nutr.* 57, 31–36. doi:10.1038/sj.ejcn.1601517

Yao, D., Zheng, L., Wang, J., Guo, M., Yin, J., and Li, Y. (2016). Perioperative alanyl-glutamine-supplemented parenteral nutrition in chronic radiation enteritis patients with surgical intestinal obstruction: A prospective, randomized, controlled study. *Nutr. Clin. Pract.* 31 (2), 250–256. doi:10.1177/0884533615591601

Yu, L., Yang, L., and Wang, T., (2014). Bioequivalence of glutamine capsules in healthy volunteers. *Chin. J. Clin. Pharmacol.* 30 (11), 1006–1009. doi:10.13699/j.cnki.1001-6821.2014.11.009

Zhang, X., Xie, X. Q., Liu, T. L., and Song, D. M. (2011). Quantitative determination and bioequivalence assessment of the drugs as endogenous compounds. *Chin. J. New Drugs* 20 (22), 2221–2228.

Zhou, Q. Q., Verne, M. L., Fields, J. Z., Lefante, J. J., Basra, S., Salameh, H., et al. (2019). Randomised placebo-controlled trial of dietary glutamine supplements for postinfectious irritable bowel syndrome. *Gut* 68, 996–1002. doi:10.1136/gutjnl-2017-315136

Zhu, M. W., Xiao, L. Y., and Liu, N. L., (2003). The pharmacokinetics study of glutamine granules in healthy volunteers. *Chin. J. Clin. Nutr.* 02, 10–13.

Ziegler, T. R., Benfell, K., Smith, R. J., Young, L. S., Brown, E., Ferrari-BaliviEra, E., et al. (1990). Safety and metabolic effects of L-glutamine administration in humans. *JPEN. J. Parenter. Enter. Nutr.* 14, 137S–146S. doi:10.1177/0148607190014004201

Zuckerman, M. J., Watts, M. T., Bhatt, B. D., and Ho, H. (1993). Intestinal permeability to [51Cr] EDTA in infectious diarrhea. *Dig. Dis. Sci.* 38, 1651–1657. doi:10.1007/BF01303174

Zuo, X. M. (2015). Clinical analysis of oral compound glutamine enteric-soluble capsule in adjuvant treatment of ulcerative colitis. *China Pract. Med.* 10 (02), 150–151. doi:10.14163/j.cnki.11-5547/r.2015.02.107

frontiers | Frontiers in Pharmacology

TYPE Original Research
PUBLISHED 05 October 2022
DOI 10.3389/fphar.2022.1012294

OPEN ACCESS

EDITED BY
Zhihao Liu,
Dalian Medical University, China

REVIEWED BY
Yukuang Guo,
Takeda Oncology, United States
Xiaokui Huo,
Dalian Medical University, China

*CORRESPONDENCE
Haimiao Yang,
haimiaoyang@outlook.com

†These authors have contributed equally to this work

SPECIALTY SECTION
This article was submitted to Drug Metabolism and Transport, a section of the journal Frontiers in Pharmacology

RECEIVED 05 August 2022
ACCEPTED 20 September 2022
PUBLISHED 05 October 2022

CITATION
Qu X, Deng Q, Li Y, Li P, Liu G, Wang Y, Liu Z, Yu S, Cheng Y, Zhou Y, Chen J, Ren Q, Yu Z, Su Z, Zhao Y and Yang H (2022), Pharmacokinetics and safety of the two oral cefaclor formulations in healthy chinese subjects in the fasting and postprandial states.
Front. Pharmacol. 13:1012294.
doi: 10.3389/fphar.2022.1012294

Pharmacokinetics and safety of the two oral cefaclor formulations in healthy chinese subjects in the fasting and postprandial states

Xinyao Qu[1†], Qiaohuan Deng[1†], Ying Li[2], Peng Li[3], Guangwen Liu[1], Yanli Wang[1], Zhengzhi Liu[1], Shuang Yu[1], Yang Cheng[1], Yannan Zhou[1], Jiahui Chen[1], Qing Ren[1], Zishu Yu[1], Zhengjie Su[1], Yicheng Zhao[4] and Haimiao Yang[1*]

[1]Phase I Clinical Trial Laboratory, Affiliated Hospital of Changchun University of Chinese Medicine, Jilin, China, [2]Disha Pharmaceutical Group Co., Ltd., Shanghai, China, [3]Shanghai Xihua Scientific Co., Ltd., Shanghai, China, [4]Puheng Technology Co., Ltd., Suzhou, China

We conducted a phase I bioequivalence trial in healthy Chinese subjects in the fasting and postprandial states. The goal of this trial was to compare the pharmacokinetics and safety of the test preparation Cefaclor granule (Disha Pharmaceutical Group Co., Ltd.) and the reference preparation Cefaclor suspension (Ceclor®, Eli Lilly and Company). In this trial, 24 subjects were selected in the fasting and postprandial states, respectively. Enrolled subjects randomly accepted a single dose of 0.125 g Cefaclor granule or Cefaclor suspension. The washout period was set as 2 days. Blood samples were collected within 8 h after administration in the fasting state and within 10 h after administration in the postprandial state. Plasma concentrations were determined by Liquid chromatography-tandem mass spectrometry (LC-MS/MS). Pharmacokinetic parameters (AUC, C_{max}) were used to evaluate bioequivalence of the two drugs. In the fasting trial, the geometric mean ratios (90% confidence intervals CIs) for C_{max}, AUC_{0-t}, and $AUC_{0-\infty}$ were 93.01% (85.96%–100.63%), 97.92% (96.49%–99.38%) and 97.95% (96.52%–99.41%), respectively. The GMR (90% CIs) for C_{max}, AUC_{0-t}, and $AUC_{0-\infty}$ in postprandial state were 89.27% (81.97%–97.22%), 97.31% (95.98%–98.65%) and 97.31% (95.93%–98.71%), respectively. The 90% CIs of AUC and C_{max} in the fasting and postprandial states were within the 80–125% bioequivalence range. Therefore, Cefaclor granule and Cefaclor suspension were bioequivalent and displayed similar safety profiles. Furthermore, food intake affected the pharmacokinetic parameters of both drugs.

KEYWORDS

antibiotic, equivalence, cefaclor, cephalosporin, pharmacokinetic

Introduction

Cefaclor, a ß-lactam antibiotic, is a second-generation cephalosporin antibiotic (Arsalan et al., 2017; Jeong et al., 2021). Cefaclor is considered as a broad-spectrum antibiotic that is effective against both Gram-positive and negative microorganisms such as *Haemophilus* influenzae and *Klebsiella*. It has a strong inhibitory effect on certain anaerobic microorganisms including Propionibacterium acnes (Wilson, 1993; Rai et al., 2010). Cefaclor is widely used in clinical to treat a variety of bacterial infections, involving otitis media, lower respiratory tract infection, upper respiratory tract infection, urinary tract infection, skin infection and sinusitis (Meyers, 2000; Sader et al., 2007; Chen et al., 2012). The anti-bactericidal activity of cefaclor is superior to other first and second generation cephalosporins (Arsalan et al., 2017).

Human pharmacokinetic (PK) studies have shown that cefaclor is well absorbed from the intestinal tract after oral administration (Sourgens et al., 1997; Chen et al., 2012). A single dose of 250 mg cefaclor reaches maximum plasma concentrations within 30–60 min, with a plasma half-life of 0.6–0.9 h (Meyers et al., 1978). At the same time, the effect of food on the absorption of oral cefaclor had also been reported, which might affect the absorption rate of oral cefaclor (Welling and Tse, 1982; Barbhaiya et al., 1990a; Barbhaiya et al., 1990b; Barbhaiya et al., 1990c; Lode et al., 1992).

Here, we conducted a phase I clinical trial to compare the pharmacokinetics and safety of Cefaclor granule and Cefaclor suspension in healthy Chinese subjects in the fasting and postprandial states. Meanwhile, we also focused on the effect of food intake for Cefaclor granule and Cefaclor suspension absorption.

Materials and methods

Study subjects

The volunteers were healthy Chinese men and women between the age of 18 and 55 years. The following screening protocols were performed in all volunteers: medical history, physical examination, blood cell count, general biochemistry (including liver function, urine routine), urine pregnancy test for women, HIV, hepatitis B and C virus serological tests, electrocardiography and imaging examinations. Excluded volunteers with one of the exclusion criteria, and the volunteers who met all of the inclusion criteria were enrolled the trial. The detailed inclusion and exclusion criteria were listed in Supplementary materials. 1.

Study design

This clinical trial was performed at the Phase I Clinical Trial Laboratory, Affiliated Hospital of Changchun University of Chinese Medicine (China). It was conducted according to the requirements of Good Clinical Practice (GCP), the Declaration of Helsinki and the relevant domestic laws and regulations and was approved by the Ethics Committee of the Affiliated Hospital of Changchun University of Chinese Medicine (Number: CCZYFYLL2019 review-006). The study was registered at Drug Clinical Trial Registration and Information Disclosure Platform (Registration No. CTR20190515). All subjects had written informed consents before the initiation of the investigation.

In the fasting state, subjects were randomly divided into two groups (1:1) to receive a single dose of 0.125 g Cefaclor granule (specification: 0.125 g, manufacturer: Disha Pharmaceutical Group Co., Ltd., Shandong, China, batch number: 190102) or Cefaclor suspension (Ceclor®, specification: 0.125 g, manufacturer: Eli Lilly and Company, Indianapolis, United States, batch number: C873035). After 2 days washout period, subjects orally administrated another formulation cefaclor with a single dose of 0.125 g. In each administration period, blood samples were collected to assay PK parameters at the following times: within 60 min (pre-dose), 5, 10, 20, 30, 45 min, 1, 1.25, 1.5, 1.75, 2, 3, 4, 6, 8 h after drug administration. The same administration protocol was used in the postprandial state, but blood samples for PK analysis were collected at the following times: within 60 min (pre-dose), 5, 10, 20, 30, 45 min, 1 h, 1 h 20 min, 1 h 40 min, 2 h, 2 h 20 min, 2 h 40 min, 3, 3.5, 4, 6, 8, 10 h after drug administration. 4 mL blood was taken in tubes containing heparin sodium anticoagulant for separation. Blood samples were centrifuged for 10 min at 2000 ± 10 g (4°C) to take plasma using a Beckman Allegra X-15R (Beckman Coulter, Inc., California, UNITED STATES), 800uL plasma was added into the detected tube. All plasma was stored at −80°C within 24 h for preservation until PK analyzed.

Analytical assays

Plasma samples were analyzed by Liquid Chromatography-Mass Spectrometry (LC-MS/MS) methods using Shimadzu LC-30AD (Kyoto, Japan). The linear quantification ranged from10 ng/mL to 8,000 ng/mL, and the lower limit of quantification was 10 ng/mL. The compounds were separated on a Acquity Uplc Hss T3 column (1.8 μm, 2.1 × 50 mm) at 40°C. Chromatographic and mass spectrometric conditions were as follows. Chromatographic separation was carried out by gradient elution with mobile phase A (0.1% formic acid in water, formic acid purchased from Merck) and mobile phase B (0.1% formic acid in acetonitrile, acetonitrile purchased from Fisher). The flow rate was 0.6 mL/min and the column pressure was 6,000 psi. The injection volume of the sample was 10 μL. Plasm samples were quantified on an API 4000 mass spectrometer using ESI in positive ion mode and multiple reaction monitoring (MRM) using characteristic parent. The mass spectrometry conditions:

ion source temperature was 550°C; curtain gas (CUR) was 10 psi; ion source gas 1 (GAS1) was 40 psi; ion source gas 2 (GAS2) was 40 psi; collision gas (CAD) was 6 uint; ion spray voltage (IS) was 5500 V; entrance potential (EP) was10 V; and collision cell exit potential (CXP1) was15 V. The dwelling time was set at 100 msec. The MRM transitions of cefaclor and Cefaclor-d5 (purchased from TLC Pharmaceutical Standards, batch number: 1900-026A3) were m/z 368.1 to 174.1 and m/z 373.1 to 179.1.

Standard solutions and the pre-sample were prepared for the determination of plasma cefaclor concentrations. The standard working solution was used to spike blank plasma samples for the calibration standards at concentrations of 10, 20, 50, 200, 1000,4800, 7200, and 8,000 ng/mL or 10, 30, 300, 4000, 6,400, 32000 ng/mL quality control samples.

Pharmacokinetic analysis

This clinical trial was a bioequivalence study with pharmacokinetic parameters as the endpoint. The primary endpoint PK parameters were the peak concentration (C_{max}), area under the curve (AUC) from time zero to the last measurable concentration (AUC_{0-t}) and AUC from time zero to observed infinity ($AUC_{0-\infty}$). Further endpoint parameters were the time of the maximum plasma concentration (T_{max}), terminal half-life of the analyte in plasma ($t_{1/2}$), terminal rate constant (λ_z).

Safety analysis

For safety evaluation, vital signs and adverse events were recorded through a questionnaire. At the end of the trial, blood cell count and general biochemical were given for all participants. The severity of AEs was graded according to the National Cancer Institute Common Terminology Criteria for Adverse Events (NCI CTCAE 5.0). All AEs were recorded throughout the trial and followed until the AEs were eliminated or stabilized.

Sample size and statistical methods

Based on Guidance for industry bioavailability and bioequivalence studies of drug administration in an account of previous clinical trials, 18–24 subjects can meet the sample size requirements for most drugs, but for some drugs with high variability, the number of subjects should be increased appropriately (European Medicines Agency, 2001; CDER, 2002; CDER, 2021). Previous reports suggest that Cefaclor suspension is not a high variability drug (Meyers et al., 1978; Chen et al., 2012). Considering the number of subjects who could not completed the trial, 24 subjects were enrolled in the fasting and postprandial states, respectively.

Statistical analysis

Plasma concentration data were analyzed using Phoenix WinNonlin software 7.0 (Phoenix WinNonlin, Certara United States, Inc., Princeton, NJ, United States) and PK parameters were calculated including C_{max}, AUC_{0-t}, $AUC_{0-\infty}$, T_{max}, λ_Z, $t_{1/2}$. The plasma drug concentration curve was log-transformed by Prism software 8.0 (GraphPad Software, San Diego, CA, United States). All data statistical analysis were performed using SAS software 9.4 (SAS Institute Inc., Cary, NC, United States). Major pharmacokinetic parameters C_{max}, AUC_{0-t} and $AUC_{0-\infty}$ were transformed natural logarithm and tested for significance by analysis of variance (ANOVA). Statistical analysis using two-side test and 90% confidence interval was used to evaluate the bioequivalence of the test and reference drug. When the 90% CI of C_{max}, AUC_{0-t} and $AUC_{0-\infty}$ GMR for two drugs were in the bioequivalent interval of 80.00–125.00%, the two drugs were considered to be bioequivalent.

Results

Subject demographics

In the trial screening for fasting and postprandial states, 62 and 64 volunteers participated, respectively. Ultimately, the trial regarding the fasting state and the postprandial state enrolled 24 subjects, respectively. Two subjects belonging to fasting state have withdrawn from the trial. NO. K014 discontinued the trial due to vomiting within the double times of medium T_{max}. The blood samples were collected prior to the first dosing period. NO. K024 withdrew from the trial due to adverse events (sweating, slow pulse). The blood samples were collected within 2 h after Cefaclor suspension administration. Besides, the two subjects were still enrolled in the full analysis set (FAS) and safety analysis set (SS), the No. K014 was not enrolled in pharmacokinetics analysis set (PKPS) and bioequivalence analysis set (BES), the No. K024 was enrolled in PKPS but not in BES. In the postprandial state, 24 subjects were all included in the safety analysis set, and no adverse events led subject withdrawn from the trial. The detailed process for this trial is shown in Figure 1. The basic information about the subjects is shown in Table 1. There were no significant differences in demographic characteristics between the two sequences. Subjects who participated in the trial were all up to the inclusion criteria.

Pharmacokinetic results

After completing 2 periods of administration, the mean ± SD plasma concentration-time curve for Cefaclor granule and Cefaclor suspension in the fasting state is shown in Figure 2A. The curve after logarithmic transformation is shown in

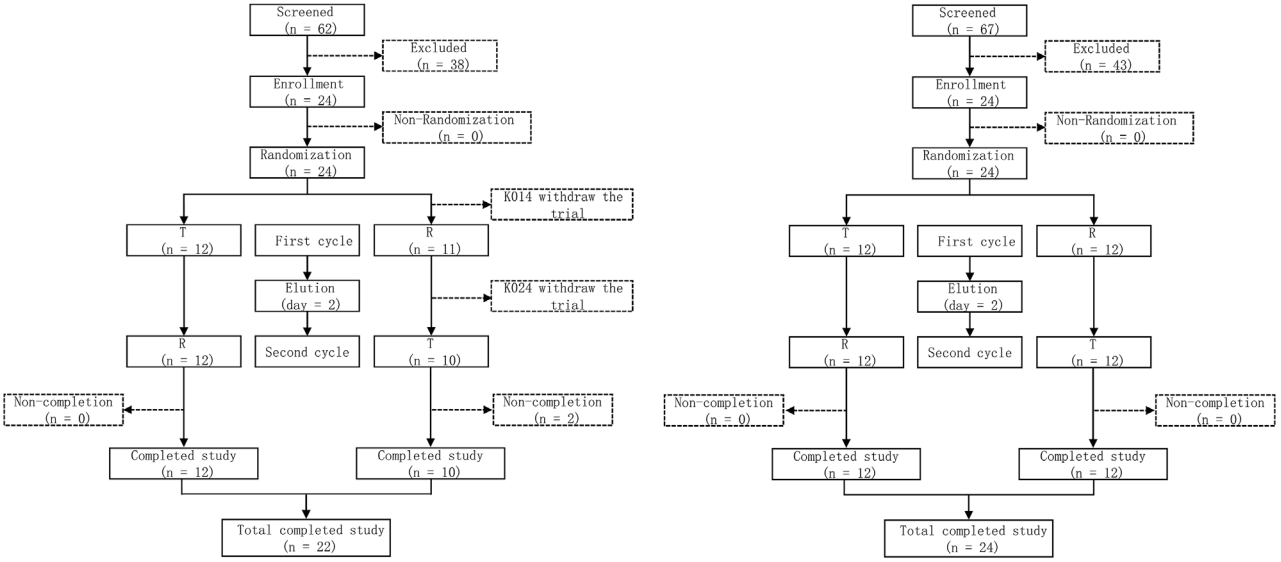

FIGURE 1
Study flow diagram under the fasting state and the postprandial state. T, test drug was Cefaclor granule; R, reference drug was Cefaclor suspension; n, number of subjects.

TABLE 1 Demographic and baseline characteristics of the study participants.

	Fasting sequence (N = 24)	Postprandial sequence (N = 24)
Age (years)		
Mean ± SD	38.96 ± 10.89	36.88 ± 9.19
Median (Q1, Q3)	42.5 (28.5, 48)	37.0 (28.5, 45)
Min–Max	19.0–53.0	23.0–50.0
Sex n (%)		
Male	13 (54.17%)	13 (54.17%)
Female	11 (45.83%)	11 (45.83%)
Ethnicity n (%)		
Ethnic Han	23 (95.83%)	24 (100%)
Others	1 (4.17%)	0 (0)
Height (cm)		
Mean ± SD	164.85 ± 8.41	167.23 ± 8.29
Median (Q1, Q3)	166.25 (159, 171)	165.5 (161.25, 174.75)
Min–Max	148.0–178.5	151.5–182
Weight (kg)		
Mean ± SD	64.72 ± 9.99	67.68 ± 9.69
Median (Q1, Q3)	61.6 (56.85, 72.45)	68.25 (61.4, 74.7)
Min–Max	48.7–81.3	49.3–84.2
BMI (kg/m^2)		
Mean ± SD	23.73 ± 2.45	24.12 ± 2.2
Median (Q1, Q3)	23.55 (22.2, 25.85)	23.95 (22.8, 26.15)
Min–Max	18.4–27.8	18.5–27.8

N, number of subjects; SD, standard deviation; Q1, 1st quartile; Median, 2nd quartile; Q3, 3rd quartile; BMI, body mass index [defined as weight/(height in meters)^2].

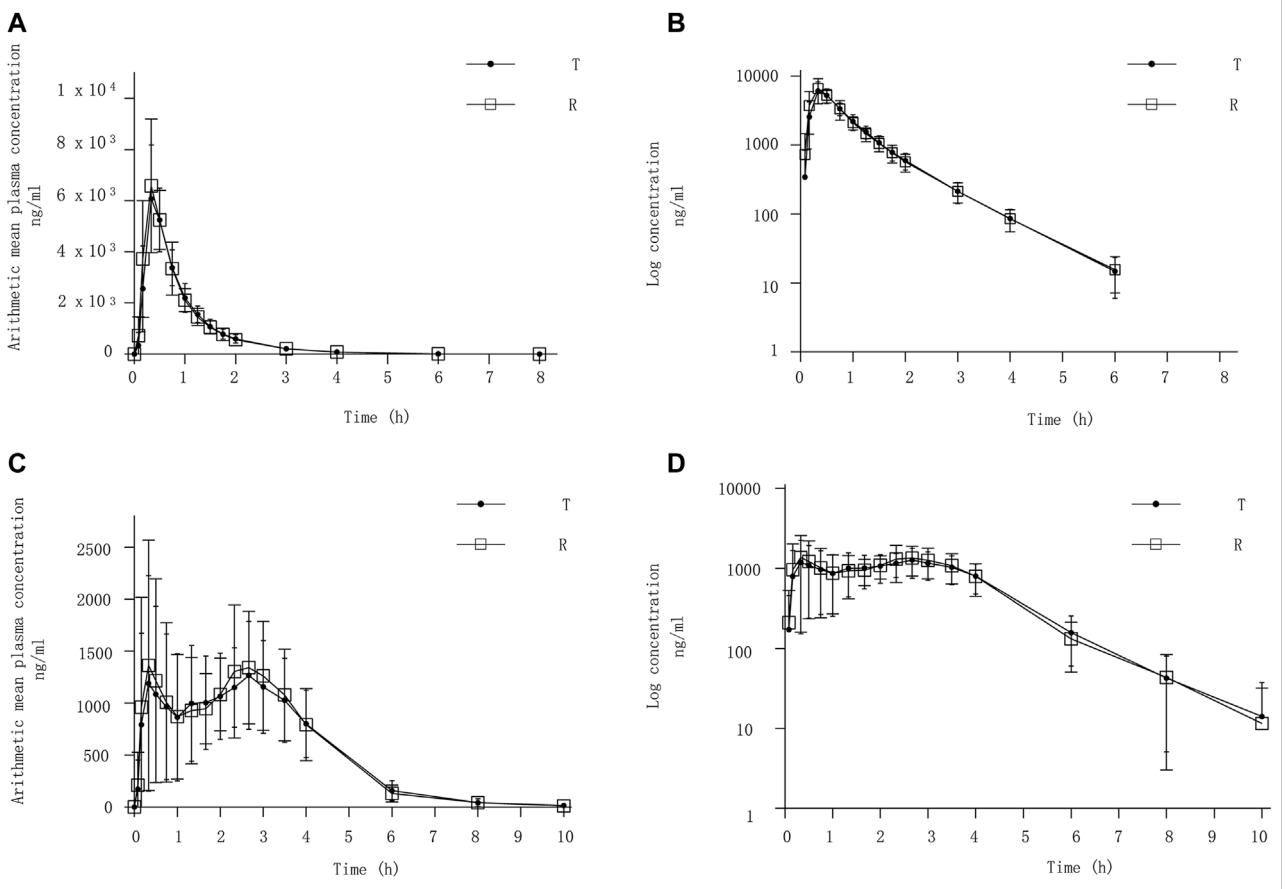

FIGURE 2
PK analysis of Cefaclor granule and Cefaclor suspension. T, test drug was Cefaclor granule; R, reference drug was Cefaclor suspension; Mean blood concentration (±SD) time curve after oral administrated Cefaclor granule and Cefaclor suspension during fasting: arithmetic mean **(A)** and log transformation **(B)**. Mean blood concentration (±SD) time curve after oral Cefaclor granule and Cefaclor suspension in postprandial state: arithmetic mean **(C)** and log transformation **(D)**.

Figure 2B. The mean ± SD (CV%) of the C_{max} values for Cefaclor granule and Cefaclor suspension were 6,432.73 ± 1645.99 ng/mL (25.59%) and 7006.52 ± 2032.34 ng/mL (29.01%), respectively; the AUC_{0-t} values were 5421.56 ± 1013.57 h*ng/mL (18.70%) and 5548.92 ± 1116.70 h*ng/mL (20.12%), respectively; and the $AUC_{0-\infty}$ values were 5446.43 ± 1013.11 h*ng/mL (18.60%) and 5573.02 ± 1118.52 h*ng/mL (20.07%), respectively. The median T_{max} of the two drugs were 0.3333 h and 0.3331 h, respectively. The mean ± SD of the $t_{1/2}$ values for Cefaclor granule and Cefaclor suspension were 0.78 ± 0.10 h and 0.79 ± 0.08 h. The mean ± SD of the λ_z values for Cefaclor granule and Cefaclor suspension were 0.91 ± 0.12 and 0.89 ± 0.09. Other detailed PK parameters are listed in Table 2. The results of ANOVA for primary PK parameters indicated that no significant difference in C_{max} for drug formulations (Cefaclor granule and Cefaclor suspension), administration periods and sequences ($p > 0.05$). Although AUC_{0-t} and $AUC_{0-\infty}$ were not statistically different during the administration periods ($p > 0.05$), there were statistical differences between drug formulations and administration sequences ($p < 0.05$) (Supplementary Table S1).

In the postprandial state, the mean ± SD plasma concentration-time curve for Cefaclor granule and Cefaclor suspension is shown in Figure 2C. The curve after logarithmic transformation is shown in Figure 2D. The mean ± SD (CV%) of the C_{max} values for Cefaclor granule and Cefaclor suspension were 1982.50 ± 601.31 ng/mL (30.33%) and 2276.25 ± 831.71 ng/mL (36.54%), respectively; the AUC_{0-t} values were 5253.26 ± 669.95 h*ng/mL (12.75%) and 5396.25 ± 661.68 h*ng/mL (12.26%), respectively; and the $AUC_{0-\infty}$ values were 5299.69 ± 691.82 h*ng/mL (13.05%) and 5442.40 ± 671.45 h*ng/mL (12.34%), respectively. The median T_{max} of the two drugs were 1.9997 h and 2.168 h, respectively. The mean ± SD of the $t_{1/2}$ values for Cefaclor granule and Cefaclor suspension were 0.98 ± 0.34 h and 1.05 ± 0.56 h. The mean ± SD of the λ_z values for Cefaclor granule and Cefaclor suspension were 0.78 ± 0.23 and 0.76 ± 0.24. Other detailed PK parameters are listed

TABLE 2 Summary of pharmacokinetic parameters after oral two drugs in fasting and postprandial sequences.

PK parameters	Fasting sequence		Postprandial sequence	
	Cefaclor granule [b]	Cefaclor suspension [b]	Cefaclor granule	Cefaclor suspension
C_{max} (ng/mL)				
N (Missing)	22 (0)	23 (0)	24 (0)	24 (0)
Mean ± SD	6,432.73 ± 1645.99	7006.52 ± 2032.34	1982.50 ± 601.31	2276.25 ± 831.71
Median (Q1, Q3)	6,470.0 (5020.0–7560.0)	7280.0 (4850.0–7900.0)	1880.0 (1665.0–2155.0)	1840.00 (1770.0–2825.0)
Min-Max	3790.0–9430.0	4280.0–11500.0	1140.0–4190.0	1240.0–3980.0
T_{max} (h)				
N (Missing)	22 (0)	23 (0)	24 (0)	24 (0)
Mean ± SD	0.42 ± 0.13	0.38 ± 0.08	1.73 ± 1.21	1.69 ± 1.23
Median (Q1, Q3)	0.3333 (0.3322–0.4983)	0.3331 (0.3322–0.4969)	1.9997 (0.3329–2.6644)	2.168 (0.3333–2.6648)
Min-Max	0.3306–0.7483	0.3297–0.4989	0.1647–3.9983	0.1664–3.4997
AUC_{0-t} (h*ng/mL)				
N (Missing)	22 (0)	22 (1) [a]	24 (0)	24 (0)
Mean ± SD	5421.56 ± 1013.57	5548.92 ± 1116.70	5253.26 ± 669.95	5396.25 ± 661.68
Median (Q1, Q3)	5275.13 (4831.20–6,054.11)	5379.47 (4771.96–6,298.42)	5195.32 (4663.40–5613.74)	5379.45 (4819.23–5935.88)
Min-Max	3500.56–7810.22	3760.36–8,071.93	4124.47–6,468.16	4145.30–6,724.68
$AUC_{0-\infty}$ (h*ng/mL)				
N (Missing)	22 (0)	22 (1) [a]	24 (0)	24 (0)
Mean ± SD	5446.43 ± 1013.11	5573.02 ± 1118.52	5299.69 ± 691.82	5442.40 ± 671.45
Median (Q1, Q3)	5289.73 (4843.23–6,079.71)	5394.24 (4787.16–6,332.56)	5222.10 (4710.78–5693.83)	5409.44 (4835.19–5965.71)
Min-Max	3542.04–7846.02	3811.80–8,104.21	4147.13–6,610.61	4177.31–6,927.89
λ_z (1/h)				
N (Missing)	22 (0)	22 (1) [a]	24 (0)	24 (0)
Mean ± SD	0.91 ± 0.12	0.89 ± 0.09	0.78 ± 0.23	0.76 ± 0.24
Median (Q1, Q3)	0.87 (0.84–1.04)	0.88 (0.80–0.96)	0.76 (0.59–0.97)	0.75 (0.62–0.95)
Min-Max	0.73–1.14	0.76–1.07	0.40–1.18	0.21–1.17
$t_{1/2}$ (h)				
N (Missing)	22 (0)	22 (1) [a]	24 (0)	24 (0)
Mean ± SD	0.78 ± 0.10	0.79 ± 0.08	0.98 ± 0.34	1.05 ± 0.56
Median (Q1, Q3)	0.79 (0.67–0.83)	0.78 (0.72–0.87)	0.91 (0.72–1.19)	0.92 (0.73–1.12)
Min-Max	0.61–0.95	0.65–0.91	0.59–1.71	0.59–3.27

N, number of subjects; C_{max}, The maximum observed drug concentration in the plasma; T_{max}, the time from administration to the maximum observed concentration of the analyte in the plasma; AUC_{0-t}, the AUC of the analyte in the plasma over the time interval from time zero to the last measurable concentration; $AUC_{0-\infty}$, the area under the curve from 0 to infinity; λ_z, terminal rate constant in the plasma; $T_{1/2}$, the terminal half-life of the analyte in the plasma.

[a]Subject with randomized number K024 discontinued the trial due to AEs 2 hours after oral administration Cefaclor suspension. Thus, PKPS only recorded T_{max} and C_{max}, while AUC_{0-t}, $AUC_{0-\infty}$, $t_{1/2}$ and λ_Z were absent.

[b]Subject with randomized number K014 discontinued the trial due to vomiting within the double medium of T_{max} of Cefaclor suspension. Only blood samples were collected prior to the first dosing period, so subject participated in SS but not PKPS and BES. Subject with random number K024 discontinued the trial due to AEs. Blood samples were collected within 2 hours after oral administration Cefaclor suspension, therefore, the subject enrolled in SS and PKPS but not BES.

in Table 2. The results of ANOVA for primary PK parameters showed that there were no significant differences in C_{max}, AUC_{0-t} and $AUC_{0-\infty}$ for administration periods and sequences ($p > 0.05$). However, both C_{max}, AUC_{0-t} and $AUC_{0-\infty}$ had statistical differences with drug formulations ($p < 0.05$) (Supplementary Table S1).

The above PK parameters suggested that food intake might affect C_{max} and T_{max} but not AUC. Meanwhile, there were no differences in the PK parameters values between Cefaclor granule and Cefaclor suspension ($p > 0.05$).

Bioequivalence results

The comparisons of the geometric mean ratios (GMRs) for the main pharmacokinetic parameters between Cefaclor granule and Cefaclor suspension in the fasting state are listed in Table 3.

TABLE 3 Results of the bioequivalence determination of Cefaclor granule and Cefaclor suspension in fasting sequence.

PK parameter		Geometric mean	GMR (%)	90% CI (%)	%CV	Power	Result
C_{max} (ng/mL)	T (N = 22)	6272.71	93.01	85.96–100.63	15.18	93.78	Bioequivalent
	R (N = 22)	6744.49					
AUC_{0-t} (h·ng/mL)	T (N = 22)	5383.22	97.92	96.49–99.38	2.83	>99.99	
	R (N = 22)	5497.41					
$AUC_{0-\infty}$ (h·ng/mL)	T (N = 22)	5409.02	97.95	96.52–99.41	2.82	>99.99	
	R (N = 22)	5522.09					

T, test drug was Cefaclor granule; R, reference drug was Cefaclor suspension; PK, Pharmacokinetic; N, number of subjects; GMR, geometric mean ratios; CI, confidence Interval; CV%, within-subject coefficient of variation; AUC_{0-t}, the AUC of the analyte in the plasma over the time interval from time zero to the last measurable concentration; $AUC_{0-\infty}$, the area under the curve from 0 to infinity; C_{max}, the maximum observed drug concentration in the plasma.

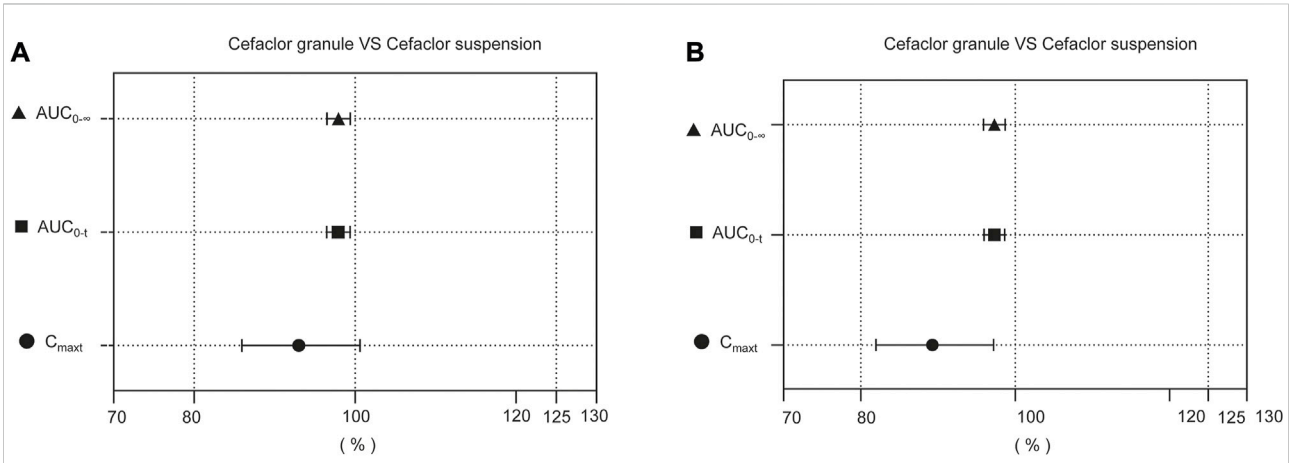

FIGURE 3
Bioequivalence analysis of Cefaclor granule and Cefaclor suspension. The bioequivalence analysis of Cefaclor granule and Cefaclor suspension during fasting **(A)** shows the ratio range of the main PK parameters of Cefaclor granule and Cefaclor suspension with 90% CI. The bioequivalence analysis of Cefaclor granule and Cefaclor suspension in postprandial state **(B)** shows the ratio range of the main PK parameters with 90% CI (bioequivalence was declared if the 90% CIs were within the prespecified acceptable ranges of 80–125%). AUC0-t: AUC of the analyte in the plasma over the time interval from time zero to the last measurable concentration; AUC0-∞: AUC of the analyte in the plasma over the time interval from time zero to infinity; Cmax: maximum observed drug concentration in the plasma.

In the fasting state, the GMRs values (power) of C_{max}, AUC_{0-t}, and $AUC_{0-\infty}$ for Cefaclor granule and Cefaclor suspension were 93.01% (93.78%), 97.92% (>99.99%) and 97.95% (>99.99%), respectively. The 90% confidence intervals (CIs) of GMRs for C_{max}, AUC_{0-t}, and $AUC_{0-\infty}$ were 85.96%–100.63%, 96.49%–99.38% and 96.52%–99.41%, respectively. The primary PK parameters were within the bioequivalence range of 80.00–125.00%. The above results indicated that Cefaclor granule was bioequivalent to Cefaclor suspension in the fasting state (Figure 3A).

The GMRs comparison for the main pharmacokinetic parameters between Cefaclor granule and Cefaclor suspension in the postprandial state are listed in Table 4. The GMRs values (power) of C_{max}, AUC_{0-t}, and $AUC_{0-\infty}$ for Cefaclor granule and Cefaclor suspension were 89.27% (68.92%), 97.31% (>99.99%) and 97.31% (>99.99%), respectively. The 90% CI of GMRs for C_{max}, AUC_{0-t}, and $AUC_{0-\infty}$ were 81.97%–97.22%, 95.98%–98.65% and 95.93%–98.71%, respectively. The primary PK parameters were within the bioequivalence range of 80.00–125.00%. These results showed that Cefaclor granule was bioequivalent to Cefaclor suspension in the postprandial state (Figure 3B).

Safety results

In general, both two drugs exhibited well safety in healthy Chinese subjects after meals or under an empty stomach

TABLE 4 Results of the bioequivalence determination of Cefaclor granule and Cefaclor suspension in postprandial sequence.

PK parameter		Geometric mean	GMR (%)	90% CI (%)	%CV	Power	Result
C_{max} (ng/mL)	T (N = 24)	1913.19	89.27	81.97–97.22	17.34	68.92	Bioequivalent
	R (N = 24)	2143.11					
AUC_{0-t} (h·ng/mL)	T (N = 24)	5213.08	97.31	95.98–98.65	2.77	>99.99	
	R (N = 24)	5357.38					
$AUC_{0-\infty}$ (h·ng/mL)	T (N = 24)	5257.47	97.31	95.93–98.71	2.88	>99.99	
	R (N = 24)	5402.92					

T, test drug was Cefaclor granule; R, reference drug was Cefaclor suspension; PK, Pharmacokinetic; N, number of subjects; GMR, geometric mean ratios; CI, confidence Interval; CV%, within-subject coefficient of variation; AUC_{0-t}, the AUC of the analyte in the plasma over the time interval from time zero to the last measurable concentration; $AUC_{0-\infty}$, the area under the curve from 0 to infinity; C_{max}, the maximum observed drug concentration in the plasma.

TABLE 5 Summary of AEs for Cefaclor granule and Cefaclor suspension in the fasting trial.

AE category	Cefaclor granule [a]		Cefaclor suspension [a]	
	N	n	N	n
Total adverse events	5	5	6	8
AEs related to the study drugs	5	5	6	8
Anemia	1	1	0	0
Vomited	0	0	1	1
Sweating	0	0	1	1
Slow pulse	0	0	1	1
Dizziness	0	0	1	1
Infection urinary tract	2	2	0	0
Urinary occult blood positive	2	2	4	4
AEs of grade 1	5	5	6)	6
AEs of grade 2	0	0	1	2
AEs of grade 3 and above	0	0	0	0
AEs leading to discontinuation of study drug	0	0	2	4

[a]Subject with random number K014 discontinued the trial due to AEs. Blood samples were collected from subjects prior to oral medication, so subject participated in SS but not PKPS and BES. Subject with random number K024 discontinued the trial due to AEs. Blood samples were collected within 2 hours after oral administration Cefaclor suspension, therefore, the subject enrolled in SS and PKPS but not BES. The number of cefaclor was 22, the number of Cefaclor suspension was 24.
N, number of the subjects with adverse events; n, the number of adverse events; AEs, adverse events.

status. In the fasting states, there were 13 adverse events (AEs) in 11 subjects caused by Cefaclor granule and Cefaclor suspension, such as anemias, vomited, sweating, slow pulse, dizziness, infection urinary tract and positive urinary occult blood. Five subjects had 5 AE cases regarding Cefaclor granule, 6 subjects had 8 AE cases in Cefaclor suspension group. The detailed AEs are shown in Table 5, there were no AEs of grade 3 or above. In the postprandial state, three subjects experienced three grade I drug-related adverse events after Cefaclor granule and Cefaclor suspension administration, such as anemia, infection urinary tract and positive urinary occult blood. There were 2 AE cases in 2 subjects caused by Cefaclor granule, and one subject had one AE in Cefaclor suspension group, the detailed AEs are shown in Table 6.

Discussion

Cefaclor is a highly absorbable oral cephalosporin antibiotic widely used in outpatient treatment for community-acquired pneumonia and other mild to moderate infections (Sader et al., 2007). This trial was designed to compare the bioequivalence and safety of Cefaclor granule and Cefaclor suspension under fasting and postprandial states. Meanwhile, the effect of food intake on Cefaclor granule and Cefaclor suspension PK parameters was

TABLE 6 Summary of AEs for Cefaclor granule and Cefaclor suspension in postprandial trial.

AE category	Cefaclor granule		Cefaclor suspension	
	N	n	N	n
Total adverse events	2	2	1	1
AEs related to the study drugs	2	2	1	1
Anemia	1	1	0	0
Infection urinary tract	0	0	0	0
Urinary occult blood positive	1	1	1	1
AEs of grade 1	2	2	1	1
AEs of grade 2	0	0	0	0
AEs of grade 3 and above	0	0	0	0
AEs leading to discontinuation of study drug	0	0	0	0

N, number of the subjects with adverse events; n, the number of adverse events; AEs, adverse events.

also investigated. The fasting and postprandial study sequences were two separate dosing sequences. The trial used a 2 × 2 cross-over study design which was up to the requirements of a bioequivalence trial. Previous studies indicated that age and gender had no significant effects on the PK parameters of Cefaclor granule and Cefaclor suspension (Satterwhite et al., 1992; Nix et al., 1997). Therefore, this study recruited male and female subjects between the ages from 18 to 55 years. In the postprandial state, the metabolic half-life of 250 mg oral cefaclor was 1–1.5 h, to avoid the influence of the previous administration of induced residue, the washout period of this trial was set as 2 days (Karim et al., 2003; FDA, 2021). The washout period was 7 times more than the drug metabolic half-life, which was enough to ensure that the drug concentration before the next administration was lower than the lower limit of the bioassay quantitation. In the fasting trial, the plasma concentrations of several samples exceeded the linear quantitative range (10.0 ng/mL to 8,000 ng/mL). Thus, we diluted the samples 5-fold for detection. 32000 ng/mL is the diluted QC sample concentrate and higher than the upper limit of quantification (8,000 ng/mL). The diluted QC was detected after a 5-fold dilution (6,400 ng/mL) which is within the quantitative linear range. The QC results met the 15% acceptance criteria and the residue was also acceptable for common compliance.

The pharmacokinetic parameter values for Cefaclor suspension in this trial were very similar to previously published data (Glynne et al., 1978; Wilson, 1993; Chen et al., 2012). At the same time, available data suggested that dietary substances can alter the absorption rate and efficiency of oral cefaclor (Oguma et al., 1991). There may be some discrepancies between the reported results. The results of the current study were quite different, with C_{max} and AUC of cefaclor showing similar changes after different types of breakfasts (Williams et al., 1996). The result of a report regarding the effects of different foods on absorption of cefaclor shows that food intake did not affect the areas under the concentration-time curves, but reduced the maximum concentration and prolonged the time to maximum concentration of drug in serum (Oguma et al., 1991). In the study of Barbhaiya, R.H., et al., food intake increased the t_{max} of cefaclor compared to fasting condition (Barbhaiya et al., 1990a). In our trial, the Cmax values of Cefaclor granule and Cefaclor suspension were significantly decreased and the Tmax values were significantly increased in the postprandial state. The presence of food did not significantly alter the AUC of cefaclor, although there was a slight decrease in AUC compared to values in the fasting state. In the postprandial group, there were significant differences in C_{max} and AUC between the two formulations. However, the 90% CI for PK parameters ranged from 80% to 125% in this trial under the fasting and postprandial states. Therefore, it can be concluded that Cefaclor granule and Cefaclor suspension were bioequivalent.

Cefaclor has high plasma concentration and a low risk of gastrointestinal side effects due to its rapid and high rate of absorption (compared to other antibiotics, cefaclor reaches peak plasma concentrations within 1 h) (Sides et al., 1988). Subjects were in good general health, with stable vital signs and no SAEs in the trial. AEs occurred in the trial included anemia, vomited, sweating, slow pulse, dizziness, infection urinary tract and positive urinary occult blood. The safety profile of this trial was similar to other bioequivalence trials (Koytchev et al., 2004; Chen et al., 2012). Adverse events associated with cefaclor treatment were rarely reported. Adverse events reported in post-marketing surveillance included allergic reaction, anaphylactoid reaction, angioedema, facial edema, hypotension, Stevens-Johnson syndrome, syncope, paresthesia, vasodilation and vertigo (Meyers, 2000). The influence of other factors cannot be determined.

An interesting phenomenon emerged in Figure 2C, a double peak was found in the plasma concentration-time curve. To

determine the cause, we plotted the plasma concentration-time curves for each subject in the postprandial state (Supplementary Figure S1). Plasma concentrations of Cefaclor granule and Cefaclor suspension for each subject in the postprandial state are shown in Supplementary Table S2 and Supplementary Table S3. We research for more literature to better explain this double peak phenomenon for Cefaclor. After a single oral dose of cefaclor, the plasma concentration-time curve of the fasting trial did not show a double-peak phenomenon, but the postprandial trial showed a double-peak phenomenon. Thus, the factor that can cause double peaks is gastric emptying and gastric motility. The residence time of a drug in the gastrointestinal tract affects the rate and extent of drug absorption after oral administration (Nimmo et al., 1975). But residence time is mainly determined by gastric emptying and gastrointestinal motility (Levine, 1970). Changes in gastric emptying and intestinal flow rates after a single dose can lead to changes in absorption rates throughout the course of absorption (Oberle and Amidon, 1987). However, in the previous studies for cefaclor after oral administration we did not find the double peek phenomenon (Barbhaiya et al., 1990a; Oguma et al., 1991; Chen et al., 2012). Further research is needed to determine the cause of this phenomenon.

Based on the results of this trial, the rate and extent of absorption for Cefaclor granule and Cefaclor suspension were comparable in the fasting and postprandial status. There was no significant difference in AUC values between 0.125 g Cefaclor granule and Cefaclor suspension. In contrast, the C_{max} and T_{max} values calculated in the fasting state were approximately 3-fold and 6-fold higher than that in the postprandial state. The PK parameters C_{max} values for the two studies after meal and under an empty stomach status were 6,432.73 ± 1645.99 ng/mL (Cefaclor granule) and 7006.52 ± 2032.34 ng/mL (Cefaclor suspension), as well as 1982.50 ± 601.31 ng/mL (Cefaclor granule) and 2276.25 ± 831.71 ng/mL (Cefaclor suspension), respectively. The results were similar to the data published (Williams and Harding, 1984; Barbhaiya et al., 1990a).

There are several limitations in the current study. First, this study merely demonstrates that the biosimilar is similar to the "originals" in terms of PK parameters. Thus, the therapeutic bioequivalence between the biosimilar and the original needs further trials to verify. The sample size is another limitation of the study, although it is up to the requirements of a bioequivalence trial. Due to sample size limitations, we were unable to conduct a comprehensive assessment for the safety of these two drugs. Lastly, our trial is single-dose administration, and there is no cumulative exposure to the drug in the human body, which will also affect the assessment of drug safety.

Conclusion

This trial is a single-center, randomized, open, single-dose, two-period crossover phase I clinical trial to compare the bioequivalence and safety of Cefaclor granule (Disha Pharmaceutical Group Co., Ltd.) and Cefaclor suspension (Ceclor®, Eli Lilly and Company) in healthy Chinese subjects under the fasting and postprandial states. By evaluating the primary PK parameters, C_{max}, AUC_{0-t}, and $AUC_{0-\infty}$ all met the bioequivalence criteria, supporting the bioequivalence of the two drugs. Cefaclor granule and Cefaclor suspension were safe in healthy Chinese subjects in the fasting and postprandial states.

Key points

1) The results of this trial indicated that Cefaclor granule and Cefaclor suspension were bioequivalent and displayed similar safety profiles.
2) Food intake reduced the maximum plasma concentration and prolonged the peak time of the two oral cefaclor.

Data availability statement

The original contributions presented in the study are included in the article/Supplementary Material, further inquiries can be directed to the corresponding author.

Ethics statement

The studies involving human participants were reviewed and approved by the trial was Ethics Committee of the Affiliated Hospital of Changchun University of Chinese Medicine (Number: CCZYFYLL2019 review-006 dated 16 January 2019). The patients/participants provided their written informed consent to participate in this study.

Author contributions

HY designed of the trial. XQ, YL, GL, YW, ZL, SY, YC, YZ, JC, and QR performed the research. PL engaged in bioanalysis process work; YZ lead the draft of the manuscript. QD, ZS, and ZY drafted the paper and drew the figures; HY finally approved of the version. All authors agreed to be accountable for all aspects of the work.

Funding

This work was supported by Disha Pharmaceutical Group Co., Ltd., Shandong, China. Funding number: phase I 2020-011. The founder helps pay for this study.

Acknowledgments

Thanks to all enrolled participants, investigators, and people who contributed to this study.

Conflict of interest

YL is employed by the Company Disha Pharmaceutical Group Co., Ltd. PL is employed by the Company Shanghai Xihua Scientific Co., Ltd. YZ is employed by the Company Puheng Technology Co., Ltd.

The remaining authors declare that the research was conducted in the absence of any commercial or financial relationships that could be construed as a potential conflict of interest.

Publisher's note

All claims expressed in this article are solely those of the authors and do not necessarily represent those of their affiliated organizations, or those of the publisher, the editors and the reviewers. Any product that may be evaluated in this article, or claim that may be made by its manufacturer, is not guaranteed or endorsed by the publisher.

Supplementary material

The Supplementary Material for this article can be found online at: https://www.frontiersin.org/articles/10.3389/fphar.2022.1012294/full#supplementary-material

References

Arsalan, A., Ahmad, I., and Ali, S. A. (2017). Cefaclor: Clinical, biochemical, analytical and stability aspects. *Adv. Med. Biol.* 123, 1–52.

Barbhaiya, R. H., Gleason, C. R., Shyu, W. C., Wilber, R. B., Martin, R. R., and Pittman, K. A. (1990). Phase I study of single-dose BMY-28100, a new oral cephalosporin. *Antimicrob. Agents Chemother.* 34 (2), 202–205. doi:10.1128/aac.34.2.202

Barbhaiya, R. H., Shukla, U. A., Gleason, C. R., Shyu, W. C., and Pittman, K. A. (1990). Comparison of the effects of food on the pharmacokinetics of cefprozil and cefaclor. *Antimicrob. Agents Chemother.* 34 (6), 1210–1213. doi:10.1128/aac.34.6.1210

Barbhaiya, R. H., Shukla, U. A., Gleason, C. R., Shyu, W. C., Wilber, R. B., and Pittman, K. A. (1990). Comparison of cefprozil and cefaclor pharmacokinetics and tissue penetration. *Antimicrob. Agents Chemother.* 34 (6), 1204–1209. doi:10.1128/aac.34.6.1204

CDER (2002). Guidance for industry bioavailability and bioequivalence studies for orally administered drug products-general considerations. Available from https://docslib.org/doc/1597843/guidance-for-industry-bioavailability-and-bioequivalence-studies-for.

CDER (2021). Guidance for industry, statisitical approaches to estabalishing bioequivalence,January. Available from: https://www.fda.gov/media/70958/download.

Chen, J., Jiang, B., Lou, H., Yu, L., and Ruan, Z. (2012). Bioequivalence studies of 2 oral cefaclor capsule formulations in Chinese healthy subjects. *Arzneimittelforschung.* 62 (3), 134–137. doi:10.1055/s-0031-1298012

European Medicines Agency (2001). Notes for guidance on the investigation of bioavailability and bioequivalence. Available from: https://www.ema.europa.eu/en/documents/scientific-guideline/guideline-investigation-bioequivalence-rev1_en.pdf.

FDA (2021) Ceclor® FDA approved information. Available at: https://www.accessdata.fda.gov/scripts/cder/daf/index.cfm?event=overview.process&ApplNo=050522.

Glynne, A., Goulbourn, R. A., and Ryden, R. (1978). A human pharmacology study of cefaclor. *J. Antimicrob. Chemother.* 4 (4), 343–348. doi:10.1093/jac/4.4.343

Jeong, S. H., Jang, J. H., Cho, H. Y., and Lee, Y. B. (2021). Population pharmacokinetic analysis of cefaclor in healthy Korean subjects. *Pharmaceutics* 13 (5), 754. doi:10.3390/pharmaceutics13050754

Karim, S., Ahmed, T., Monif, T., SahaN.and Sharma, P. L. (2003). The effect of four different types of food on the bioavailability of cefaclor. *Eur. J. Drug Metab. Pharmacokinet.* 28 (3), 185–190. doi:10.1007/BF03190484

Koytchev, R., Ozalp, Y., Erenmemisoglu, A., Tyutyulkova, N., Gatchev, E., and Alpan, R. S. (2004). Studies on the bioequivalence of second generation cephalosporins: Cefaclor capsules and suspension. *Arzneimittelforschung.* 54 (9A), 583–587. doi:10.1055/s-0031-1297053

Levine, R. R. (1970). Factors affecting gastrointestinal absorption of drugs. *Am. J. Dig. Dis.* 15 (2), 171–188. doi:10.1007/BF02235648

Lode, H., Muller, C., Borner, K., Nord, C. E., and KoePPe, P. (1992). Multiple-dose pharmacokinetics of cefprozil and its impact on intestinal flora of volunteers. *Antimicrob. Agents Chemother.* 36 (1), 144–149. doi:10.1128/aac.36.1.144

Meyers, B. R. (2000). Cefaclor revisited. *Clin. Ther.* 22 (2), 154–166. doi:10.1016/S0149-2918(00)88477-5

Meyers, B. R., Hirschman, S. Z., Wormser, G., GartenberG, G., and SrulEvitch, E. (1978). Pharmacologic studies with cefaclor, a new oral cephalosporin. *J. Clin. Pharmacol.* 18 (4), 174–179. doi:10.1002/j.1552-4604.1978.tb01590.x

Nimmo, W. S., Heading, R. C., Wilson, J., Tothill, P., and Prescott, L. F. (1975). Inhibition of gastric emptying and drug absorption by narcotic analgesics. *Br. J. Clin. Pharmacol.* 2 (6), 509–513. doi:10.1111/j.1365-2125.1975.tb00568.x

Nix, D. E., Symonds, W. T., Hyatt, J. M., Wilton, J. H., Teal, M. A., Reidenberg, P., et al. (1997). Comparative pharmacokinetics of oral ceftibuten, cefixime, cefaclor, and cefuroxime axetil in healthy volunteers. *Pharmacotherapy* 17 (1), 121–125.

Oberle, R. L., and Amidon, G. L. (1987). The influence of variable gastric emptying and intestinal transit rates on the plasma level curve of cimetidine; an explanation for the double peak phenomenon. *J. Pharmacokinet. Biopharm.* 15 (5), 529–544. doi:10.1007/BF01061761

Oguma, T., Yamada, H., SawakiM.and NaritaN. (1991). Pharmacokinetic analysis of the effects of different foods on absorption of cefaclor. *Antimicrob. Agents Chemother.* 35 (9), 1729–1735. doi:10.1128/aac.35.9.1729

Rai, A., Prabhune, A., and Perry, C. C. (2010). Antibiotic mediated synthesis of gold nanoparticles with potent antimicrobial activity and their application

in antimicrobial coatings. *J. Mat. Chem.* 20 (32), 6789–6798. doi:10.1039/c0jm00817f

Sader, H. S., Jacobs, M. R., and Fritsche, T. R. (2007). Review of the spectrum and potency of orally administered cephalosporins and amoxicillin/clavulanate. *Diagn. Microbiol. Infect. Dis.* 57, 5S–12S. doi:10.1016/j.diagmicrobio.2006.12.014

Satterwhite, J. H., Cerimele, B. J., Coleman, D. L., Hatcher, B. L., Kisicki, J., and DeSante, K. A. (1992). Pharmacokinetics of cefaclor AF: Effects of age, antacids and H2-receptor antagonists. *Postgrad. Med. J.* 68, S3–S9.

Sides, G., Franson, T. R., DeSante, K. A., and Black, H. R. (1988). A comprehensive review of the clinical pharmacology and pharmacokinetics of cefaclor. *Clin. Ther.* 11, 5–19.

Sourgens, H., Derendorf, H., and Schifferer, H. (1997). Pharmacokinetic profile of cefaclor. *Int. J. Clin. Pharmacol. Ther.* 35 (9), 374–380.

Welling, P. G., and Tse, F. L. (1982). The influence of food on the absorption of antimicrobial agents. *J. Antimicrob. Chemother.* 9 (1), 7–27. doi:10.1093/jac/9.1.7

Williams, L., Hill, D. P., Davis, J. A., and Lowenthal, D. T. (1996). The influence of food on the absorption and metabolism of drugs: An update. *Eur. J. Drug Metab. Pharmacokinet.* 21 (3), 201–211. doi:10.1007/BF03189714

Williams, P. E., and Harding, S. M. (1984). The absolute bioavailability of oral cefuroxime axetil in male and female volunteers after fasting and after food. *J. Antimicrob. Chemother.* 13 (2), 191–196. doi:10.1093/jac/13.2.191

Wilson, R. (1993). *Int. J. Antimicrob. Agents* 2 (3), 185–198. doi:10.1016/0924-8579(93)90053-8

frontiers | Frontiers in Pharmacology

TYPE Original Research
PUBLISHED 19 October 2022
DOI 10.3389/fphar.2022.1027627

OPEN ACCESS

EDITED BY
Zhihao Liu,
Dalian Medical University, China

REVIEWED BY
Qian Xiang,
First Hospital, Peking University, China
Fen Yang,
Beijing Cancer Hospital, China
Yukuang Guo,
Takeda Oncology, United States

*CORRESPONDENCE
Xitong Ju,
xitong.ju@hengrui.com
Runbin Sun,
runbinsun@gmail.com
Juan Li,
juanli2003@njglyy.com

†These authors have contributed equally to this work

SPECIALTY SECTION
This article was submitted to Drug Metabolism and Transport, a section of the journal Frontiers in Pharmacology

RECEIVED 25 August 2022
ACCEPTED 05 October 2022
PUBLISHED 19 October 2022

CITATION
Ma T, Dong Y, Huang L, Yang Y, Geng Y, Fei F, Xie P, Zhao Y, Lin H, Yang Z, Jin Y, Ju X, Sun R and Li J (2022), SHR2285, the first selectively oral FXIa inhibitor in China: Safety, tolerability, pharmacokinetics and pharmacodynamics combined with aspirin, clopidogrel or ticagrelor. *Front. Pharmacol.* 13:1027627. doi: 10.3389/fphar.2022.1027627

SHR2285, the first selectively oral FXIa inhibitor in China: Safety, tolerability, pharmacokinetics and pharmacodynamics combined with aspirin, clopidogrel or ticagrelor

Tingting Ma[1†], Yanli Dong[2†], Lei Huang[1], Yuanxun Yang[1], Yan Geng[1], Fei Fei[1], Pinhao Xie[1], Yu Zhao[1], Hui Lin[1], Zeyu Yang[2], Yun Jin[2], Xitong Ju[2*], Runbin Sun[1*] and Juan Li[1*]

[1]Phase I Clinical Trials Unit, Nanjing Drum Tower Hospital Clinical College of Jiangsu University, Nanjing, China, [2]Jiangsu Hengrui Pharmaceuticals Co.,Ltd., Lianyungang, China

Purpose: To evaluate the safety, tolerability, pharmacokinetics and pharmacodynamics of SHR2285, the first oral coagulation factor XIa (FXIa) inhibitor developed in China in combination with aspirin, clopidogrel or ticagrelor in healthy subjects.

Methods: This study was a single-center, randomized, double-blind, placebo-controlled (only SHR2285) design (NCT04945616). A total of 52 healthy subjects, 29 male and 23 female, were completed in this study. The subjects were divided into three groups: A, B and C, 16 subjects in group A [aspirin + clopidogrel + placebo or SHR2285 200 mg bid (1:3, 4 received placebo and 12 received SHR2285)] 16 subjects in group B [aspirin + clopidogrel + placebo or SHR2285 300 mg bid (1:3, 3 received placebo and 13 received SHR2285)] and 20 subjects in group C (aspirin + ticagrelor + placebo or SHR2285 300 mg bid (2:3, 8 received placebo and 12 received SHR2285)), respectively. All groups were administered orally for six consecutive days. Safety, tolerability, pharmacokinetics and pharmacodynamics parameters were assessed.

Results: 1) SHR2285 was well tolerated, and all adverse events were mild. There was no evidence of an increased risk of bleeding. 2) After 6 days of twice-daily administration, SHR2285 could reach a steady state. The mean half-life of SHR2285 in group A, group B and group C was 13.9 h, 14.5 h and 13.8 h, respectively. 3) SHR2285 markedly inhibited FXI activity and prolonged activated partial thromboplastin time (APTT). In group A, group B and group C, the mean maximum inhibition rate of FXI activity was 84.8%, 89.3% and 92.2% and the mean maximum prolongation of APTT was 2.08-fold, 2.36-fold and 2.26-fold, respectively.

Conclusion: These data suggest that SHR2285, a potential oral FXIa inhibitor, is expected to become a novel, safe and effective anticoagulant when combined with aspirin, clopidogrel or ticagrelor.

KEYWORDS

anticoagulants, coagulation factor inhibitor, dual antiplatelet therapy, pharmacodynamics, pharmacokinetics

Introduction

With the aging of the population and the change in people's lifestyles and habits, thromboembolic diseases have increasingly become a major global health problem and the top-ranked cause of global population death (Abbafati et al., 2020). Thromboembolic conditions were estimated to account for one in 4 deaths worldwide in 2010 and are the leading cause of mortality. Ischemic heart disease, ischemic stroke and atrial fibrillation are all included in the global disease burden project (Wendelboe and Raskob, 2016).

The short-term use of dual antiplatelet therapy (DAPT) based on aspirin and platelet P2Y12 receptor inhibitors (commonly clopidogrel and ticagrelor used in China) is the cornerstone of the treatment of cardiac and systemic ischemic events in patients with coronary heart disease with an elevated risk of ischemia (Degrauwe et al., 2017; Wang et al., 2017). DAPT has been shown to reduce recurrent major ischemic events. However, there are still about 5.0%–8.7% of cardiovascular death or ischemic events and 8.3% stroke recurrence rate (Degrauwe et al., 2017; Pan et al., 2021), indicating the involvement of hypercoagulability. In addition, DAPT significantly increases the risk of severe bleeding.

In recent years, drugs targeting coagulation factors have become a new research hot spot for anticoagulant therapy. Non-vitamin K antagonist oral anticoagulants (NOACs) are also known as novel oral anticoagulants directly inhibiting Xa (such as rivaroxaban, apixaban and edoxaban) or factor IIa (such as dabigatran) are widely used in clinical (Levi, 2016). The most important complication of anticoagulant therapy is haemorrhage, which may be severe or even life-threatening, limiting its clinical application. Consequently, the research and development of new antithrombotic drugs are extremely important for the treatment of thrombotic diseases, and it is urgent to explore a safe and effective distinctive oral anticoagulant to meet the clinical demands.

Human FXI is a dimer composed of 607 amino acids (Emsley et al., 2010). It belongs to the trypsin-like serine protease factor and is necessary to maintain the endogenous pathway. FXI forms a complex with high molecular weight (HMW) kininogen and circulates in plasma. It is disconnected between Arg369 and Ile370 by FXIIa and thrombin, and finally transformed into the active form FXIa, which participates in the amplification effect of the coagulation cascade (Emsley et al., 2010). Genomic studies show that individuals with genetic defects in FXIa do not have spontaneous bleeding, and high levels of FXI are closely related to coronary artery diseases such as venous thrombosis and myocardial infarction; On the contrary, FXI deficiency does not have a great impact on physiological hemostasis (Key, 2014; Georgi et al., 2019; Wang et al., 2021). Severe FXI deficiency (10%–20% of the normal value) can protect against venous thrombosis and reduce the incidence of thrombosis (Salomon et al., 2008; Preis et al., 2017). Therefore, FXIa inhibitor is expected to become a new, safe and effective anticoagulant drug.

FXIa inhibitors currently under clinical development include monoclonal antibodies [Osocimab [BAY-1213790] (Weitz et al., 2020), Abelacimab [MAA868] (Koch et al., 2019)]antisense oligonucleotides [FXI-ASO (ISIS 416858)] (Büller et al., 2015) and small molecules [BMS-986177 (Gómez-Outes et al., 2017), BMS-962212 (Perera et al., 2018), ONO-7684 (Beale et al., 2021), EP-7041 (Pollack et al., 2020)]. This indicates that FXIa inhibitors have great potential for treating thrombotic diseases without a substantial risk of bleeding. However, these compounds are in phase I or phase II clinical trials.

SHR2285 is a small molecule compound that selectively inhibits human FXIa, independently developed by Jiangsu Hengrui Pharmaceutical Co., Ltd. It is the first oral inhibitor of coagulation factor XIa (FXIa) developed in China and a new potential antithrombotic drug. At present, systematic preclinical pharmacology, pharmacokinetics and toxicology studies have been completed, and animal tests have confirmed that it selectively inhibits human FXIa, reduces thrombosis weight, prolongates APTT and reduces bleeding risk. Up to now, SHR2285 has completed three clinical trials (including SHR2285-101, SHR2285-102 and SHR2285-104), all of which are phase I trials in healthy subjects (Perera et al., 2018; Chen et al., 2022).

Triple antithrombotic therapy with warfarin plus two antiplatelet agents is the standard of care after percutaneous coronary intervention (PCI) for patients with a trial fibrillation. Recently, most guidelines recommended both anticoagulation and dual antiplatelet therapy (triple therapy) (Cannon et al., 2018). However, these therapies are associated with a high risk of bleeding. In the first-in-human study of SHR2285 (Chen et al., 2022), no bleeding events of SHR2285 were reported, indicating that SHR2285 might be a potential choice of anticoagulants for patients with a trial fibrillation who underwent PCI and required a combination of dual antiplatelet therapy with the anticoagulant drug. Refer to most guidelines for recommendations (Degrauwe et al., 2017; Wang et al., 2017), SHR2285 may be combined with aspirin, clopidogrel, or ticagrelor in the phase II clinical study planned to be carried out, and the patients are given multiple times of medication for a long time. In SHR2285-104 study (data not disclosed), it was predicted that the effective dose of SHR2285 tablets was 200 mg bid and above. Therefore, the dose of SHR2285 in this study is 200 mg bid or 300 mg bid. Still, when combined with dual antiplatelet agents, subjects have

increased safety risks, especially the possibility of increased risk of bleeding, as well as the potential of pharmacokinetic (PK) and pharmacokinetic (PD) interactions. Therefore, the objective of this study was to evaluate the safety, tolerability, PK and PD of SHR2285 tablets in combination with aspirin, clopidogrel or ticagrelor in healthy subjects.

Methods

This study (NCT04945616) was consensus on ethical principles based on international ethical guidelines, including the declaration of Helsinki, the international ethical guidelines of the Council for International Organization of Medical Sciences (CIOMS), the International Council for Harmonisation of Technical Requirements for Pharmaceuticals for Human Use (ICH) guidelines, and other applicable laws and regulations. The study was reviewed and approved in writing by the ethics committee of Nanjing Drum Tower Hospital, the Affiliated Hospital of Nanjing University Medical School, and the research plan, plan amendment, informed consent and other relevant documents such as recruitment advertisement were provided to the ethics committee. This trial strictly followed the good clinical practice (GCP) issued by National Medical Products Administration (NMPA). All subjects provided written informed consent.

Study design

The overall study was a single-center, randomized, double-blind, placebo (SHR2285 only) control design. A total of 52 healthy subjects were completed in this study, including 29 males and 23 females. The subjects were divided into groups A, B and C. 16 subjects were randomised according to a Randomization and trial supply management (RTSM) by a study doctor using a SAS software program in group A and group B (1:3, four received placebo and 12 received SHR2285), 20 subjects in group C (2:3, 8 received comfort 12 received SHR2285). Each subject can only participate in the trial of one dose group.

For group A, the dosing regimen was aspirin + clopidogrel + placebo or SHR2285 200 mg. Specifically, aspirin: 100 mg was taken orally every morning from day 1 to day 6; clopidogrel: 300 mg in the morning of the first day, 75 mg in the morning of the second day to the sixth day; placebo or SHR2285 (1:3): 200 mg orally every morning and evening until the morning of the sixth day.

For group B, the dosing regimen was aspirin + clopidogrel + placebo or SHR2285 300 mg. The use of aspirin and clopidogrel was the same as that of group A; Placebo or SHR2285: added the amount to 300 mg based on group A.

For group C, the administration regimen was aspirin + ticagrelor + placebo or SHR2285 300 mg. The use of aspirin, placebo or SHR2285 was the same as that in group B. Clopidogrel in group B was adjusted to ticagrelor: 180 mg orally in the morning of the first day, 90 mg in the morning and evening from the second day to the morning of the sixth day.

The subjects were administered continuously from day 1 to day 6 by oral administration with about 240 ml of normal temperature water. They were required to fast for at least 8 h before administration in the morning and take it 1 h (±10 min) before breakfast; the administration time in the evening is 12 h (+15 min) from the administration in the morning. The administration of group B and group C was initiated after the researchers and the sponsor evaluated the safety data of all subjects in group A at 48 h after the last dosing. During the whole trial period, it was forbidden to take tea, coffee and other beverages containing coffee and alcohol, eat grapefruit or grapefruit juice, and smoke. Required work and rest regularly and avoided strenuous exercise.

SHR2285 was identical to the placebo except for the drug number. The blind state must be maintained from the enrollment of subjects, the recording and evaluation of study results, the inspection of the study process to data management. All subjects, researchers, the sponsor's investigator participating in the clinical evaluation, and the supervisors (CRA) participating in the study were not informed about which drugs the subjects received for the study. The blind remained unbroken.

PK blood collection points: the blood of each group was collected in the morning of day 1 before administration (within 1 h before administration), 4 h and 12 h after administration (before administration in the evening); in the morning of day 3, day 4, and day 5 before administration (within 1 h before administration), within 1 h before administration on the morning of the sixth day, and 0.5 h, 1 h, 1.5 h, 2 h, 2.5 h, 3 h, 4 h, 5 h, 6 h, 8 h, 10 h, 12 h, 15 h, 24 h, 36 h, and 48 h after administration. About 7 ml of venous blood was collected, and the plasma was collected for concentration determination of aspirin and its active metabolites (salicylic acid) and clopyridine (group A, group B), ticagrelor and its active metabolite AR-C124910XX (group C), SHR2285 and its active metabolite SHR164471.

PD blood collection points: the blood of each group was collected in the morning of the first day before administration (within 1 h before administration) and 4 h and 12 h after administration (before evening administration); the morning of the third, fourth, and fifth days before administration (within 1 h before administration), before administration on the morning of the sixth day (within 1 h before administration), and 1.5 h, 2 h, 2.5 h, 3 h, 4 h, 6 h, 8 h, 12 h, 24 h, 36 h, and 48 h after administration. About 6 ml of venous blood was collected for FXIa (about 3 ml) and coagulation function testing (about 3 ml).

Subjects

Subjects were healthy volunteers aged 18–55 years, both male and female (No pregnant or breastfeeding; Contraception for at least 30 days before screening; The next menstrual period is at least five drug half-lives, about 5 days). The body mass index (BMI) of the subjects was 19–28 kg/m^2, the male body weight was ≥50.0 Kg and <90.0 Kg and the female body weight was ≥45.0 Kg and <90.0 Kg; No smoker within 1 month before screening; The average daily alcohol intake in a week was less than 15 g. Strict contraception should be used during the trial and for 90 days after administration. The subjects could understand the research procedures and methods, voluntarily participate in the trial and sign written informed consent.

The subjects should not have any allergy to the suspected study drug or any related components, or have a history of abnormal coagulation function, high-risk bleeding risk and affecting drug absorption. Subjects were not allowed to take any prescription drugs, over-the-counter drugs and Chinese herbal medicine within 14 days before taking the study drug.

Research objectives and indicators

The primary objective of this study was to evaluate the safety and tolerability of SHR2285 tablets combined with aspirin, clopidogrel or ticagrelor in healthy subjects, that is, the incidence and severity of adverse events (rated as mild, moderate and severe), including subjects' main complaint, physical examination, vital signs, laboratory examination and ECG, *etc.*

The secondary objective was to evaluate 1) the pharmacokinetic (PK) of aspirin and its active metabolite salicylic acid, clopidogrel, SHR2285 and its active metabolite SHR164471 in group A and group B. In group C, the PK of aspirin and its active metabolite salicylic acid, ticagrelor and its active metabolite AR-C124910XX, SHR2285 and its active metabolite SHR164471 were measured. 2) The pharmacodynamics (PD) of aspirin plus clopidogrel or ticagrelor with or without SHR2285 tablets in healthy subjects. PD indexes included coagulation factor XIa (FXIa) activity, activated partial thromboplastin time (APTT), prothrombin time (PT), and international normalized ratio (INR). On the first day before administration, the measured values of coagulation FXI activity and coagulation function (APTT, PT, INR) were taken as the baseline.

Data analysis and statistical methods

Full analysis set (FAS), safety analysis set: all subjects who have received the study drug at least once. PK concentration and parameter analysis set: all randomized subjects who have used the study drug and have at least one PK concentration or parameter data. PD analysis set: all randomized subjects who have used the test drug and have a pre-medication baseline and at least one post-medication PD evaluation data.

The classified data are summarized by frequency and percentage. Continuous data are summarized by subject number, mean, standard deviation, median, maximum and minimum. Blood drug concentration data and PK parameters were summarized by subject number, mean, standard deviation, median, maximum, minimum, coefficient of variation, geometric mean, geometric standard deviation and geometric coefficient of variation.

Based on the PK concentration analysis set, the blood drug concentration was listed and summarized by descriptive statistics according to the medication group at the planned time. The mean and median blood concentration-time curved and semi-logarithmic diagrams were drawn according to the medication. In addition, the actual blood sample collection time was used to draw the blood concentration-time curve and semi-logarithmic diagram of individual subjects.

Based on the actual sampling time, the PK parameters of each component were calculated as a non-compartmental model by WinNonlin (Certara United States Inc, version 8.1). The pharmacokinetic parameters after multiple administrations were investigated: C_{max}, AUC_{tau}, $AUC_{0\text{-}last}$, $AUC_{0\text{-}inf}$, T_{max}, $t_{1/2}$, CL_{ss}/F, V_{ss}/F, C_{trough} and $C_{average}$. The main pharmacokinetic parameters such as $AUC_{0\text{-}last}$, $AUC_{0\text{-}inf}$ and C_{max} were tabulated and summarized by descriptive statistics.

After logarithmic conversion, the AUC_{ss} and C_{max} of each component in the SHR2285 group (aspirin + clopidogrel/ticagrelor + SHR2285) and placebo group (aspirin + clopidogrel/ticagrelor + placebo) were statistically analyzed by ANOVA model. The medication group was used as the independent variable. The geometric mean ratio of the corresponding PK parameter (SHR2285/placebo group) and the estimated value of its 90% confidence interval was obtained by taking the exponential conversion from the mean difference estimated by the model (SHR2285 group-placebo group) and its 90% confidence interval. SHR2285 and its metabolite SHR164471, aspirin/salicylic acid, clopidogrel, ticagrelor and its metabolite AR-C124910XX were determined by Frontage Laboratories Co., Ltd. (Shanghai, China) using high-performance liquid chromatography-tandem mass spectrometry (HPLC-MS, Sciex API 4000). The chromatographic column is WATERS CORTECS®T3 (50 mm × 4.6 mm, id 2.7 μm), column temperature is set at 40°C. Mobile phase A is ultrapure water (containing 0.1% formic acid), and mobile phase B is acetonitrile/water (90:10, containing 0.1% formic acid). The elution gradient is: 0–0.4 min, A-B (50:50), 0.4–0.8 min, A-B (5:95), 0.8–2 min, A-B (5:95), 2–2.4 (50:50), 2.4–3.5 min, A-B (50:50). The total time was 3.5 min and the flow rate was 1.0 ml/min. The ion source was ESI source at positive ion mode. The heating capillary temperature was 400°C; CAD was nine; curtain gas was 30; GS1

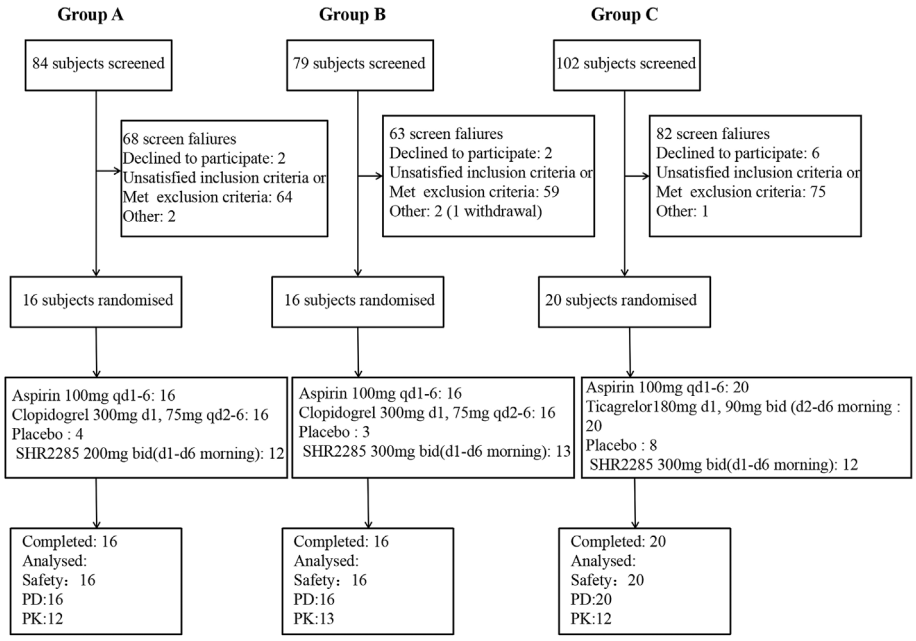

FIGURE 1
(A) Subject disposition of participants in group A of the study **(B)** Subject disposition of participants in group B of the study. **(C)** Subject disposition of participants in group C of the study. PD, pharmacodynamics; PK, pharmacokinetics; qd, once daily; bid, twice a day, once in the morning and once in the evening. There was unwilling to see an error in the randomization system, resulting in three placebos and 13 trial drugs in group **(B)** (One subject withdrew due to an adverse event, and the substitute subject accepted the drug randomization).

(N2) was 50; GS2 (N2) was 50; The method used was multiple reaction monitoring (MRM), and the ion reactions used for quantitative analysis were m/z 545.1→408.0 (SHR2285) and m/z 721.2→408.1 (SHR164471), respectively. The calibration ranges of SHR2285 and SHR164471 were 5 ng/ml (lower limit of quantification) to 5,000 ng/ml. The calibration model was linear regression, quality control samples (15–4,000 ng/ml) were determined with accuracies of 98.0%–104.5% and 100.9%–104.2%, precision of ≤6.2% and ≤6.6%, and recovery of 98.7%–103.6% and 97.3%–102.1%, respectively for both analytes.

The absolute value and relative baseline change percentage of coagulation factor XI (FXI) activity, APTT, PT, INR (placebo group, SHR2285 group) and planned sampling time points of healthy subjects after administration were summarized and plotted (if applicable). FXI activity was measured by the Institute of Blood Transfusion, Chinese Academy of Medical Sciences of China using coagulation method. APTT was measured by Guangzhou Kingmed Center For Clinical Laboratory Co., Ltd. (China) using the coagulation method. PT was counted on the coagulation analyzer, and INR was calculated through parameter calculation. PD parameters APTT, PT, INR and FXI activity were measured with validated assays at Guangzhou KingMed Diagnostics Group Co., Ltd. and the Institute of Blood Transfusion, Chinese Academy of Medical Sciences of China. APTT and PT was evaluated using Dade Actin FSL activated APTT reagent and Tromborel S reagent respectively, automated on the instrument Sysmex CS5100 with a within-batch and inter-batch precision of both not high than 5%, and INR was calculated based on PT test results. FXI activity was measured using a clotting method by Dade actin activated cephaloplastin reagent, automated on Sysmex CS 2000i Coagulation analyser. The result data are presented as a percentage of normal, and its calibration range was 6.25%–150.0%.

Results

Subject demographics

The study was conducted from 16 July 2021 to 16 November 2021. In group A and group B, all 32 subjects completed the study; in group C, all 20 subjects completed the study (Figure 1). All subjects were Chinese. The demographics of the subjects are shown in Table 1.

Safety and tolerability

At least one treatment emergent adverse event (TEAE) occurred in 26 of 37 (70.3%) healthy subjects who received SHR2285 and 10 of 15 (66.7%) subjects who received placebo. The TEAEs of subjects are shown in Table 2.

TABLE 1 Subject demographics.

	Treatment (placebo or SHR2285)				
	Placebo (A + B) n = 7	Placebo(C) n = 8	SHR2285 (A) n = 12	SHR2285(B) n = 13	SHR2285(C) n = 12
Age, years	26.4 (6.21)	27.3 (9.82)	36.0 (14.29)	33.1 (10.32)	29.3 (9.48)
Female, n (%)	3 (42.9)	4 (50.0)	7 (58.3)	4 (30.8)	5 (41.7)
Male, n (%)	4 (57.1)	4 (50.0)	5 (41.7)	9 (69.2)	7 (58.3)
Han nationality, n (%)	7 (100)	7 (87.5)	12 (100)	13 (100)	11 (91.7)
Height, cm	168.79 (5.322)	163.31 (5.548)	162.92 (6.704)	166.73 (11.088)	167.25 (10.947)
Weight, kg	67.13 (8.195)	62.01 (7.406)	62.66 (7.269)	63.22 (8.438)	67.36 (9.537)
BMI, kg/m^2	23.5 (1.90)	23.2 (1.76)	23.6 (2.25)	22.7 (2.10)	24.0 (2.03)

Age, Height, Weight and BMI, are presented as mean (standard deviation). BMI, body massindex.

TABLE 2 Summary of adverse events.

Term, n (%)	Placebo			SHR2285				Total n = 52
	A + B n = 7	C n = 8	Total n = 15	A n = 12	B n = 13	C n = 12	Total n = 37	
Epistaxis	0	0	0	2 (16.7)	0	0	2 (5.4)	2 (3.8)
Gingival bleeding	0	0	0	1 (8.3)	1 (7.7)	0	2 (5.4)	2 (3.8)
Oral Ulcer	1 (14.3)	0	1 (6.7)	1 (8.3)	2 (15.4)	0	3 (8.1)	4 (7.7)
Scratch	0	0	0	0	1 (7.7)	0	1 (2.7)	1 (1.9)
Subcutaneous hemorrhage	0	2 (25.0)	2 (13.3)	1 (8.3)	0	0	1 (2.7)	3 (5.8)
Diarrhea	0	0	0	0	2 (15.4)	0	2 (5.4)	2 (3.8)
Constipation	0	0	0	0	1 (7.7)	0	1 (2.7)	1 (1.9)
Ecchymosis	0	3 (37.5)	3 (20.0)	0	0	5 (41.7)	5 (13.5)	8 (15.4)
Rash	0	0	0	0	0	1 (8.3)	2 (2.7)	1 (1.9)
URTI	0	1 (12.5)	1 (6.7)	0	0	2 (16.7)	2 (5.4)	3 (5.8)
Abdominalburning sensation	0	0	0	0	0	1 (8.3)	1 (2.7)	1 (1.9)
Decreased Hb	0	1 (12.5)	1 (6.7)	2 (16.7)	1 (7.7)	0	3 (8.1)	4 (7.7)
Increased WBC	0	0	0	1 (8.3)	0	0	1 (2.7)	1 (1.9)
Increased N	0	0	0	1 (8.3)	0	0	1 (2.7)	1 (1.9)
Increased M	0	0	0	1 (8.3)	0	0	1 (2.7)	1 (1.9)
Fecal OB(+)	1 (14.3)	1 (12.5)	2 (13.3)	2 (16.7)	0	0	2 (5.4)	4 (7.7)
Urine OB(+)	0	1 (12.5)	1 (6.7)	0	0	0	0	1 (1.9)
Elevated ALT	0	0	0	0	1 (7.7)	0	1 (2.7)	1 (1.9)
Elevated TBil	0	1 (12.5)	1 (6.7)	0	1 (7.7)	0	1 (2.7)	2 (3.8)
Elevated Ca	0	0	0	0	1 (7.7)	0	1 (2.7)	1 (1.9)
Elevated TG	2 (28.6)	0	2 (13.3)	5 (41.7)	2 (15.4)	3 (25.0)	10 (27.0)	12 (23.1)
Hypercholesterolemia	0	0	0	0	1 (7.7)	0	1 (2.7)	1 (1.9)
Elevated UA	2 (28.6)	1 (12.5)	3 (20.0)	2 (16.7)	1 (7.7)	5 (41.7)	8 (21.6)	11 (21.2)
Elevated CK	0	1 (12.5)	1 (6.7)	0	0	0	0	1 (1.9)
ECG T wave changes	1 (14.3)	3 (37.5)	4 (26.7)	2 (16.7)	0	1 (8.3)	3 (8.1)	7 (13.5)
Prolonged QTc	0	0	0	0	0	1 (8.3)	1 (2.7)	1 (1.9)

URTI, upper respiratory tract infection; Hb, Hemoglobin; WBC, white blood cell count; N, neutrophil count; M, monocyte count; OB(+), occult blood positive; ALT, alanine aminotransferase; TBil, total bilirubin; Ca, blood calcium; TG, triglycerides; UA, serum uric acid; CK, creatine kinase; ECG, electrocardiogram; QTc, QTc interval of ECG. There were no serious adverse events during the entire study and no TEAEs, that led to treatment discontinuation or interruption.

Gingival bleeding and/or epistaxis occurred in three subjects in the SHR2285 dose group (A and B), but not in the placebo group. TEAE that occurred in or more of healthy subjects receiving SHR2285 compared with subjects treated with placebo included subcutaneous hemorrhage (2.7% vs. 13.3%), ecchymosis (13.5% vs. 20.0%), oral ulcer (8.1% vs. 6.7%), abdominal burning sensation (2.7% vs. 0), scratch (2.7% vs. 0), diarrhea (5.4% vs. 0), constipation (2.7% vs. 0), rash (2.7% vs. 0).

We also observed abnormalities in clinically relevant laboratory values in the SHR2285 dose group compared with the placebo group, including decreased hemoglobin (8.1% vs. 6.7%), fecal occult blood positive (5.4% vs. 13.3%), urine occult blood positive (0 vs. 6.7%), elevated alanine aminotransferase (2.7% vs. 0), elevated total bilirubin (2.7% vs. 6.7%), elevated triglycerides (27% vs. 13.3%), elevated serum uric acid (21.6% vs. 20.0%), elevated blood calcium (2.7% vs. 0), hypercholesterolemia (2.7% vs. 0), elevated creatine kinase (0 vs. 6.7%), electrocardiogram T wave abnormal (8.1% vs. 26.7%), prolonged QTc interval of electrocardiogram (2.7% vs. 0).

All TEAE in healthy subjects were mild. AEs in the SHR2285 group did not increase apparently compared with the placebo group, suggesting that the AEs may be caused by the combination of aspirin, clopidogrel or ticagrelor, indicating that the combination of SHR2285 with dual antiplatelet treatment did not increase the TEAE. The challenge of FXIa inhibitor combined with dual antiplatelet therapy is the risk of bleeding. In this trial, three subjects with transient mild gingival bleeding and epistaxis in SHR2285 dose group A and B compared with the placebo group. The AE of bleeding mentioned in SHR2285 300 mg dose group C was only ecchymosis, which occurred in five of 12 subjects, compared with three of eight subjects with placebo. No higher risk of bleeding was observed in group C than in the placebo group. These data suggest that it may be an adverse reaction of aspirin combined with clopidogrel or ticagrelor, and less likely to be related to SHR2285. Importantly, there was no evidence of a severe hemorrhage risk or serious adverse event (SAE). All events were resolved without treatment. None of the healthy subjects died or stopped taking TEAE.

Pharmacokinetics

Combined with aspirin, clopidogrel or ticagrelor, three SHR2285 dose groups were administered 200 mg or 300 mg SHR2285 bid for six consecutive days, SHR2285 and its active metabolite SHR164471 in plasma reached a steady-state (Figures 2A,B). The mean plasma concentration of SHR2285 in each group peaked at approximately 1.5 h after the last administration on day 6 and then gradually decreased to baseline levels by 48 h (Figure 2A).

In the three groups, the peak of SHR2285 in plasma was faster, T_{max} was about 1.5 h. The mean $t_{1/2}$ for SHR2285 after Day 6 was roughly the same (13.8–14.5 h). The peak of SHR164471 in plasma was later than the prototype, T_{max} was 2.5–4 h, and the $t_{1/2}$ was 12.3–14.3 h (Tables 3, 4).

Dose proportionality in SHR2285 exposure in group A and group B was observed as follows: C_{max} and AUC_{tau} values increased about 1.6- and 1.38-fold with a 1.5-fold increase in dose, respectively (geometric means of 3,780–6,020 ng/ml for C_{max} and 14,300–19700 h*ng/mL for AUC_{tau}; Table 3). Correspondingly, SHR164471 exposure (C_{max} and AUC_{tau}) increased by 1.3- and 1.1- fold, respectively (Table 4).

Aspirin was administered once a day for six consecutive days. The median T_{max} of aspirin in groups A, B, C and placebo (A + B, C) were similar, which were 4.5 h, 6.0 h, 7.0 h, 8.0 h and 4.0 h, respectively (Supplementary Table S1), which was in line with the PK characteristics of delayed absorption of enteric-coated tablets in the drug instructions (Figure 3). The T_{max} of its active metabolite salicylic acid was slightly later than that of the prototype, with a median of 8.0 h, 8.0 h, 9.0 h, 8.0 h and 5.0 h, respectively (Supplementary Table S2). It was similar to the prototype, and T_{max} had a certain degree of inter-individual variation (Figure 3). The PK exposure (AUC_{tau}, C_{max}) of salicylic acid in the SHR2285 group and placebo group were similar, and no apparent difference was found between the two groups (Supplementary Tables S1, S2, S6).

The peak of clopidogrel T_{max} in plasma was fast, ranging from one to 1.5 h. The clopidogrel exposure (C_{max}, AUC) of group A and placebo were similar and slightly lower than that of group B with extremely high exposure in some individuals (Supplementary Tables S3, S6, Figure 4). CYP2C19 was involved in forming the active metabolite and intermediate metabolite 2-oxygen-clopidogrel, which is suspected to be related to gene polymorphism.

Six days after administration, ticagrelor and its metabolite AR-C124910XX in plasma reached a steady state, and T_{max} peaked rapidly, ranging from 1.5 to 1.75 h. PK exposure (AUC_{tau}, C_{max}) of the SHR2285 dose group and placebo group were similar, and no noticeable difference was found between the groups (Supplementary Tables S4–S6, Figure 5).

Pharmacodynamics

Following repeated administration of SHR2285 200 mg or 300 mg, the inhibition of FXI activity in the SHR2285 group was apparently higher than that in the placebo group (Table5), and there was no evident change in the inhibition level of FXI activity in the placebo group (Figure 2C).

In the 200 mg SHR2285 group, there was a mean minimum on treatment ratio-to-baseline of 15.2%, corresponding to a mean maximum on treatment percentage inhibition vs baseline of

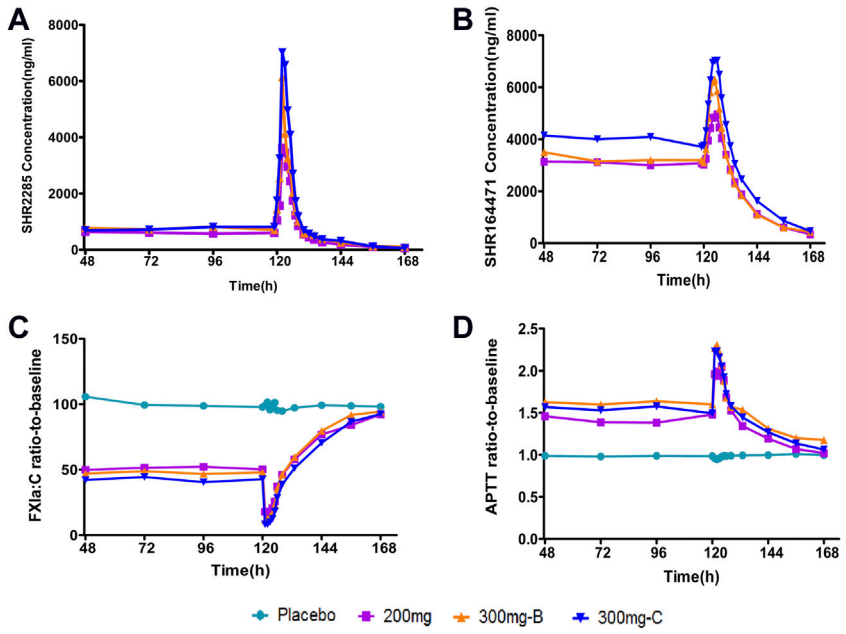

FIGURE 2
Mean PK and PD data following administration of multiple doses of SHR2285 for 6 days **(A)** Time course of mean SHR2285 concentrations; **(B)** Time course of mean SHR164471 (metabolite of SHR2285) concentrations **(C)** Time course of mean ratio-to-baseline values for FXIa:C; **(D)** Time course of mean ratio-to-baseline values for APTT. APTT, activated partial thromboplastin time; FXIa:C, factor XIa coagulation activity; PD, pharmacodynamics; PK, pharmacokinetics.

TABLE 3 SHR2285 Pharmacokinetic parameters.

	Treatment (SHR2285)		
	Group A n = 12	**Group B n = 13**	**Group C n = 12**
C_{max}, ng/mL	3,780 (28.8)	6,020 (36.7)	7,290 (16.1)
T_{max}, h	1.5 (1.5–2.5)	1.5 (1.5–2.0)	1.5 (1.5–2.0)
AUC_{tau}, h*ng/mL	14,300 (26.4)	19,700 (33.7)	25,200 (22.9)
$AUC_{0\text{-last}}$, h*ng/mL	19,400 (32.5)	28,100 (31.0)	33,800 (21.5)
$AUC_{0\text{-inf}}$, h*ng/mL	19,600 (33.0)	29,500 (27.5)	34,900 (24.9)
$t_{1/2}$, h	13.9 (5.56)	14.5 (5.43)	13.8 (7.02)
CL_{ss}/F, L/h	14.8 (3.68)	15.7 (4.15)	12.2 (2.75)
V_{ss}/F, L	283 (87.8)	343 (213)	227 (76.4)
C_{trough}, ng/mL	337 (43.9)	501 (40.1)	505 (29.1)
$C_{average}$, ng/mL	1,190 (26.4)	1,650 (33.7)	2,100 (22.9)

C_{max}, AUC_{tau}, $AUC_{0\text{-last}}$ and $AUC_{0\text{-inf}}$ are presented as geometric mean (GCV), T_{max} as median (range), $t_{1/2}$, CL_{ss}/F and V_{ss}/F as mean (standard deviation).
GCV, geometric coefficient of variation; C_{max}, maximum concentration; T_{max}, time to reach maximum concentration; AUC_{tau}, area under the plasma concentration-time curveat steady-state (one dose interval); $AUC_{0\text{-last}}$, area under the plasma concentration-time curve from time 0 to last time of quantifiable concentration; $AUC_{0\text{-inf}}$, area under the plasma concentration-time curve from time 0 extrapolated to infinite time; $t_{1/2}$, elimination half-life; CL_{ss}/F, steady state clearance rate of oral administration; V_{ss}/F, apparent volume of distribution; C_{trough}, valley concentration; $C_{average}$, steady-state average concentration.

84.8%. The mean of the maximum inhibition rate of FXI activity in groups B and C were 89.3% and 92.2%, respectively (Table 5). The maximum inhibition of FXI activity occurred at 2 h, 1.5 h and 1.5 h (median) after administration; The FXI activity of the SHR2285 group gradually returned to the baseline level 48 h after administration (Figure 2C).

TABLE 4 SHR164471 Pharmacokinetic parameters.

	Treatment (SHR2285)		
	Group A n = 12	Group B n = 13	Group C n = 12
C_{max}, ng/mL	5,030 (18.7)	6,330 (25.1)	7,050 (34.3)
T_{max}, h	4.0 (1.5–4.0)	2.5 (2.0–4.0)	3.0 (2.5–4.0)
AUC_{tau}, h*ng/mL	43,200 (23.3)	48,000 (24.6)	57,600 (37.2)
$AUC_{0\text{-}last}$, h*ng/mL	76,000 (30.6)	80,800 (30.5)	102,000 (42.8)
$AUC_{0\text{-}inf}$, h*ng/mL	82,100 (33.6)	83,800 (31.0)	111,000 (40.8)
$t_{1/2}$, h	13.1 (2.52)	12.3 (2.52)	14.3 (3.69)
CL_{ss}/F, L/h	6.29 (1.53)	8.69 (2.08)	7.36 (3.12)
V_{ss}/F, L	116 (20.7)	151 (29.5)	165 (119)
C_{trough}, ng/mL	2,250 (32.0)	2,220 (26.2)	2,830 (45.7)
$C_{average}$, ng/mL	3,600 (23.3)	4,000 (24.6)	4,800 (37.2)

C_{max}, AUC_{tau}, $AUC_{0\text{-}last}$ and $AUC_{0\text{-}inf}$ are presented as geometric mean (GCV), T_{max} as median (range), $t_{1/2}$, CL_{ss}/F and V_{ss}/F as mean (standard deviation).
GCV, geometric coefficient of variation; C_{max}, maximum concentration;T_{max}, time to reach maximum concentration; AUC_{tau}, area under the plasma concentration-time curveat steady-state (one dose interval); $AUC_{0\text{-}last}$, area under the plasma concentration-time curve from time 0 to last time of quantifiable concentration; $AUC_{0\text{-}inf}$, area under the plasma concentration-time curve from time 0 extrapolated to infinite time; $t_{1/2}$, elimination half-life; CL_{ss}/F, steady state clearance rate of oral administration; V_{ss}/F, apparent volume of distribution; C_{trough}, valley concentration; $C_{average}$, steady-state average concentration.

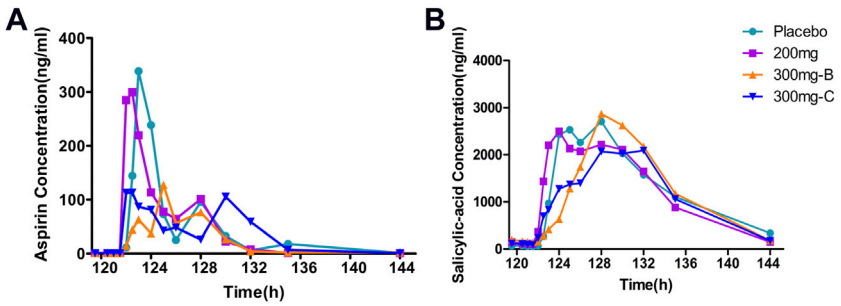

FIGURE 3
Mean PK data following administration of multiple doses of aspirin for 6 days **(A)** Time course of mean aspirin concentrations; **(B)** Time course of mean salicylic acid (metabolite of aspirin) concentrations. PK, pharmacokinetics.

Similar to the observed inhibitory effect of FXI activity, the APTT in the SHR2285 group was apparently more prolonged than that in the placebo group after repeated administration of 200 mg SHR2285 tablets in healthy subjects. There was almost no APTT prolongation in the placebo group (Figure 2D). The mean of the maximum APTT prolongation in the three SHR2285 dose groups were 2.08-, 2.36- and 2.26-fold, which appeared at 2 h, 1.5 h and 1.5 h (median), respectively (Table 5), and gradually returned to the baseline level at 48 h after administration. SHR2285 did not affect PT or INR (Figure 6).

The above data showed that the inhibition level of FXI activity was consistent with the increasing trend of plasma exposure of SHR2285 and its metabolite SHR164471, and they were positively correlated. In contrast, the correlation between APTT prolonged and plasma exposure of SHR2285 and SHR164471 was slightly weak.

Pharmacokinetics and pharmacodynamic relationship

As the *in vitro* PD study showed that both SHR2285 and its main metabolite SHR164471 inhibited human FXI activity and prolonged the APTT, FXI activity and APTT in the study were plotted against the sum of SHR2285/SHR164471 unbound plasma concentration (Figure 7). There is an obvious positive correlation between pharmacokinetics and inhibition of FXI activity and APTT prolongation.

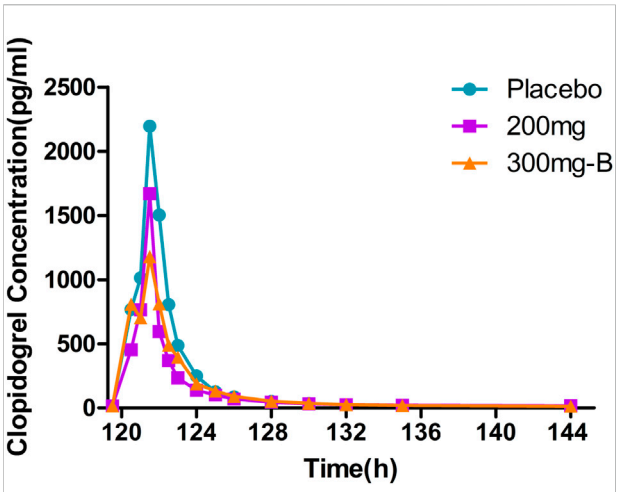

FIGURE 4
Mean PK data following administration of multiple doses of clopidogrel for 6 days. Time course of mean clopidogrel concentrations. PK, pharmacokinetics.

Discussion

The emergence of antithrombotic drugs with different action mechanisms provides more choices for preventing and treating thrombotic diseases. Although the commonly used antithrombotic drugs have significant effects, some deficiencies still exist, such as adverse reactions, including bleeding, osteoporosis and thrombocytopenia, and undesired drug interactions. Therefore, the research and development of new antithrombotic drugs are crucial for treating thrombotic diseases. Severe FXI deficiency reduces the incidence of thrombosis without the risk of major bleeding, which provides a new strategy for FXIa inhibition as an anticoagulant therapy.

The PD parameters of SHR2285 in this clinical trial were similar to several developed FXI inhibitors. The phase II clinical trial data of antisense oligonucleotide FXI-ASO showed that subcutaneous injection of 300 mg FXI-ASO reduced FXI activity in patients undergoing total knee arthroplasty by 80%, APTT prolonged by 1.4 imes, and venous thromboembolism

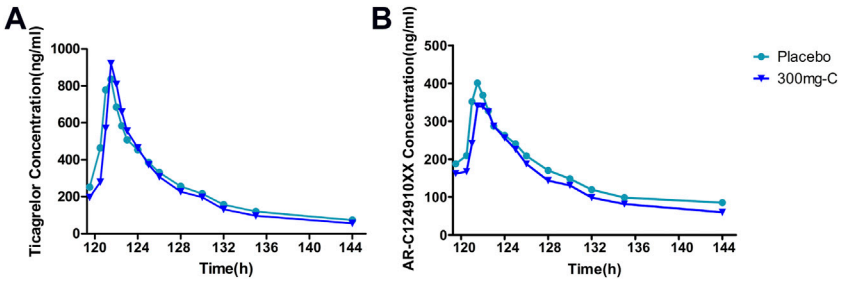

FIGURE 5
Mean PK data following administration of multiple doses of ticagrelor for 6 days **(A)** Time course of mean ticagrelor concentrations; **(B)** Time course of mean AR-C124910XX (metabolite of ticagrelor) concentrations. PK, pharmacokinetics.

TABLE 5 Pharmacodynamics indexes.

	Treatment (placebo or SHR2285)				
	Placebo (A + B) n = 7	Placebo(C) n = 8	SHR2285 (A) n = 12	SHR2285 (B) n = 13	SHR2285 (C) n = 12
FXIa:C					
Inhibition maximum	8.07 (3.37)	14.6 (6.88)	84.8 (4.66)	89.3 (3.85)	92.2 (1.66)
Inhibition average	-0.33 (4.88)	5.6 (7.06)	62.2 (6.53)	63.8 (5.50)	70.0 (5.33)
APTT					
RTB maximum	1.08 (0.0877)	1.04 (0.0372)	2.08 (0.199)	2.36 (0.224)	2.26 (0.125)
RTB average	0.988 (0.0619)	0.976 (0.0599)	1.67 (0.132)	1.78 (0.115)	1.76 (0.0866)

FXIa:C and APTT, values are presented as mean (standard deviation).
Percentage inhibition values are calculated using the percentage from baseline values (100% - FXI, activity%/baseline FXI, activity). FXIa:C, factor XIa, coagulation activity; APTT, activated partial thromboplastin time; RTB, ratio-to-baseline.

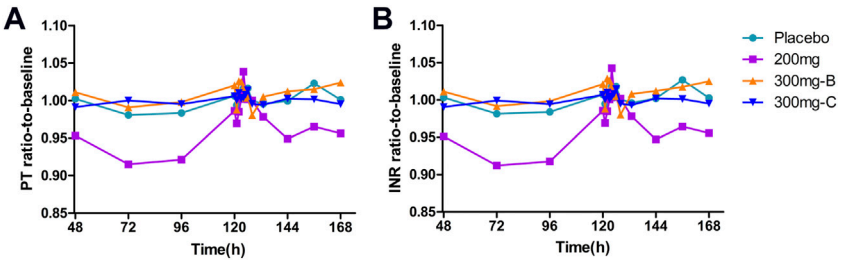

FIGURE 6
Mean PD data following administration of multiple doses of SHR2285 for 6 days **(A)** Time course of mean ratio-to-baseline values for PT; **(B)** Time course of mean ratio-to-baseline values for INR. PT, prothrombin time; INR, international normalized ratio; PD, pharmacodynamics.

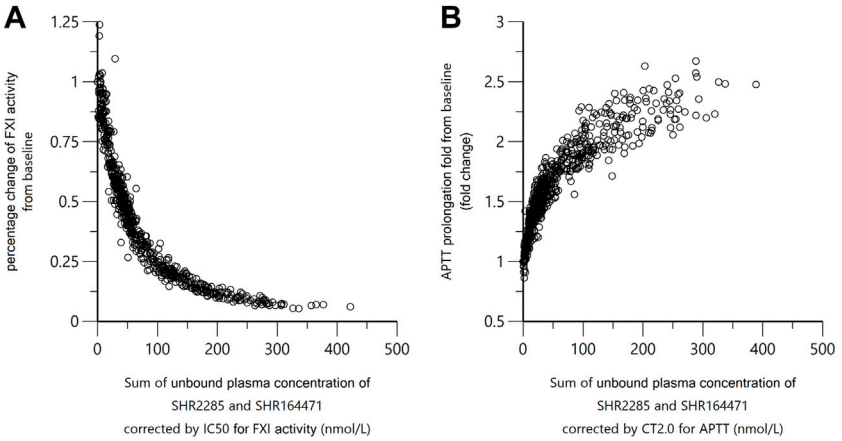

FIGURE 7
Correlation of SHR2285/SHR164471 unbound plasma concentrations with inhibition of FXI activity and APTT prolongation. In panel **(A)**, the *x*-axis indicates sum of unbounded plasma concentration of SHR2285 and SHR164471*IC50 of SHR2285 on FXI activity/IC50 of SHR164471 on FXI activity. In panel **(B)**, the *x*-axis represents the sum of unbounded plasma concentration of SHR2285 and SHR164471*CT2.0 of SHR2285 on APTT/CT2.0 of SHR164471 on APTT. The plasma-protein binding rate was measured using rapid equilibrium dialysis. Unbound plasma concentration = total plasma concentration*(1−protein binding%).

incidence rate was 4%, significantly lower than that in the enoxaparin group. However, it works slowly and may cause thrombocytopenia and an increased risk of postoperative bleeding (Büller et al., 2015). Some FXI inhibitors are administered intravenously; this invasive way of administration increases the adverse events of the infusion reaction and also limits the place of use, preferably in the hospital (Perera et al., 2018; Pollack et al., 2020; Weitz et al., 2020). Moreover, the risk of bleeding and the prevention of venous thromboembolism is not more effective than existing anticoagulants (Weitz et al., 2020). Highly selective oral FXIa inhibitors showed rapid onset and offset, the maximum inhibition rate of FXI activity is more than 90%, and the extension multiple of APTT is as high as 2.78 times (Gómez-Outes et al., 2017; Beale et al., 2021). In the SHR2285-101 study, the maximum FXI inhibition was 60.92%, and the APTT pro longed 1.52 times, slightly inferior to the PD of SHR2585 in this study (different dosage forms). In the first-in-human study of SHR2285, no bleeding events were reported, suggesting that SHR2285 may be a potential anticoagulant option for patients who underwent PCI and required DAPT in combination with anticoagulants (Chen et al., 2022). However, the antithrombotic effect and bleeding risk after FXIa inhibitor combined with the existing standard dual antiplatelet therapy, the standard treatment of myocardial infarction and stroke recommended by the international and China, has not been studied.

In this study, SHR2285 was well tolerated in healthy subjects. All randomized subjects completed the study as planned without any significant tolerance problems. All adverse events observed were mild and resolved without intervention. The incidence of AEs was similar in the placebo and SHR2285 dose groups. Importantly, there is no evidence of a risk of massive bleeding after combined

administration, which remains a common problem of existing anticoagulant therapy. The mild bleeding events observed in the study may be the drug reaction of dual antiplatelet. The PK parameters of SHR2285 were comparable with other small molecule FXIa inhibitors such as BMS-986177, BMS-962212, ONO-7684 and EP-7041 (Gómez-Outes et al., 2017; Perera et al., 2018; Pollack et al., 2020; Beale et al., 2021). The pharmacokinetics of SHR2285 and its main active metabolite were well characterized. The $t_{1/2}$ of SHR2285 and its active metabolite SHR164471 is 12.3–14.5 h, similar to the SHR2285-101 study (Chen et al., 2022), which supports oral administration twice a day, both inside and outside the hospital. In this study, C_{max} and AUC of SHR2285 were apparent higher than 101 study, and T_{max} was significantly apparent. In this study, SHR2285 was a solid dispersible tablet, and SHR2285-101 was a nanocrystalline preparation. It may be that different dosage forms lead to different absorption and bioavailability. PD studied in this trial included APTT, FXI activity and PT/INR. The increasing exposure could result in the prolongation of APTT and the decrease of FXI activity but had no effect on PT/INR, which may explain why SHR2285 does not increase the risk of bleeding.

Previous studies have suggested that anticoagulant drugs (including vitamin K antagonists, factor Xa inhibitors, *etc.*) combined with dual antiplatelet drugs showed a trend of reducing thrombotic events (not statistically significant), but it was also accompanied by an increased risk of bleeding, which was limited in clinical application (Lou et al., 2018). Therefore, to reduce the occurrence of thromboembolism without increasing the risk of bleeding, we can choose the treatment scheme of DAPT combined with FXIa (a new anticoagulant) to meet the clinical needs better. The relationship between SHR2285 and the prevention of thromboembolic events needs to be determined in subsequent phase II and III clinical trials.

In conclusion, SHR2285 significantly inhibited the activity of FXI in a dose-dependent manner. When combined with aspirin, clopidogrel or ticagrelor, it was well tolerated in healthy subjects without apparent safety or tolerance issues. There was no significant effect on PT or INR, and there was no evidence of an increased risk of bleeding. These results suggest that the FXIa inhibitor represented by SHR2285 is expected to be an effective and safe oral anticoagulant for combined dual antiplatelet therapy.

Data availability statement

The raw data supporting the conclusions of this article will be made available by the authors, without undue reservation.

Ethics statement

The studies involving human participants were reviewed and approved by the ethics committee of Nanjing Drum Tower Hospital, the Affiliated Hospital of Nanjing University Medical School. The participants provided their written informed consent to participate in this study.

Author contributions

XJ and YD designed the research. All authors performed the research, TM, YD, and ZY analysed the data. TM, JL, RS, and YD contributed to the writing of the manuscript.

Funding

This study was funded by the National Natural Science Foundation of China (No. 31371399) and Jiangsu Hengrui Pharmaceuticals Co., Ltd.

Acknowledgments

The authors would like to thank the following people for their contributions: all volunteers who participated in this study, all the investigators, CRA and CRC who participated in supporting the trial.

Conflict of interest

Authors YD, ZY, YJ, and XJ were employed by Jiangsu Hengrui Pharmaceuticals Co., Ltd.

The remaining authors declares that the research was conducted in the absence of any commercial or financial relationships that could be construed as a potential conflict of interest.

Publisher's note

Supplementary material

The Supplementary Material for this article can be found online at: https://www.frontiersin.org/articles/10.3389/fphar.2022.1027627/full#supplementary-material

References

Abbafati, C., Abbas, K. M., Abbasi, M., Abbasifard, M., Abbasi-Kangevari, M., Abbastabar, H., et al. (2020). Global burden of 369 diseases and injuries in 204 countries and territories, 1990-2019: A systematic analysis for the global burden of disease study 2019. *LANCET* 396, 1204–1222. doi:10.1016/S0140-6736(20)30925-9

Beale, D., Dennison, J., Boyce, M., Mazzo, F., Honda, N., Smith, P., et al. (2021). ONO-7684 a novel oral FXIa inhibitor: Safety, tolerability, pharmacokinetics and pharmacodynamics in a first-in-human study. *Br. J. Clin. Pharmacol.* 87, 3177–3189. doi:10.1111/bcp.14732

Büller, H. R., Bethune, C., Bhanot, S., Gailani, D., Monia, B. P., Raskob, G. E., et al. (2015). Factor XI antisense oligonucleotide for prevention of venous thrombosis. *N. Engl. J. Med.* 372, 232–240. doi:10.1056/NEJMoa1405760

Cannon, C. P., Lip, G. Y. H., and Oldgren, J. (2018). Dual antithrombotic therapy with dabigatran after PCI in atrial fibrillation. *N. Engl. J. Med.* 378, 485–486. doi:10.1056/NEJMc1715183

Chen, R., Guan, X., Hu, P., Dong, Y., Zhu, Y., Zhang, T., et al. (2022). First-in-human study to assess the safety, pharmacokinetics, and pharmacodynamics of SHR2285, a small-molecule factor XIa inhibitor in healthy subjects. *Front. Pharmacol.* 13, 821363. doi:10.3389/fphar.2022.821363

Degrauwe, S., Pilgrim, T., Aminian, A., Noble, S., Meier, P., and Iglesias, J. F. (2017). Dual antiplatelet therapy for secondary prevention of coronary artery disease. *Open Heart* 4, e000651. doi:10.1136/openhrt-2017-000651

Emsley, J., Mcewan, P. A., and Gailani, D. (2010). Structure and function of factor XI. *Blood* 115, 2569–2577. doi:10.1182/blood-2009-09-199182

Georgi, B., Mielke, J., Chaffin, M., Khera, A. V., Gelis, L., Mundl, H., et al. (2019). Leveraging human genetics to estimate clinical risk reductions achievable by inhibiting factor XI. *Stroke* 50, 3004–3012. doi:10.1161/STROKEAHA.119.026545

Gómez-Outes, A., García-Fuentes, M., and Suárez-Gea, M. L. (2017). Discovery methods of coagulation-inhibiting drugs. *Expert Opin. Drug Discov.* 12, 1195–1205. doi:10.1080/17460441.2017.1384811

Key, N. S. (2014). Epidemiologic and clinical data linking factors XI and XII to thrombosis. Hematology. *Am. Soc. Hematol. Educ. Prog.* 1, 66–70. doi:10.1182/asheducation-2014.1.66

Koch, A. W., Schiering, N., Melkko, S., Ewert, S., Salter, J., Zhang, Y., et al. (2019). MAA868, a novel FXI antibody with a unique binding mode, shows durable effects on markers of anticoagulation in humans. *Blood* 133, 1507–1516. doi:10.1182/blood-2018-10-880849

Levi, M. (2016). Management of bleeding in patients treated with direct oral anticoagulants. *Crit. Care* 20, 249. doi:10.1186/s13054-016-1413-3

Lou, B., Liang, X., Wu, Y., Deng, Y., Zhou, B., Yuan, Z., et al. (2018). Meta-analysis comparing dual versus single antiplatelet therapy in combination with antithrombotic therapy in patients with atrial fibrillation who underwent percutaneous coronary intervention with stent implantation. *Am. J. Cardiol.* 122, 604–611. doi:10.1016/j.amjcard.2018.04.050

Pan, Y., Li, Z., Li, J., Jin, A., Lin, J., Jing, J., et al. (2021). Residual risk and its risk factors for ischemic stroke with adherence to guideline-based secondary stroke prevention. *J. Stroke* 23, 51–60. doi:10.5853/jos.2020.03391

Perera, V., Luettgen, J. M., Wang, Z., Frost, C. E., Yones, C., Russo, C., et al. (2018). First-in-human study to assess the safety, pharmacokinetics and pharmacodynamics of BMS-962212, a direct, reversible, small molecule factor XIa inhibitor in non-Japanese and Japanese healthy subjects. *Br. J. Clin. Pharmacol.* 84, 876–887. doi:10.1111/bcp.13520

Pollack, C. V., Kurz, M. A., and Hayward, N. J. (2020). EP-7041, a factor XIa inhibitor as a potential antithrombotic strategy in extracorporeal membrane oxygenation: A brief report. *Crit. Care Explor.* 2, e0196. doi:10.1097/CCE.0000000000000196

Preis, M., Hirsch, J., Kotler, A., Zoabi, A., Stein, N., Rennert, G., et al. (2017). Factor XI deficiency is associated with lower risk for cardiovascular and venous thromboembolism events. *Blood* 129, 1210–1215. doi:10.1182/blood-2016-09-742262

Salomon, O., Steinberg, D. M., Koren-Morag, N., Tanne, D., and Seligsohn, U. (2008). Reduced incidence of ischemic stroke in patients with severe factor XI deficiency. *Blood* 111, 4113–4117. doi:10.1182/blood-2007-10-120139

Wang, H., Rosendaal, F. R., Cushman, M., and Van Hylckama Vlieg, A. (2021). Procoagulant factor levels and risk of venous thrombosis in the elderly. *J. Thromb. Haemost.* 19, 186–193. doi:10.1111/jth.15127

Wang, W., Jiang, B., Sun, H., Ru, X., Sun, D., Wang, L., et al. (2017). Prevalence, incidence, and mortality of stroke in China: Results from a nationwide population-based survey of 480 687 adults. *Circulation* 135, 759–771. doi:10.1161/CIRCULATIONAHA.116.025250

Weitz, J. I., Bauersachs, R., Becker, B., Berkowitz, S. D., Freitas, M. C. S., Lassen, M. R., et al. (2020). Effect of osocimab in preventing venous thromboembolism among patients undergoing knee arthroplasty: The FOXTROT randomized clinical trial. *JAMA* 323, 130–139. doi:10.1001/jama.2019.20687

Wendelboe, A. M., and Raskob, G. E. (2016). Global burden of thrombosis: Epidemiologic aspects. *Circ. Res.* 118, 1340–1347. doi:10.1161/CIRCRESAHA.115.306841

frontiers | Frontiers in Pharmacology

TYPE Clinical Trial
PUBLISHED 04 November 2022
DOI 10.3389/fphar.2022.1057949

OPEN ACCESS

EDITED BY
Zhihao Liu,
Dalian Medical University, China

REVIEWED BY
Yanna Zhu,
Dalian Medical University, China
Ziqiang Li,
Tianjin University of Traditional Chinese Medicine, China

*CORRESPONDENCE
Qing He,
heqing0510@163.com

†These authors have contributed equally to this work and share first authorship

SPECIALTY SECTION
This article was submitted to Drug Metabolism and Transport, a section of the journal Frontiers in Pharmacology

RECEIVED 30 September 2022
ACCEPTED 18 October 2022
PUBLISHED 04 November 2022

CITATION
Huang K, Ding Y, Que L, Chu N, Shi Y, Qian Z, Qin W, Chen Y, Gu X, Wang J, Zhang Z, Xu J and He Q (2022), Safety, tolerability and pharmacokinetics of WXFL10203614 in healthy Chinese subjects: A randomized, double-blind, placebo-controlled phase I study. *Front. Pharmacol.* 13:1057949. doi: 10.3389/fphar.2022.1057949

Safety, tolerability and pharmacokinetics of WXFL10203614 in healthy Chinese subjects: A randomized, double-blind, placebo-controlled phase I study

Kai Huang[1†], Ying Ding[1†], Linling Que[1], Nannan Chu[1], Yunfei Shi[1], Zhenzhong Qian[1], Wei Qin[1], Yuanxin Chen[1], Xianghong Gu[1], Jiakun Wang[1], Zhiwei Zhang[2], Jianguo Xu[2] and Qing He[1]*

[1]Drug Clinical Trial Institution, Affiliated Wuxi People's Hospital of Nanjing Medical University, Wuxi, China, [2]Wuxi Fuxin Pharmaceutical Research and Development Co, Ltd, Wuxi, China

Objective: This study was conducted to investigate the safety, tolerability and pharmacokinetics (PK) of WXFL10203614 after single and multiple oral doses in healthy Chinese subjects.

Methods: A single-center, randomized, double-blind, placebo-controlled phase I study was performed on healthy Chinese subjects. In the single-dose study, Subjects were randomized into 7 dose levels of WXFL10203614 (1 mg group, n = 2; 2, 5, 10, 17, 25 and 33 mg groups with placebo, 8 subjects per group, 2 of them given placebo). In the multiple-dose study, subjects received 5 or 10 mg WXFL10203614 once daily (QD), 5 mg twice daily (BID) or placebo for 7 consecutive days. Safety, tolerability and PK of WXFL10203614 were all assessed.

Results: A total of 592 subjects were screened, 50 subjects were enrolled in the single-dose study and 30 in the multiple-dose study. All adverse events (AEs) were mild or moderate and resolved spontaneously. No Serious Adverse Events (SAEs) or deaths were reported during the study. WXFL10203614 was absorbed rapidly after dosing with T_{max} of 0.48–0.98 h, C_{max}, AUC_{0-t} and $AUC_{0-\infty}$ were all increased in a dose-related manner over the range of 1–33 mg. Renal excretion was the major route of elimination of WXFL10203614. Steady-state PK parameters ($C_{max,ss}$, $AUC_{0-t,ss}$ and $AUC_{0-\infty,ss}$) were elevated after once-daily administration of 5–10 mg WXFL10203614 and non- and weak drug accumulations were observed, whereas moderate drug accumulation occurred in the 5 mg BID group.

Conclusion: WXFL10203614 exhibited good safety, tolerability and favorable PK profiles in healthy Chinese subjects, supporting further clinical development in patients with rheumatoid arthritis.

Clinical Trials Registration Number: http://www.chinadrugtrials.org.cn/index.html, #CTR20190069 and CTR20200143.

KEYWORDS

WXFL10203614, pharmacokinetics, JAK1 inhibitor, rheumatoid arthritis, first-in-human

Introduction

Rheumatoid arthritis (RA) is a chronic systemic autoimmune disease. It is characterized by joint synovitis, bone erosion, progressive cartilage destruction and disability, which seriously influence life quality and even increase mortality (Mohamed et al., 2016; Sparks, 2019). So far, however, the exact etiology of RA has still been unclear (Li et al., 2020).

Although significant progress has been made in non-steroidal anti-inflammatory drugs (NSAIDs), conventional synthetic disease-modifying anti-rheumatic drugs (csDMARDs) and biological therapeutics for the treatment of RA, some shortcomings were still inevitable during the treatments, such as inadequate or no response to traditional therapies, serious complications of infection, inconvenient injection and high cost of biological therapy, which limited their long-term use (Lin et al., 2020; Xie et al., 2020). A more effective and better tolerated oral treatment may be preferable for RA patients. A great deal of attention has been paid to the Janus kinase (JAK) family when JAK-mediated signal pathways were confirmed to play a pivotal role in the pathologic processes of RA (Norman, 2014; Alqarni and Zeidler, 2020; You et al., 2020). Therefore, inhibition of JAK isoforms was considered a potential therapeutic approach for RA.

JAK family comprises JAK1, JAK2, JAK3 and tyrosine kinase 2 (TYK2), mediating the signal pathways of numerous cytokines and growth factors which participate in the regulation of immune function, inflammation and hematopoiesis (Vazquez et al., 2018). However, among 4 JAK isoforms, JAK1 mainly regulated various cytokine signal pathways related to the pathophysiology of multiple inflammatory diseases (Kotenko and Pestka, 2000; Peeva et al., 2018), JAK2 was involved in the essential regulatory functions of granulocyte-macrophage colony-stimulating factor (GM-CSF) and erythropoietin (Broxmeyer, 2013), JAK3 was more selectively expressed in hematopoietic cells and Tyk2 was a target for treating psoriasis and inflammatory bowel disease rather than RA (Norman, 2014). Immunoregulation and anti-inflammation were the keys for JAK inhibitors in RA treatment *via* inhibiting the JAK-mediated signal pathways. A series of small molecule inhibitors of JAK isoforms have been approved for treating RA since 2009 (Choy, 2019), including tofacitinib (the first JAK1/JAK3 inhibitor), baricitinib (JAK1/JAK2 inhibitor), upadacitinib and filgotinib (JAK1 inhibitor) and peficitinib (pan-JAK inhibitor) (Norman, 2014; Kaneko, 2020). Therefore, developing selective JAK1 inhibitors not only minimizes the potential side effects but also maximizes the therapeutic efficacy for RA patients.

WXFL10203614, a potential selective JAK1 inhibitor, was under development as an oral DMARD for RA treatment. The preclinical studies confirmed that WXFL10203614 was effective for RA with acceptable safety and tolerability profiles and superior to tofacitinib (data not shown). Based on these promising preclinical data, the clinical trials of WXFL10203614 were eventually approved by National Medical Products Administration (NMPA) in 2018 (Approval Number: 2018L03083 and 2018L03084).

This single- and multiple-dose study aimed to evaluate the safety, tolerability and pharmacokinetics (PK) of WXFL10203614 in healthy Chinese subjects. Results supported the dose selection and design of phaseIIclinical trials of WXFL10203614 in RA patients.

Methods

Study population

Healthy Chinese subjects aged 18–45 years, with a body mass index of 19.0–26.0 kg/m^2 and body weight ≥50 kg (male) or ≥45 kg (female), were enrolled in this study. Subjects were included if they were evaluated to be healthy by vital signs, physical examination, medical history, laboratory tests, virological examinations, electrocardiograph (ECG), chest X-ray, abdominal ultrasound, urine nicotine test, alcohol breath analysis and urine drug screening test within 2 weeks before dosing. Subjects were excluded if they had any of the following: allergic to any medication, a history of corrected Q-T (QTc) interval prolongation, QTc interval ≥450 milliseconds, PR interval ≥210 milliseconds, QRS ≥120 milliseconds, positive for T-SPOT® TB test, took any prescription or nonprescription medicine (including vitamins, herbal products or dietary supplements) within 1 month before the screening, or participated in any clinical trial within the past 3 months. Besides, pregnant or lactating women were also excluded.

Compliance with ethical standards

This study was conducted according to Good Clinical Practice guidelines and the ethical principle of the Declaration of Helsinki. The study protocol and informed consent form were approved by the independent Ethics Committee of Affiliated Wuxi People's Hospital of Nanjing Medical University (Approval Number: 2018LLPJ-I-45 for the single-dose study and 2020LLPJ-I-08 for the multiple-dose study). The written informed consent was signed by each subject freely and voluntarily before the screening.

Study design

A single-center, randomized, double-blind, placebo-controlled, single- and multiple-dose phase I study of WXFL10203614 was conducted in the phase I center of Wuxi people's hospital from 7 March 2019 to 13 December 2019 (the single-dose study) and from 31 March 2020 to 10 July 2020 (the multiple-dose study) (Chinese Clinical Trial Registry, Registration Number: CTR20190069 and CTR20200143, http://www.chinadrugtrials.org.cn/index.html). The WXFL10203614 tablet (1 mg, Lot Number: XS180902B; 5 mg, Lot Number: XS180902C) and the placebo tablet (Lot Number: XS180901A) were manufactured and supplied by Wuxi Fuxin Pharmaceutical Research and Development Co., Ltd.

In the single-dose study, 50 subjects were randomly allocated to receive a single ascending dose of 1, 2, 5, 10, 17, 25 and 33 mg WXFL10203614. In the initial dose cohort, 2 subjects received 1 mg WXFL10203614 only for the safety evaluation. After that, 8 subjects per cohort randomly received WXFL10203614 (2, 5, 10, 17, 25 or 33 mg) or placebo at a 3:1 ratio in a dose-escalation manner. All subjects fasted overnight for at least 10 h before dosing and received a single oral dose of WXFL10203614 with 240 ml water. Moreover, none of the subjects was permitted to drink water within 1 h before and after dosing or eat anything within 4 h after dosing. Subjects remained in the center for 4 days and completed follow-up on day 7 after discharge. Safety, tolerability and PK evaluations were performed before escalation to the next dose level.

In the multiple-dose study, three doses of WXFL10203614 (5 or 10 mg once daily [QD] or 5 mg twice daily [BID]) were selected on the basis of the single-dose study. 30 subjects were enrolled, 10 subjects per cohort were randomly assigned to receive WXFL10203614 or placebo at a 4:1 ratio for 7 consecutive days (QD: once daily on day 1–7; BID: once daily on day 1 and 7, and twice daily on day 2–6). Subjects fasted overnight before the first and last dosing and orally received WXFL10203614 with 240 ml water at each dosing time. Subjects remained in the center until day 10 and completed follow-up on day 7 after discharge. Safety, tolerability and PK were also evaluated at the end of the study. Dose escalation was only allowed when the previous dose was safe and well-tolerated in subjects.

Safety and tolerability evaluations

Safety and tolerability were assessed on the basis of Adverse Events (AEs), the clinically significant changes in physical examination, vital signs, laboratory tests and ECG. The severity of AEs was referenced in terms of the National Cancer Institute- Common Terminology Criteria for Adverse Events (NCI-CTCAE) (version 5.03). Furthermore, the relationship of AEs to WXFL10203614 was evaluated by the investigator.

Pharmacokinetic analysis

In the single-dose study, blood samples (4 ml) were collected in Ethylene Diamine Tetraacetie Acid (EDTA)-2K vacuum tubes at 0 (pre-dose), 0.25, 0.5, 1, 1.5, 2, 3, 4, 6, 8, 12, 24, 36, 48 and 72 h. Urine samples were collected at -2-0 h (pre-dose), 0–4, 4–8, 8–12, 12–24, 24–36, 36–48 and 48–72 h. In the multiple-dose study, blood samples (4.0 ml) were collected on day 1 at the same points as in the single-dose study until 24 h (before the second dosing) and on day 5 and 6 before dosing. Moreover, the sampling time points were 0 (pre-dose), 0.25, 0.5, 0.75, 1, 1.5, 2, 4, 8, 12, 24, 36 and 48 h after the last dosing on day 7. Blood samples were gently mixed 6–8 times after collecting and centrifuged at 1500 g for 10 min at 4°C. All plasma and urine samples were stored at −80°C until analyzed.

Samples were prepared by simple protein precipitation with acetonitrile containing $^{13}CD_3$-Target as internal standard (IS). Briefly, 50 μL of IS working solution (50 ng/ml for plasma or 200 ng/ml for urine) and 300 μl of acetonitrile were added to 50 μl of the sample. The mixture was vortexed for 15 min, followed by centrifugation at 2,510 *g* for 15 min. The supernates were assayed for the WXFL10203614 concentration in plasma. For the urine sample, the supernate should be diluted 10-fold before analysis.

The concentrations of WXFL10203614 in plasma and urine were analyzed using a validated liquid chromatography-tandem mass spectrometry (LS-MS/MS) method. WXFL10203614 and IS were chromatographed by injecting 1 μl sample into a BEH C18 column (1.7 μm, 2.1 mm × 50 mm, Waters, USA) with a column temperature at 40°C. The mobile phase consisted of solvent A (0.05% formic acid in a 2 mM aqueous ammonium acetate solution) and solvent B (acetonitrile). The gradient elution was programmed as follows: 90% solvent A for 0.3 min, and then gradually decreased to 5% for 1.4 min, followed by re-equilibration at 90% for 0.8 min. The total analytical run time was 2.5 min and the flow rate was 0.55 ml/min. The mass transitions of WXFL10203614 and IS monitored in multiple reaction monitoring (MRM) were m/z 294.1→146.0 and 298.2→146.1. The retention times of WXFL10203614 and IS were 1.06 and 1.05 min, and no apparent interference affected the detection. The linearity ranges of WXFL10203614 were 0.4–500 ng/ml and 5–8,000 ng/ml, the lower limit of quantitation (LLOQ) was 0.4 and 5 ng/ml, and the recoveries were 90.9–94.2% and 92.0–94.0% in plasma and urine, respectively. The intra-and inter-day precision did not exceed 6.1% with an accuracy of −4.2-2.9% in plasma (Low QC: 1.2 ng/ml, Middle QC: 50 ng/ml and High QC: 400 ng/ml). The plasma samples were stable at room temperature for 18 h, and −20°C and −80°C for

105 days. The intra-and inter-day precision did not exceed 10.7% and the accuracy was within ±7.2% in urine (Low QC: 15 ng/ml, Middle QC: 500 ng/ml and High QC: 6,400 ng/ml). The urine samples were stable at room temperature for 24 h, and −20°C and −80°C for 69 days. The concentrations of WXFL10203614 in plasma or urine that exceed the upper limit of quantification (ULOQ) should be diluted, and 10-fold dilutions did not affect the accuracy and precision.

Statistical analysis

PK analysis was performed by a non-compartmental method using Phoenix WinNonlin software (version 8.2) to calculate PK parameters. In the single-dose study, the primary PK parameters included maximum concentration in plasma (C_{max}), time to maximum concentration (T_{max}), area under the plasma concentration-time curve from time 0 to the last measurable concentration (AUC_{0-t}), area under the plasma concentration-time curve from time 0 to infinity ($AUC_{0-\infty}$), terminal elimination half-life ($t_{1/2}$), mean residence time of 0 to the last measurable concentration (MRT_{0-t}), apparent clearance rate (CL/F), apparent volume of distribution (Vd) and the cumulative urinary excretion in 72 h (Ae_{0-72}). In the multiple-dose study, the primary PK parameters were C_{max} at steady state ($C_{max,ss}$), Tmax at steady state ($T_{max,ss}$), AUC_{0-t} at steady state ($AUC_{0-t,ss}$), $AUC_{0-\infty}$ at steady state ($AUC_{0-\infty,ss}$), CL/F at steady state (CL_{ss}/F) and the accumulation index (Ra). Ra (AUC) was calculated as the ratio of $AUC_{0-t,ss}$ to AUC_{0-t} and Ra (C_{max}) was the ratio of $C_{max,ss}$ to C_{max}.

The Full Analysis Set (FAS) and Safety Set (SS) included all randomized subjects receiving at least one dose of WXFL10203614 or placebo. The pharmacokinetic concentration set (PKCS) included all subjects with at least one drug concentration result. The pharmacokinetic parameter set (PKPS) included all subjects with at least one viable PK parameter.

Dose-PK parameter (C_{max}, AUC_{0-t} and $AUC_{0-\infty}$) proportionality was assessed with linear regression by using natural logarithm value based on the power model. The corresponding 90% confidence intervals (CIs) for the slopes of the log-transformed C_{max}, AUC_{0-t} and $AUC_{0-\infty}$ were compared with the modified acceptance range (Smith et al., 2000). PK parameters and demographic characteristics were summarized using descriptive statistics. All statistical analyses were performed with SAS software (version 9.4). Variance analysis and *t*-test for normally distributed data and Wilcoxon rank test for non-normally distributed data were used for data analysis. $p < 0.05$ was considered statistically significant.

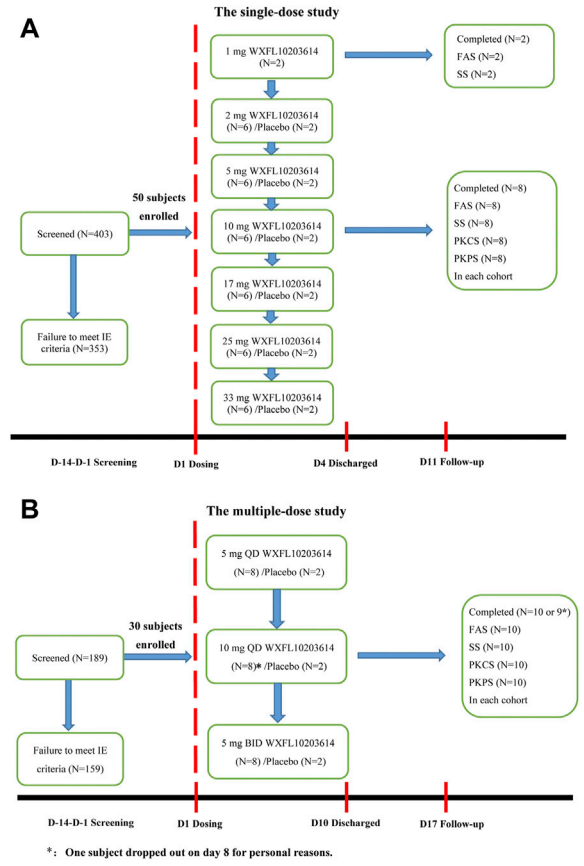

FIGURE 1
Subject disposition. **(A)** The single-dose study, **(B)** The multiple-dose study. FAS: The Full Analysis Set, SS: Safety set, PKCS: Pharmacokinetic concentration set, PKPS: Pharmacokinetic parameter set, IE: inclusion/exclusion.

Results

Demographic data of subjects

In the single-dose study, 403 subjects were screened, 50 healthy subjects randomized and exposed to oral administration. Among them, 32 were male and 18 were female, all subjects completed the study. Two subjects who received 1 mg WXFL10203614 were only evaluated for FAS and SS, and others were included in FAS, SS, PKCS and PKPS analyses. In the multiple-dose study, 189 subjects were screened, 30 subjects were enrolled and randomized, 18 were male and 12 were female, 29 subjects completed the study and 1 subject who received 10 mg QD WXFL10203614 dropped out on day 8 for personal reasons. All subjects were included in FAS, SS, PKCS and PKPS analyses (Figure 1). Age, weight and BMI were similar between WXFL10203614 groups and placebo in the single- and multiple-dose study. Baseline demographic characteristics are shown in Table 1.

TABLE 1 Demographics and baseline characteristics of subjects.

	Single-dose study								Multiple-dose study			
	1 mg (N = 2)	2 mg (N = 6)	5 mg (N = 6)	10 mg (N = 6)	17 mg (N = 6)	25 mg (N = 6)	33 mg (N = 6)	Placebo (N = 12)	5 mg QD (N = 8)	10 mg QD (N = 8)	5 mg BID (N = 8)	Placebo (N = 6)
Sex, N (%)												
Male	1 (50.0)	4 (66.7)	2 (33.3)	4 (66.7)	4 (66.7)	5 (83.3)	4 (66.7)	8 (66.7)	3 (37.5)	5 (62.5)	6 (75.0)	4 (66.7)
Female	1 (33.3)	2 (33.3)	4 (66.7)	2 (33.3)	2 (33.3)	1 (16.7)	2 (33.3)	4 (33.3)	5 (62.5)	3 (37.5)	2 (25.0)	2 (33.3)
Ethnicity (Han/other)	2/0	5/1	6/0	6/0	6/0	6/0	6/0	12/0	8/0	7/1	8/0	6/0
Age (years)	22.5 ± 0.7	27.8 ± 4.2	28.0 ± 5.1	26.8 ± 6.9	32.0 ± 4.4	27.2 ± 6.6	28.7 ± 5.2	27.6 ± 5.9	24.3 ± 4.4	26.3 ± 5.4	32.8 ± 8.0	28.7 ± 7.1
Height (cm)	159.5 ± 7.1	162.5 ± 5.0	162.6 ± 7.9	170.7 ± 8.1	165.3 ± 8.4	168.6 ± 8.7	164.2 ± 8.6	164.7 ± 7.3	163.9 ± 10.9	168.8 ± 6.9	168.7 ± 7.1	166.2 ± 9.0
Weight (kg)	55.0 ± 2.3	59.9 ± 6.7	60.8 ± 6.7	65.5 ± 8.1	64.3 ± 7.9	64.2 ± 9.0	55.9 ± 5.9	59.2 ± 6.9	59.3 ± 8.5	62.6 ± 8.3	61.4 ± 7.7	60.6 ± 8.4
BMI (kg/m^2)	21.6 ± 1.1	22.7 ± 2.1	23.0 ± 1.3	22.5 ± 2.4	23.5 ± 0.8	22.5 ± 1.2	20.8 ± 1.6	21.8 ± 1.9	22.0 ± 1.0	21.9 ± 1.6	21.5 ± 1.8	21.8 ± 1.7

BMI: body mass index; Data are presented in mean ± SD, unless otherwise indicated.

TABLE 2 The primary pharmacokinetic parameters of WXFL10203614 in the single-dose study.

Parameter	2 mg (N = 6)	5 mg (N = 6)	10 mg (N = 6)	17 mg (N = 6)	25 mg (N = 6)	33 mg (N = 6)
C_{max} (ng/ml)	52.9 ± 15.6	118.0 ± 19.7	192.0 ± 54.4	322.3 ± 61.0	577.0 ± 65.0	748.3 ± 276.9
T_{max} (h)[a]	0.48 (0.23–0.98)	0.48 (0.48–0.98)	0.98 (0.23–2.00)	0.73 (0.48–1.48)	0.48 (0.23–0.98)	0.98 (0.23–2.00)
AUC_{0-t} (h•ng/mL)	504 ± 94	1250 ± 183	2,400 ± 382	4,710 ± 455	6,940 ± 535	10800 ± 1580
$AUC_{0-\infty}$ (h•ng/mL)	518 ± 93	1270 ± 176	2,420 ± 385	4,760 ± 456	7,090 ± 596	11100 ± 1740
$t_{1/2}$ (h)	9.2 ± 1.1	9.9 ± 1.7	9.5 ± 0.8	10.4 ± 1.1	12.4 ± 3.1	12.4 ± 3.8
MRT_{0-t} (h)	11.6 ± 1.2	12.6 ± 0.8	13.8 ± 2.1	15.0 ± 1.4	16.6 ± 2.7	17.1 ± 2.5
CL/F (L/h)	3.95 ± 0.65	4.02 ± 0.58	4.23 ± 0.65	3.60 ± 0.35	3.54 ± 0.29	3.04 ± 0.50
Vd (L)	52.9 ± 11.5	56.7 ± 6.4	57.2 ± 7.2	54.2 ± 7.3	63.1 ± 13.6	53.0 ± 11.4
Ae_{0-72} (mg)	1.29 ± 0.13	2.97 ± 0.30	5.34 ± 0.79	8.88 ± 1.45	15.80 ± 1.28	17.70 ± 2.09

[a]Median (minimum, maximum).

Pharmacokinetic and statistical analyses

The primary PK parameters and plasma concentration-time profiles of WXFL10203614 in the single-dose study are shown in Table 2 and Figure 2, respectively. WXFL10203614 was absorbed rapidly following single doses of 2–33 mg under fasted conditions and the median T_{max} was 0.48–0.98 h. CL/F ranged from 3.04 to 4.23 L/h, Vd was 52.9–63.1 L, $t_{1/2}$ was 9.2–12.4 h, and MRT_{0-t} was 11.6–17.1 h which was slightly prolonged with the increasing doses of WXFL10203614. C_{max}, AUC_{0-t} and $AUC_{0-\infty}$ were all increased across the dose range. However, the results of statistical analyses showed that the 90% CIs for the slopes of the log-transformed C_{max}, AUC_{0-t} and $AUC_{0-\infty}$ were not wholly contained within the acceptance range of 0.92–1.08 (C_{max}: 0.87–1.01, AUC_{0-t}:1.04–1.12 and $AUC_{0-\infty}$:1.04–1.12), it was inconclusive that PK parameters were proportional to dose within the dose range (Smith et al., 2000). In addition, Ae_{0-72} ranged from 1.29 to 17.70 mg almost reaching the plateau of total cumulative urinary excretion and exceeding 50% of the administered dose in each group (Table 2 and Figure 3), suggesting that renal excretion was the main excretion route of WXFL10203614.

Table 3 and Figure 4 shows PK parameters and plasma concentration-time profiles in the multiple-dose study. Similar to the single-dose study, WXFL10203614 rapidly reached peak concentrations (median T_{max} was 0.48–0.88 h) on day 1 following 5–10 mg QD WXFL10203614, the median $T_{max, ss}$ and $t_{1/2}$ was 0.73–1.23 h and 9.2–12.0 h on day 7, while CL_{ss}/F

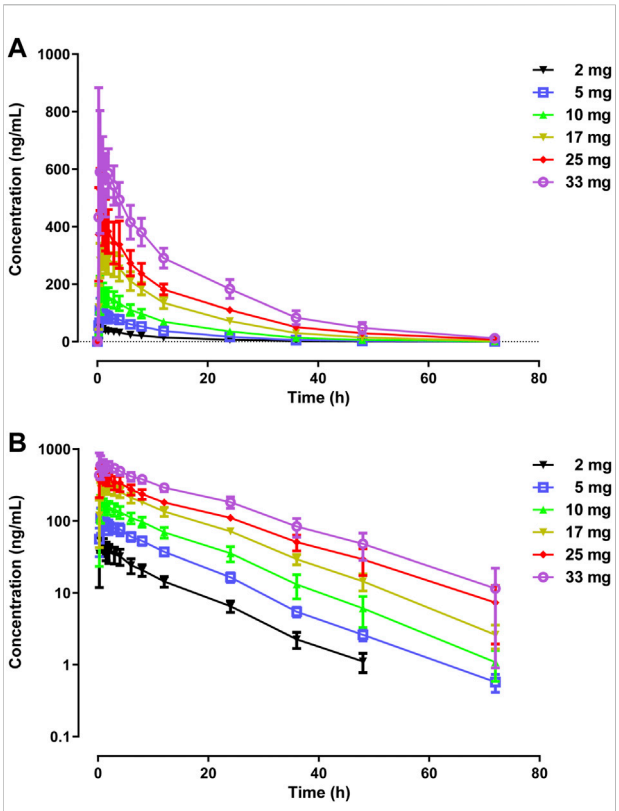

FIGURE 2
Mean plasma concentrations *versus* time profiles following a single dose of WXFL10203614 (2–33 mg) in healthy Chinese subjects on linear **(A)** and semilogarithmic scales **(B)**.

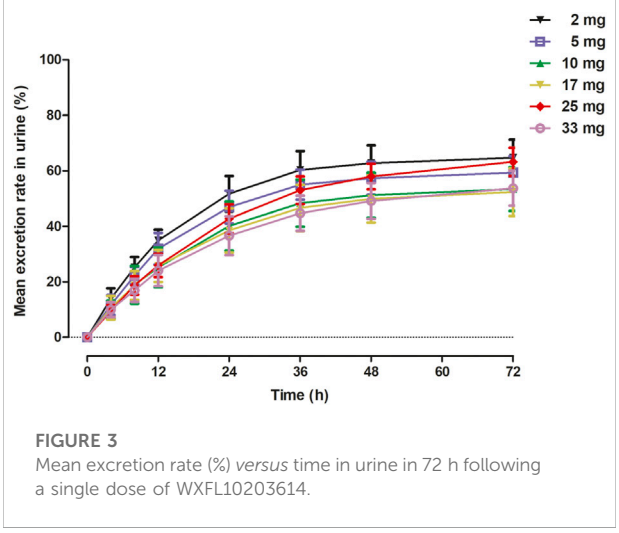

FIGURE 3
Mean excretion rate (%) *versus* time in urine in 72 h following a single dose of WXFL10203614.

remained constant (3.6 L/h) regardless of the dose. Steady-state trough concentrations were 26.2 ± 11.8, 25.5 ± 13.4 and 25.6 ± 13.4 ng/ml for 5 mg QD WXFL10203614, as well as 59.3 ± 15.5, 58.8 ± 17.9 and 58.9 ± 19.4 ng/ml for 10 mg QD WXFL10203614 in day 5, 6 and 7 mornings, indicating that the steady state of WXFL10203614 in plasma has been reached after multiple doses. $AUC_{0-t,ss}$ and $C_{max,ss}$ were increased with the dose ranging from 5 to 10 mg. Ra (AUC) and Ra (C_{max}) were 1.17–1.34 and 1.14–1.37, respectively. In the 5 mg BID group, Steady-state trough concentrations of WXFL10203614 in 3 days were 97.5 ± 12.6, 96.5 ± 13.9 and 95.8 ± 14.9 ng/ml, which confirmed the steady-state trough concentration was stable. The median $T_{max,\ ss}$ was 0.48 h and $t_{1/2}$ was 11.1 h, Ra (AUC) and Ra (C_{max}) were 2.17 ± 0.15 and 1.85 ± 0.21, indicating that the obvious accumulation might occur following multiple doses of 5 mg BID WXFL10203614.

Safety analysis

The numbers and percentages of subjects who experienced AEs are summarized in Tables 4, 5.

In the single-dose study, 58 AEs occurred in 28 (73.7%) of the 38 subjects who received 1–33 mg WXFL10203614. The most common AEs included polyuria (11/28.9%), the proportion of neutrophils decreased (9/23.7%), fecal occult blood (positive for transferrin) (7/18.4%), neutrophil counts decreased (6/15.8%), white blood cell count decreased (3/8.0%) and creatinine increased (3/8.0%), all deemed related to WXFL10203614 before unblinding. 20 AEs were reported in 8 (66.7%) of the 12 subjects who received placebo, mainly including white blood cell count decreased (3/25.0%), polyuria (3/25.0%) and fecal occult blood (positive for transferrin) (2/16.7%). All AEs were mild or moderate and resolved spontaneously.

In the multiple-dose study, 28 AEs occurred in 11 (68.8%) of the 16 subjects in the 5 and 10 mg QD groups. The most frequency AEs were polyuria (8/50.0%), fecal occult blood (positive for transferrin) (5/31.3%), creatinine increased (3/18.8%), mucositis oral (3/18.8%) and the proportion of neutrophils decreased (3/18.8%), respectively. Meanwhile, 21 AEs occurred in all subjects (8/100%) who received 5 mg BID WXFL10203614, mainly including polyuria (8/100%), fecal occult blood (positive for transferrin) (2/25.0%) and constipation (2/25.0%). All AEs were considered to be related to WXFL10203614 before unblinding. However, 15 AEs occurred in the placebo group (6/100%), which was similar to WXFL10203614 groups, such as polyuria (4/66.7%), mucositis oral (3/50.0%), fecal occult blood (positive for transferrin) (2/33.3%). All AEs were mild and subsided without treatment.

There were no AEs, Serious Adverse Events (SAEs) or deaths leading to withdrawal from the single- and multiple-dose study. All AEs were reported to the Ethics Committee of Wuxi people's hospital.

TABLE 3 The primary pharmacokinetic parameters of WXFL10203614 on day 1 and 7 in the multiple-dose study.

	Parameter	5 mg QD (N = 8)	10 mg QD (N = 8)	5 mg BID (N = 8)
Day 1	C_{max} (ng/ml)	126.0 ± 16.8	216.0 ± 86.6	124.0 ± 24.6
	T_{max} (h)[a]	0.48 (0.48–1.00)	0.88 (0.48–3.98)	0.50 (0.48–1.48)
	AUC_{0-12} (h•ng/ml)	886 ± 132	1500 ± 397	753 ± 88
	AUC_{0-24} (h•ng/ml)	1260 ± 218	2,210 ± 489	1060 ± 125
Day7	$C_{max, ss}$ (ng/ml)	143.0 ± 42.0	264.0 ± 72.8	226.0 ± 36.1
	$T_{max, ss}$ (h)[a]	1.23 (0.50–1.98)	0.73 (0.48–1.48)	0.48 (0.48–0.50)
	$AUC_{0-12, ss}$ (h•ng/ml)	1080 ± 319	1960 ± 400	1640 ± 255
	$AUC_{0-24, ss}$ (h•ng/ml)	1500 ± 500	2,920 ± 602	2,400 ± 402
	$AUC_{0-t, ss}$ (h•ng/ml)	1750 ± 651	3,620 ± 936	2,950 ± 549
	$AUC_{0-\infty, ss}$ (h•ng/ml)	1810 ± 711	3,940 ± 1080	3,110 ± 618
	$t_{1/2}$ (h)	9.2 ± 1.6	12.0 ± 2.6	11.1 ± 1.1
	CLss/F (L/h)	3.6 ± 1.0	3.6 ± 0.8	3.1 ± 0.5
	Ra (AUC)	1.17 ± 0.20	1.34 ± 0.22	2.17 ± 0.15
	Ra (C_{max})	1.14 ± 0.31	1.37 ± 0.51	1.85 ± 0.21

[a]Median (minimum, maximum).

Discussion

As far as we know, none of the domestically produced JAK1 inhibitors are marketed in China. It is the first-in-human clinical trial of WXFL10203614, a potent and selective JAK1 inhibitor, conducted in healthy Chinese subjects. The study showed that WXFL10203614 was well-tolerated after a single dose and multiple doses. The most frequent AEs were polyuria, the proportion of neutrophils decreased, fecal occult blood (positive for transferrin), neutrophil count decreased, white blood cell count decreased and creatinine increased, most of which were more common with the higher doses, and have previously been reported in healthy subjects or patients treated with JAK inhibitors (Shi et al., 2014; Taylor et al., 2017; Li et al., 2022). As for polyuria and fecal occult blood (positive for transferrin), they were not reported in JAK inhibitor before and the incidence was not associated with the increasing dose of WXFL10203614. Meanwhile, they were also found in the placebo group. Therefore, the exact reason is unclear yet, which might be related to personal water-drinking habits and diet, and should be explored and paid more attention in future studies. All AEs were mild to moderate without treatment. No SAEs, deaths or clinically significant changes in laboratory tests were observed. Only 1 subject in the 10 mg QD group was discontinued on day 8 for personal reasons.

WXFL10203614 was absorbed rapidly after single dosing with the median T_{max} of 0.48–0.98 h, which was in accordance with the PK profiles of JAK1 inhibitors (Krishnaswami et al., 2015; Peeva et al., 2018; Gao et al., 2022), whereas the elimination rate was slightly slow and $t_{1/2}$ was 9.2–12.4 h. Moreover, MRT_{0-t} was gradually prolonged from 11.6 to 17.1 h with the increase of dose, indicating that there might be a trend of saturable distribution and/or elimination of WXFL10203614. Although PK parameters ($C_{max,}$ AUC_{0-t} and $AUC_{0-\infty}$) were elevated in a dose-related manner, the conclusion of an obvious linear correlation could not be made yet. Renal excretion was proved to be the main excretion route of WXFL10203614. The slow elimination of WXFL10203614 might increase AEs caused by drug accumulation when multiple doses were given consecutively. The kidney was the main route of WXFL10203614 excretion, and chronic kidney disease was reported in 10.4% of RA patients before and 89.6% of RA patients after treatment (Fayed et al., 2019). Thus, more attention should be paid to renal function in clinical trials.

In the multiple-dose study, steady-state trough concentrations of WXFL10203614 had achieved after once daily or twice daily dosing for 5 consecutive days. Steady-state PK parameters were also elevated with increasing of the once-daily dose, and $AUC_{0-t, ss}$ and $C_{max, ss}$ in the 10 mg QD group were higher than those in the 5 mg BID group, though the daily dose was the same. In addition, non- and weak accumulations of WXFL10203614 *in vivo* were observed in the 5 and 10 mg QD groups while moderate accumulation in the 5 mg BID group, which were assessed by the calculation method for Ra. The crucial values for non-, weak, moderate, and strong accumulation can be set at $Ra < 1.2$, $1.2 \leq Ra < 2$, $2 \leq Ra < 5$ and $Ra \geq 5$, respectively (Li et al., 2013). RA treatment is a long-term process, the twice-daily regimen may cause drug accumulation of WXFL10203614 *in vivo*, resulting in severe adverse reactions. Thus, the once-daily regimen could be a

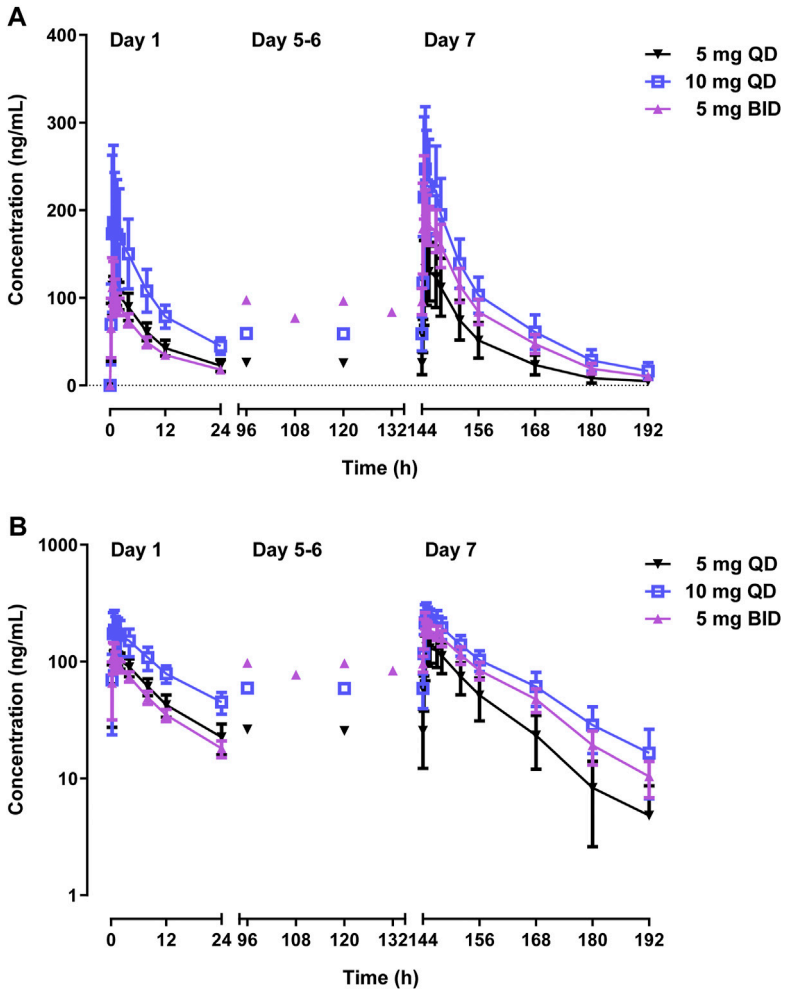

FIGURE 4
Mean plasma concentrations *versus* time profiles following multiple doses of WXFL10203614 (5 mg QD, 10 mg QD and 5 mg BID) in healthy Chinese subjects on linear **(A)** and semilogarithmic scales **(B)**.

safer and better way for patients with RA to avoid drug accumulation.

As a first-in-human clinical trial, the oral doses of WXFL10203614 were based on the no observed adverse effect levels (NOAELs) originating from the long-term toxicological studies of WXFL10203614 conducted in Sprague Dawley rats and beagle dogs (2 and 6 mg/kg). The NOAELs were finally converted to human equivalent doses (HEDs) according to the guidelines issued by US Food and Drug Administration (US Department of Health and Human ServicesFood and Drug AdministrationCenter for Drug Evaluation and Research, 2005). The safety factor was selected as 20 to decrease the possible risk of WXFL10203614. The maximum starting dose (MRSD) was obtained by dividing the HED by the safety factor. Consequently, 1 mg was calculated as MRSD given to healthy subjects weighing 60 kg. Additionally, in an efficacy study conducted in the rat model of arthritis, the minimal effective dose (MED) of WXFL10203614 was 1 mg/kg converted to HED of 21.5 mg, and the final estimated MRSD was 1.1 mg. To sum up, the starting dose of WXFL10203614 was set at 1 mg, and dose increments were 1, 2, 5, 10, 17, 25 and 33 mg, which was designed according to the modified Fibonacci method and the specifications of WXFL10203614 (1 mg per tablet and 5 mg per tablet) (Simon et al., 1997). The increments of dose for succeeding levels were 100%, 150%, 100%, 70%, 47% and 32%.

Once-daily and twice-daily treatment regimens are two options for treating RA. According to the results of the preclinical pharmacodynamics studies of WXFL10203614, the efficacy of 3 mg/kg WXFL10203614 was equal to 5 mg/kg

TABLE 4 Summary of adverse events at each dose level in the single-dose study.

System organ class preferred term	1 mg (N = 2)	2 mg (N = 6)	5 mg (N = 6)	10 mg (N = 6)	17 mg (N = 6)	25 mg (N = 6)	33 mg (N = 6)	Placebo (N = 12)
Total adverse event (%)	1 (50.0)	2 (33.3)	5 (83.3)	4 (66.7)	5 (83.3)	5 (83.3)	6 (100.0)	8 (66.7)
Metabolism and nutrition disorders (%)								
Hypokalemia	0	0	0	0	0	0	0	1 (8.3)
Investigations (%)								
Fecal occult blood (positive for transferrin)	0	1 (16.7)	2 (33.3)	1 (16.7)	0	1 (16.7)	2 (33.3)	2 (16.7)
Electrocardiogram ST segment abnormal	0	0	2 (33.3)	0	0	0	0	0
Erythrocyte sedimentation rate elevated	1 (50.0)	0	0	0	0	0	0	0
White blood cell count decreased	0	0	1 (16.7)	0	0	0	2 (33.3)	3 (25.0)
Neutrophil count decreased	0	0	1 (16.7)	0	1 (16.7)	2 (33.3)	2 (33.3)	1 (8.3)
The proportion of neutrophils decreased	0	0	0	0	0	4 (66.7)	5 (83.3)	0
Alanine aminotransferase increased	0	0	0	0	0	1 (16.7)	0	0
Triiodothyronine decreased	0	0	0	0	0	0	1 (16.7)	0
Thyroid stimulating hormone elevated	0	0	0	0	0	0	1 (16.7)	0
Fibrinogen decreased	0	0	0	0	0	0	1 (16.7)	1 (8.3)
Glomerular filtration rate decreased	0	0	0	0	0	0	0	1 (8.3)
Creatinine increased	0	0	0	0	3 (50.0)	0	0	1 (8.3)
Positive for urine protein	0	0	0	0	0	0	1 (16.7)	0
Gastrointestinal disorders (%)								
Dental ulcer	0	0	1 (16.7)	0	0	0	0	1 (8.3)
Nausea	0	1 (16.7)	0	0	0	0	0	0
Renal and urinary disorders (%)								
Polyuria	0	0	2 (33.3)	3 (50.0)	4 (66.7)	0	2 (33.3)	3 (25.0)
Blood and lymphatic system disorders (%)								
Anemia	0	0	1 (16.7)	0	0	0	0	0
Infections and infestations (%)								
Bacterial tonsillitis	0	0	0	0	0	0	1 (16.7)	0

tofacitinib in the rat model of RA, and the steady plasma concentration of tofacitinib with the therapeutic dose of 5 mg BID. It is speculated that when WXFL10203614 achieved the same clinical efficacy as tofacitinib, the steady-state peak concentration and steady-state exposure should reach 39.23 ng/ml and 287.90 ng*h/mL, respectively. PK model of WXFL10203614 after multiple dosing developed by WinNonlin software which predicted that administration of 5 mg QD, 10 mg QD, 5 mg BID or 10 mg BID WXFL10203614 for 7 consecutive days could achieve this PK profile. Thus, 5 mg QD, 10 mg QD, 5 mg BID and 10 mg BID were chosen as the administration dosages in the multiple-dose study. However, due to the drug accumulation (Ra: 2.17 ± 0.15) of the 5 mg twice-daily regimen, the 10 mg BID study was not performed.

The present study will help to optimize the WXFL10203614 dosing regimen for the phaseⅡstudy of WXFL10203614 in patients with moderate to severe active RA (Registration Number: CTR20202,463), and the drug-drug interaction (DDI) of WXFL10203614 with methotrexate in patients with RA (Registration Number: CTR20212,562) to evaluate the efficacy, safety and DDI of WXFL10203614 better.

Conclusion

WXFL10203614, the potential selective JAK1 inhibitor, was well-tolerated and safe in healthy Chinese subjects, and plasma exposure increased in a dose-related manner after

TABLE 5 Summary of adverse events at each dose level in the multiple-dose study.

System organ class preferred term	5 mg QD (N = 8)	10 mg QD (N = 8)	5 mg BID (N = 8)	Placebo (N = 6)
Total adverse event (%)	6 (75.0)	5 (62.5)	8 (100)	6 (100)
Investigations (%)				
Fecal occult blood (positive for transferrin)	4 (50.0)	1 (12.5)	2 (25.0)	2 (33.3)
The proportion of neutrophils decreased	0	3 (37.5)	1 (12.5)	0
Creatinine increased	2 (25.0)	1 (12.5)	1 (12.5)	0
Positive for urine protein	0	1 (12.5)	0	0
Nervous system disorders (%)	1 (12.5)	0	0	0
Dizziness	1 (12.5)	0	0	0
Gastrointestinal disorders (%)				
Mucositis oral	0	3 (37.5)	0	3 (50.0)
Dry mouth	0	1 (12.5)	0	0
Constipation	0	0	2 (25.0)	1 (16.7)
Renal and urinary disorders (%)				
Polyuria	4 (50.0)	4 (50.0)	8 (100)	4 (66.7)
Infections and infestations (%)				
Pharyngitis	0	1 (12.5)	0	0
Bacterial tonsillitis	1 (12.5)	0	0	0
Respiratory, thoracic and mediastinal disorders (%)				
Epistaxis	0	0	0	1 (16.7)

QD: once daily, BID: twice daily.

single-dose and once-daily administration, supporting further evaluation of WXFL10203614 in patients with RA.

Data availability statement

The original contributions presented in the study are included in the article/Supplementary Material, further inquiries can be directed to the corresponding author.

Ethics statement

The studies involving human participants were reviewed and approved by the Ethics Committee of Wuxi people's hospital. The patients/participants provided their written informed consent to participate in this study.

Author contributions

KH, ZZ, JX, and QH designed this experiment. KH, YD, LQ, NC, YS, ZQ, WQ, YC, XG, and JW performed this clinic trial. KH and ZQ analyzed the data. KH and YD wrote and edited the paper, and drew the figures.

Funding

This work was supported by the Wuxi Public Service Platform for Clinical Research and Evaluation of New Drugs and Medical Devices (GGFWPT 2019) and Wuxi Fuxin Pharmaceutical Research and Development Co., Ltd., Wuxi, China.

Conflict of interest

Authors ZZ and JX were employed by Wuxi Fuxin Pharmaceutical Research and Development Co, Ltd.

The remaining authors declare that the research was conducted in the absence of any commercial or financial relationships that could be construed as a potential conflict of interest.

Publisher's note

References

Alqarni, A. M., and Zeidler, M. P. (2020). How does methotrexate work? *Biochem. Soc. Trans.* 48, 559–567. doi:10.1042/BST20190803

Broxmeyer, H. E. (2013). Erythropoietin: Multiple targets, actions, and modifying influences for biological and clinical consideration. *J. Exp. Med.* 210, 205–208. doi:10.1084/jem.20122760

Choy, E. H. (2019). Clinical significance of Janus Kinase inhibitor selectivity. *Rheumatol. Oxf.* 58, 953–962. doi:10.1093/rheumatology/key339

Fayed, A., Shaker, A., Hamza, W. M., and Wadie, M. (2019). Spectrum of glomerulonephritis in Egyptian patients with rheumatoid arthritis: A university hospital experience. *Saudi J. Kidney Dis. Transpl.* 30, 803–811. doi:10.4103/1319-2442.265455

Gao, X., He, X., Oshima, H., Miyatake, D., Otsuka, Y., Kato, K., et al. (2022). Pharmacokinetics and safety of single and multiple doses of peficitinib (ASP015K) in healthy Chinese subjects. *Drug Des. devel. Ther.* 16, 1365–1381. doi:10.2147/DDDT.S359501

Kaneko, Y. (2020). Efficacy and safety of peficitinib in rheumatoid arthritis. *Mod. Rheumatol.* 30, 773–778. doi:10.1080/14397595.2020.1794103

Kotenko, S. V., and Pestka, S. (2000). Jak-Stat signal transduction pathway through the eyes of cytokine class II receptor complexes. *Oncogene* 19, 2557–2565. doi:10.1038/sj.onc.1203524

Krishnaswami, S., Boy, M., Chow, V., and Chan, G. (2015). Safety, tolerability, and pharmacokinetics of single oral doses of tofacitinib, a Janus kinase inhibitor, in healthy volunteers. *Clin. Pharmacol. Drug Dev.* 4, 83–88. doi:10.1002/cpdd.171

Li, L., Li, X., Xu, L., Sheng, Y., Huang, J., and Zheng, Q. (2013). Systematic evaluation of dose accumulation studies in clinical pharmacokinetics. *Curr. Drug Metab.* 14, 605–615. doi:10.2174/13892002113149990002

Li, N., Du, S., Wang, Y., Zhu, X., Shu, S., Men, Y., et al. (2022). Randomized, double-blinded, placebo-controlled phase I study of the pharmacokinetics, pharmacodynamics, and safety of KL130008, a novel oral JAK inhibitor, in healthy subjects. *Eur. J. Pharm. Sci.* 176, 106257. doi:10.1016/j.ejps.2022.106257

Li, Z., Xu, M., Li, R., Zhu, Z., Liu, Y., Du, Z., et al. (2020). Identification of biomarkers associated with synovitis in rheumatoid arthritis by bioinformatics analyses. *Biosci. Rep.* 40, BSR20201713. doi:10.1042/BSR20201713

Lin, Y. J., Anzaghe, M., and Schülke, S. (2020). Update on the pathomechanism, diagnosis, and treatment options for rheumatoid arthritis. *Cells* 9, 880. doi:10.3390/cells9040880

Mohamed, M. F., Camp, H. S., Jiang, P., Padley, R. J., Asatryan, A., and Othman, A. A. (2016). Pharmacokinetics, safety and tolerability of ABT-494, a novel selective JAK 1 inhibitor, in healthy volunteers and subjects with rheumatoid arthritis. *Clin. Pharmacokinet.* 55, 1547–1558. doi:10.1007/s40262-016-0419-y

Norman, P. (2014). Selective JAK inhibitors in development for rheumatoid arthritis. *Expert Opin. Investig. Drugs* 23, 1067–1077. doi:10.1517/13543784.2014.918604

Peeva, E., Hodge, M. R., Kieras, E., Vazquez, M. L., Goteti, K., Tarabar, S. G., et al. (2018). Evaluation of a Janus kinase 1 inhibitor, PF-04965842, in healthy subjects: A phase 1, randomized, placebo-controlled, dose-escalation study. *Br. J. Clin. Pharmacol.* 84, 1776–1788. doi:10.1111/bcp.13612

Shi, J. G., Chen, X., Lee, F., Emm, T., Scherle, P. A., Lo, Y., et al. (2014). The pharmacokinetics, pharmacodynamics, and safety of baricitinib, an oral JAK 1/2 inhibitor, in healthy volunteers. *J. Clin. Pharmacol.* 54, 1354–1361. doi:10.1002/jcph.354

Simon, R., Freidlin, B., Rubinstein, L., Arbuck, S. G., Collins, J., and Christian, M. C. (1997). Accelerated titration designs for phase I clinical trials in oncology. *J. Natl. Cancer Inst.* 89, 1138–1147. doi:10.1093/jnci/89.15.1138

Smith, B. P., Vandenhende, F. R., DeSante, K. A., FaridM, N. A., Welch, P. A., Callaghan, J. T., et al. (2000). Confidence interval criteria for assessment of dose proportionality. *Pharm. Res.* 17, 1278–1283. doi:10.1023/a:1026451721686

Sparks, J. A. (2019). Rheumatoid arthritis. *Rheum. Arthritis. Ann. Intern. Med.* 170, ITC1–ITC16. doi:10.7326/AITC201901010

Taylor, P. C., Keystone, E. C., van der Heijde, D., Weinblatt, M. E., Del Carmen Morales, L., Reyes Gonzaga, J., et al. (2017). Baricitinib versus placebo or adalimumab in rheumatoid arthritis. *N. Engl. J. Med.* 376, 652–662. doi:10.1056/NEJMoa1608345

US Department of Health and Human Services, Food and Drug Administration, Center for Drug Evaluation and Research (CDER) (2005). *Guidance for industry: Estimating the maximum safe starting dose in initial clinical trials for therapeutics in adult healthy volunteers.* .

Vazquez, M. L., Kaila, N., Strohbach, J. W., Trzupek, J. D., Brown, M. F., Flanagan, M. E., et al. (2018). Identification of N-{cis-3-[Methyl(7H-pyrrolo[2, 3-d] pyrimidin-4-yl)amino] cyclobutyl}propane-1-sulfonamide (PF-04965842): A selective JAK1 clinical candidate for the treatment of autoimmune diseases. *J. Med. Chem.* 61, 1130–1152. doi:10.1021/acs.jmedchem.7b01598

Xie, S., Li, S., Tian, J., and Li, F. (2020). Iguratimod as a New drug for rheumatoid arthritis: Current landscape. *Front. Pharmacol.* 11, 73. doi:10.3389/fphar.2020.00073

You, H., Xu, D., Zhao, J., Li, J., Wang, Q., Tian, X., et al. (2020). JAK inhibitors: Prospects in connective tissue diseases. *Clin. Rev. Allergy Immunol.* 59, 334–351. doi:10.1007/s12016-020-08786-6

frontiers | Frontiers in Pharmacology

TYPE Clinical Trial
PUBLISHED 24 November 2022
DOI 10.3389/fphar.2022.1066895

OPEN ACCESS

EDITED BY
Zhihao Liu,
Dalian Medical University, China

REVIEWED BY
Runbin Sun,
Nanjing Drum Tower Hospital, China
Xiangmeng Wu,
University of Arizona, United States

*CORRESPONDENCE
Qing He,
heqing0510@163.com

†These authors have contributed equally to this work and share first authorship

SPECIALTY SECTION
This article was submitted to Drug Metabolism and Transport, a section of the journal Frontiers in Pharmacology

RECEIVED 11 October 2022
ACCEPTED 15 November 2022
PUBLISHED 24 November 2022

CITATION
Huang K, Shi Y, Chu N, Que L, Ding Y, Qian Z, Qin W, Gu X, Wang J, Zhang Z, Xu J and He Q (2022), The effect of food on the pharmacokinetics of WXFL10203614, a potential selective JAK1 inhibitor, in healthy Chinese subjects.
Front. Pharmacol. 13:1066895.
doi: 10.3389/fphar.2022.1066895

The effect of food on the pharmacokinetics of WXFL10203614, a potential selective JAK1 inhibitor, in healthy Chinese subjects

Kai Huang[1†], Yunfei Shi[1†], Nannan Chu[1], Linling Que[1], Ying Ding[1], Zhenzhong Qian[1], Wei Qin[1], Xianghong Gu[1], Jiakun Wang[1], Zhiwei Zhang[2], Jianguo Xu[2] and Qing He[1*]

[1]Drug Clinical Trial Institution, Affiliated Wuxi People's Hospital of Nanjing Medical University, Wuxi, China, [2]Wuxi Fuxin Pharmaceutical Research and Development Co., Ltd., Wuxi, China

Objective: This study was performed to investigate the effect of food on the pharmacokinetics (PK) of WXFL10203614 in healthy Chinese subjects.

Methods: This was a randomized, open-label, single-dose, two-treatment (fed vs fasted), two-period, two-sequence, crossover study. 14 eligible subjects were averagely randomized into 2 sequences and then received 10 mg WXFL10203614 under fasted or fed condition. In each period, the blood samples were collected from 0 h (pre-dose) and serially up to 72 h post-dose, and plasma concentrations were detected using the high-performance liquid chromatography-tandem mass spectrometry (HPLC-MS/MS) method. The effect of food on the PK profile and safety of WXFL10203614 were assessed.

Results: 70 subjects were screened, and 14 subjects (10 male and 4 female) were enrolled and completed the study. Under the fasted condition, WXFL10203614 was absorbed rapidly with a T_{max} of 0.98 h. The absorption rate was slower, T_{max} delayed by 2.98 h, and the C_{max} decreased by 16.3% when WXFL10203614 administered after the high-fat and high-calorie diet, other PK parameters were not affected. The 90% confidence intervals (CIs) for the ratio (fed/fasted) of geometric means of the C_{max}, AUC_{0-t} and $AUC_{0-\infty}$ were 0.73–1.01, 0.90–1.03 and 0.90–1.03, indicating that the high-fat and high-calorie diet might impact the absorption process of WXFL10203614. Although the C_{max} was slightly decreased, there was no significant difference in the C_{max} under fasted and fed conditions. Thus, it was not considered clinically significant owing to the small magnitude of changes in C_{max}. All Treatment-emergent adverse events (TEAEs) were mild and resolved spontaneously without treatment.

Conclusion: Food had no clinically relevant effects on drug system exposure of WXFL10203614. It was well tolerated under fasted and fed conditions in healthy Chinese subjects, so WXFL10203614 could be administered orally with or without food.

Clinical Trial Registration: http://www.chinadrugtrials.org.cn/index.html, identifier CTR20191636.

KEYWORDS

WXFL10203614, pharmacokinetics, JAK1 inhibitor, rheumatoid arthritis, absorption

Introduction

Rheumatoid arthritis (RA) is an autoimmune disease associated with chronic and painful joint inflammation, which gradually causes joint synovitis, bone erosion, progressive cartilage destruction, and even physical disability (Sparks, 2019). However, the exact pathogenesis of RA is unknown (Li et al., 2020). It has been reported that Janus kinase (JAK)/signal transducers and activators of transcription (STAT) signal pathway was closely related to various inflammatory cytokines exerting and integrating their functions in inflammatory diseases, such as RA (Fragoulis et al., 2019). As the key initiators of the JAK/STAT signal pathway, JAK was increasingly regarded as one of the critical factors in the pathogenesis of RA (Crispino et al., 2021). Therefore, inhibiting the JAK/STAT signal pathway with specific JAK inhibitors is a new therapeutic option for RA.

WXFL10203614, a potential selective JAK1 inhibitor, is being developed for RA treatment. At present, WXFL10203614 has entered Phase III clinical trial stage. As a part of the new drug application, assessing the effects of food on oral drugs was strongly recommended by guidelines (EMA, 2012; NMPA, 2021; USFDA, 2022). Food-drug interaction was often associated with changes in drug pharmacokinetics (PK), which inadvertently affected the drug effect. However, the reasons for food-drug interaction were complicated, such as the chelation of drug with components in food, the direct interactions between drug and food, delayed gastric emptying, gastric acid or bile secretion increased, and food-induced increase in drug solubility, etc. (Singh, 1999; Schmidt et al., 2002; EMA, 2012). This interaction would result in decreased, delayed, increased or accelerated drug absorption. Therefore, food-drug interaction, on the one hand, might cause a high risk of treatment failure due to a remarkably reduced systemic drug exposure. On the other hand, it might obtain the desired pharmacological effect but with severe toxicity (Schmidt et al., 2002). Great importance should be attached to this issue in the process of developing a new drug.

Although the effects of food on the PK profiles of JAK inhibitors have been reported previously, the consequences were not completely consistent. The C_{max} of INCB018424, filgotinib and upadacitinib was partly reduced by food which had little effect on AUC (Shi et al., 2011; Mohamed et al., 2017; Anderson et al., 2019). In contrast, the C_{max} of tofacitinib and peficitinib was elevated to different degrees under the fed state (Lamba et al., 2016; Shibata et al., 2021). However, it is not yet clear whether food interferes with the PK profile of WXFL10203614.

This study was conducted on healthy Chinese subjects to assess the effect of the high-calorie and high-fat diet on the PK profile of WXFL10203614. Meanwhile, safety was also evaluated.

Methods

Subjects

Healthy Chinese subjects, 18–45 years old, with body weight ≥50 for males and ≥45 kg for females, and body mass index (BMI) ranging from 19.0 to 26.0 kg/m^2 were enrolled. Meanwhile, they were assessed as healthy by vital signs, physical examination, medical history, laboratory tests, abdominal ultrasound, chest X-ray and electrocardiograph (ECG). Subjects could not participate if they were confirmed to meet one of the exclusion criteria as follow: 1) the history of the cardiovascular, nervous, respiratory, digestive or other systems, 2) allergic constitution or severe allergies to any medicine or food, 3) abnormal ECG, such as QTc interval ≥450 ms, PR interval ≥210 ms or QRS ≥120 ms, 4) severe infection, 5) the positive result for hepatitis B surface antigen, hepatitis C antibody, human immunodeficiency virus (HIV) antibody or treponema pallidum antibody, 6) medicine taken within 1 month before screening (including vitamins, herbal products and dietary supplements), 7) the positive result for the urine drug test, urine nicotine test or breath alcohol test, 8) pregnant or lactating women, 9) participated in any clinical trial in the past 3 months, 10) any clinically significant abnormal findings judged by investigators, 11) other special situations confirmed by investigators for exclusion.

Study design

This randomized, open-label, single-dose, two-treatment (fed vs fasted), two-period, two-sequence, crossover study was conducted on healthy Chinese subjects to evaluate the effect of food on the PK profile of WXFL10203614. The study was approved by National Medical Products Administration (NMPA) (Chinese Clinical Trial Registry, http://www.chinadrugtrials.org.cn/index.html, Registration Number: CTR20191636) and carried out on the basis of Good Clinical Practice guidelines and the ethical principle of the Declaration of Helsinki. The final protocol and informed consent form were reviewed and permitted by the ethics committee of the Affiliated

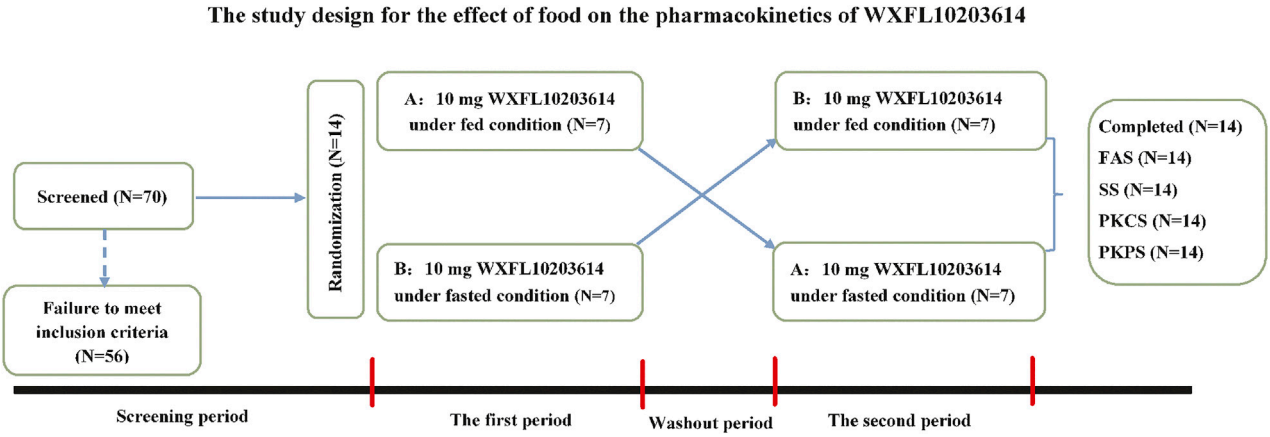

FIGURE 1
The study design for the effect of food on the pharmacokinetics of WXFL10203614. FAS, The Full Analysis Set; SS, Safety set; PKCS, Pharmacokinetic concentration set; PKPS, Pharmacokinetic parameter set.

Wuxi People's Hospital of Nanjing Medical University (Approval Number: 2019LLPJ-I-24). All subjects were fully informed of the study procedures, objectives, basic information and potential risks of the investigational drug and provided written informed consent before enrollment.

This two-period clinical trial was conducted in the Phase I center of Wuxi people's hospital from August to September 2019. 14 subjects were randomly allocated into sequence A and sequence B in a 1:1 ratio, and then received a single oral dose of 10 mg WXFL10203614 (5 mg*2 tablets, Lot Number: XS180902C) with 240 ml water under fasted or fed condition with the high-fat and high-calorie diet (800–1000 calories with 150 calories from protein, 250 calories from carbohydrates and 400–600 calories from fat) (USFDA, 2022). Among them, 7 subjects in sequence A received 10 mg WXFL10203614 with food in the first period and without food in the second period, the remaining 7 subjects in sequence B received 10 mg WXFL10203614 without food in the first period and with food in the second period. The protocol design was described in detail in Figure 1. All subjects fasted overnight for at least 10 h and ate up the meal within 30 min before dosing. Moreover, none of the subjects was permitted to drink water within 1 h before and after dosing or eat anything within 4 h after dosing. All subjects were allowed to leave the clinical center on Day 3 after dosing in each period, and the washout between the 2 periods was 7 days.

Pharmacokinetic assessment

In each period, 4 ml of blood samples were collected in EDTA-K_2 tubes at 15 time points: 0 (pre-dose), 0.25, 0.5, 1, 1.5, 2, 3, 4, 6, 8, 12, 24, 36, 48 and 72 h following oral administration of WXFL10203614. The plasma samples were obtained after centrifuging at 1500 g for 10 min at 4°C and then stored at -80°C until analysis.

Determination of plasma concentration of WXFL10203614

Samples were prepared by simple protein precipitation with acetonitrile. Briefly, 50 μL of internal standard (IS) solution (50 ng/ml $^{13}CD_3$-Target) and 300 μL of acetonitrile were added to 50 μL of the plasma sample. The mixture was vortexed for 15 min and then centrifuged at 2510 g for 15 min. The supernates were used to determine the WXFL10203614 concentration.

The validated high-performance liquid chromatography-tandem mass spectrometry (HPLC-MS/MS) method was used to determine the concentrations of WXFL10203614 in plasma (Huang et al., 2022). The HPLC-MS/MS system consisted of the UPLC 30A system (Shimadzu, Japan) and the AB SCIEX Triple Quad 5500 system with an electrospray ionization (ESI) source and Analyst 1.6.3 software (AB SCIEX, USA) for data acquisition and processing. Multiple reaction monitoring (MRM) transitions of WXFL10203614 and $^{13}CD_3$-Target (IS) were m/z 294.1→146.0 and 298.2→146.1 for quantification, respectively. Additionally, 1 μL sample was injected into a BEH C18 column (1.7 μm, 2.1 mm × 50 mm, Waters, USA) to chromatograph WXFL10203614 and IS with the gradient elution. The calibration of WXFL10203614 ranged from 0.4 to 500 ng/ml with the lower limit of quantitation (LLOQ) of 0.4 ng/ml. The accuracy of the assay was -4.2%–2.9%, and the precision was within the 6.1% coefficient of variation. Additionally, Samples were stable in blood for 2 h at room temperature and in plasma at 4°C for 17 h and -20°C and -80°C for 105 days. The 10-fold dilutions did not affect the accuracy and precision of the samples.

TABLE 1 Demographics and baseline characteristics of subjects.

Characteristic	Sequence A (N = 7)	Sequence B (N = 7)
Sex, N (%)		
Male	5 (71.4)	5 (71.4)
Female	2 (28.6)	2 (28.6)
Ethnicity (Han/other)	6/1	6/1
Age (years)	29.3 ± 5.8	25.3 ± 6.7
Height (cm)	165.0 ± 9.0	161.9 ± 7.5
Weight (kg)	61.7 ± 8.2	60.2 ± 9.7
BMI (kg/m^2)	22.6 ± 1.0	22.9 ± 2.2

N, number; BMI, body mass index. Data are presented as mean ± standard deviation unless otherwise indicated.

TABLE 2 The primary pharmacokinetic parameters of WXFL10203614 after dosing under fed and fasted conditions.

Parameter	Fed condition (N = 14)	Fasted condition (N = 14)
C_{max} (ng/ml)	170.0 ± 29.8	203.0 ± 55.3
T_{max} (h)	2.98 (0.23–3.98)	0.98 (0.48–3.98)
AUC_{0-t} (h·ng/mL)	2780 ± 453	2890 ± 467
$AUC_{0-\infty}$ (h·ng/mL)	2800 ± 459	2910 ± 474
$t_{1/2}$ (h)	10.2 ± 1.3	9.9 ± 1.2
MRT_{0-t} (h)	15.2 ± 1.6	14.8 ± 1.6
CL/F (L/h)	3.66 ± 0.61	3.53 ± 0.61

C_{max}, maximum concentration; T_{max}, time of maximum concentration; AUC_{0-t}, area under the plasma concentration-time curve from time 0 to the last measurable concentration; $AUC_{0-\infty}$, area under the plasma concentration-time curve from time 0 to infinity; $t_{1/2}$, terminal elimination half-life; MRT_{0-t}, mean residence time of 0 to the last measurable concentration and CL/F, apparent clearance rate. T_{max} is presented as median (minimum, maximum) and other data are presented as mean ± standard deviation.

Safety assessment

Treatment-emergent adverse events (TEAEs) were defined and graded according to the National Cancer Institute-Common Terminology Criteria for Adverse Events (NCI-CTCAE) (version 5.03). The severity, duration and clinical outcome of TEAEs and their association with WXFL10203614 were all evaluated. In addition, any clinically significant changes in physical examination, vital signs, laboratory tests as well as ECG were all included in the safety assessment.

Statistical analysis

Descriptive statistics were calculated for Pharmacokinetic (PK) parameters and demographical data. The primary PK parameters were maximum concentration (C_{max}), time of maximum concentration (T_{max}), area under the plasma concentration-time curve from time 0 to the last measurable concentration (AUC_{0-t}), area under the plasma concentration-time curve from time 0 to infinity ($AUC_{0-\infty}$), terminal elimination half-life ($t_{1/2}$), mean residence time of 0 to the last measurable concentration (MRT_{0-t}), and apparent clearance rate (CL/F) analyzed by the non-compartmental method with the WinNonlin software (version 8.2). The PK parameters were summarized descriptively. Variance analysis was used to compare the log-transformed PK parameters (C_{max}, AUC_{0-t} and $AUC_{0-\infty}$) between the fed and fasted treatment groups. If the 90% confidence intervals (CIs) for the ratio (fed/fasted) of geometric means of the C_{max}, AUC_{0-t} and $AUC_{0-\infty}$ fell within 0.80–1.25, confirming that food has no significant effect on the PK profile of WXFL10203614. Variance analysis and *t*-test for normally distributed data and Wilcoxon rank test for non-normally distributed data were used for data analysis. All statistical analyses were conducted with SAS software (version 9.4) and $p < 0.05$ was considered statistically significant.

Results

Demographic data of subjects

70 subjects were screened and 56 failed to meet the inclusion criteria. Finally, 14 eligible healthy subjects (10 male and 4 female) were randomized into 2 sequences to receive 10 mg WXFL10203614 orally under fed or fasted condition. All subjects completed the study and were included in the full analysis set

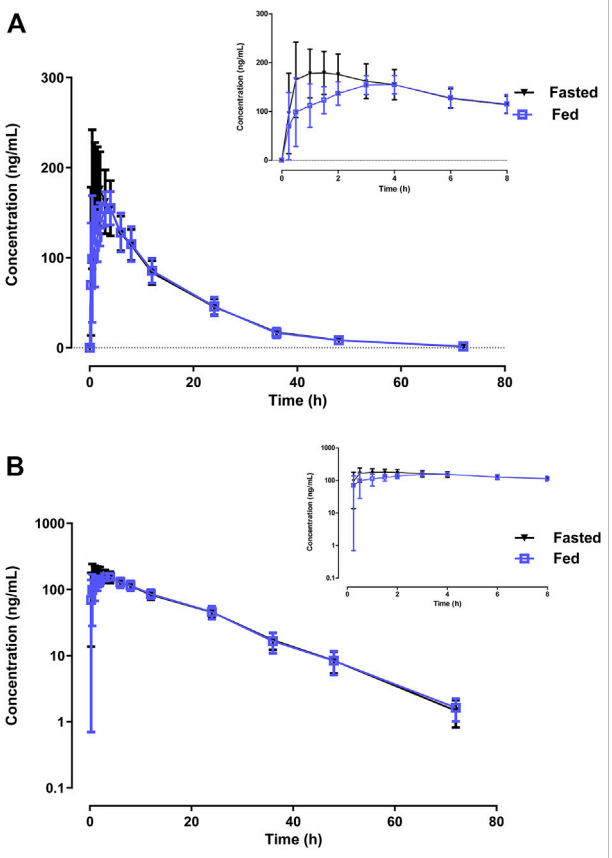

FIGURE 2
The linear **(A)** and semi-logarithmic **(B)** mean plasma concentrations-time profiles after a single dose of 10 mg WXFL10203614 under fed and fasted conditions. The data are expressed as mean ± standard deviation.

(FAS), safety set (SS), pharmacokinetic concentration set (PKCS) and pharmacokinetic parameter set (PKPS) (Figure 1). Baseline demographic characteristics were summarized in Table 1 using descriptive statistics. There were no significant differences in age, height, weight and BMI between the 2 groups.

Pharmacokinetic and statistical analyses

The effect of food on the primary PK parameters and mean plasma concentration-time profile of 10 mg WXFL10203614 were shown in Table 2 and Figure 2, respectively. Under the fasted condition, WXFL10203614 was absorbed rapidly with a median T_{max} of 0.98 h, but the absorption rate was delayed and T_{max} was 2.98 h, C_{max} was decreased by 16.3% after food intake (from 203.0 ± 55.3 ng/ml to 170.0 ± 29.8 ng/ml). Although the 90% CIs for the geometric mean ratios (GMRs) of the C_{max}, AUC_{0-t} and $AUC_{0-\infty}$ were 0.73–1.01, 0.90–1.03 and 0.90–1.03 (Table 3), confirming that the C_{max} was beyond the acceptable range of 0.80–1.25, there was no significant difference in these PK parameters (C_{max}, AUC_{0-t}, $AUC_{0-\infty}$, $t_{1/2}$, MRT_{0-t} and CL/F) between the 2 groups ($p > 0.05$). In view of the change in the C_{max} was slight, thus it was indicated that food intake delayed the absorption of WXFL10203614 to a certain extent, but did not significantly influence the PK profiles (C_{max}, AUC_{0-t} and $AUC_{0-\infty}$) of the WXFL10203614 under the fasted and fed conditions.

Safety analysis

10 mg WXFL10203614 was well-tolerated in the subjects. A total of 26 TEAEs occurred in 13 subjects (92.9%, 13/14) who received 10 mg WXFL10203614. 4 TEAEs reported in 2 subjects (14.3%, 2/14) were not associated with WXFL10203614 while 22 TEAEs reported in 12 subjects (85.7%, 12/14) were associated with WXFL10203614.

Under the fasted condition, 15 TEAEs occurred in 10 subjects (71.4%, 10/14) after dosing (Table 4), 14 TEAEs associated with WXFL10203614 occurred in 10 subjects (71.4%, 10/14), including polyuria (28.6%, 4/14), creatinine increased (21.4%, 3/14), fecal occult blood (positive for transferrin) (14.3%, 2/14), neutrophil count decreased (7.1%, 1/14), neutrophil count increased (7.1%, 1/14), white blood cell count increased (7.1%, 1/14) and fibrinogen decreased (7.1%, 1/14). 1 TEAE (soft tissue injury) was considered unrelated to WXFL10203614.

Under the fed condition, 11 TEAEs occurred in 8 subjects (57.1%, 8/14) after receiving WXFL10203614 (Table 4), 8 TEAEs associated with WXFL10203614 occurred in 7 subjects (50.0%, 7/14), including polyuria (21.4%, 3/14), creatinine increased (21.4%, 3/14), triglycerides increased (7.1%, 1/14) and fibrinogen decreased (7.1%, 1/14), 3 TEAEs were unassociated with WXFL10203614, including diarrhea (7.1%, 1/14) and fecal occult blood (positive for transferrin) (7.1%, 1/14), because NO.005 subject had diarrhea, the results of stool routine tests were abnormal twice.

All AEs were mild and resolved spontaneously without any special intervention. None of the subjects was discontinued from the study due to AEs. There were no serious adverse events (SAEs) or deaths reported. At the end of the study, the investigator collected related information on all AEs observed in this trial, such as the name, severity, duration and clinical outcome of AEs and their association with WXFL10203614. According to the requirements of the Ethics Committee of Wuxi people's hospital, these AEs should be reported within 3 months after the completion of the study. Finally, 26 AEs were submitted to the Ethics Committee as paper reports.

Discussion

It is the first clinical trial conducted on healthy Chinese subjects to investigate the food effect on the PK profile of WXFL10203614. Generally, the food effect on drug exposure

TABLE 3 Statistical comparison of primary pharmacokinetic parameters of WXFL10203614.

Parameter	Geometric mean		Fed/fasted ratio (%)	90% CI of the Fed/Fasted ratio	Intra-CV
	Fed condition (N = 14)	Fasted condition (N = 14)			
C_{max} (ng/ml)	167.3	195.2	85.7	0.73–1.01	0.250
AUC_{0-t} (h·ng/mL)	2741.8	2852.1	96.1	0.90–1.03	0.098
$AUC_{0-\infty}$ (h·ng/mL)	2767.8	2873.9	96.3	0.90–1.03	0.099

The acceptance range of 90% confidence interval is 0.80–1.25. C_{max}, maximum concentration; AUC_{0-t}, area under the plasma concentration-time curve from time 0 to the last measurable concentration; $AUC_{0-\infty}$, area under the plasma concentration-time curve from time 0 to infinity; CI, confidence interval; CV, coefficient of variation.

TABLE 4 Summary of treatment emergent adverse events.

System organ class preferred term	Fed condition (N = 14)	Fasted condition (N = 14)
Total TEAE n (%)	8 (57.1)	10 (71.4)
Investigations	6 (42.9)	7 (50.0)
Fecal occult blood (positive for transferrin)	1 (7.1)*	2 (14.3)
Neutrophil count decreased	0	1 (7.1)
Neutrophil count increased	0	1 (7.1)
White blood cell count increased	0	1 (7.1)
Triglycerides increased	1 (7.1)	0
Fibrinogen decreased	1 (7.1)	1 (7.1)
Creatinine increased	3 (21.4)	3 (21.4)
Renal and urinary disorders	3 (21.4)	4 (28.6)
Polyuria	3 (21.4)	4 (28.6)
Skin and subcutaneous tissue disorders	0	1 (7.1)
Soft tissue injury	0	1 (7.1)*
Gastrointestinal disorders	1 (7.1)	0
Diarrhea	1 (7.1)*	0

TEAT, treatment emergent adverse events; n, number of subjects; %, incidence of subjects reporting TEAEs. Data are reported as n (%). *: TEAEs were considered unrelated to the WXFL10203614.

depends mainly on the biopharmaceutical properties and formulation of the drug, which may affect its efficacy (Sun et al., 2019). For this reason, the effect of food on oral drug should be explored at the early stage of drug development to make the dose recommendation in Phase II and III studies (EMA, 2012). Thus, a randomized, open-label, single-dose, two-treatment (fed vs fasted), two-period, two-sequence, crossover study was designed in Phase I clinical trial stage to evaluate the potential food-drug interaction. Our data showed that food delayed the absorption rate of WXFL10203614.

The design of our study is mainly based on the following considerations: Firstly, the greatest advantage of a crossover study is that the subjects act as self-controls allowing for greater biological homogeneity, which is strongly recommended by guidelines. Additionally, 7 days of washout is enough to eliminate WXFL10203614 based on the short half-life. Secondly, for safety concerns, healthy male and female subjects were enrolled, which was easier for investigators to observe AEs and the changes in clinical data after dosing. Thirdly, according to the guideline of NMPA, a minimum of 12 subjects should complete the study to statistically assess the food effects on drug (NMPA, 2021). The final sample size was set as 14 on the basis of the dropout rate of 10%. Fourthly, in our single dose-escalation study, 10 mg WXFL10203614 was intended to be the highest recommended dose for RA treatment, so the dose of WXFL10203614 used to evaluate the food effect was 10 mg. Finally and most importantly, in order to provide the most significant impact on gastrointestinal physiology, thereby affecting the PK profile of the drug maximally, a high-fat and high-calorie meal is generally recommended before dosing, and the compositions and calories of the meal should be followed the guidelines strictly (NMPA, 2021; USFDA, 2022).

In terms of PK profile, the results showed that the $t_{1/2}$, MRT_{0-t} and CL/F of WXFL10203614 were similar under the fasted and fed conditions, indicating the elimination phase of

WXFL10203614 was not influenced. Furthermore, the AUC was not obviously changed after food intake and the 90% CIs for the ratios (fed/fasted) of the AUC_{0-t} and $AUC_{0-\infty}$ were all within the range of 0.80–1.25, confirming that food did not affect the systemic exposure of WXFL10203614. However, for the absorption phase, the T_{max} was delayed approximately 3-fold and C_{max} decreased by 16.3% under the fed condition. More importantly, the 90% CI for the ratio (fed/fasted) of the C_{max} was not totally within the range of 0.80–1.25. The above results indicated that the high-fat and high-calorie diet slowed down the absorption rate of WXFL10203614, similar to the previously results reported in other selective JAK1 inhibitors. Administration of 3 mg upadacitinib immediate-release capsules after a high-fat meal, C_{max} decreased by 23%, and AUC was not impacted compared with the fasted condition (Mohamed et al., 2017). High- and low-fat meals decreased C_{max} by 20% and 11% and delayed the absorption of filgotinib, with T_{max} prolonging about 2-3 folds, but little effect on systemic exposure was observed (Anderson et al., 2019). In general, the delayed absorption or reduced absorption rate originated from the slower gastric emptying rate and/or increased gastric pH in the fed state, which exhibited a decreased C_{max} and a corresponding longer T_{max} in the PK profile (Singh, 1999). The onset of drug absorption usually occurred in the proximal bowel, which might be delayed due to a slower gastric emptying rate (Lennernäs et al., 1997). The drug delivered from the stomach to the small intestine became the rate-limiting step in drug absorption (Singh, 1999). Therefore, we speculated that the delayed absorption of WXFL10203614 is perhaps related to the slow gastric emptying rate, but the exact mechanism needs to be studied further. Although the C_{max} decreased by 16.3% and 90% CI did not fall within the range of 0.8–1.25, this slight decrease in C_{max} did not need the dose adjustment owing to the small magnitude of changes (<25%) and was not considered clinically significant (Shen et al., 2019). Therefore, WXFL10203614 could be taken with or without food. However, due to the limitation of the sample size in our study, it is hard to compare the effect of gender difference on PK profile.

Regarding safety, WXFL10203614 was well tolerated in all subjects under fed or fasted condition. The TEAEs were consistent with previous studies of WXFL10203614 and JAK inhibitors (Shi et al., 2014; Taylor et al., 2017; Choy, 2019; Li et al., 2022). All TEAEs were mild and resolved spontaneously without any intervention. Additionally, the number and incidence of TEAEs (the changes in the neutrophil count and white blood cell count) were slightly reduced under the fed condition. These AEs were associated with the JAK2 inhibition which interfered with the regulatory functions of granulocyte-macrophage colony-stimulating factor (GM-CSF) that stimulated the proliferation of granulocytes and macrophages from bone marrow precursor cells (Furuya et al., 2018). WXFL10203614 has a slight inhibition effect on JAK2, and the inhibition effect of WXFL10203614 on JAK1 was 9-fold than that on JAK2 *in vitro*. It is inferred that when the absorption process of WXFL10203614 is delayed and concentration in the blood is reduced under the fed condition, the inhibition on the JAK2 signal pathway is weakened, which might reduce the risk of adverse events. However, more samples will be needed to confirm this speculation in future studies.

Conclusion

This study demonstrated that food could delay the absorption rate of WXFL10203614 but not significantly affect systemic exposure, which had no clinically relevant impact on the pharmacokinetics of the WXFL10203614 tablet. In addition, WXFL10203614 was well tolerated under fed or fasted condition so that it could be administered orally with or without food.

Data availability statement

The original contributions presented in the study are included in the article/Supplementary Material, further inquiries can be directed to the corresponding author.

Ethics statement

The studies involving human participants were reviewed and approved by Ethics Committee of Wuxi people's hospital. The patients/participants provided their written informed consent to participate in this study.

Author contributions

KH, ZZ, JX, and QH designed this experiment. KH, YS, NC, LQ, YD, ZQ, WQ, XG, and JW performed this clinic trial. KH, YS, and ZQ analyzed the data. KH and YS wrote and edited the paper, and drew the figures.

Funding

This work was supported by the Wuxi Public Service Platform for Clinical Research and Evaluation of New Drugs and Medical Devices (GGFWPT2019) and Wuxi Fuxin Pharmaceutical Research and Development Co., Ltd., Wuxi, China.

Conflict of interest

The authors declare that this study received funding from Wuxi Fuxin Pharmaceutical Research and Development Co.,

Ltd. The funder had the following involvement with the study: study design. ZZ and JX are employed by Wuxi Fuxin Pharmaceutical Research and Development Co., Ltd.

The remaining authors declare that the research was conducted in the absence of any commercial or financial relationships that could be construed as a potential conflict of interest.

Publisher's note

References

Anderson, K., Zheng, H., Kotecha, M., Cuvin, J., Scott, B., Sharma, S., et al. (2019). The relative bioavailability and effects of food and acid-reducing agents on filgotinib tablets in healthy subjects. *Clin. Pharmacol. Drug Dev.* 8, 585–594. doi:10.1002/cpdd.659

Center for drug evaluation, National Medical Products Administration (2021). *Technical guidelines for the food-effect studies in the development of new drugs*. https://www.cde.org.cn/main/news/viewInfoCommon/4f21fc720672cf26ad0efbe0207fdced.

Choy, E. H. (2019). Clinical significance of Janus Kinase inhibitor selectivity. *Rheumatol. Oxf.* 58, 953–962. doi:10.1093/rheumatology/key339

Crispino, N., and Ciccia, F. (2021). JAK/STAT pathway and nociceptive cytokine signalling in rheumatoid arthritis and psoriatic arthritis. *Clin. Exp. Rheumatol.* 39, 668–675. doi:10.55563/clinexprheumatol/e7ayu8

European medicines agency (2012). *Guideline on the investigation of drug interactions*. https://www.ema.europa.eu/en/documents/scientific-guideline/guideline-investigation-drug-interactions-revision-1_en.pdf.

Fragoulis, G. E., McInnes, I. B., and Siebert, S. (2019). JAK-inhibitors. New players in the field of immune-mediated diseases, beyond rheumatoid arthritis. *Rheumatol. Oxf.* 58, i43–i54. doi:10.1093/rheumatology/key276

Furuya, M. Y., Asano, T., Sumichika, Y., Sato, S., Kobayashi, H., Watanabe, H., et al. (2018). Tofacitinib inhibits granulocyte-macrophage colony-stimulating factor-induced NLRP3 inflammasome activation in human neutrophils. *Arthritis Res. Ther.* 20, 196. doi:10.1186/s13075-018-1685-x

Huang, K., Ding, Y., Que, L., Chu, N., Shi, Y., Qian, Z., et al. (2022). Safety, tolerability and pharmacokinetics of WXFL10203614 in healthy Chinese subjects: A randomized, double-blind, placebo-controlled phase I study. *Front. Pharmacol.* 13, 1057949. doi:10.3389/fphar.2022.1057949

Lamba, M., Wang, R., Fletcher, T., Alvey, C., Kushner, J. 4th., and Stock, T. C. (2016). Extended-release once-daily formulation of tofacitinib: Evaluation of pharmacokinetics compared with immediate-release tofacitinib and impact of food. *J. Clin. Pharmacol.* 56, 1362–1371. doi:10.1002/jcph.734

Lennernäs, H., and Fager, G. (1997). Pharmacodynamics and pharmacokinetics of the HMG-CoA reductase inhibitors. Similarities and differences. *Clin. Pharmacokinet.* 32, 403–425. doi:10.2165/00003088-199732050-00005

Li, N., Du, S., Wang, Y., Zhu, X., Shu, S., Men, Y., et al. (2022). Randomized, double-blinded, placebo-controlled phase I study of the pharmacokinetics, pharmacodynamics, and safety of KL130008, a novel oral JAK inhibitor, in healthy subjects. *Eur. J. Pharm. Sci.* 176, 106257. doi:10.1016/j.ejps.2022.106257

Li, Z., Xu, M., Li, R., Zhu, Z., Liu, Y., Du, Z., et al. (2020). Identification of biomarkers associated with synovitis in rheumatoid arthritis by bioinformatics analyses. *Biosci. Rep.* 40, BSR20201713. doi:10.1042/BSR20201713

Mohamed, M. F., Jungerwirth, S., Asatryan, A., Jiang, P., and Othman, A. A. (2017). Assessment of effect of CYP3A inhibition, CYP induction, OATP1B inhibition, and high-fat meal on pharmacokinetics of the JAK1 inhibitor upadacitinib. *Br. J. Clin. Pharmacol.* 83, 2242–2248. doi:10.1111/bcp.13329

Schmidt, L. E., and Dalhoff, K. (2002). Food-drug interactions. *Drugs* 62, 1481–1502. doi:10.2165/00003495-200262100-00005

Shen, Z., Lee, C. A., Valdez, S., Yang, X., Wilson, D. M., Flanagan, T., et al. (2019). Effects of food and antacids on pharmacokinetics and pharmacodynamics of lesinurad, a selective urate reabsorption inhibitor. *Clin. Pharmacol. Drug Dev.* 8, 647–656. doi:10.1002/cpdd.663

Shi, J. G., Chen, X., Lee, F., Emm, T., Scherle, P. A., Lo, Y., et al. (2014). The pharmacokinetics, pharmacodynamics, and safety of baricitinib, an oral JAK 1/2 inhibitor, in healthy volunteers. *J. Clin. Pharmacol.* 54, 1354–1361. doi:10.1002/jcph.354

Shi, J. G., Chen, X., McGee, R. F., Landman, R. R., Emm, T., Lo, Y., et al. (2011). The pharmacokinetics, pharmacodynamics, and safety of orally dosed INCB018424 phosphate in healthy volunteers. *J. Clin. Pharmacol.* 51, 1644–1654. doi:10.1177/0091270010389469

Shibata, M., Toyoshima, J., Kaneko, Y., Oda, K., Kiyota, T., Kambayashi, A., et al. (2021). The bioequivalence of two peficitinib formulations, and the effect of food on the pharmacokinetics of peficitinib: Two-way crossover studies of a single dose of 150 mg peficitinib in healthy volunteers. *Clin. Pharmacol. Drug Dev.* 10, 283–290. doi:10.1002/cpdd.843

Singh, B. N. (1999). Effects of food on clinical pharmacokinetics. *Clin. Pharmacokinet.* 37, 213–255. doi:10.2165/00003088-199937030-00003

Sparks, J. A. (2019). Rheumatoid arthritis. *Rheum. Arthritis. Ann. Intern. Med* 170, ITC1-ITC16. ITC16. doi:10.7326/AITC201901010

Sun, L., McDonnell, D., Liu, J., and von Moltke, L. (2019). Effect of food on the pharmacokinetics of a combination of olanzapine and samidorphan. *Clin. Pharmacol. Drug Dev.* 8, 503–510. doi:10.1002/cpdd.688

Taylor, P. C., Keystone, E. C., van der Heijde, D., Weinblatt, M. E., Del Carmen Morales, L., Reyes Gonzaga, J., et al. (2017). Baricitinib versus placebo or adalimumab in rheumatoid arthritis. *N. Engl. J. Med.* 376, 652–662. doi:10.1056/NEJMoa1608345

US Department of Health and Human Services, Food and Drug Administration, Center for Drug Evaluation and Research (CDER) (2022). *Assessing the effects of food on drugs in INDs and NDAs-clinical Pharmacology considerations guidance for industry*. https://www.fda.gov/media/121313/download.

frontiers | Frontiers in Pharmacology

TYPE Original Research
PUBLISHED 12 December 2022
DOI 10.3389/fphar.2022.1075309

OPEN ACCESS

EDITED BY
Zhihao Liu,
Dalian Medical University, China

REVIEWED BY
Jiaqi Mi,
Boehringer Ingelheim, Germany
Hong Zhang,
First Affiliated Hospital of Jilin University, China

*CORRESPONDENCE
Juan Li,
juanli2003@njglyy.com
Runbin Sun,
runbinsun@gmail.com
Chunhe Wang,
wangc@dartsbio.com

SPECIALTY SECTION
This article was submitted to Drug Metabolism and Transport, a section of the journal Frontiers in Pharmacology

RECEIVED 20 October 2022
ACCEPTED 29 November 2022
PUBLISHED 12 December 2022

CITATION
Ma T, Cao B, Huang L, Yang Y, Geng Y, Xie P, Zhao Y, Lin H, Wang K, Wang C, Sun R and Li J (2022), First-in-human study to assess the safety, tolerability, pharmacokinetics and immunogenicity of DS002, an anti-nerve growth factor monoclonal antibody.
Front. Pharmacol. 13:1075309.
doi: 10.3389/fphar.2022.1075309

First-in-human study to assess the safety, tolerability, pharmacokinetics and immunogenicity of DS002, an anti-nerve growth factor monoclonal antibody

Tingting Ma[1], Bei Cao[1], Lei Huang[1], Yuanxun Yang[1], Yan Geng[1], Pinhao Xie[1], Yu Zhao[1], Hui Lin[1], Kun Wang[2], Chunhe Wang[3]*, Runbin Sun[1]* and Juan Li[1]*

[1]Phase I clinical Trials Unit, Nanjing Drum Tower Hospital, The Affiliated Hospital of Nanjing University Medical School, Nanjing, China, [2]Beijing Highthink Pharmaceutical Technology Service Co., Ltd., Beijing, China, [3]Dartsbio Pharmaceuticals Ltd., Zhongshan, Guangdong, China

Purpose: To evaluate the safety, tolerability, pharmacokinetics and immunogenicity of DS002 injection, an anti-nerve growth factor (anti-NGF) monoclonal antibody for treating pain conditions, in healthy Chinese subjects.

Methods: This study was a single-center, randomized, double-blind, single-dose escalation, placebo-controlled design (CTR20210155). A total of 53 healthy subjects, 27 male and 26 female, were enrolled in this study, and one subject withdrew from the study before administration. Seven dose groups were set up, which were 0.5 mg, 1.0 mg, 2.0 mg, 4.0 mg, 7.0 mg, 12.0 mg and 20.0 mg, respectively. The drug was administered by single subcutaneous injection. Four subjects were enrolled in the first dose group (0.5 mg) received DS002. Other dose groups enrolled eight subjects each, six of whom received DS002 while the other two received a placebo. Safety, tolerability, pharmacokinetic parameters and immunogenicity of DS002 were assessed.

Results: DS002 was well tolerated; all adverse events were Grade 1–2, and did not reach the termination standard of dose increment within the range of 0.5–20.0 mg. Adverse event rates were generally similar across treatments. After a single subcutaneous injection, the median T_{max} in different dose groups ranged 167.77–337.38 h; mean $t_{1/2}$ ranged 176.80–294.23 h, the volume of distribution (V_z) ranged 5265.42–7212.00 ml, and the clearance rate (CL) ranged 12.69–24.75 ml/h. In the dose range of 0.5–20.0 mg, C_{max} ranged from 51.83 ± 22.74 ng/ml to 2048.86 ± 564.78 ng/ml, AUC_{0-t} ranged from 20615.16 ± 5698.28 h·ng/mL to 1669608.11 ± 387246.36 h·ng/mL, and AUC_{0-inf} ranged from 21852.45 ± 5920.21 h·ng/mL to 1673504.66 ± 389106.13 h·ng/mL. They all increased with dose escalation, and C_{max} and AUC_{0-t} did not have a significant dose-linear relationship, whilst AUC_{0-t} was not dose-dependent

at all. anti-drug antibody test results of each group of all subjects in this trial were negative.

Conclusion: DS002 showed satisfactory safety within the dose range of 0.5 mg–20.0 mg. The absorption and metabolism of DS002 were slow, it exhibited a low volume of distribution and the clearance rate was low. These data suggest that DS002, by blocking nerve growth factor, is expected to become a novel, safe and non-addictive treatment for pain conditions.

KEYWORDS

DS002, anti-nerve growth factor antibody, first-in-human trial, pharmacodynamics, novel analgesic

Introduction

Chronic pain affects more than 30% of people in the world. The individual and societal burden of chronic pain are substantial (Cohen et al., 2021). In the state of chronic pain, the protective effect of pain becomes disordered and morbid. The pain attack leads to sleep disorder, anorexia, mental collapse, personality distortion and other consequences. Many patients even choose to commit suicide because they can't bear the long-term pain, which jeopardized their lives and quality of life (Hooley et al., 2014). Non-steroidal anti-inflammatory drugs (NSAIDs) and opioid analgesics are the traditional main treatment for chronic pain (Chang et al., 2016). However, long-term use of NSAIDs causes adverse effects related to gastric bleeding and cardiovascular (Schjerning et al., 2020). Opioids are effective short-term treatment but have addictive and respiratory inhibitory effects (Coussens et al., 2019; Kiyatkin 2019), which limits their clinical application. Therefore, the successful management of chronic pain remains a significant medical challenge.

The nerve growth factor (NGF) belongs to the neurotrophic factor family. It was originally extracted from mouse submandibular gland and snake venom, and exists in almost all vertebrates (Tong et al., 2012). NGF exists in various species as different polymers (precursors), among which the β subunit has NGF biological activity and is called β-NGF; Mature dissociation β-NGF is composed of two 118-amino acid peptides connected through non-covalent bonds (Shooter 2001). Although NGF has a critical role in early neural development, in adults, this role changes to other functions, including neuronal plasticity, hypersensitization to noxious stimuli, and pain signaling. (Enomoto et al., 2019; Wise et al., 2021). When NGF binds to the functional receptor tropomyosin receptor kinase A (TrkA) on the nociceptor, it activates cytoplasmic ERK, PLC/PKC and other signal pathways. NGF-TrkA signaling reduces the threshold of the neuronal action potential, improves neuronal excitability, and then sensitizes pain (Tong et al., 2012; Wise et al., 2021). Elevated NGF levels have been associated with acute and chronic pain conditions and injured and inflamed tissues. NGF is expected to become a potential non-addictive analgesic target. The anti-NGF antibody can bind to NGF and block its interaction with TrkA to interrupt the pain-sensing neurons to send signals.

Anti-NGF antibody drugs include Pfizer/Lilly's Tanezumab and Regeneron/Tiva's Fasinumab, both of which have achieved significant efficacy in the treatment of moderate to severe osteoarthritis and chronic lower back pain. However, both drugs reported severe adverse reactions in joints, including osteonecrosis and rapidly progressive osteoarthritis (RPOA), (Jayabalan and Schnitzer 2016). Therefore, it is of great social significance and clinical prospect to develop safer anti-NGF antibodies, in order to meet clinical needs and improve patients' quality of life.

DS002 is an anti-NGF monoclonal antibody independently developed by Dartsbio Pharmaceuticals, Ltd. *In vitro* studies have shown that DS002 can successfully block the binding of NGF to TrkA receptors. In pre-clinical studies, DS002 treatment demostrated potent analgesic effects in several pain models including OA pain, chemotherapy-induced pain, and cancer pain. Based on the preclinical repeated toxicity test and efficacy test, as well as the clinical trial of drugs at the same target (Jonsson et al., 2016), the dose range selection of this first-in-human trial for the healthy subject was set as 0.5 mg–20.0 mg. The objective of this first-in-human study was to evaluate the safety, tolerability, pharmacokinetics and immunogenicity of a single subcutaneous injection of DS002 in healthy volunteers.

Methods

This study (CTR20210155) was approved by the ethics committee of Nanjing Drum Tower Hospital, The Affiliated Hospital of Nanjing University Medical School, and carried out according to the Declaration of Helsinki (2013 version), the Guideline For Good Clinical Practice issued by the International Council for Harmonisation (ICH), the Good

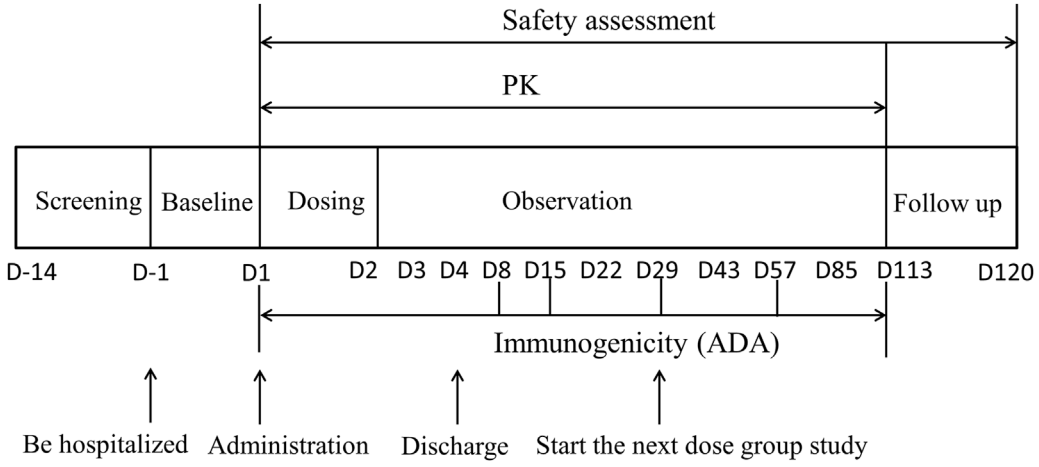

FIGURE 1
The flow chart of DS002 single-dose administration. PK, pharmacokinetics; ADA, anti-drug antibody.

Clinical Practice (GCP) issued by the National Medical Products Administration (NMPA) and relevant regulations. Written informed consent was obtained from all subjects.

Study design

The overall study was a single-center, randomized, double-blind, single-dose escalation, placebo-controlled phase I clinical trial. A total of 53 Chinese healthy subjects were enrolled in this study, including 27 males and 26 females, and 52 subjects completed this clinical trial.

The dose-escalation design was used to evaluate the safety, tolerability, pharmacokinetics and immunogenicity of DS002 after a single administration. Seven dose groups were set up, including 0.5, 1.0, 2.0, 4.0, 7.0, 12.0 and 20.0 mg, not per kg, respectively. DS002 was administered by subcutaneous injection. Four subjects were enrolled in the first dose group (0.5 mg), and each subject received a singledose of DS002 subcutaneously. In the 2nd to 7th dose groups, eight subjects were enrolled in each group, among whom 6 received DS002 and two subjects received placebo. A series of blood samples were collected before and after DS002 administration to evaluate the PK parameters and immunogenicity of DS002 in healthy subjects. Subjects were clinically followed up on the 4th, 8th, 15th, 22nd, 29th, 43rd, 57th, 85th and 113th days, biological samples were collected and safety and tolerability were assesseded. Subjects were followed up by telephone on the 120th day, which was the end of each dose group. (Figure 1). The next dose escalation group could only be started after the assessment results on the 29th day of all subjects in the previous dose group were confirmed as safe.

During hospitalization in the research center, the subjects were managed with a unified diet and rest protocol. On the day before DS002 administration, the subjects stayed in the Phase I trials unit, took a unified dinner, and then fasted overnight for at least 10 h. The next morning, they ate a small amount of standard breakfast and then received DS002 injection subcutaneously. After injection, they ate the standard meals. Within 48 h prior to enrollment and during the whole trial period, it was forbidden to take any food and drink rich in caffeine or xanthine (such as tea, coffee, chocolate, cola, etc.), smoking and drinking alcohol-containing products were also not allowed. Strenuous exercise (exceeding normal daily activities) were avoided during the whole trial period. Subjects were told to take proper contraception from the start of the study period to 6 months after DS002 administration.

This study was a double-blind trial design (except for the first dose group). Blindness was maintained for the generation of random numbers, the coding of drugs used in the trial, the drug matched to each subject, the recording and evaluation of test results, the monitoring of the test process and data management. On the day of DS002 administration, the investigator checked the information of all subjects to ensure that they met the inclusion criteria of the trial, and then administered according to the drug number matched with the random number of the subject. All relevant personnel remained blind during the clinical study.

PK blood sampling time points: for determination of the concentration of DS002, blood samples were collected at 17 time points in each dose group: within 1 h before DS002 administration, and 6 h, 8 h, 12 h, D2 (24 h), D2 (36 h), D3 (48 h), D3 (60 h), D4 (72 h), D8 (168 h), D15 (336 h), D22 (504 h), D29 (672 h), D43 (1,008 h), D57 (1,344 h), D85 (2016 h), and D113 (2688 h) after administration. About 3 ml of venous blood was collected at each time point (Figure 1).

Immunogenicity (ADA) blood sampling time points: blood samples were collected at 6 time points in each dose group, including within 1 h before administration, D8 (168 h), D15 (336 h), D29 (672 h), D57 (1,344 h) and D113 (2688 h) after administration, and about 3 ml of venous blood was collected at each time point (Figure 1).

Subjects

Subjects were healthy volunteers aged 18–45 years, including both males and females (not pregnant or breastfeeding). The body mass index (BMI) of the subjects was 19.0–26.0 kg/m^2, the male body weight was ≥50 kg and female ≥45 kg. Effective contraception should be used during the trial and continued for 6 months after administration. Subjects fully understood the content, objectives and characteristics of the study and could complete the study as planned, voluntarily participated in the study and signed written informed consent.

Subjects were excluded if they met one of the following: Those who had an allergic history or allergic constitution in the past; Those who had a history of bone or joint diseases, peripheral or autonomic neuropathy, spontaneous bleeding of unknown causes and (or) disease or medical history of continuous bleeding after trauma, abnormal thyroid function or thyroid hormone, or malignant tumor; Smokers, alcoholics or drug abusers. Subjects were not allowed to take any prescription drugs, over-the-counter drugs and natural health products within 14 days before screening.

Objectives

The primary objective of this study was to evaluate the safety and tolerability of DS002 as a single administration in healthy subjects. The secondary objective was to evaluate the pharmacokinetic parameters and immunogenicity of DS002 in healthy subjects after a single administration.

Research indicators

The safety indicators of this study included the incidence of adverse event (AE, Graded according to CTCAE v5.0) and serious adverse event (SAE); Laboratory examinations; Neurological examination; Injection site reaction; 12-lead electrocardiogram (ECG); Abdominal B ultrasound; Vital signs; Physical examination.

PK indexes: PK parameters of DS002 after a single administration, including but not limited to C_{max}, T_{max}, $AUC_{0\text{-}t}$, $AUC_{0\text{-}inf}$, $t_{1/2}$, MRT, λ_z; Immunogenicity index: ADA after single administration of DS002.

The methods for detecting DS002 and anti-DS002 antibody

Electrochemiluminescence Immunoassay (ECLIA) methods for the analysis of the pharmacokinetics (PK) and anti-drug antibody (ADA) of DS002 in serum were established.

For PK samples, the MSD plate was pre-coated with huNGF-his, and after adding the sample, it was incubated to form an antigen-antibody complex. After incubation, the unbound DS002 was washed away with a washing solution. Detection antibody Sulfo-Anti-DS002 antibody was then added and incubated; after incubation, unbound antibody was washed off with washing solution; finally the reading buffer was added, and MSD (MESO QuickPlexSQ120, acquisition software MSD Workbench V4.0.12) was used to collect the signal. The data were analyzed and processed with Watson LIMS (V7.4.1 and V7.6.1). The calibration ranges of DS002 were 2.50 ng/ml~500.00 ng/ml. The quality control samples (7.5, 50 and 400 ng/ml) were determined with an accuracy of 89.0%–114.3%, the precision of 17.6% (CV) for inter-assay and accuracy of 104.0%–106.1%, precision of 19.8% (CV) for intra-assay. There was no matrix effect for human serum. No hook effect was observed for samples up to 5000.00 ng/ml. The sample can be diluted up to 1,250 fold with a total CV(%) of 5.5%.

The ADA samples were measured by screening assay, confirmatory assay, and titer assay. The method is based on the multivalency of antibodies and the specific binding of antigen-antibody. First, each control sample and the test sample were diluted by 1:20 times of acidification. Then each diluted sample solution was added to TrkA-hFc working solution for purification to remove interferences. The purified solution was then added with Biotin-DS002 and Suflo-DS002 Master Mixture (with or without drug), incubating on a dilution plate to allow a bridging reaction between the drug and the anti-drug antibody to form a bridging complex. After the reaction was completed, it was transferred to the MSD plate for incubation. After incubation, the plate was washed and then the reading buffer was added, and the signal was read on the MSD. For the screening assay, the HPC samples (5000 ng/ml) were determined with a precision of 4.4% (CV) for inter-assay and 11.9% (CV) for intra-assay. The LPC samples (16 ng/ml) were determined with a precision of 14% (CV) for inter-assay and 10.8% (CV) for intra-assay. For the confirmatory assay, the HPC samples (5000 ng/ml) were determined with a precision of 0.1% (CV) for inter-assay and 0.1% (CV) for intra-assay. The LPC samples (16 ng/ml) were determined with a precision of 25.9% (CV) for inter-assay and 18.3% (CV) for intra-assay. There was no matrix effect for human serum. No hook effect was observed for samples up to 41000.00 ng/ml.

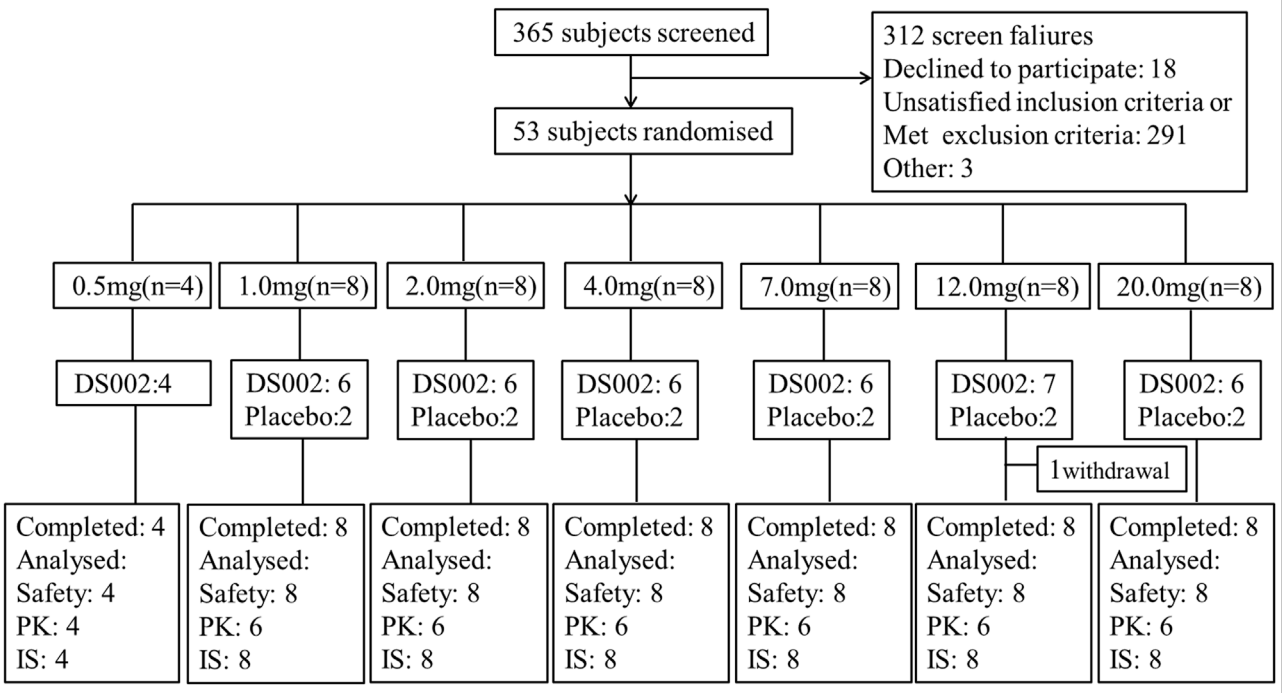

FIGURE 2
Subject disposition of participants in the study. PK, pharmacokinetics; IS, Immunogenicity analysis set.

Data analysis and statistical methods

Unless otherwise specified, SAS (version 9.4 and above) and Phoenix™ WinNonlin ® (Version 8.0 and above) were used for statistical analysis. The classified variables were summarized by frequency and percentage. Continuous variables were summarized by sample size, mean, standard deviation, median, minimum and maximum. For some continuous variables, the coefficient of variation or the geometric coefficient of variation, geometric mean, lower quartile and upper quartile were also counted. The number of subjects enrolled in each dose group and the situation of dropped cases were summarized. A descriptive statistical analysis on baseline characteristics of the enrolled cases were made. Safety and PK data were summarized using appropriate statistical tables and diagrams.

Full analysis set (FAS): all randomized subjects. Safety analysis set (SS): all subjects who have received the study drug at least once and have at least one safety evaluation index. PK concentration and parameter analysis set (PKCS and PKPS): all subjects who have used the study drug and have at least one PK concentration or parameter data. Immunogenicity analysis set (IS): all subjects who have received the study drug at least once and have at least one post-baseline immunogenicity evaluation data.

Based on the PKCS, the concentration data were tabulated and described by dose groups. The drug concentration-time curves (linear and semi-logarithmic) were drawn according to the planned blood collection time.

Based on PKPS, a Non-Compartmental Analysis by Phoenix™ WinNonlin® (version 8.0 or above) was adopted. PK parameters were calculated according to the actual blood collection time, and PK parameters were listed and described statistically. A power model was used to analyze the linear relationship between main PK parameters (C_{max}, AUC) and dose.

Results

Subject demographics

The study was conducted from 22 February 2021 to 24 May 2022. In this trial, a total of 53 healthy Chinese subjects in seven dose groups were included in the FAS, and 52 were included in the SS (one subject withdrew from the study before administration), including 40 subjects receiving DS002, four in the 0.5 mg dose group, and six in other dose groups; There were 12 subjects receiving placebo. All 52 subjects completed the study (Figure 2). The demographics and baseline characteristics analysis of the subjects are shown in Table 1.

TABLE 1 Subject demographics.

	0.5 mg *n* = 4	1.0 mg *n* = 6	2.0 mg *n* = 6	4.0 mg *n* = 6	7.0 mg *n* = 6	12.0 mg *n* = 7	20.0 mg *n* = 6	Placebo *n* = 12	Total *n* = 52
Age, years	27.00 (2.16)	31.00 (5.87)	28.33 (8.21)	26.83 (8.93)	31.00 (7.95)	28.86 (8.69)	29.33 (5.61)	27.83 (6.24)	28.74 (6.77)
Female, n (%)	1 (25.0)	2 (33.3)	3 (50.0)	4 (66.7)	5 (83.3)	3 (42.86)	3 (50.0)	5 (41.7)	26 (49.06)
Male, n (%)	3 (75.0)	4 (66.7)	3 (50.0)	2 (33.3)	1 (16.7)	4 (57.14)	3 (50.0)	7 (58.3)	27 (50.94)
Han, n (%)	4 (100)	6 (100)	6 (100)	6 (100)	6 (100)	7 (100)	5 (83.33)	12 (100)	52 (98.11)
Height, cm	165.13 (3.35)	164.25 (11.23)	164.33 (6.84)	164.33 (6.46)	162.58 (8.65)	163.21 (8.35)	164.67 (10.60)	165.88 (8.26)	164.42 (7.93)
Weight, kg	64.68 (5.19)	62.60 (10.84)	63.92 (8.62)	56.15 (3.89)	57.78 (6.91)	59.16 (5.04)	61.57 (7.67)	62.43 (9.90)	61.02 (7.91)
BMI, kg/m^2	23.68 (1.13)	23.08 (2.05)	23.58 (1.95)	20.83 (1.71)	21.83 (1.35)	22.21 (1.38)	22.72 (2.23)	22.60 (2.12)	22.52 (1.90)

Age and BMI are presented as mean (standard deviation). BMI, body mass index; Han, Han Nationality.

Safety and tolerability

At least one adverse event (AE) occurred in 36 of 40 (90%) healthy subjects who received DS002 and 12 of 12 (100%) subjects who received placebo. Forty-five subjects (86.54%) had adverse reactions (ARs). 12 (25.00%) subjects of DS002 had AEs of grade 2 (vs. placebo, 1/12, 8.33%). No grade 3 or grade 4 AEs were reported. The TEAEs of subjects are shown in Table 2.

Among the 40 subjects injected DS002, the AEs with an incidence rate of more than 5% include the following: upper respiratory tract infection (25.00%, 10/40); decreased triiodothyronine, and elevated serum uric acid (22.50%, 9/40); elevated amylase (20.00%, 8/40); elevated serum thyrotropin (15.00%, 6/40); decreased white blood cell count (12.50%, 5/40); arthralgia (10.00%, 4/40); positive urine red blood cell, positive urine occult blood, elevated triglycerides, elevated alanine aminotransferase, prolonged QTc interval of ECG, hypokalemia, and decreased free thyroxine (7.50%, 3/40); increased neutrophil count, abnormal ECG T wave, increased white blood cell count, elevated free thyroxine, elevated γ-glutamyltransferase, elevated aspartate aminotransferase, elevated serum calcium and elevated free triiodothyronine (5.00%, 2/40).

In the placebo group, 12 subjects (100.00%) had AEs. The incidence rates from high to low were elevated amylase (33.33%, 4/12); elevated serum thyrotropin, decreased leukocyte count, and increased neutrophil count (25.00%, 3/12); decreased triiodothyronine, abnormal ECG T wave, and positive urine protein (16.67%, 2/12); all (100.00%) had ARs. Of which one subject (8.33%) had 2 times Grade 2 AE.

The incidences of AEs and ARs in each dose group showed an overall upward trend with dose escalation, and the incidence of AEs and ARs between DS002 and placebo subjects was similar. One case of Grade 2 AE (elevated amylase without symptom) was reported in the 12.0 mg dose group, whilst the rest of elevated amylase AEs were all Grade 1. No serious adverse event (SAE) was reported in subjects who received DS002 injection. None of the subjects died or dropped out to TEAE.

In brief, after a single dose of DS002, none of the dose groups reached the termination standard of dose escalation, and the safety and tolerability profiles of DS002 were satisfied.

Pharmacokinetics

All 40 subjects receiving DS002 were included in the PK analysis. The PK parameters of the DS002 and placebo groups are shown in Table 3.

In this study, $AUC_{\_\%\ Extrap}$ of DS002 in the dose range of 0.5 mg–20 mg was less than 5.81% (Table 3), which indicated that the design of the blood sampling time points for PK test was reasonable, and the calculated terminal clearance rate constant and related parameters were reliable.

After a single subcutaneous injection of DS002 in healthy subjects, the median T_{max} was 167.77–337.38 h; The mean $t_{1/2}$ was 176.80–294.23 h. Except for the 0.5 mg dose group, of which $t_{1/2}$ was 176.80 h, $t_{1/2}$ of the remaining dose groups ranged 205.46–294.23 h (Table 3). In the dose range of 0.5–20.0 mg, C_{max}, $AUC_{0\text{-}t}$ and $AUC_{0\text{-}inf}$ of prototype drug DS002 increased with the increase of dose (Table 3; Figures 3A,B).

After a single DS002 administration to healthy subjects, C_{max}, $AUC_{0\text{-}t}$, $AUC_{0\text{-}inf}$ and dose were simultaneously logarithmically converted to perform linear PK analysis. The 90% confidence interval of C_{max} slope was 90.61%–106.92%, the 90% confidence

TABLE 2 Summary of adverse events.

n (%)	0.5 mg *n* = 4	1.0 mg *n* = 6	2.0 mg *n* = 6	4.0 mg *n* = 6	7.0 mg *n* = 6	12.0 mg *n* = 6	20.0 mg *n* = 6	Placebo *n* = 12	Total *n* = 52
All AEs	3 (75.00)	5 (83.33)	5 (83.33)	5 (83.33)	6 (100)	6 (100)	6 (100)	12 (100)	48 (92.31)
All ARs	2 (50.00)	4 (66.67)	5 (83.33)	4 (66.67)	6 (100)	6 (100)	6 (100)	12 (100)	45 (86.54)
Grade 2 AEs	1 (25.00)	1 (16.67)	0	3 (50.00)	3 (50.00)	2 (33.33)	2 (33.33)	1 (8.33)	13 (25.00)
Grade 2 ARs	0	0	0	0	0	1 (16.67)	0	0	1 (1.92)
Term									
Various inspections									
Elevated AMY	1 (25.00)	1 (16.67)	1 (16.67)	1 (16.67)	1 (16.67)	2 (33.33)	1 (16.67)	4 (33.33)	12 (23.08)
Reduced T3	0	1 (16.67)	2 (33.33)	0	3 (50.00)	0	3 (50.00)	2 (16.67)	11 (21.15)
Elevated UA	1 (25.00)	1 (16.67)	3 (50.00)	1 (16.67)	1 (16.67)	0	2 (33.33)	1 (8.33)	10 (19.23)
Elevated TSH	0	0	1 (16.67)	1 (16.67)	1 (16.67)	2 (33.33)	1 (16.67)	3 (25.00)	9 (17.31)
Decreased WBC	0	0	0	0	1 (16.67)	2 (33.33)	2 (33.33)	3 (25.00)	8 (15.38)
Increased N	0	0	1 (16.67)	0	0	0	1 (16.67)	3 (25.00)	5 (9.62)
Elevated ALT	0	0	1 (16.67)	0	0	2 (33.33)	0	1 (8.33)	4 (7.69)
Urine RBC(+)	0	0	0	1 (16.67)	1 (16.67)	0	1 (16.67)	1 (8.33)	4 (7.69)
Urine OB(+)	0	0	0	1 (16.67)	1 (16.67)	0	1 (16.67)	1 (8.33)	4 (7.69)
Abnormal ECG T wave	0	0	0	2 (33.33)	0	0	0	2 (16.67)	4 (7.69)
Elevated TG	0	0	1 (16.67)	0	1 (16.67)	1 (16.67)	0	1 (8.33)	4 (7.69)
Increased WBC	0	0	0	1 (16.67)	0	0	1 (16.67)	1 (8.33)	3 (5.77)
Prolonged QTc	0	2 (33.33)	0	0	0	0	1 (16.67)	0	3 (5.77)
Hypokalemia	0	1 (16.67)	0	0	0	1 (16.67)	1 (16.67)	0	3 (5.77)
Decreased FT4	0	1 (16.67)	1 (16.67)	0	1 (16.67)	0	0	0	3 (5.77)
Elevated FT4	0	0	0	1 (16.67)	0	1 (16.67)	0	1 (8.33)	3 (5.77)
Elevated γ-GT	0	0	1 (16.67)	0	0	1 (16.67)	0	0	2 (3.85)
Decreased T4	0	0	0	0	0	0	1 (16.67)	1 (8.33)	2 (3.85)
Urine protein (+)	0	0	0	0	0	0	0	2 (16.67)	2 (3.85)
Elevated AST	0	0	1 (16.67)	0	0	1 (16.67)	0	0	2 (3.85)
Elevated TBil	0	0	1 (16.67)	0	0	0	0	1 (8.33)	2 (3.85)

(Continued on following page)

10.3389/fphar.2022.1075309

TABLE 2 (*Continued*) Summary of adverse events.

n (%)	0.5 mg *n* = 4	1.0 mg *n* = 6	2.0 mg *n* = 6	4.0 mg *n* = 6	7.0 mg *n* = 6	12.0 mg *n* = 6	20.0 mg *n* = 6	Placebo *n* = 12	Total *n* = 52
Elevated Ca	0	0	0	2 (33.33)	0	0	0	0	2 (3.85)
Elevated FT3	1 (25.00)	0	1 (16.67)	0	0	0	0	0	2 (3.85)
Abnormal liver ultrasound	0	0	1 (16.67)	0	0	0	0	0	1 (1.92)
Decreased L	0	0	0	0	0	0	0	1 (8.33)	1 (1.92)
Elevated FT3	0	0	0	0	0	0	1 (16.67)	0	1 (1.92)
Increased Eos	0	0	0	0	1 (16.67)	0	0	0	1 (1.92)
Increased heart rate	0	0	0	1 (16.67)	0	0	0	0	1 (1.92)
Decreased Ca	0	0	0	0	0	0	0	1 (8.33)	1 (1.92)
Decreased Hb	0	0	0	0	1 (16.67)	0	0	0	1 (1.92)
Decreased P	0	0	0	0	0	1 (16.67)	0	0	1 (1.92)
Elevated Glu	0	0	1 (16.67)	0	0	0	0	0	1 (1.92)
Decreased FT3	0	0	1 (16.67)	0	0	0	0	0	1 (1.92)
Increased N%	0	0	0	0	0	0	0	1 (8.33)	1 (1.92)
Infections and infectious diseases									
URTI	1 (25.00)	0	0	1 (16.67)	4 (66.67)	1 (16.67)	3 (50.00)	0	10 (19.23)
Urinary tract infection	0	0	0	0	0	0	0	1 (8.33)	1 (1.92)
Vaginal fungal infection	0	0	0	0	1 (16.67)	0	0	0	1 (1.92)
Pharyngitis	0	1 (16.67)	0	0	0	0	0	0	1 (1.92)
Tinea pedis	0	0	0	0	1 (16.67)	0	0	0	1 (1.92)
Various musculoskeletal and connective tissue diseases									
Arthralgia	0	0	0	1 (16.67)	0	1 (16.67)	2 (33.33)	1 (8.33)	5 (9.62)
Joint swelling	0	0	0	0	0	0	1 (16.67)	0	1 (1.92)
Diseases of hepatobiliary system									
Gallbladder polyps	1 (25.00)	0	0	0	0	0	0	1 (8.33)	2 (3.85)
Hepatic steatosis	0	0	1 (16.67)	0	0	0	0	0	1 (1.92)
Systemic diseases and various reactions at the administration site									
Bleeding	0	0	0	0	0	0	0	1 (8.33)	1 (1.92)
Erythema	0	0	0	1 (16.67)	0	0	0	0	1 (1.92)

(Continued on following page)

10.3389/fphar.2022.1075309

TABLE 2 (*Continued*) Summary of adverse events.

n (%)	0.5 mg $n = 4$	1.0 mg $n = 6$	2.0 mg $n = 6$	4.0 mg $n = 6$	7.0 mg $n = 6$	12.0 mg $n = 6$	20.0 mg $n = 6$	Placebo $n = 12$	Total $n = 52$
Metabolic and nutritional diseases									
Hypoglycemia	0	0	0	0	0	0	1 (16.67)	0	1 (1.92)
Skin and subcutaneous tissue diseases									
Urticaria	0	0	0	1 (16.67)	0	0	0	0	1 (1.92)
Heart Organ Diseases									
Ventricular extrasystole	0	1 (16.67)	0	0	0	0	0	0	1 (1.92)
Eye organ diseases									
Keratitis	0	0	0	1 (16.67)	0	0	0	0	1 (1.92)

AEs, adverse events; AR, adverse reactions, the adverse events that are positively related, likely related, and possibly related. AMY, amylase; T3, triiodothyronine; UA, serum uric acid; TSH, serum thyrotropin; WBC, white blood cell count; N, neutrophil count; ALT, alanine aminotransferase; RBC, red blood cell; OB(+), occult blood positive; TG, triglycerides; QTc, QTc interval of ECG; FT4, free thyroxine; GT, glutamyltransferase; T4, thyroxine; AST, aspartate aminotransferase; TBil, total bilirubin; Ca, serum calcium; FT3, free triiodothyronine; L, lymphocyte count; Eos, eosinophil count; Hb, Hemoglobin; P, serum phosphorus; Glu, serum glucose; URTI, upper respiratory tract infection. There were no serious adverse events during the entire study and no TEAEs that led to treatment discontinuation or interruption.

interval of $AUC_{0\text{-}t}$ slope was 107.41%–121.13%, and the 90% confidence interval of $AUC_{0\text{-}inf}$ slope was 106.05%–119.33%. The results indicated that C_{max} and $AUC_{0\text{-}inf}$ increased with dose, but did not have a significant dose-linear relationship, whilst AUC0-t was not dose dependent at all. (Table 4).

Immunogenicity

The ADA test results of every group of subjects in this trial were negative at all follow-up visits, indicating that the immunogenicity of the DS002 injection was low.

Discussion

Pain can be treated more effectively with analgesics that operate on different mechanisms. Traditional NSAIDs and opioids are the most widely used analgesics, but their long-term use causes side effects and addiction, which is unable to meet clinical needs (Chang et al., 2016; Coussens et al., 2019; Kiyatkin 2019; Schjerning et al., 2020). DS002, an anti-NGF monoclonal antibody, is developed as a potential analgesic. Preclinical studies have shown that it could effectively supress NGF/TrkA signalingand reset the pain threshold without obvious adverse reactions and addiction problems. Here in this first-in-human study, we evaluated the safety, tolerability and PK parameters of DS002 as a single subcutaneous injection in healthy subjects. DS002 was well tolerated and safe within the dose range of 0.5–20.0 mg. PK results showed that the absorption and metabolism of DS002 was slow, and had a long effect time. Immunogenicity results suggested that ADA was negative throughout all follow-up visits.

In terms of safety, all subjects receivied DS002 injection completed the trial. No dose-limiting toxicity was observed, and the dose increment termination criteria were not reached within the dose range of 0.5–20 mg. Five subjects suffered from arthralgia, including four subjects receiving DS002 (one in 4.0 mg, one in 12.0 mg and two in 20.0 mg group) and one subject in the placebo group. The symptoms were mild without any discomfort such as activity disorder, and were all resolved without intervention. It is worth noting that no severe bone and joint events or peripheral neuropathy/paresthesia were found. No rapid progression of osteoarthritis (RPOA) was observed even at high doses, which was the most prominent concern when the US Food and Drug Administration shelved the development plan of similar anti-NGF drugs. Collectively, the safety data of DS002 indicate that it may serve as provide a new therapeutic strategy for the target of analgesic treatment.

In adults, NGF and its interaction with TrkA have been found to play a vital role in the nociception and plasticity of the nervous system under pain conditions. Therefore, various monoclonal antibody therapies targeting this pathway have been studied to treat chronic pain. Although the Food and Drug Administration

TABLE 3 The pharmacokinetic parameters of DS002.

	0.5 mg *n* = 4	1.0 mg *n* = 6	2.0 mg *n* = 6	4.0 mg *n* = 6	7.0 mg *n* = 6	12.0 mg *n* = 6	20.0 mg *n* = 6
T_{max} (h)	167.77 (48.00–335.78)	168.63 (168.58–336.25)	251.90 (35.93–335.88)	168.54 (168.50–504.58)	337.38 (35.95–337.48)	168.61 (168.58–337.82)	169.61 (59.50–337.35)
C_{max} (ng/ml)	51.83 ± 22.74	85.69 ± 37.80	157.92 ± 63.52	295.97 ± 69.58	374.02 ± 42.75	956.21 ± 213.41	2048.86 ± 564.78
$t_{1/2}$(h)	176.80 ± 66.67	205.46 ± 55.76	235.16 ± 48.83	214.06 ± 29.67	223.92 ± 39.93	294.23 ± 24.17	287.18 ± 45.24
AUC_{0-t} (h·ng/mL)	20615.16 ± 5698.28	48976.41 ± 13712.08	107834.02 ± 49871.96	238871.15 ± 62280.97	332402.49 ± 84014.77	717276.99 ± 113683.18	1669608.11 ± 387246.36
AUC_{0-inf} (h·ng/mL)	21852.45 ± 5920.21	50946.19 ± 13253.08	112353.93 ± 48514.62	242206.02 ± 61448.70	336848.83 ± 84030.42	726968.53 ± 112493.19	1673504.66 ± 389106.13
λ_z (1/h)	0.0043 ± 0.0012	0.0036 ± 0.0009	0.0031 ± 0.0007	0.00 ± 0.00	0.0033 ± 0.0005	0.0032 ± 0.0006	0.0024 ± 0.0002
CL (mL/h)	24.75 ± 9.18	20.99 ± 6.49	20.53 ± 8.28	17.45 ± 4.55	21.89 ± 5.42	16.87 ± 2.86	12.69 ± 3.91
V_z (mL)	6119.27 ± 2314.67	6517.12 ± 3671.56	6851.26 ± 2815.53	5365.67 ± 1,437.83	6967.68 ± 1778.05	7212.00 ± 1,618.54	5265.42 ± 1896.20
MRT_{0-t} (h)	297.91 ± 126.91	398.31 ± 83.78	457.03 ± 98.71	519.61 ± 107.44	556.17 ± 126.16	557.95 ± 54.15	589.40 ± 46.42
MRT_{0-inf} (h)	343.10 ± 139.90	443.53 ± 108.34	505.59 ± 103.18	539.77 ± 105.51	576.68 ± 126.44	583.91 ± 62.09	595.14 ± 49.79
$AUC_{\_\% Extrap}$ (%)	5.81 ± 1.09	4.42 ± 3.59	4.66 ± 5.41	1.50 ± 1.21	1.41 ± 1.26	1.38 ± 0.47	0.23 ± 0.17

T_{max} as median (range); C_{max}, $t_{1/2}$, AUC_{0-t}, AUC_{0-inf}, λ_z, CL, V_z, MRT_{0-t} and MRT_{0-inf} are presented as mean ± standard deviation. T_{max}, time to reach maximum concentration; C_{max}, maximum concentration; $t_{1/2}$, elimination half-life; AUC_{0-t}, area under the plasma concentration-time curve from time 0 to last time of quantifiable concentration; AUC_{0-inf}, area under the plasma concentration-time curve from time 0 extrapolated to infinite time; λ_z, elimination rate constant; CL, clearance rate; V_z, apparent volume of distribution; MRT_{0-t}, mean residence time from time 0 to last time of quantifiable concentration; MRT_{0-inf}, mean residence time from time 0 extrapolated to infinite time. $AUC_{\_\% Extrap}$ values are calculated using the percentage of AUC_{0-t} and AUC_{0-inf} values (100%–AUC_{0-t}%/AUC_{0-inf}).

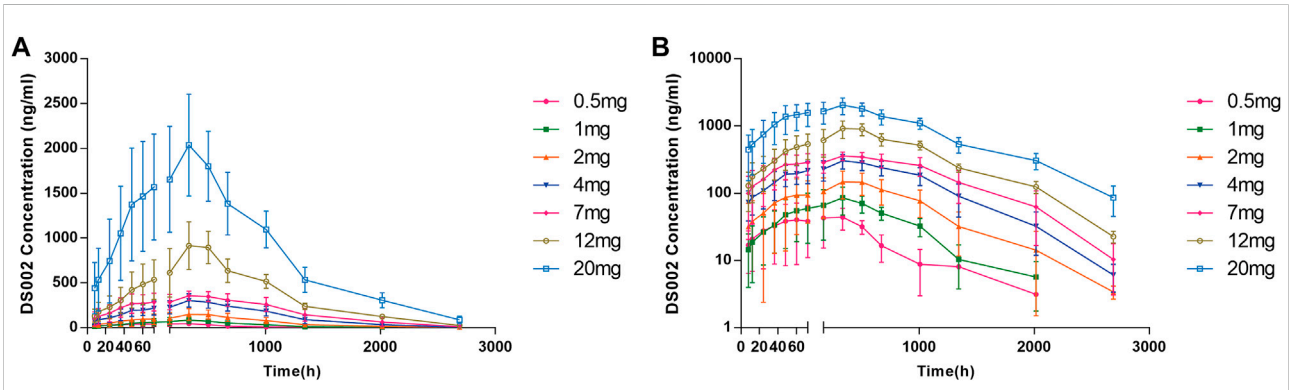

FIGURE 3
Plasma concentration-time profile (PKCS) of DS002. **(A)** DS002 concentrations time curves of subjects; **(B)** Semi-logarithmic curves of DS002 concentrations time of subjects. PKCS, pharmacokinetics concentration set. Data are presented as mean ± SD.

once shelved the development plan for an anti-NGF monoclonal antibody due to safety concerns, this target still has great clinical value and application prospect. Currently, no anti-NGF monoclonal antibody has been approved for clinical use, but three anti-NGF drugs are under development: tanezumab, fulranumab and fasinumab (Enomoto et al., 2019; Zhao et al., 2022). Tanezumab was designated as a fast track (Hochberg et al., 2016). The monoclonal antibody has unique pharmacokinetic parameters such as non-linear pharmacokinetics metabolism, time dependence and long half-life; Target-mediated distribution (TMD) and clearance (TMC) are important pathways for macromolecular drug metabolism. The occurrence of TMD and TMC are the important sources of non-linear PK characteristics. The $t_{1/2}$ of tanezumab is about 21 day (Jonsson et al., 2016), while that of DS002 was around 7–12 days. In the dose range of 0.5–20.0 mg, C_{max}, AUC_{0-t} and AUC_{0-inf} of prototype drug DS002 increased with the increase in dosage. C_{max} and AUC_{0-inf} did not show a significant dose linear relationship, whilst AUC_{0-t}

TABLE 4 DS002 Linear pharmacokinetic analysis of indicators (C_{max}, AUC_{0-t}, AUC_{0-inf}).

Parameters	Dose range (mg)	Interval (%)	Regression equation	Slope		Linear relationship
				Point estimate (%)	90%CI (%)	
C_{max}(ng/mL)	0.5–20.0	93.95–106.49	Y = 0.99*x+4.35	98.77	(90.61,106.92)	Unidentified
AUC_{0-t} (ng·h/mL)	0.5–20.0	93.95–106.49	Y = 1.14*x+10.70	114.27	(107.41,121.13)	No
AUC_{0-inf} (ng·h/mL)	0.5–20.0	93.95–106.49	Y = 1.13*x+10.75	112.69	(106.05,119.33)	Unidentified

C_{max}, maximum concentration; AUC_{0-t}, area under the plasma concentration-time curve from time 0 to last time of quantifiable concentration; AUC_{0-inf}, area under the plasma concentration-time curve from time 0 extrapolated to infinite time. CI, confidence interval.

was not dose dependent at all. The PK parameters of DS002 conform to the metabolic characteristics of monoclonal antibodies. Moreover, the immunogenicity of DS002 injection was low (ADA was negative).

In conclusion, the absorption and metabolism of a single subcutaneous injection of DS002 in healthy subjects were slow, it exhibited a low volume of distribution, and the clearance rate was low. Single subcutaneous injection of DS002 was well tolerated and non-immunogenic within the dose range of 0.5 mg–20.0 mg. The anti-NFG antibody represented by DS002 shows promise as a novel, safe and non-addictive approach for pain treatment. This first-in-human study supports further development of DS002 as a potential analgesic treatment.

Data availability statement

The original contributions presented in the study are included in the article/Supplementary Material, further inquiries can be directed to the corresponding authors.

Ethics statement

The studies involving human participants were reviewed and approved by the ethics committee of Nanjing Drum Tower Hospital, the Affiliated Hospital of Nanjing University Medical School. The participants provided their written informed consent to participate in this study.

Author contributions

CW and JL designed the research. All authors performed the research. TM and CW analyzed the data. TM and RS contributed to the writing of the manuscript.

Funding

This study was funded by the National Natural Science Foundation of China (No. 31371399), Major Scientific and Technological Special Project of Zhongshan City (210205143867019/2021A1012) and Dartsbio Pharmaceuticals, Ltd.

Acknowledgments

The authors would like to thank the following people for their contributions: All volunteers who participated in this study, all the investigators, clinical research associates and clinical research coordinators who participated in supporting the trial.

Conflict of interest

CW was employed by the Company Dartsbio Pharmaceuticals, Ltd. KW was employed by the Company Beijing Highthink Pharmaceutical Technology Service Co., Ltd.

The remaining authors declare that the research was conducted in the absence of any commercial or financial relationships that could be construed as a potential conflict of interest.

Publisher's note

References

Chang, D. S., Hsu, E., Hottinger, D. G., and Cohen, S. P. (2016). Anti-nerve growth factor in pain management: Current evidence. *J. Pain Res.* 9, 373–383. doi:10.2147/JPR.S89061

Cohen, S. P., Vase, L., and Hooten, W. M. (2021). Chronic pain: An update on burden, best practices, and new advances. *Lancet* 397 (10289), 2082–2097. doi:10.1016/S0140-6736(21)00393-7

Coussens, N. P., Sittampalam, G. S., Jonson, S. G., Hall, M. D., Gorby, H. E., Tamiz, A. P., et al. (2019). The opioid crisis and the future of addiction and pain therapeutics. *J. Pharmacol. Exp. Ther.* 371 (2), 396–408. doi:10.1124/jpet.119.259408

Enomoto, M., Mantyh, P. W., Murrell, J., Innes, J. F., and Lascelles, B. D. X. (2019). Anti-nerve growth factor monoclonal antibodies for the control of pain in dogs and cats. *Vet. Rec.* 184 (1), 23. doi:10.1136/vr.104590

Hochberg, M. C., Tive, L. A., Abramson, S. B., Vignon, E., Verburg, K. M., West, C. R., et al. (2016). When is osteonecrosis not osteonecrosis?: Adjudication of reported serious adverse joint events in the tanezumab clinical development program. *Arthritis Rheumatol.* 68 (2), 382–391. doi:10.1002/art.39492

Hooley, J. M., Franklin, J. C., and Nock, M. K. (2014). Chronic pain and suicide: Understanding the association. *Curr. Pain Headache Rep.* 18 (8), 435. doi:10.1007/s11916-014-0435-2

Jayabalan, P., and Schnitzer, T. J. (2016). Tanezumab in the treatment of chronic musculoskeletal conditions. *Expert Opin. Biol. Ther.* 17 (2), 245–254. doi:10.1080/14712598.2017.1271873

Jonsson, E. N., Xie, R., Marshall, S. F., and Arends, R. H. (2016). Population pharmacokinetics of tanezumab in phase 3 clinical trials for osteoarthritis pain. *Br. J. Clin. Pharmacol.* 81 (4), 688–699. doi:10.1111/bcp.12850

Kiyatkin, E. A. (2019). Respiratory depression and brain hypoxia induced by opioid drugs: Morphine, oxycodone, heroin, and fentanyl. *Neuropharmacology* 151, 219–226. doi:10.1016/j.neuropharm.2019.02.008

Schjerning, A.-M., McGettigan, P., and Gislason, G. (2020). Cardiovascular effects and safety of (non-aspirin) NSAIDs. *Nat. Rev. Cardiol.* 17 (9), 574–584. doi:10.1038/s41569-020-0366-z

Shooter, E. M. (2001). Early days of the nerve growth factor proteins. *Annu. Rev. Neurosci.* 24 (1), 601–629. doi:10.1146/annurev.neuro.24.1.601

Tong, Q., Wang, F., Zhou, H.-Z., Sun, H.-L., Song, H., Shu, Y.-Y., et al. (2012). Structural and functional insights into lipid-bound nerve growth factors. *FASEB J.* 26 (9), 3811–3821. doi:10.1096/fj.12-207316

Wise, B. L., Seidel, M. F., and Lane, N. E. (2021). The evolution of nerve growth factor inhibition in clinical medicine. *Nat. Rev. Rheumatol.* 17 (1), 34–46. doi:10.1038/s41584-020-00528-4

Zhao, D., Luo, M.-h., Pan, J.-k., Zeng, L.-f., Liang, G.-h., Han, Y.-h., et al. (2022). Based on minimal clinically important difference values, a moderate dose of tanezumab may be a better option for treating hip or knee osteoarthritis: A meta-analysis of randomized controlled trials. *Ther. Adv. Musculoskelet. Dis.* 14, 1759720X2110676. doi:10.1177/1759720x211067639

frontiers | Frontiers in Pharmacology

TYPE Original Research
PUBLISHED 14 December 2022
DOI 10.3389/fphar.2022.1073535

OPEN ACCESS

EDITED BY
Zhihao Liu,
Dalian Medical University, China

REVIEWED BY
Linling Que,
Wuxi People's Hospital, China
Aijie Zhang,
Chinese Academy of Medical Sciences and Peking Union Medical College, China
Yukuang Guo,
Takeda Oncology, United States

*CORRESPONDENCE
Peiyong Zheng,
zpychina@sina.com
Ming Yang,
yangpluszhu@sina.com

†These authors have contributed equally to this work

SPECIALTY SECTION
This article was submitted to Drug Metabolism and Transport, a section of the journal Frontiers in Pharmacology

RECEIVED 18 October 2022
ACCEPTED 30 November 2022
PUBLISHED 14 December 2022

CITATION
Li X, Chen C, Ding N, Zhang T, Zheng P and Yang M (2022), Physiologically based pharmacokinetic modelling and simulation to predict the plasma concentration profile of schaftoside after oral administration of total flavonoids of *Desmodium styracifolium*. *Front. Pharmacol.* 13:1073535. doi: 10.3389/fphar.2022.1073535

Physiologically based pharmacokinetic modelling and simulation to predict the plasma concentration profile of schaftoside after oral administration of total flavonoids of *Desmodium styracifolium*

Xue Li[1†], Chao Chen[1†], Nan Ding[1], Tianjiao Zhang[1], Peiyong Zheng[2]* and Ming Yang[1,2]*

[1]Phase I Clinical Research Lab, LongHua Hospital, Shanghai University of Traditional Chinese Medicine, Shanghai, China, [2]Clinical Research Center, LongHua Hospital, Shanghai University of Traditional Chinese Medicine, Shanghai, China

Introduction: The total flavonoids of *Desmodium styracifolium* (TFDS) are the flavonoid extracts purified from Desmodii Styracifolii Herba. The capsule of TFDS was approved for the treatment of urolithiasis by NMPA in 2022. Schaftoside is the representative compound of TFDS that possesses antilithic and antioxidant effects. The aim of this study was to develop a physiologically based pharmacokinetic (PBPK) model of schaftoside to simulate its plasma concentration profile in rat and human after oral administration of the total flavonoids of *Desmodium styracifolium*.

Methods: The physiologically based pharmacokinetic model of schaftoside was firstly developed and verified by the pharmacokinetic data in rats following intravenous injection and oral administration of the total flavonoids of *Desmodium styracifolium*. Then the PBPK model was extrapolated to human with PK-Sim® software. In order to assess the accuracy of the extrapolation, a preliminary multiple-dose clinical study was performed in four healthy volunteers aged 18–45 years old. The predictive performance of PBPK model was mainly evaluated by visual predictive checks and fold error of C_{max} and AUC_{0-t} of schaftoside (the ratio of predicted to observed). Finally, the adult PBPK model was scaled to several subpopulations including elderly and renally impaired patients.

Results: Schaftoside underwent poor metabolism in rat and human liver microsomes *in vitro*, and *in vivo* it was extensively excreted into urine and bile as an unchanged form. By utilizing literature and experimental data, the PBPK model of schaftoside was well established in rat and human. The predicted plasma concentration profiles of schaftoside were consistent with the corresponding observed data, and the fold error values were within the 2-fold acceptance criterion. No significant pharmacokinetic differences were observed after

extrapolation from adult (18–40 years old) to elderly populations (71–80 years) in PK-Sim®. However, the plasma concentration of schaftoside was predicted to be much higher in renally impaired patients. The maximum steady-state plasma concentrations in patients with chronic kidney disease stage 3, 4 and 5 were 3.41, 12.32 and 23.77 times higher, respectively, than those in healthy people.

Conclusion: The established PBPK model of schaftoside provided useful insight for dose selection of the total flavonoids of *Desmodium styracifolium* in different populations. This study provided a feasible way for the assessment of efficacy and safety of herbal medicines.

KEYWORDS

physiologically based pharmacokinetic model, schaftoside, total flavonoids of *Desmodium* styracifolium, urolithiasis, rat, human

1 Introduction

Urolithiasis, also known as urinary calculi or stones, is a widespread disease. It is the most frequent diagnosis in the urology departments, and affects 1–20% of the adult population (Li et al., 2020). The prevalence rate of urolithiasis is approximately 5–9% in Europe, 12–15% in North America, and 1–5% in Asia (Ramello et al., 2000; López and Hoppe, 2010). Moreover, the relapse rate of this disease is approximately 50% within the subsequent 5–10 years after the first episode (Fisang et al., 2015). Surgical managements are widely applied to remove the calculi in patients (Jiang et al., 2021). However, the risk of a symptomatic stone episode remains an important unresolved problem due to the stone fragments remaining in the urinary system after the intervention (Ozdedeli and Cek, 2012). To facilitate the passage of ureteral stones, α-blockers or calcium-channel inhibitors are usually recommended, such as tamsulosin, silodosin and nifedipine (Hollingsworth et al., 2006; Turk et al., 2016). Yet, it seems that this class of medicine can only increase passage in larger stones (>5 mm) rather than smaller stones (Hollingsworth et al., 2016). Furthermore, these drugs increase the risk of orthostatic hypotension, which can be particularly problematic in older subjects (Gottlieb et al., 2018). Presently, numerous drugs have been studied for the management of urolithiasis, allopathic medicine are still limitedly available (Ahmad et al., 2021).

The total flavonoids of *Desmodium styracifolium* (TFDS) are the flavonoid-enriched natural extracts purified from Desmodii Styracifolii Herba, which is a traditional herbal medicine for treating urolithiasis in China (Hou et al., 2018). It was reported that TFDS can significantly reduce crystalluria and improve the impaired renal function in the urolithiasis rat models (Zhou et al., 2018). The results of a randomized, double-blind, multi-center clinical trial performed in China (CTR20171265) showed that TFDS had a significant effect on the efficiency of stone removal and improvement of TCM Symptoms. The Capsule of TFDS was approved by National Medical Products Administration (NMPA) in China for the treatment of urinary calculi (https://www.nmpa.gov.cn/yaowen/ypjgyw/20220915152305161.html) in 2022 (Z20220003).

The main active constituents of TFDS are the flavone glycosides, including schaftoside, vicenin-1, vicenin-2, vicenin-3, et al. (Li et al., 2022). Schaftoside is the marker component of *Desmodium styracifolium* in Chinese Pharmacopeia (2020 edition). An *in vivo* study demonstrated that the plasma concentration of schaftoside was the highest among these components after oral intake of TFDS (Li et al., 2022). Previous studies indicated that schaftoside could protect against cholesterol gallstone and calcium oxalate kidney stone formation (Liu et al., 2017; Liu et al., 2020). To some extent, schaftoside is the representative compound of TFDS. Although the pharmacokinetic (PK) characteristics of schaftoside following administration of TFDS have been studied in animals, the PK profiles of it in humans remain unknown (Li et al., 2022).

The crystalline deposits in kidney tubular cells lead to acute or chronic tubular injury and interstitial fibrosis, which contributes to a progressive chronic kidney disease (CKD) (Khan et al., 2016). However, PK studies in the CKD patients are difficult to conduct due to ethical and logistic challenges. Physiologically based pharmacokinetic (PBPK) modeling is a mathematical modeling technique to describe and predict drug disposition in various populations (Jones and Rowland-Yeo, 2013). By integrating population-specific physiologic parameters with drug-specific physicochemical and pharmacokinetics information, PBPK models are increasingly used for the prediction of drug distribution, drug-drug interactions (DDI), transporter evaluation, and extrapolation of drug exposure in age-specific or special subgroups of patients (Jones et al., 2009; Maharaj and Edginton, 2014; Reig-Lopez et al., 2021). However, the application of PBPK modeling for the active ingredients of herbal medicine was limitedly reported. Thus, the aim of this study was to establish a PBPK model of schaftoside after oral administration of TFDS in rats and humans, and to extrapolate the adult PBPK model to several subpopulations including elderly and renally impaired

population for the prediction of plasma concentration-time profiles of schaftoside.

2 Materials and methods

2.1 Chemicals and reagents

TFDS Capsules (0.2 g/capsule), containing 133 mg of TFDS extract with 8.5 mg schaftoside per capsule, and the TFDS APIs were supplied by Humanwell Healthcare (Group) Co., Ltd. The reference standards of schaftoside and sulfamethoxazole were provided by Chinese National Institutes for Food and Drug Control (Beijing, China). Midazolam was supplied by Toronto Research Chemicals INC (Toronto, Canada). D-glucose-6-phosphate disodium salt hydrate, glucose-6-phosphate dehydrogenase, β-nicotinamide adenine dinucleotide phosphate sodium salt hydrate, and midazolam were the products of Sigma-Aldrich Co. (St. Louis, United States). The liver microsomes of rat and human were purchased from Corning Gentest (Woburn, MA, United States). High-performance liquid chromatography (HPLC) grade acetonitrile, methanol and formic acid were supplied by Merck KGaA (Darmstadt, Germany). Ultrapure water was prepared by a Milli-Q water system (Millipore, United States) in our own lab. All the other reagents and solvents were commercially available.

2.2 Software

Pharmacokinetic parameters of schaftoside were calculated by non-compartmental model analysis using Phoenix WinNonlin software (version 8.3, Certara Corporation, United States). The establishment of PBPK models was used PK-Sim v9.0 which is part of the Open Systems Pharmacology suite (www.open-systems-pharmacology.org). The optimization and sensitivity analysis of model input parameters were carried out by PK-Sim. *Python* Software (Version 3.7, https://www.python.org/) was used for graph plotting.

2.3 Metabolic stability in liver microsomes

The *in vitro* metabolic stability of schaftoside was investigated in rat and human liver microsomes. All incubations were conducted in triplicate at 37°C with a final volume of 400 μL. The incubation mixture contained schaftoside (1 μM, 10 μM), liver microsomes (0.5 mg protein/mL), and NADPH-generating system (3.3 mM glucose 6-phosphate, 1.3 mM $NADP^+$, 4 mM $MgCl_2$, and 0.4 U/mL glucose 6-phosphate dehydrogenase) in Tris-HCl buffer (50 mM, pH 7.4). The mixture was incubated for 5 min at 37°C before the addition of NADPH to initiate the reaction. The reaction was terminated by the addition of a 2-fold volume of ice-chilled acetonitrile at specific time points (0, 0.5, 1.0 and 1.5 h). Then the mixture was vortexed for 1 min and centrifuged at 12,000 rpm for 10 min at 4°C. The supernatant was stored at −20°C until HPLC-MS/MS analysis. Midazolam (5 uM) was used as a positive control and the total organic solvent concentration did not exceed 1% (v/v) in the experiment.

2.4 Pharmacokinetic and excretion studies in rats

Male Sprague-Dawley rats (6 weeks, 200–220 g) were purchased from Vital River Experimental Animal Co., Ltd (Beijing, China). The rats were housed under standard laboratory conditions at room temperature (20°C–25°C) with relative humidity (50–60%) and 12-h day/night rhythm cycle. Rats were fasted overnight with free access to water before the experiment. The experimental protocols were approved by the Animal Care and Welfare Committee of Shanghai University of Traditional Chinese Medicine.

For determination of pharmacokinetic characteristics of schaftoside in TFDS, rats were either administered a single intravenous dose of 1.2 mg/kg of schaftoside solution (5% ethanol +5% PEG400 in saline) or an oral dose of 50, 100, or 200 mg/kg TFDS suspension (0.5% CMC-Na, equivalent to 3.03, 6.06, 12.12 mg/kg schaftoside). The oral dose of TFDS was chosen based on the results of our previous pharmacological experiments and relevant literature (Zhou et al., 2018), which showed that the effective dose range of TFDS was between 50 and 400 mg/kg. Due to the low oral bioavailability of schaftoside (<5%), ten percent of the amount of schaftoside in the high-dose group of TFDS (12.12 mg/kg) was selected as the intravenous dose.

Six rats were used per experimental group in the pharmacokinetic studies. Blood samples (approximately 0.15 ml) were collected in 1.5 ml heparinized tubes pre-dose (0 h), and 0.033, 0.083, 0.167, 0.333, 0.50, 0.75, 1, 2, 3, 4, 6, 8, and 12 h post-dose for intravenous dosing, and pre-dose (0 h), and 0.083, 0.25, 0.50, 0.75, 1, 1.5, 2, 3, 4, 6, 8, 12, 24 h post-dose for oral administration. Plasma was prepared by centrifugation at 4,000 rpm for 10 min at 4°C, and samples were stored at −80°C until analysis.

For the excretion studies of schaftoside, six rats received 1.2 mg/kg of schaftoside solution through tail vein injection. Three rats were placed in metabolic cages individually and urine was collected during the following intervals: 0–4, 4–16, 16–24, 24–36, 36–48 h post dosing. Another three rats were anesthetized and cannulated with PE-10 polyethylene tubing for the collection of bile. Bile samples were collected during the following intervals: 0–2, 2–4, 4–16, 16–24, 24–36, 36–48 h post dosing. In addition, urine was collected following the same

protocols after six rats were orally administered 100 mg/kg TFDS suspension. The volumes of urine and bile samples were measured and recorded. Renal clearance (CLr) was calculated through the determination of the total amount of drug excreted in urine (Ae) and drug exposure in plasma (AUC_{0-t}) after a single administration, which was described as $CLr = Ae/AUC_{0-t}$.

2.5 Clinical pharmacokinetic studies in healthy volunteers

This clinical study was an open-label, single-center, single- and multiple-dose study, which was conducted at Longhua Hospital, Shanghai University of Traditional Chinese Medicine. The study protocol was approved by the Institutional Review Board of Longhua Hospital (Approved Number 2019LCSY069) and registered at Chinese Clinical Trials Platform (CTR20192424). All subjects provided written informed consent before this study. The trial strictly complied with the Declaration of Helsinki and the International Conference on Harmonization (ICH) Good Clinical Practice Guidelines.

Four healthy volunteers (two men and two women) aged 18–45 years with body mass index (BMI) of 19–24 kg/m^2 and body weight ≥50 kg were enrolled into this study. Participants were excluded for any abnormal screening laboratory results, HIV/HBV/HCV infection, and clinically significant abnormality on physical examination or electrocardiogram. Additional exclusion criteria included a history of hypersensitivity to study drugs or excipients; drug abuse within the past 12 months or alcohol abuse within the past 6 months; pregnancy; vaccination within 4 weeks; intake of prescription or non-prescription medications within 2 weeks before hospital admission.

The subjects were asked to fast for at least 10 h before the first oral administration. The subjects were orally administered of TFDS Capsules once a day for day 1 and day 6 (0.6 g/day), and three times a day from day 2 to day 5 (0.6 g q 8 h). TFDS Capsules were administered at 08: 00, 16: 00, 00: 00 from day 2 to day 5, and at 08:00 on day 1 and day 6. Venous blood samples (~4 ml) were collected into K_2EDTA vacuum tubes on day 1 and day 6 at pre-dose (0 h) and 0.25, 0.5, 1, 1.5, 2, 2.5, 3, 4, 5, 6, 7, 8, 12, 24 h post-dose. Blood trough samples were collected before the first dose (08: 00) on day 2 to day 5. Plasma was separated from the blood samples by centrifugation at 3,500 rpm for 10 min at 4°C, and stored at −80°C until analysis.

2.6 HPLC-MS/MS analysis

2.6.1 Sample pretreatment

For the rat sample pretreatment, an aliquot of 50 μl plasma/urine/bile sample was spiked with 10 μL of sulfamethoxazole solution (500.0 ng/ml, internal standard) and 240 μl methanol. Then the mixture was vortexed for 1 min and centrifuged at 12,000 rpm for 10 min at 4°C. The supernatant was collected and analyzed by HPLC-MS/MS.

For the human sample pretreatment, an aliquot of 100 μl plasma sample was spiked with 10 μl of sulfamethoxazole solution (100.0 ng/ml) and 500 μl mixed solvent (acetonitrile: methanol = 3:2, v/v). Then the mixture was vortexed for 1 min and centrifuged at 12,000 rpm for 10 min at 4°C. The supernatant was dried for 3 h at 30°C using a vacuum centrifugal concentrator (Concentrator plus, Eppendorf AG, Hamburg, Germany). The residues were reconstituted with 100 μl of 50% methanol and centrifuged again. The supernatant was analyzed by HPLC-MS/MS.

2.6.2 Instrumentation and chromatographic conditions

The plasma concentration of schaftoside was determined using a liquid chromatography tandem mass spectrometry method (HPLC-MS/MS) as previously reported (Li et al., 2022). Briefly, the HPLC-MS/MS system was comprised of an Agilent 1260 HPLC system and a tandem mass spectrometer (AB SCIEX QTRAP®5500, Canada). The chromatographic separation was performed on an ACQUITY UPLC HSS T3 column (1.8 μm, 2.1 mm i. d. × 50 mm; Waters, United States), and a gradient elution was adopted using water containing 0.1% (v/v) formic acid (A) and methanol (B) as the mobile phase. The following gradient program was used: 0–1.0 min, 10% B; 1.0–4.0 min, 10–30% B; 4.0–6.0 min, 30–50% B; 6.0–10.0 min, 50% B; 10.0–11.0 min, 50–10% B; 11.0–15.0 min, 10% B. Mass spectrometry was performed under negative electrospray ionization condition. The selected mass transitions for schaftoside and its internal standard sulfamethoxazole were m/z 563.2→353.2 and m/z 252.0→156.0, respectively.

The calibration curves for schaftoside in rat and human plasma samples were linear over ranges from 0.5 to 200 ng/ml and 0.05–10 ng/ml, respectively. The analytical methods were well validated in this study. The intra-day and inter-day precision and accuracy values met the acceptance criteria (± 15%) according to the FDA and NMPA guidelines.

2.7 Establishment of PBPK models

The overall scheme of the PBPK model-building workflow including development, verification, and application is listed in Figure 1. Briefly, the PBPK model of schaftoside was firstly built for rats, which was subsequently evaluated with experimental data to promote confidence in the parametrization of the model, and then the model was scaled to humans. The basic physicochemical and biopharmaceutical parameters of schaftoside were mainly gained from the literature, online

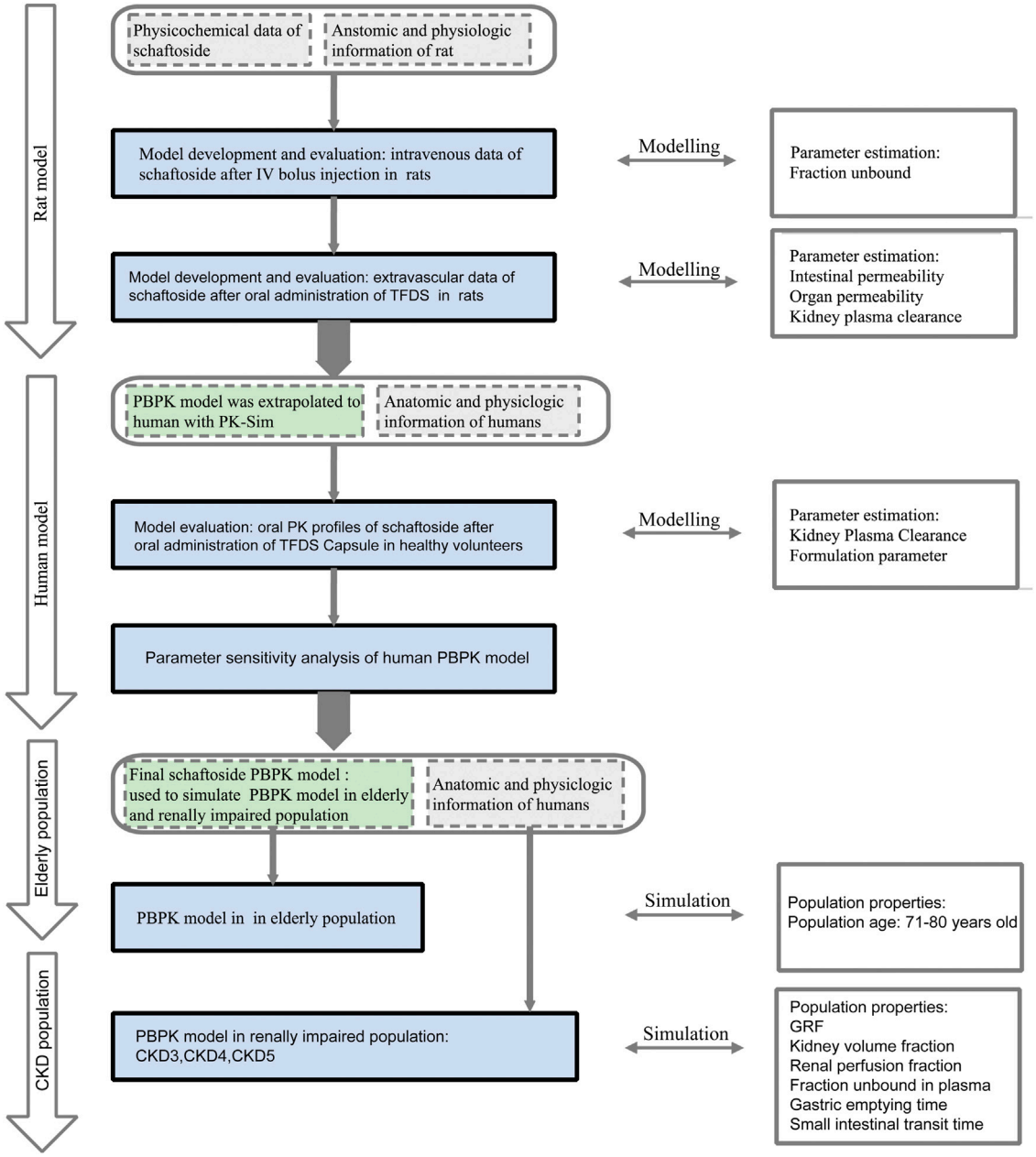

FIGURE 1
Schaftoside PBPK model-building workflow in rats and humans after oral administration of TFDS. The overall scheme included development, verification, and application.

databases and PK-Sim® software prediction and optimization (Table 1) (Mendez et al., 2019; Shen et al., 2021). The default physiological parameters of animals and humans in software were modified to represent our experiments such as weight, age and gender. All relevant anatomical and physiological parameters for rat and human including tissue volume, blood flow and vascular permeability were contained in the integrated database within the software.

By utilizing the plasma concentration data of schaftoside after a bolus intravenous injection of this chemical, the elimination PK model of schaftoside in rats was firstly established. After getting accurate distribution and elimination parameters, a PBPK model for extravascular administration was further developed. The parameters related with absorption, distribution and metabolism/excretion were fixed and modified (Kuepfer et al., 2016). In this study, the plasma

TABLE 1 Parameters used to establish the PBPK models of schaftoside in rat and human.

Parameter	Value	Unit	Source	Description
Mwt	596.494	g/mol	ZINC000084817379[a]	Molecular weight
LogP	−2.427	—	ZINC000084817379[a]	Lipophilicity
Acidic_pKa	6.35	—	CHEMBL532274[b]	First acid dissociation constant
Solubility (PH-7)	0.02	g/L	Calculated by XLOGS[c]	Solubility
f_u	26.65%	%	Optimized	Fraction unbound
Intestinal permeability	1.08*1E-4	dm/min	Optimized	Transcellular intestinal permeability
Organ permeability	2.98*1E-6	cm/s	Optimized	Organ permeability
Formulation (rat)	Suspension	—	—	—
Kidney Plasma Clearance (rat)	2.57*1E-3	L/min/kg	Optimized	Kidney Plasma Clearance
Dis time (rat)	0.92	Min	Optimized	Dissolution time (50% dissolved)
Dis shape (rat)	1.08*1E-3	—	Optimized	Shape parameter of Welbull function
Formulation (Human)	Capsule	—	—	—
Kidney Plasma Clearance (human)	1.24*1E-3	L/min/kg	Optimized	Kidney plasma clearance
Dis time (human)	8.16	Min	Optimized	Dissolution time (50% dissolved)
Dis shape (human)	3.74*1E-4	—	Optimized	Shape parameter of Welbull function

[a]Available at https://zinc.docking.org/substances/ZINC000084817379/
[b]Literature report (Mendez et al., 2019).
[c]Available at http://www.sioc-ccbg.ac.cn/?p=42&software=xlogs

concentration data of schaftoside after an oral dose of 100 mg kg^{-1} TFDS suspension were used to perform and optimize the extravascular PBPK model. The plasma concentration profile of schaftoside obtained from the dose groups of 50 and 200 mg/kg were used for the validation of PBPK model.

For the development of human PBPK model for schaftoside after oral administration of TFDS Capsules, the formulation of drug was changed from suspension to capsule, so we reset the parameters of dissolution time and shape. We selected the pre-existing individual option in PK-Sim® software which was a 28-year-old Japanese male with 56.35 kg of body weight and 162.1 cm of height. In order to assess the accuracy of the extrapolation, the predicted and observed data obtained from a clinical PK study performed in healthy volunteers were compared.

2.8 PBPK model validation

The predictive performance of PBPK model was mainly evaluated by visual predictive checks, fold error of each concentration-time points and main PK parameters such as C_{max} and $AUC_{0\text{-}t}$. Agreement between the predicted and observed profiles was evaluated by comparing the predicted mean concentration-time profiles with mean observed data in goodness-of-fit plots. The observed data were obtained from our experimental data and previous literature reports (Li et al., 2022).

The fold error of each point (FE_i), average fold error (AFE) and absolute average fold error (AAFE) were three commonly used test criteria to evaluate the accuracy of models (Tan et al., 2021). FE_i showed the predictive accuracy of data at time point *i*, as calculated in Eq. 1. AFE showed whether the predicted profile overestimated or underestimated the observed values, as calculated in Eq. 2 (Huang and Isoherranen, 2020). AAFE indicated the absolute error from the observed values, as calculated in Eq. 3 (Rasool et al., 2021).

$$FE_i = \frac{Predicted_i}{Observed_i} \tag{1}$$

$$AFE = 10^{\frac{1}{n}*\sum log\left(\left|\frac{Predicted_i}{Observed_i}\right|\right)} \tag{2}$$

$$AAFE = 10^{\frac{1}{n}*\sum\left|log\left(\frac{Predicted_i}{Observed_i}\right)\right|} \tag{3}$$

In which $predicted_i$ is the predicted concentration at time point *i*, $observed_i$ is the observed concentration at time point *i*, *n* is the number of time points. For each point, it can be considered as a successful simulation if the FE_i ranges from 0.3 to 3 and the *AFE* and *AAFE* both range from 0.5 to 2.

The fold error (FE) of PK parameters (C_{max} and $AUC_{0\text{-}t}$) was also commonly used to evaluate the accuracy of prediction (Eq.

4). A good prediction model is achieved when FE is between 0.5 and 2 (Ke et al., 2022).

$$FE = \frac{Predicted\ values\ of\ parameter}{Observed\ values\ of\ parameter} \quad (4)$$

2.9 Parameter sensitivity analysis

Parameter sensitivity analysis was performed using PBPK model established in human with the sensitivity analysis tool provided with the PK-Sim® software (Yellepeddi and Baker, 2020). C_{max} and $AUC_{0\text{-}t}$ of schaftoside were evaluated to find out the key factors that influenced the simulated schaftoside plasma concentration-time profiles.

Sensitivities of the PBPK models were calculated as the relative changes of the predicted PK parameter of schaftoside to the relative variation of model input parameters. The analyses were investigated with a relative perturbation of initial input values of 10%. Sensitivity analysis to a model parameter was calculated as follows:

$$S = \frac{\Delta PK}{\Delta p} \cdot \frac{p}{PK} \quad (5)$$

where S is the sensitivity of the PK parameter to the examined model parameter, ΔPK is the difference between the values of PK values in the new simulation and the original simulation. PK is the simulated value with the original parameter value, p is the original input parameter and Δp is the change of the p.

The sensitivity value of −1.0 shows that a 10% increase of the parameters causes a 10% decrease of the PK parameter values, and a sensitivity of +0.5 implies that a 10% increase of the parameters causes a 5% increase of the PK parameter values (Kovar et al., 2020).

2.10 PBPK model prediction in elderly and renally impaired population

The PBPK model in adults was scaled to elderly individuals by adjusting age to 70 years old. The changes of whole-body anatomical and physiological parameters related based on age were induced using the in-built calculation methods and integrated database in PK-Sim® software. Population simulations were used to quantify the relationship between PK parameter and inter-individual variability. It was designed in PK-Sim to create a virtual population using manual settings for the number of simulated subjects, sex ratio, age range, *etc.* Simulations of elderly population were conducted by setting with 100 subjects with 50% male, age ranging from 71 to 80 years based on elderly individual parameters.

For the renal impairment simulations, 100 subjects with 50% male, age ranging from 18 to 40 years with demographic properties according to the clinical study data were created. CKD is the most prevalent form of renal impairment. In this study, we used three levels of CKD, classified based on the GFR ranges 30–60, 15–30, and <15 ml/min/1.73 m^2 (Yoon et al., 2019). PBPK models for populations with "healthy" "CKD *stage3*" "CKD *stage4*" "CKD *stage5*" were established, respectively. The final virtual healthy individual models were replaced with individuals whose parameter sets were adapted for renal impairment meanwhile the parameters of drug were left unchanged. The whole-body anatomy and physiology in patients throughout the progressive stages of CKD such as kidney volume fraction, renal perfusion fraction, fraction unbound in plasma, gastric emptying time and small intestinal transit time were changed according to literatures (Malik et al., 2020). Changes in the physiological parameters, resulting from decreased renal function, were listed in Table 2. Single-dose (0.6 g or 1 g) and multi-dose simulations (0.6 g q 8 h or 1 g q 8 h) of TFDS Capsules were performed in patients with different stages of renal impairment. The influence of renal impairment on plasma exposure of schaftoside was conducted *via* visual inspection of the plasma concentration time profile and by comparison of PK parameters (Cui et al., 2021).

3 Results

3.1 *In vitro* metabolism by liver microsomes

The results of microsomal metabolic stability of schaftoside are shown in Figure 2. After 1.5 h incubation with rat liver microsomes, the remaining amount of schaftoside accounted for 102.66 ± 2.41% (C_0 = 1 μM) and 97.66 ± 3.30% (C_0 = 10 μM) of the initial amounts. Similar to the results above, the residual schaftoside amounts in human liver microsomes were 100.25 ± 1.04% (C_0 = 1 μM) and 98.36 ± 1.34% (C_0 = 10 μM) after 1.5 h. In contrast, midazolam (5 μM), a representative substrate of CYP3A4/5 enzyme, was metabolized quickly in rat and human liver microsomes, in which the residual amounts of midazolam were 0.24 ± 0.05% and 13.47 ± 0.75%, respectively. These results indicated schaftoside was poorly metabolized by the liver microsomes.

3.2 Pharmacokinetic and excretion studies in rat

The mean concentration-time profiles and pharmacokinetic parameters of schaftoside in rats are presented in Figure 3 and Table 3, respectively. After a single intravenous injection at 1.2 mg/kg dose, the mean maximum plasma concentration (C_{max}) of schaftoside in rats reached 5567.22 ng/ml. Schaftoside was quickly eliminated from the blood circulation

TABLE 2 Categorical parameters in healthy adults and renally impaired patients with different CKD stages (age range: 18–40, 50% female).

Parameter	Fraction of Healthy Values (normal Coefficient of Variation %)			
	Healthy	Stage 3	Stage 4	Stage 5
	110.57 ml/min/1.73 m^2	30–60 ml/min/1.73 m^2	15–30 ml/min/1.73 m^2	<15 ml/min/1.73 m^2
GRF	110.57	60.00	30.00	15.00
Kidney volume fraction	1.00	0.81	0.61	0.51
renal perfusion fraction	1.00	0.55	0.36	0.29
Fraction unboun in plasma	1.00	1.07	1.16	1.55
Gastric emptying time	1.00	1.00	1.60	1.60
Small intestinal transit time	1.00	1.00	1.40	1.40
Large intestinal transit time	1	1	1	1

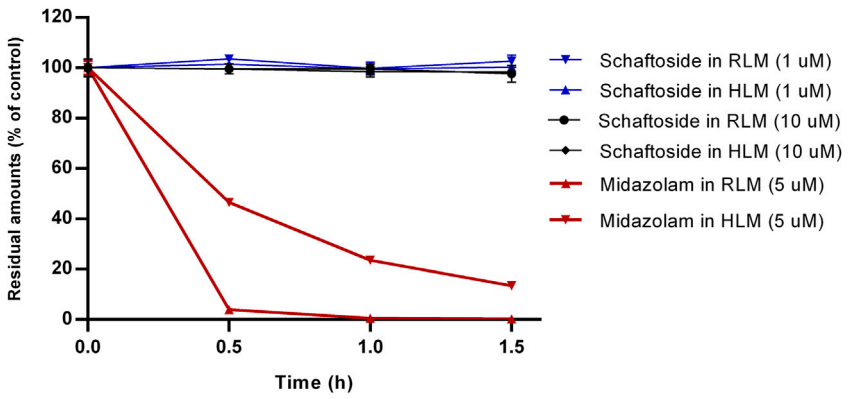

FIGURE 2
In vitro metabolism of schaftoside in rat liver microsomes (RLM) and human liver microsomes (HLM). Midazolam, a representative substrate of CYP3A4/5 enzyme in liver microsomes, was used a positive control of this study.

with a terminal half-life ($t_{1/2}$) of 0.64 h. Meanwhile, schaftoside exhibited a low volume of distribution in rats following the intravenous administration. After oral administration of TFDS suspension at 50, 100 and 200 mg/kg doses, the plasma concentration of schaftoside reached its peak at 0.25–1.50 h. Schaftoside plasma exposures were generally proportional to the administered doses. The C_{max} and $AUC_{0\text{-}t}$ values of schaftoside in low, medium, high groups were 23.17, 46.25, 91.75 ng/ml and 76.39, 204.75, 357.09 hng/mL, respectively. In addition, no significant between-group differences were observed in $t_{1/2}$, Vz_F and CL_F variables.

In the current study, the excretion pathways of schaftoside in rats were firstly investigated after an intravenous injection of schaftoside solution. After drug administration, the total cumulative urinary and biliary excretion of schaftoside accounted for 54.59 ± 9.11% and 24.78 ± 3.07% of the dose, respectively (Figure 4). The calculated renal clearance was 50.67 ± 11.67 ml/h (Table 3; Figure 3, Figure 4). Moreover, the cumulative urinary amounts of schaftoside were measured in rats after oral administration of TFDS, and the results showed 57.56 ± 5.88% of the absorbed schaftoside were was excreted unaltered through kidney. The results indicated that the urinary and biliary excretions of the parent form are the major elimination routes of schaftoside.

3.3 Clinical pharmacokinetic studies in healthy volunteers

In the current study, 29 subjects signed informed consent, and 4 subjects met all the enrollment criteria and entered the

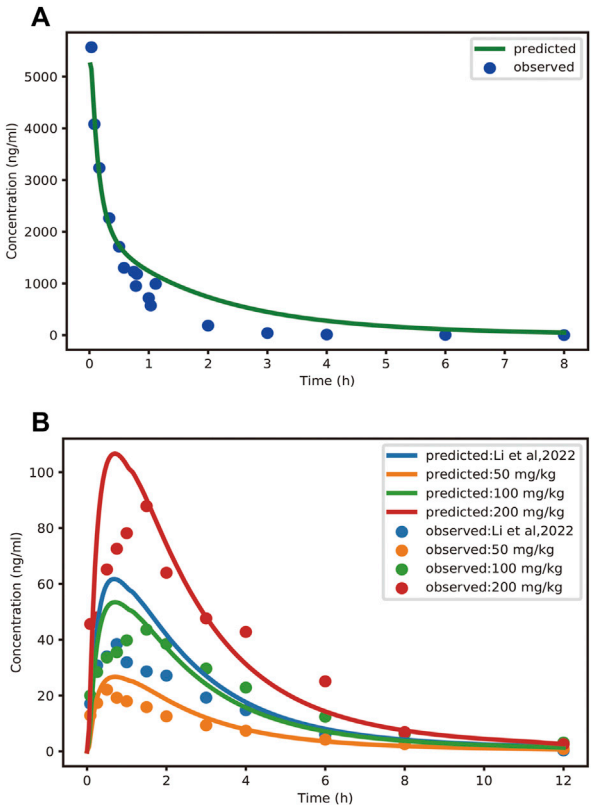

FIGURE 3
Observed and PBPK-model-predicted plasma concentration-time profiles of schaftoside after intravenous injection of schaftoside solution **(A)** and oral administration of TFDS suspension **(B)**. Solid circles represent observed mean data, and solid lines represent the profiles predicted from the PBPK model in PK-Sim. Doses were 1.2 mg/kg (iv) and 50, 100, 200 mg/kg (po), respectively. Additionally, the dose of TFDS in the previous report (Li et al., 2022) is 100 mg/kg.

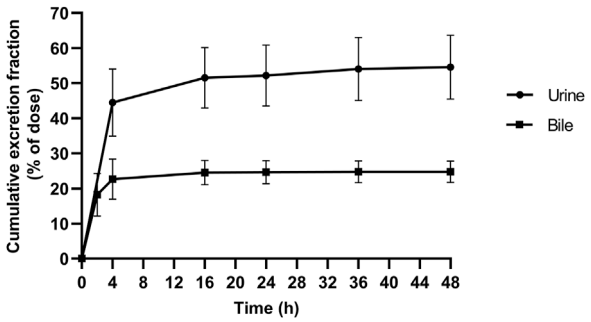

FIGURE 4
Cumulative excretion of schaftoside into urine and bile after an intravenous administration in rats.

clinical trial. The primary reasons for exclusion included withdrawal of consents, electrocardiographic abnormality, and liver or kidney function alterations. All participants completed this study. Demographic data on the participants (4 subjects) showed the mean age was 28 years old (range: 23–32 years old) and 50% were female. The body mass index ranged from 20.8 to 21.9 kg/m^2 and the median index was 21.5 kg/m^2. No serious adverse events related to the drug were observed during the clinical trial.

The pharmacokinetic parameters of schaftoside in human subjects following single- and multiple-dose administration of TFDS Capsules are shown in Table 4, and the concentration-time profiles are presented in Figure 5. After the oral dose of TFDS Capsules on day 1 (0.6 g), the maximum concentration of schaftoside was reached within 1.0–1.5 h. The mean C_{max} and AUC_{0-t} values were 2.43 ng/ml and 13.19 hng/mL, respectively. The plasma concentrations were close to the detection limit (0.05 ng/ml) at 12 h after dosing. In the multiple-dose part, the trough concentration of schaftoside was determined for 3 consecutive days. The mean trough concentrations on day 3, 4 and 5 were 0.72, 0.64, 0.70 ng/ml, respectively. The values were analyzed by one-way ANOVA, and no significant differences were observed ($p > 0.05$). Therefore, steady-state of schaftoside concentrations appeared to be achieved after three doses of TFDS Capsules. Compared with the first-dose on day 1, the C_{max} and AUC_{0-t} values of schaftoside on day 6 were slightly elevated. The R_{Cmax} (ratio of C_{max6} *versus* C_{max1}) and R_{AUC} (ratio of AUC_{last6} *versus* AUC_{last1}) were 1.64 and 1.23, respectively. The accumulation index of schaftoside was 1.12 in this study.

TABLE 3 Pharmacokinetic parameters of schaftoside in rats after intravenous bolus of schaftoside solution or oral administration of TFDS suspension (n = 6). Data are presented as the mean ± standard deviation except for T_{max} as median (range).

Drug	Dose (mg/kg)	C_{max} (ng/ml)	t_{max} (h)	AUC_{0-t} (h·ng/mL)	$t_{1/2}$ (h)	Vz_F (L/kg)	CL_F (L/h/kg)
Schaftoside (iv)	1.2	5567.22 ± 1007.46	—	2776.80 ± 449.16	0.64 ± 0.10	0.41 ± 0.10	0.44 ± 0.07
TFDS (po)	50[a]	23.17 ± 5.07	0.50 (0.25–1.5)	76.39 ± 20.26	2.22 ± 0.47	132.72 ± 26.39	39.00 ± 9.76
TFDS (po)	100[b]	46.25 ± 15.94	1.00 (0.50–1.50)	204.75 ± 59.50	2.18 ± 0.53	114.70 ± 44.07	30.22 ± 9.87
TFDS (po)	200[c]	91.75 ± 18.59	1.25 (0.50–1.50)	357.09 ± 123.71	2.03 ± 0.09	105.42 ± 29.09	35.86 ± 9.31

[a,b,c]Equivalent to 3.03, 6.06, 12.12 mg/kg schaftoside, respectively.

TABLE 4 Pharmacokinetic parameters of schaftoside in human subjects (n = 4) after single- and multiple-dose of TFDS Capsules. Data are presented as the mean ± standard deviation except for T_{max} as median (range).

Variable	Units	Day 1	Day 6
C_{max}	ng/mL	2.43 ± 1.00	4.32 ± 3.54
T_{max}	h	1.25 (1.00–1.50)	1.50 (1.00–2.00)
AUC_{0-t}	h·ng/mL	13.19 ± 4.16	15.62 ± 5.77
$t_{1/2}$	h	1.62 ± 0.21	2.41 ± 0.86
Cl_F	L/h	2048 ± 655	—
Vz_F	L	4740 ± 1530	—
Vss	L	—	6845 ± 2668
C_{avg}	ng/mL	—	1.69 ± 0.65
$AUC_{\_TAU}$	h·ng/mL	—	13.55 ± 5.19

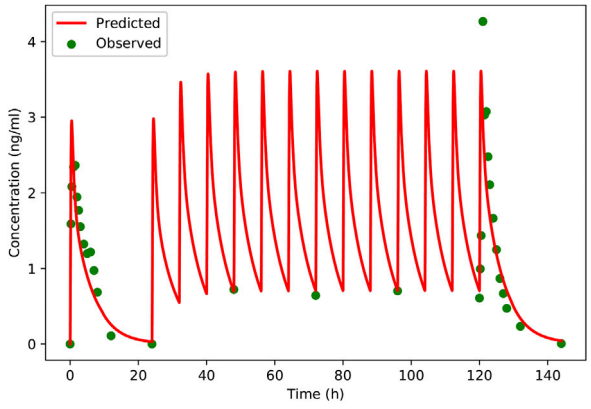

FIGURE 5
Predicted and observed plasma concentration-versus-time profiles of schaftoside after single- and multiple-dose of TFDS Capsules to healthy volunteers (two male and two female). Clinically observed data are shown as dots; solid lines indicate the model prediction.

3.4 PBPK modelling and evaluation in rat and human

In this study, the PBPK model was initially optimized and validated in rats by using the obtained preclinical data. The observed and predicted plasma concentration-time profiles of schaftoside in rat are presented in Figure 3, and the predicted and observed values of PK parameters such as C_{max} and AUC_{0-t} are shown in Table 5. As shown in Figure 3, the predicted plasma concentration profiles of schaftoside were in close concordance with observed data except that the predicted maximum plasma concentration was generally higher than the observed values in the oral intake groups. The fold error (FE) of C_{max} ranged from 0.94 to 1.41, and FE of AUC_{0-t} was between 0.87 and 1.65, which all fell within the 2-fold acceptance criterion (Table 5). These results indicated that the PBPK model successfully predicted schaftoside pharmacokinetics in rats.

A PBPK model was constructed for the healthy adults based on the rat model, and then the model was verified using clinical PK data. The predicted and observed plasma concentration-time profiles of schaftoside in human are presented in Figure 5. As shown in the figure, the predicted plasma profiles are in close agreement with the observed data. The pharmacokinetic parameters of schaftoside were calculated for day 1 and day 6. The predicted C_{max} and AUC_{0-t} values were 1.38- and 1.05-fold of the observed data in the single-dose section (day 1), while the predicted values for C_{max} and AUC_{0-t} of in the multi-dose regimens were 0.95 and 1.18 (day 6). The fold error of PK parameters met the acceptance criteria of 2-fold.

In order to further evaluate the accuracy of the PBPK models in rat and human, each point of the models was validated by FEi. As shown in Figure 6, most of the FEi values were close to 2, but there were a few outliers. The FE_i value of time at 12 h of model in rat simulating 100 mg/kg TFDS (literature report) was without 3-fold error (FE_i = 4.47. These may be caused by experiment errors in the blood sampling or detection for the last time point (Tan et al., 2021). In addition, the AFE and AAFE values for models in rat and human were all within 2-fold error (Table 5). These results indicated the PBPK models in rat and human are accurate and reliable.

3.5 Parameter sensitivity analysis

The results of parameter sensitivity analysis performed on the human PBPK model are demonstrated in Figure 7. Figures 7A,B suggested that the predicted C_{max} values of schaftoside both on day 1 and day 6 were most sensitive to changes in the dissolution shape of drugs. The parameter was also sensitive to changes in fraction unbound, gastric emptying time, kidney-volume, kidney-plasma clearance, and kidney-specific blood flow rate. Whereas, C_{max} was insensitive to the following factors: pKa value 0, solubility at reference pH, solubility gain per charge. Figures 7C,D showed the AUC_{0-t} values of schaftoside both on day 1 and day 6 were significantly sensitive to dissolution shape, kidney-volume, kidney-plasma clearance and fraction unbound. In addition, the AUC_{0-t} was also influenced by kidney-specific blood flow rate, intestinal permeability, large intestinal transit time and small intestinal transit time. However, the influences of gastric emptying time, solubility, pKa, and lipophilicity on AUC_{0-t} were not significant. Altogether, "dissolution shape", "fraction unbound", "kidney-volume", and "kidney-plasma clearance" were identified to be the key factors that influenced the simulated schaftoside plasma concentration-time profiles in human.

TABLE 5 Predicted and observed pharmacokinetic parameters of schaftoside in rats. The accuracy of the prediction is expressed as fold error (the ratio of predicted to observed).

	1.2 mg/kg (schaftoside, iv)		50 mg/kg (TFDS, po)[a]		100 mg/kg (TFDS, po)[b]		200 mg/kg (TFDS, po)[c]		100 mg/kg (TFDS, po)[d]	
	C_{max} (ng/mL)	AUC_{0-t} (h·ng/mL)	C_{max} (ng/mL)	AUC_{0-t} (h·ng/mL)	C_{max} (ng/mL)	AUC_{0-t} (h·ng/mL)	C_{max} (ng/mL)	AUC_{0-t} (h·ng/mL)	C_{max} (ng/mL)	AUC_{0-t} (h·ng/mL)
Observed	5567.22	2776.8	23.17	76.39	46.25	204.75	91.75	357.09	43.86	127.56
Predicted	5230.70	4587.42	26.69	89.09	53.41	178.26	106.64	356.62	61.72	201.76
FE	0.94	1.65	1.15	1.17	1.15	0.87	1.16	1.00	1.41	1.58
AFE	—		1.03		0.86		1.02		1.51	
AAFE	—		1.35		1.47		1.33		1.64	

[abc]Equivalent to 3.03, 6.06, 12.12 mg/kg schaftoside, respectively.
[d]Data from literature report (Li et al., 2022).

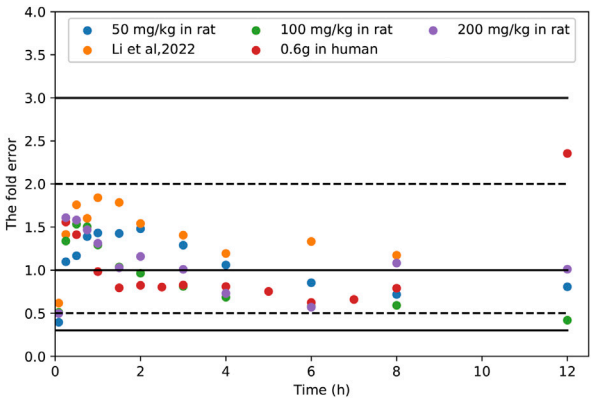

FIGURE 6
The fold errors of all the predicted and observed concentration points (FE_i) in Figure 3 and Figure 5. The data was calculated by $Predicted_i/Observed_i$. The 2-fold and 3-fold errors are indicated by dashed and solid black lines, respectively.

3.6 PBPK simulation in elderly and renally impaired population

Following verification of the model in healthy volunteers, the PK-Sim was used to predict systemic exposure in elderly population and patients with "CKD *stage3*" (GFR = 60 ml/min/1.73 m^2), "CKD *stage4*" (GFR = 30 ml/min/1.73 m^2) and "CKD *stage5*" (GFR = 15 ml/min/1.73 m^2). In order to further evaluate the safety of the drug in renally impaired patients, we also simulated healthy population taking a high dose of TFDS Capsules (1 g q 8 h), which was confirmed to be a safe dose in previous clinical study. The PK profiles of schaftoside in special subgroups were compared with those in the healthy population (18–40 years old).

The predicted schaftoside plasma concentration-time profiles for these populations (n = 100) are shown in Figure 8. The predicted C_{max} and AUC_{0-t} values of schaftoside in the high-dose group (1 g) were 1.67 times higher than that in the regular-dose group (0.6 g) following single- and multiple-dose administration of TFDS in healthy population. Compared to the healthy subjects, the plasma exposure of schaftoside was higher in CKD patients. After the single dose of 0.6 g TFDS, the mean AUC_{0-t} values in CKD3, CKD4, CKD5 patients were 2.14, 3.47, 4.02-fold of the data in healthy population (0.6 g), but the maximum plasma concentration of schaftoside did not differ significantly in these populations (Table 6). After multiple-dose administration (0.6 g q 8 h), the mean C_{max} and AUC_{0-t} values on day 6 were increased by 0.72, 2.62, 4.91-fold and 2.41, 11.32, 22.77-fold, respectively, in CKD3, CKD4, CKD5 patients. Additionally, compared to the high-dose group of TFDS (1 g) in the healthy population, the plasma exposure (C_{max} and AUC_{0-t}) of schaftoside in the regular-dose group (0.6 g) were increased more than two times for the patients with CKD4-5. Furthermore, the drug exposure in the elderly population was explored in this study. The plasma concentrations of schaftoside after oral administration of TFDS did not vary greatly between elderly people (71–80 years) and adult population (18–40 years).

4 Discussion

With the rapid development of economies over the past few decades, the incidence of urolithiasis is increasing annually worldwide (Raheem et al., 2017). For example, the prevalence was increased from 5.95% to 10.63% during the period 1991–2016 in mainland China (Wang et al., 2017). Although surgery operations and various drugs are used to treat urolithiasis, high recurrence and side effects of drugs are still problematic. Flavonoids are a large group of plant polyphenols in

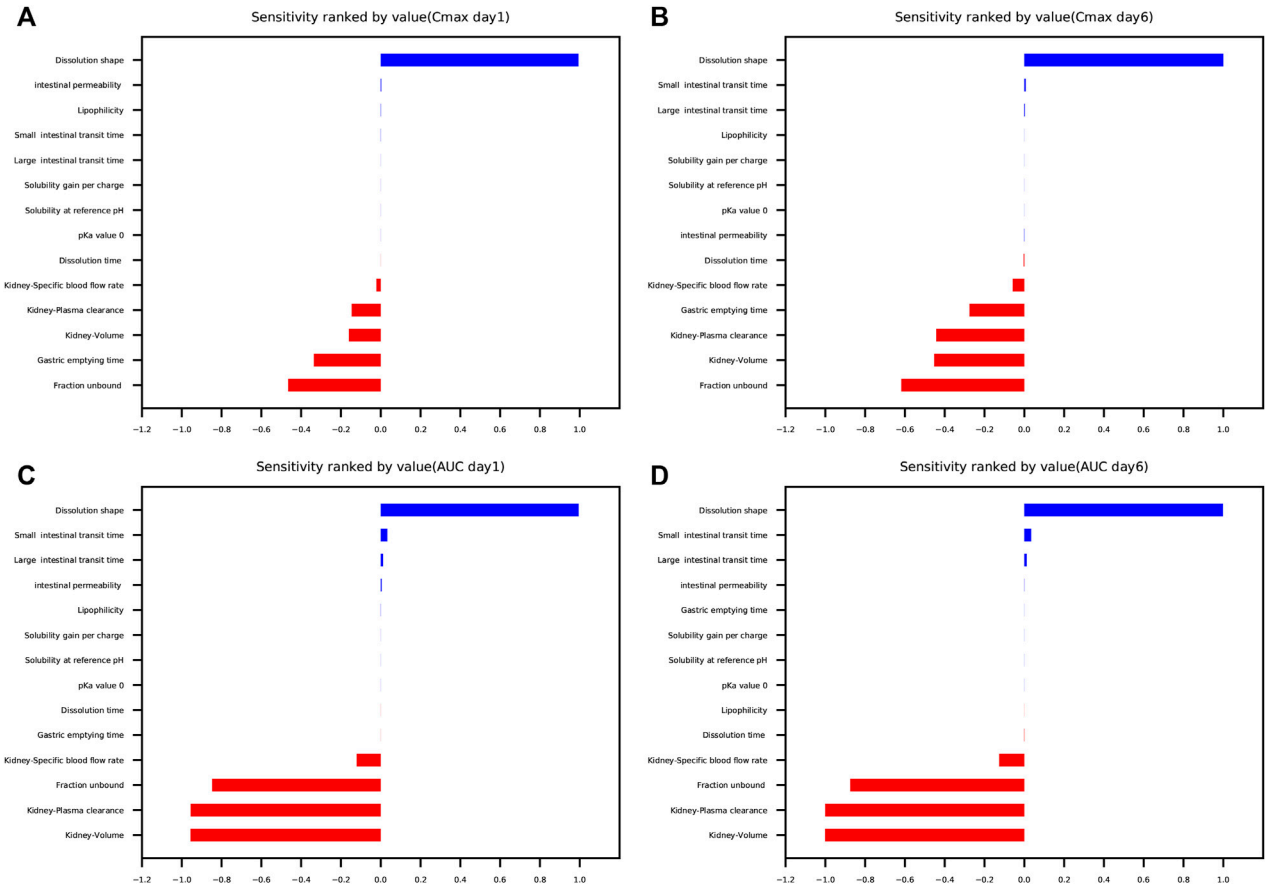

FIGURE 7
Parameter sensitivity analysis performed on the human PBPK model with PK-Sim®. Sensitivity was measured as the relative changes of C_{max} on day 1 **(A)**, C_{max} on day 6 **(B)**, AUC_{0-t} on day 1 **(C)**, AUC_{0-t} on day 6 **(D)** of schaftoside in the clinical study. Variation range was 0.1 with maximum number of steps = 2.

nature which are endowed with pleiotropic activities, such as anti-crystallization of stones, antioxidant, anti-inflammatory and other protective effects (Zeng et al., 2019). Thus, flavonoids are presumed to have beneficial effects on the disease, yet a very few of them have reached clinical use. Therefore, it is exciting when the total flavonoids of *Desmodium styracifolium* (TFDS) have shown good efficacy and tolerability in randomized clinical trials. However, many unresolved questions remain, such as the PK profiles of active constituents in human, the safety and efficacy in patients with impaired kidney or liver function, and the dosage recommendations across a wide range of ages. To address these issues, we developed a PBPK model in human to predict the plasma concentration profile of schaftoside in different populations. This method could provide useful insight for safety evaluation and dose selection of TFDS.

There are many tricky problems to be solved about the development of PBPK models of herbal medicines. Herbal extracts usually contain complex chemical compositions, and interactions between the components may influence the establishment of PBPK models. Metabolism mediated by intestinal microflora or hepatic enzymes is one of the most important factors restricting the building of models (Meng and Liu, 2014; Feng et al., 2019). Therefore, we conducted *in vitro* and *in vivo* experiments to investigate the metabolic features of schaftoside. The *in vitro* results showed schaftoside underwent poor metabolism in rat and human liver microsomes, and *in vivo* studies demonstrated schaftoside was mainly excreted into the urine (~55%) and bile (~25%) in forms of the parent drug itself, rather than various metabolites. To compare the metabolic characteristics of schaftoside in pure form and mixture, we analyzed the drug components and metabolites in rats after oral administration of TFDS in previous studies, and no obvious phase I and II metabolites of schaftoside were observed (data not shown). These findings indicated the possibility of metabolism-mediated interactions was relatively small between schaftoside and other compounds in TFDS. In line with our results, Tremmel and colleagues reported schaftoside underwent poor metabolism in an intestinal and epithelial metabolism

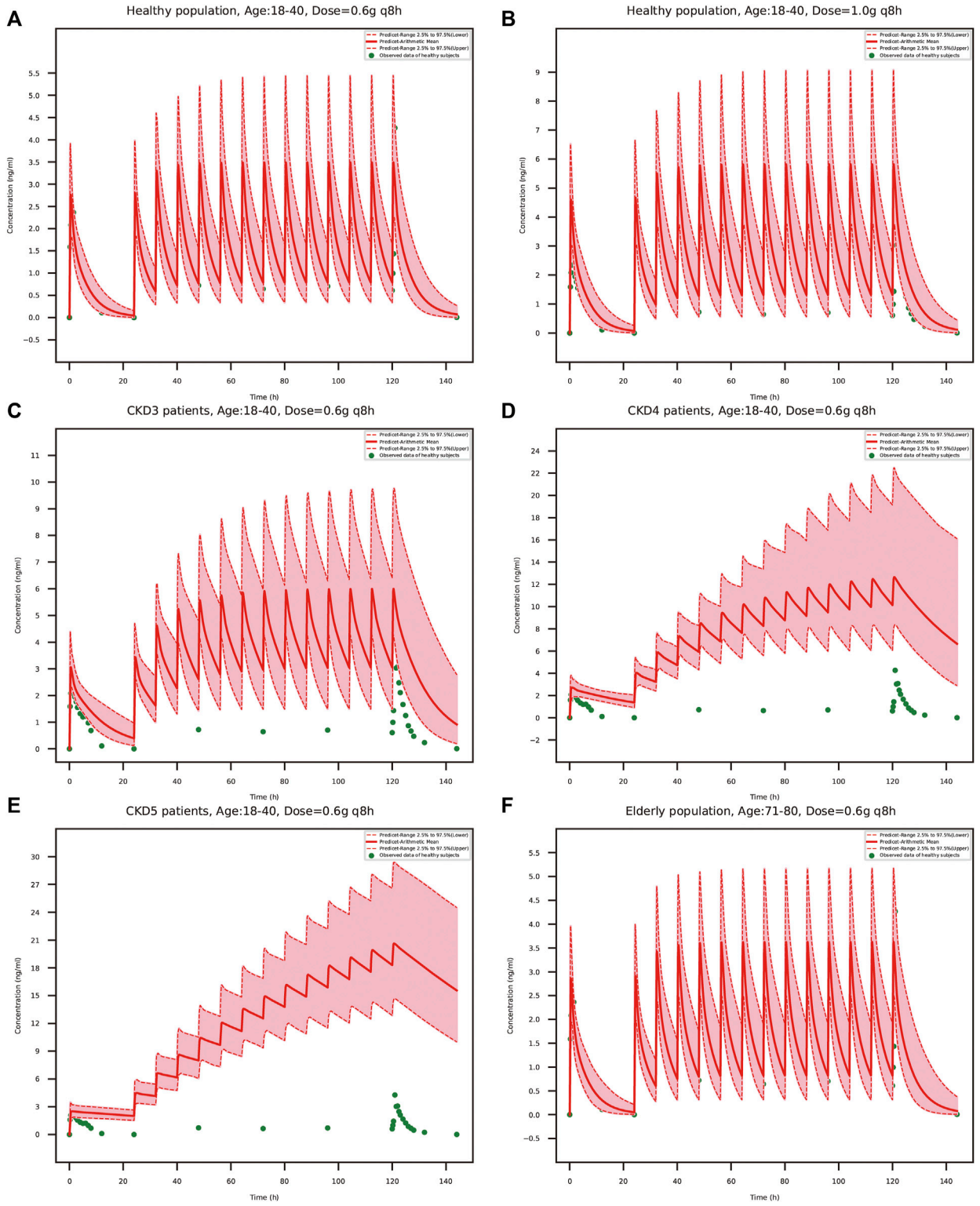

FIGURE 8
PBPK model-simulated schaftoside plasma concentration-time profiles in healthy population (18–40 years) at the TFDS regular dosage **(A)**: 0.6 g q 8 h) or a higher dosage **(B)**: 1 g q 8 h), renally impaired patients with CKD *stage3* **(C)**, GFR = 60 ml/min/1.73 m^2), CKD *stage4* **(D)**, GFR = 30 ml/min/1.73 m^2), CKD *stage5* **(E)**, GFR = 15 ml/min/1.73 m^2), and elderly population **(F)**, 71–80 years). Simulated data included the mean values, 97.5th percentile and 2.5th percentile concentration range. The green solid circles represent mean observed data obtained from the healthy volunteers in the present clinical study.

TABLE 6 Predicted pharmacokinetic parameters of schaftoside following oral administration of TFDS at 0.6 g/1 g q 8 h.

Parameter		Healthy (0.6 g q 8 h)		Healthy (1 g q 8 h)		CKD3 (0.6 g q 8 h)		CKD4 (0.6 g q 8 h)		CKD5 (0.6 g q 8 h)		Eldly (0.6 g q 8 h)	
		Day 1	Day 6	Day 1	Day 6	Day 1	Day 6	Day 1	Day 6	Day 1	Day 6	Day 1	Day 6
C_{max} (ng/mL)	Mean	2.76	3.49	4.6	5.82	3.06	6	2.72	12.65	2.52	20.64	2.86	3.62
	Range 2.5%	1.81	2.25	3.02	3.75	2.32	4.27	1.93	8.38	1.89	14.7	1.94	2.5
	Range 97.5%	3.91	5.44	6.52	9.07	4.39	9.76	3.82	22.49	3.49	29.38	3.96	5.17
R_{Cmax}[a]	Mean	1.26		1.27		1.96		4.65		8.19		1.27	
	Range 2.5%	1.24		1.24		1.84		4.34		7.78		1.29	
	Range 97.5%	1.39		1.39		2.22		5.89		8.42		1.30	
AUC_{0-t} (h·ng/mL)	Mean	13.33	18.25	22.22	30.42	28.49	62.21	46.31	224.85	53.54	433.77	13.71	18.98
	Range 2.5%	7.69	9.35	12.81	15.59	18.5	30.79	34.39	128.03	40.5	296.5	7.74	9.45
	Range 97.5%	22.05	34.91	36.75	58.19	44.21	133.06	60.96	451.02	69.65	647.54	23.02	39.48
R_{AUC}[b]	Mean	1.37		1.37		2.18		4.86		8.10		1.38	
	Range 2.5%	1.22		1.22		1.66		3.72		7.32		1.22	
	Range 97.5%	1.58		1.58		3.01		7.40		9.30		1.72	

[a]Ratio of C_{max} of schaftoside on day 6 *versus* day 1.
[b]Ratio of AUC_{0-t} of schaftoside on day 6 *versus* day 1.

model (Tremmel et al., 2021). They found schaftoside, isoschaftoside, and vitexin were poorly metabolized in phase I and II reactions, while orientin, isoorientin, and isovitexin were highly metabolized. By comparing the structures of these C-glycosylated flavones, we speculated that the hydroxy groups at C-4'/C-5' in the B-ring and sugar residues linked to C-8 in the A-ring were the meaningful structural features for the metabolism of these compounds.

TFDS contains several flavonoid glycosides including schaftoside, which are poorly soluble in nature. Therefore, the oral formulation for PK studies in rat is a TFDS suspension solution, which means the dissolution during administration may be incomplete. In order to simulate possible solubility, the dissolution time and dissolution shape in rat were set 0.92 min and 1.08*1E-3, respectively. Nevertheless, there was still an overestimation in schaftoside plasma concentration especially for C_{max}. According to the literature, intestinal absorption may be limited by solubility, thus imposing an upper limit on the absorption of compounds (Gerner and Scherf-Clavel, 2021). Even so, the predicted C_{max} and AUC_{0-t} values of schaftoside after oral administration of TFDS in rats were within ~1.5-fold of the observed values, which met the acceptance criteria (<2-fold). Likewise, the predicted profiles of schaftoside in human model were consistent with the observed data obtained from our clinical study, demonstrating the reliability and robustness of the PBPK model.

To evaluate the efficacy and safety of TFDS in various populations, the adult PBPK model in healthy population was scaled to elderly people and renally impaired patients. After multiple-dose administration, the predicted C_{max} and AUC_{0-t} of schaftoside on day 6 were obviously higher in CKD patients than the healthy people. The drug exposure increased with the decline of renal function. Compared to the healthy people, both the C_{max} and AUC_{0-t} values of schaftoside were increased more than two times in the CKD4-5 patients. We speculated that the renal function could greatly affect the excretion of schaftoside, and declined renal function in CKD patients led to the accumulation of shaftoside. The increased ratio of C_{max} and AUC_{0-t} of schaftoside on day 6 *versus* day 1 verified this speculation. Thus, exposure-related adverse events may be more frequently experienced by patients with impaired renal function during TFDS treatment. On the contrary, the drug exposure of schaftoside in the elderly population (71–80 years old) did not differ with the adult people (18–40 years old), indicating age was not a key factor influencing the safety and efficacy of TFDS.

There are some limitations to this study. One limitation which might reduce the applicability of the model was the lack of iv data of schaftoside in human (Gerner and Scherf-Clavel, 2021). Although the rat PBPK model utilized the iv and oral plasma concentration-time profiles of schaftoside and TFDS, the establishment of human PBPK model only based on the oral data of schaftoside after oral administration of TFDS. However, clearance processes could not be transferred from rat to human completely due to species differences. This may lead to some uncertainties and inaccuracies of PBPK models. However, the excellent model fit indexes such as FE, AFE and AAFE values which were within 2-fold error indicated the schaftoside PBPK model in human was generally accurate and

reliable. We speculated it may be related to the metabolic characteristics of schaftoside in animals and human. Schaftoside underwent poor metabolism and was extensively excreted as an unchanged form. Another shortcoming of the present study was the relatively small clinical sample size (Gao et al., 2015) and the lack of pharmacokinetic data of TFDS in CKD patients. Because TFDS was recently approved for the treatment of urolithiasis, the clinical data was not adequate. Therefore, model validation in patients was not sufficient. In the future, more clinical data could be incorporated into the human PBPK model. Then the patient model can be refined and expanded with the availability of additional information. Third, the drug transporters were not included in the current PBPK models. It was reported drug transporters played important roles in the disposition of flavonoid C-glycosides. Schaftoside was identified as the substrate of multidrug resistance protein in previous studies (Fang et al., 2019; Song et al., 2020; Shen et al., 2021). A future investigation of the activities of drug transporters related with schaftoside will be proper for the optimization of PBPK models. Last, PBPK model was only applied to simulate pharmacokinetic profiles of schaftoside in this study. Although schaftoside is the representative compound of TFDS, we cannot exclude the important roles of the other constituents in TFDS such as vicenin-1, vicenin-2, and vicenin-3. More studies need to be performed to investigate their pharmacology activities and pharmacokinetic profiles in the future.

5 Conclusion

In conclusion, the established PBPK models of schaftoside in rats and humans are both reliable and valid. Using this model, we successfully simulated the pharmacokinetic profiles of schaftoside in elderly and renally impaired patients after oral administration of TFDS. The results indicated there is no PK-based need for dose adjustment in elderly population, however, dosage reduction may be recommended for patients with severe renal impairment. This study provided a feasible way for the assessment of efficacy and safety of herbal medicines.

Data availability statement

The raw data supporting the conclusion of this article will be made available by the authors, without undue reservation.

Ethics statement

The studies involving human participants were reviewed and approved by the Institutional Review Board of Longhua Hospital (Approved Number 2019LCSY069). The participants provided their written informed consent to participate in this study.

Author contributions

All of the authors have read and approved the final manuscript. MY and PZ conceived and designed the research; XL and CC contributed to data collection, statistical analysis, and manuscript writing; ND and TZ were responsible for data collection. MY and PZ helped revising the manuscript.

Funding

This study was supported by National Natural Science Foundation of China (No. 81803825), LongHua Hospital research projects (YM2021016 and RC-2020-02-04), Natural Science Foundation of Shanghai (22ZR1462100), Evidence based capacity building project of traditional Chinese Medicine (1749), and National Science and Technology Major Projects (2017ZX09304001).

Conflict of interest

The authors declare that the research was conducted in the absence of any commercial or financial relationships that could be construed as a potential conflict of interest.

Publisher's note

All claims expressed in this article are solely those of the authors and do not necessarily represent those of their affiliated organizations, or those of the publisher, the editors and the reviewers. Any product that may be evaluated in this article, or claim that may be made by its manufacturer, is not guaranteed or endorsed by the publisher.

References

Ahmad, W., Khan, M. A., Ashraf, K., Ahmad, A., Daud Ali, M., Ansari, M. N., et al. (2021). Pharmacological evaluation of safoof-e-pathar phori- A polyherbal unani formulation for urolithiasis. *Front. Pharmacol.* 12, 597990. doi:10.3389/fphar.2021.597990

Cui, C., Li, X., Liang, H., Hou, Z., Tu, S., Dong, Z., et al. (2021). Physiologically based pharmacokinetic model of renally cleared antibacterial drugs in Chinese renal impairment patients. *Biopharm. Drug Dispos.* 42 (1), 24–34. doi:10.1002/bdd.2258

Fang, Y., Cao, W., Liang, F., Xia, M., Pan, S., and Xu, X. (2019). Structure affinity relationship and docking studies of flavonoids as substrates of multidrug-resistant associated protein 2 (MRP2) in MDCK/MRP2 cells. *Food Chem.* 291, 101–109. doi:10.1016/j.foodchem.2019.03.111

Feng, W., Ao, H., Peng, C., and Yan, D. (2019). Gut microbiota, a new frontier to understand traditional Chinese medicines. *Pharmacol. Res.* 142, 176–191. doi:10.1016/j.phrs.2019.02.024

Fisang, C., Anding, R., Muller, S. C., Latz, S., and Laube, N. (2015). Urolithiasis-an interdisciplinary diagnostic, therapeutic and secondary preventive challenge. *Dtsch. Arztebl. Int.* 112 (6), 83–91. doi:10.3238/arztebl.2015.0083

Gao, Z. W., Zhu, Y. T., Yu, M. M., Zan, B., Liu, J., Zhang, Y. F., et al. (2015). Preclinical pharmacokinetics of TPN729MA, a novel PDE5 inhibitor, and prediction of its human pharmacokinetics using a PBPK model. *Acta Pharmacol. Sin.* 36 (12), 1528–1536. doi:10.1038/aps.2015.118

Gerner, B., and Scherf-Clavel, O. (2021). Physiologically based pharmacokinetic modelling of cabozantinib to simulate enterohepatic recirculation, drug-drug interaction with rifampin and liver impairment. *Pharmaceutics* 13 (6), 778. doi:10.3390/pharmaceutics13060778

Gottlieb, M., Long, B., and Koyfman, A. (2018). The evaluation and management of urolithiasis in the ed: A review of the literature. *Am. J. Emerg. Med.* 36 (4), 699–706. doi:10.1016/j.ajem.2018.01.003

Hollingsworth, J. M., Canales, B. K., Rogers, M. A., Sukumar, S., Yan, P., Kuntz, G. M., et al. (2016). Alpha blockers for treatment of ureteric stones: Systematic review and meta-analysis. *BMJ* 355, i6112. doi:10.1136/bmj.i6112

Hollingsworth, J. M., Rogers, M. A., Kaufman, S. R., Bradford, T. J., Saint, S., Wei, J. T., et al. (2006). Medical therapy to facilitate urinary stone passage: A meta-analysis. *Lancet* 368 (9542), 1171–1179. doi:10.1016/S0140-6736(06)69474-9

Hou, J., Chen, W., Lu, H., Zhao, H., Gao, S., Liu, W., et al. (2018). Exploring the therapeutic mechanism of *Desmodium styracifolium* on oxalate crystal-induced kidney injuries using comprehensive approaches based on proteomics and network pharmacology. *Front. Pharmacol.* 9, 620. doi:10.3389/fphar.2018.00620

Huang, W., and Isoherranen, N. (2020). Novel mechanistic PBPK model to predict renal clearance in varying stages of CKD by incorporating tubular adaptation and dynamic passive reabsorption. *CPT. Pharmacometrics Syst. Pharmacol.* 9 (10), 571–583. doi:10.1002/psp4.12553

Jiang, P., Xie, L., Arada, R., Patel, R. M., Landman, J., and Clayman, R. V. (2021). Qualitative review of clinical guidelines for medical and surgical management of urolithiasis: Consensus and controversy 2020. *J. Urol.* 205 (4), 999–1008. doi:10.1097/JU.0000000000001478

Jones, H. M., Gardner, I. B., and Watson, K. J. (2009). Modelling and PBPK simulation in drug discovery. *AAPS J.* 11 (1), 155–166. doi:10.1208/s12248-009-9088-1

Jones, H., and Rowland-Yeo, K. (2013). Basic concepts in physiologically based pharmacokinetic modeling in drug discovery and development. *CPT. Pharmacometrics Syst. Pharmacol.* 2, e63. doi:10.1038/psp.2013.41

Ke, C., You, X., Lin, C., Chen, J., Guo, G., Wu, W., et al. (2022). Development of physiologically based pharmacokinetic model for pregabalin to predict the pharmacokinetics in pediatric patients with renal impairment and adjust dosage regimens: PBPK model of pregabalin in pediatric patients with renal impairment. *J. Pharm. Sci.* 111 (2), 542–551. doi:10.1016/j.xphs.2021.10.026

Khan, S. R., Pearle, M. S., Robertson, W. G., Gambaro, G., Canales, B. K., Doizi, S., et al. (2016). Kidney stones. *Nat. Rev. Dis. Prim.* 2, 16008. doi:10.1038/nrdp.2016.8

Kovar, L., Schräpel, C., Selzer, D., Kohl, Y., Bals, R., Schwab, M., et al. (2020). Physiologically-based pharmacokinetic (PBPK) modeling of buprenorphine in adults, children and preterm neonates. *Pharmaceutics* 12 (6), 578. doi:10.3390/pharmaceutics12060578

Kuepfer, L., Niederalt, C., Wendl, T., Schlender, J. F., Willmann, S., Lippert, J., et al. (2016). Applied concepts in PBPK modeling: How to build a PBPK/PD model. *CPT. Pharmacometrics Syst. Pharmacol.* 5 (10), 516–531. doi:10.1002/psp4.12134

Li, J., Xun, Y., Li, C., Han, Y., Shen, Y., Hu, X., et al. (2020). Estimation of renal function using unenhanced computed tomography in upper urinary tract stones patients. *Front. Med.* 7, 309. doi:10.3389/fmed.2020.00309

Li, X., Chen, C., Zhang, T., Ding, N., Zheng, P., and Yang, M. (2022). Comparative pharmacokinetic studies of five C-glycosylflavones in normal and urolithiasis model rats following administration of total flavonoids from *Desmodium styracifolium* by liquid chromatography-tandem mass spectrometry. *J. Sep. Sci.* 45 (15), 2901–2913. doi:10.1002/jssc.202200010

Liu, M., Liu, C., Chen, H., Huang, X., Zeng, X., Zhou, J., et al. (2017). Prevention of cholesterol gallstone disease by schaftoside in lithogenic diet-induced C57BL/6 mouse model. *Eur. J. Pharmacol.* 815, 1–9. doi:10.1016/j.ejphar.2017.10.003

Liu, R., Meng, C., Zhang, Z., Ma, H., Lv, T., Xie, S., et al. (2020). Comparative metabolism of schaftoside in healthy and calcium oxalate kidney stone rats by UHPLC-Q-TOF-MS/MS method. *Anal. Biochem.* 597, 113673. doi:10.1016/j.ab.2020.113673

López, M., and Hoppe, B. (2010). History, epidemiology and regional diversities of urolithiasis. *Pediatr. Nephrol.* 25 (1), 49–59. doi:10.1007/s00467-008-0960-5

Maharaj, A. R., and Edginton, A. N. (2014). Physiologically based pharmacokinetic modeling and simulation in pediatric drug development. *CPT. Pharmacometrics Syst. Pharmacol.* 3, e150. doi:10.1038/psp.2014.45

Malik, P. R. V., Yeung, C. H. T., Ismaeil, S., Advani, U., Djie, S., and Edginton, A. N. (2020). A physiological approach to pharmacokinetics in chronic kidney disease. *J. Clin. Pharmacol.* 60 (1), S52–S62. doi:10.1002/jcph.1713

Mendez, D., Gaulton, A., Bento, A. P., Chambers, J., De Veij, M., Felix, E., et al. (2019). ChEMBL: Towards direct deposition of bioassay data. *Nucleic Acids Res.* 47 (D1), D930–D940. doi:10.1093/nar/gky1075

Meng, Q., and Liu, K. (2014). Pharmacokinetic interactions between herbal medicines and prescribed drugs: Focus on drug metabolic enzymes and transporters. *Curr. Drug Metab.* 15 (8), 791–807. doi:10.2174/1389200216666150223152348

Ozdedeli, K., and Cek, M. (2012). Residual fragments after percutaneous nephrolithotomy. *Balk. Med. J.* 29 (3), 230–235. doi:10.5152/balkanmedj.2012.082

Raheem, O. A., Khandwala, Y. S., Sur, R. L., Ghani, K. R., and Denstedt, J. D. (2017). Burden of urolithiasis: Trends in prevalence, treatments, and costs. *Eur. Urol. Focus* 3 (1), 18–26. doi:10.1016/j.euf.2017.04.001

Ramello, A., Vitale, C., and Marangella, M. (2000). Epidemiology of nephrolithiasis. *J. Nephrol.* 13, S45–S50.

Rasool, M. F., Ali, S., Khalid, S., Khalid, R., Majeed, A., Imran, I., et al. (2021). Development and evaluation of physiologically based pharmacokinetic drug-disease models for predicting captopril pharmacokinetics in chronic diseases. *Sci. Rep.* 11 (1), 8589. doi:10.1038/s41598-021-88154-2

Reig-Lopez, J., Garcia-Arieta, A., Mangas-Sanjuan, V., and Merino-Sanjuan, M. (2021). Current evidence, challenges, and opportunities of physiologically based pharmacokinetic models of atorvastatin for decision making. *Pharmaceutics* 13 (5), 709. doi:10.3390/pharmaceutics13050709

Shen, W., Hu, X., Niu, Y., Lu, Y., Wang, B., and Wang, H. (2021). Bioaccessibility and absorption of flavonoid C-glycosides from Abrus mollis using simulated digestion, caco-2 cell, and *in Situ* single-pass perfusion models. *Planta Med.* 87 (7), 570–580. doi:10.1055/a-1363-2088

Song, P., Xiao, S., Zhang, Y., Xie, J., and Cui, X. (2020). Mechanism of the intestinal absorption of six flavonoids from zizyphi spinosi semen across caco-2 cell monolayer model. *Curr. Drug Metab.* 21 (8), 633–645. doi:10.2174/1389200221666200714100455

Tan, Z., Zhang, Y., Wang, C., and Sun, L. (2021). Physiologically based pharmacokinetic modeling of cefadroxil in mouse, rat, and human to predict concentration-time profile at infected tissue. *Front. Pharmacol.* 12, 692741. doi:10.3389/fphar.2021.692741

Tremmel, M., Kiermaier, J., and Heilmann, J. (2021). *In vitro* metabolism of six C-glycosidic flavonoids from passiflora incarnata L. *Int. J. Mol. Sci.* 22 (12), 6566. doi:10.3390/ijms22126566

Turk, C., Petrik, A., Sarica, K., Seitz, C., Skolarikos, A., Straub, M., et al. (2016). EAU guidelines on diagnosis and conservative management of urolithiasis. *Eur. Urol.* 69 (3), 468–474. doi:10.1016/j.eururo.2015.07.040

Wang, W., Fan, J., Huang, G., Li, J., Zhu, X., Tian, Y., et al. (2017). Prevalence of kidney stones in mainland China: A systematic review. *Sci. Rep.* 7, 41630. doi:10.1038/srep41630

Yellepeddi, V. K., and Baker, O. J. (2020). Predictive modeling of aspirin-triggered resolvin D1 pharmacokinetics for the study of Sjögren's syndrome. *Clin. Exp. Dent. Res.* 6 (2), 225–235. doi:10.1002/cre2.260

Yoon, S., Yi, S., Rhee, S. J., Lee, H. A., Kim, Y., Yu, K. S., et al. (2019). Development of a physiologically-based pharmacokinetic model for cyclosporine in Asian children with renal impairment. *Transl. Clin. Pharmacol.* 27 (3), 107–114. doi:10.12793/tcp.2019.27.3.107

Zeng, X., Xi, Y., and Jiang, W. (2019). Protective roles of flavonoids and flavonoid-rich plant extracts against urolithiasis: A review. *Crit. Rev. Food Sci. Nutr.* 59 (13), 2125–2135. doi:10.1080/10408398.2018.1439880

Zhou, J., Jin, J., Li, X., Zhao, Z., Zhang, L., Wang, Q., et al. (2018). Total flavonoids of *Desmodium styracifolium* attenuates the formation of hydroxy-L-proline-induced calcium oxalate urolithiasis in rats. *Urolithiasis* 46 (3), 231–241. doi:10.1007/s00240-017-0985-y

frontiers | Frontiers in Pharmacology

TYPE Original Research
PUBLISHED 15 December 2022
DOI 10.3389/fphar.2022.1064364

OPEN ACCESS

EDITED BY
Yurong Lai,
Gilead, United States

REVIEWED BY
Hong Shen,
Bristol Myers Squibb, United States
Yuan Wei,
Jiangsu University, China

*CORRESPONDENCE
Li Ding,
dingli@cpu.edu.cn
Jintong Li,
gcpljt@189.cn

SPECIALTY SECTION
This article was submitted to Drug Metabolism and Transport, a section of the journal Frontiers in Pharmacology

RECEIVED 08 October 2022
ACCEPTED 21 November 2022
PUBLISHED 15 December 2022

CITATION
Gao H, Li J, Chen X, Sun Z, Cui G, Cheng M and Ding L (2022), Pharmacokinetics, metabolite profiling, safety, and tolerability of inhalation aerosol of 101BHG-D01, a novel, long-acting and selective muscarinic receptor antagonist, in healthy Chinese subjects.
Front. Pharmacol. 13:1064364.
doi: 10.3389/fphar.2022.1064364

Pharmacokinetics, metabolite profiling, safety, and tolerability of inhalation aerosol of 101BHG-D01, a novel, long-acting and selective muscarinic receptor antagonist, in healthy Chinese subjects

Huaye Gao[1], Jintong Li[2]*, Xiaoping Chen[3], Zhanguo Sun[3], Gang Cui[2], Minlu Cheng[4] and Li Ding[1]*

[1]Department of Pharmaceutical Analysis, China Pharmaceutical University, Nanjing, China, [2]Drug Clinical Trial Research Center, China-Japan Friendship Hospital, Beijing, China, [3]Beijing Shuobai Pharmaceutical Technology Co., Ltd., Beijing, China, [4]Nanjing Jiening Pharmaceutical Technology Co., Ltd., Nanjing, China

101BHG-D01 is a novel, long-acting, selective muscarinic receptor antagonist for the treatment of chronic obstructive pulmonary disease (COPD). A single-site, randomized, double-blind, placebo-controlled and dose-escalation study of 101BHG-D01 inhalation aerosol was conducted to evaluate its pharmacokinetics, metabolite profiling, safety and tolerability following the single inhaled doses ranged from 20 to 900 μg in healthy Chinese subjects. After inhalation, 101BHG-D01 was absorbed rapidly into plasma with the time to maximum concentration about 5 min, and eliminated slowly with the terminal phase half-life about 30 h. The cumulative excretion rates of 101BHG-D01 in feces and urine were about 30% and 2%, respectively, which showed the study drug was mainly excreted in feces. The maximum drug concentration and area under the plasma concentration-time curve increased with dose escalation in the range of 20–600 μg, but their values increased out of proportion to the whole studied doses. The main metabolic pathways were loss of phenyl group and hydroxylation. No metabolite that presented at greater than 10 percent of total drug-related exposure was observed. 101BHG-D01 was safe and well tolerated after administration. The study results indicate that 101BHG-D01 is a good candidate for the treatment of COPD and enable further clinical development in subsequent studies in patients.

Clinical Trial Registration: http://www.chinadrugtrials.org.cn; Identifier: CTR20192058.

KEYWORDS

101BHG-D01, chronic obstructive pulmonary disease, long-acting muscarinic antagonist, pharmacokinetics, metabolite, safety

1 Introduction

Chronic obstructive pulmonary disease (COPD) is a common, treatable and preventable chronic respiratory disease (Xu et al., 2022), characterized by persistent airflow limitation and associated with an abnormal inflammatory response in the airways and lungs (da Silva et al., 2022). According to the World Health Organization, COPD is the third leading cause of death worldwide, with 65 million people suffering from it and over 4 million people dying each year globally (Alfahad et al., 2021). Bronchodilators are the mainstay of pharmacological treatment of COPD (Anzueto and Kaplan, 2020). Two classes of bronchodilators can be distinguished: β_2-adrenoreceptor agonists and muscarinic antagonists (Kabir and Morshed, 2015; van Haarst et al., 2019; Calzetta et al., 2021), with long-acting bronchodilators considered to provide more convenient and effective symptom relief than short-acting bronchodilators (Quinn et al., 2018). Long-acting muscarinic antagonists (LAMAs) are recommended as the first-line maintenance bronchodilator therapy in patients with stable COPD without significant symptoms but who have a high risk of exacerbations and those without a history of exacerbation but with significant symptoms (Rhee et al., 2019). The most frequently prescribed LAMA is tiotropium that reduces airflow limitation, dynamic hyperinflation and COPD exacerbations, and improves patients' quality of life (Tashkin et al., 2008; Yohannes et al., 2013). Tiotropium has similar affinity to the subtypes of muscarinic receptors, M1 to M3 (Barnes, 2000), and it exhibits pharmacological effects through inhibition of M3 receptor at the smooth muscle leading to bronchodilation (Donohue et al., 2002). However, its action on the muscarinic M2 receptor in the heart may increase the risk of adverse cardiovascular outcomes in patients (Oba et al., 2015), and a variety of studies suggested a significantly increased risk of acute urinary retention associated with tiotropium in patients with COPD (Loke and Singh, 2013). Given the high prevalence of COPD and the undesirable safety profiles of tiotropium, the development of additional options is clearly warranted.

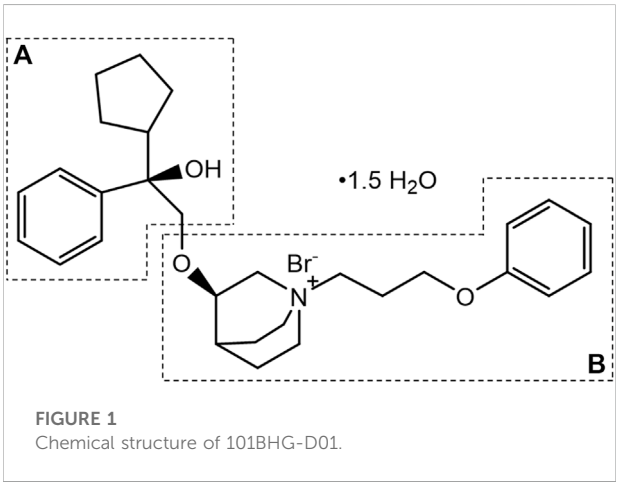

FIGURE 1
Chemical structure of 101BHG-D01.

101BHG-D01, chemically known as (R)-3-((R)-2-cyclopentyl-2-hydroxy-2-phenylethoxy)-1-(3-phenoxypropyl) quinuclidin-1-ium bromide sesquihydrate (Figure 1), is a novel, long-acting, selective muscarinic receptor antagonist for the treatment of COPD. The preparation method and medical use thereof have been patented in the United States (Patent No. US9751875B2). Compared with tiotropium, 101BHG-D01 has a greater affinity to M3 subtype and dissociates more rapidly from M2 subtype (Chu et al., 2022), resulting in a more preferable safety profile. Furthermore, 101BHG-D01 is considered to be administrated by inhalation and delivered *via* metered dose inhaler (MDI) due to its stable physical-chemical properties. Currently, 101BHG-D01 inhalation aerosol is undergoing Phase Ib clinical trial in China, and it has shown the potential efficacy for the treatment of COPD.

Pharmacokinetics describes the fate of a drug in the body (i.e., the processes of absorption, distribution, metabolism, and excretion), which is necessary to evaluate the safety and effectiveness of the drug. Pharmacokinetic (PK) information is essential in establishing the most effective and safe therapeutic dose schedules for initiating and adjusting therapy in patient population. For instance, the half-life of a drug could help researchers to explain the accumulation of the drug in the body and optimize the frequency of administration. If a drug has a long half-life, the continuous administration could cause drug accumulation, which would raise safety concern, and the frequency of administration should be reduced. Meanwhile, metabolite profiling is strongly recommended by the U.S. Food and Drug Administration (FDA) to be conducted as early as feasible. Generally, metabolites identified only in human plasma or metabolites present at higher levels in humans than in any of the animal test species should be considered for safety assessment. If the human metabolites exceed 10 percent of total drug-related exposure at steady state, nonclinical pharmacodynamic and toxicity studies of the metabolites should be conducted. On the contrary, the above studies are not necessary temporarily. Therefore, we conducted this study to evaluate the pharmacokinetics, metabolite profiling, safety and tolerability of 101BHG-D01 following the single inhaled doses in healthy Chinese subjects.

2 Materials and methods

2.1 Chemicals and reagents

101BHG-D01 inhalation aerosols and placebo, as well as the reference substance of 101BHG-D01, were provided by Beijing Shuobai Pharmaceutical Technology Co., Ltd. (Beijing, China). The study drug was delivered *via* MDI, which containing 101BHG-D01 20 or 150 μg per actuation. The placebo formulation had no active substance, and the other substances were consistent with the corresponding 101BHG-D01 inhalation aerosol. Pooled human liver microsomes (HLMs, n = 50) were purchased from XenoTech, LLC (Lenexa, KS, United States).

Nicotinamide adenine dinucleotide phosphate (NADPH) was obtained from Roche Diagnostic GmbH (Mannheim, Germany), and uridine diphosphate galacturonic acid (UDPGA) was purchased from Sigma-Aldrich (St. Louis, MO, United States). HPLC grade methanol and acetonitrile were from Merck KGaA (Darmstadt, Germany). All the other chemicals and reagents were of analytical grade and commercially available.

2.2 Study population

Subjects were male or female (non-lactating and non-pregnant) volunteers, 18–65 years old, with a body mass index (BMI) between 19–28 kg/m^2, and assessed as healthy by review of medical history, physical examination, vital sign measurements, 12-lead electrocardiogram (ECG), and clinical laboratory evaluations. All subjects were non- or ex-smokers (<10 years and who had stopped smoking more than 3 months prior to screening) and had normal lung function. Subjects unable to tolerate the inhaled administration or with clinically significant medical conditions (based on the judgement of the investigators), including abnormal physical examination, laboratory tests and X-ray of the chest, or abnormal vital signs or ECG abnormalities were excluded. Other exclusion criteria were as follows: 1) a history of clinically diagnosed disease in circulatory, endocrine, nervous, digestive, urinary, respiratory, hematological, immunological system, malignant tumor, metabolic abnormality, or psychiatric disease; 2) a history of glaucoma, functional constipation, benign prostatic hyperplasia, urinary obstruction; 3) subjects with bronchitis, sinusitis, urinary tract infection, or cellulitis within 1 week prior to screening; 4) subjects with drug allergy history or allergic constitution; 5) subjects who received any medicine that inhibited or induced drug metabolic enzyme CYP2D6 or CYP3A4 (the study drug is a substrate for CYP2D6 and CYP3A4), or received systemic corticosteroid therapy and/or antibiotic therapy within 30 days before screening; 6) subjects who received any other medicine within 14 days preceding screening; 7) subjects who participated in another clinical trial with an investigational product within about 3 months prior to screening; 8) subjects with positive findings for human immunodeficiency virus, *Treponema pallidum* antibody, hepatitis B virus surface antigen, or anti-hepatitis C virus antibody; 9) a positive alcohol breathalyzer or urine screen for abused drugs and nicotine; (10) blood donation/loss more than 400 mL during the 3 months preceding screening. Written informed consents were obtained from all of the eligible subjects before the initiation of any study-related procedures.

2.3 Clinical study design

This was a single-site, randomized, double-blind, placebo-controlled and dose-escalation study consisting of six dose cohorts (20, 60, 150, 300, 600, and 900 μg) to evaluate the pharmacokinetics, metabolite profiling, safety and tolerability of 101BHG-D01 after inhalation in healthy Chinese subjects. Dose escalation was continued sequentially after review of all safety data and each subject could participate in only one dose cohort. In the 20 μg dose cohort, four subjects all received 101BHG-D01. In the 60–900 μg dose cohorts, the ten subjects of each cohort were randomized in a 4:1 ratio such that eight subjects received 101BHG-D01 inhalation aerosol and two subjects received the placebo. The sample size was determined to provide adequate PK, safety and tolerability data at each dose. For the allocation of the subjects, the randomization list was generated by using SAS statistical package version 9.4 (SAS Research and Development Co., Ltd., Chapel Hill, NC, United States). In this study, the study drug and placebo were identical in appearance to ensure both the investigators and the subjects were blind. The drug administration was conducted in accordance with the standard operating procedure (SOP) strictly. Prior to administration, all subjects received adequate administration training. The SOPs were as follows: 1) before using, remove the cap from the mouthpiece, shake the inhaler well and discard the first 2 sprays; 2) breathe out as fully as possible for 5 s, put the inhaler into mouth, and then close lips, keeping tongue below the mouthpiece; 3) while breathing in deeply and slowly for 4 s, press down on the center of the inhaler until the actuator stops moving; 4) after finishing breathing in, hold breath for 10 s and then breathe out gently for 5 s; 5) after using, rinse mouth with water to remove any excess medicine and do not swallow. As the clinical study was in progress, the metabolite profiling of 101BHG-D01 in human liver microsomes was conducted. According to the results of metabolite profiling *in vitro* (see the Section 3.3 "Metabolite profiling in human liver microsomes"), the main metabolite of 101BHG-D01was identified as M6, which corresponding to the loss of phenyl group compared with the parent drug. The pharmacokinetic profiles of M6 were also studied in the 600 and 900 μg dose cohorts. This study was carried out in accordance with the principles of the Declaration of Helsinki and the International Conference for Harmonization (ICH) E6 guidelines for Good Clinical Practice (GCP). The study protocol and informed consent form (ICF) were approved by the Clinical Research Ethics Committee of China-Japan Friendship Hospital (Beijing, China).

2.4 Sample collection and processing

In the 20–300 μg dose cohorts, blood samples were taken for pharmacokinetic analysis of 101BHG-D01. In the 600 and 900 μg dose cohorts, blood, urine and fecal samples were collected for the pharmacokinetic evaluation of 101BHG-D01 and M6, and estimation of the relative quantification of the parent drug and its metabolites.

In the 20 and 60 μg dose cohorts, blood samples were taken before dosing and at 5, 15, 30 min and 1, 2, 3, 4, 6, 8, 12, 24, 36, and 48 h after dosing. In the 150–900 μg dose cohorts, blood samples were taken before dosing and at 5, 15, 30 min and 1, 2, 4, 8, 12, 24, 36, 48, 72, and 96 h after dosing. Plasma was separated and stored at −60 to −90°C until analysis. Urine samples were collected within 24 h pre-dosing and the following time intervals: 0–2, 2–4, 4–8, 8–12, 12–24, 24–48, 48–72 and 72–96 h. The total volume of the urine in each time interval was recorded. The urine samples were stored at −60 to −90°C until analysis. Fecal samples were collected within the following time intervals: 24 h before dosing and 0–24, 24–48, 48–72 and 72–96 h. The fecal samples in each time interval were weighed. The fecal samples were stored at −20°C until analysis.

2.5 Pharmacokinetic assessments

Determination of 101BHG-D01 and M6 in plasma, urine and feces was performed by high performance liquid chromatography tandem mass spectrometry method (HPLC-MS/MS) using multiple reaction monitoring (MRM) detection. HPLC was performed with Shimadzu LC30AD (Shimadzu, Kyoto, Japan). Mass spectrometric detection was performed with Triple Quad 6500 (AB Sciex, Foster, United States) for plasma and urine, and QTrap5500 (AB Sciex, Foster, United States) for feces. These assays were all fully validated. The validated ranges were 1.00–800 pg/mL for 101BHG-D01 and 1.00–20.0 pg/mL for M6 in plasma, 0.0500–20.0 ng/mL for 101BHG-D01 and M6 in urine, 0.400–400 ng/mL for 101BHG-D01 and 0.100–100 ng/mL for M6 in feces.

The data acquisition was performed by AB Sciex Analyst software (version 1.6.3, AB Sciex, Foster, United States), and the data analysis was supported by Watson LIMS software (version 7.5, Thermo Fisher Scientific, Waltham, MA, United States). The pharmacokinetic parameters were calculated with WinNonlin version 8.0 (Pharsight Corporation, Mountain View, California) using non-compartmental analysis method. The main pharmacokinetic parameters of 101BHG-D01 and M6 in the study included the following: maximum concentration in plasma (C_{max}); time to maximum concentration (T_{max}); area under the concentration-time curve from time zero to the last measurable concentration (AUC_{0-t}) or infinity ($AUC_{0-\infty}$); terminal phase half-life ($t_{1/2z}$); renal clearance (CLr); the cumulative excretion rates of 101BHG-D01 in urine (fe_u%) and feces (fe_f%).

Statistical analysis was performed by using SAS statistical package version 9.4 (SAS Research and Development Co., Ltd., Chapel Hill, NC, United States). The relationship between the dose and systemic exposure to 101BHG-D01 was assessed using the method combining the log-linearized power model and the confidence interval (CI) criterion (Hummel et al., 2009). The model can be described as: $PK = \alpha \times dose^{\beta}$. Linear regression of ln-transformed PK parameters by the ln-transformed dose was described in the form of $\ln(PK) = \ln(\alpha) + \beta \times \ln(dose)$, where β was the dose proportionality coefficient (Hummel et al., 2009). Dose proportionality would be concluded if the 90% CI for β was within the acceptance range $[1 + \ln(0.8)/\ln(r); 1 + \ln(1.25)/\ln(r)]$, where r was the ratio of the highest to the lowest doses (Luo et al., 2021).

2.6 Metabolite profiling in human liver microsomes

The metabolite profiling of 101BHG-D01 in human liver microsomes was investigated by *in vitro* incubation with HLMs. The incubation mixture, in 0.1 M phosphate buffer (pH 7.4), consisted of 101BHG-D01 (1 μM), UDPGA (1 mM), NADPH (1 mM) and pooled human liver microsomes (1 mg/mL). The total incubation volume was 200 μL. After pre-incubation for 3 min at 37°C, the human liver microsomes were added to initiate the 1 h reaction at 37°C, which was then terminated with ice-cold acetonitrile. The negative control samples were prepared as described above with the addition of inactivated HLMs.

By using high performance liquid chromatography-quadrupole-time of flight mass spectrometry (HPLC-Q-TOF/MS) method, the metabolite profiling of 101BHG-D01 in human liver microsomes was conducted. The analysis platform was established by using a Shimadzu LC30AD HPLC system (Kyoto, Japan) followed a X500B QTOF (AB Sciex, CA, United States). The strategy was mainly divided into the following steps. The first step was on-line data acquisition. The OS software (version 1.6.1, AB Sciex, CA, United States) was applied for the data acquisition. A full mass scan was performed and the accurate MS/MS data sets were obtained using multiple mass defect filtering (MMDF)-dynamic background subtraction (DBS)-dependent data acquisition method. The application of MMDF and DBS could enable the mass spectrometry to distinguish between the background interfering ions and metabolite ions effectively and intelligently, and simultaneously gain the molecular ion peaks and MS/MS spectrum of the metabolites (Zhang et al., 2018). The second step was post acquisition data mining. Full scan mass spectra corresponding to the incubation and negative control samples were compared to look for potential metabolites. Only those analytes just presenting in the incubation samples were considered as potential metabolites. The extracted ion

chromatograms (XIC) and MS/MS spectra of the possible components were investigated. Based on the qualitative information, such as the retention time (t_R) and fragmentation ions, the metabolites were identified.

2.7 Relative quantification of 101BHG-D01 and metabolites in human plasma, urine and feces

Because of the low dose and poor systemic exposure after inhalation of 101BHG-D01, the concentrations of the parent drug and the metabolites *in vivo* was too low to be detected in the full mass scan by using HPLC-Q/TOF-MS method. Hence, the relative quantification of 101BHG-D01 and the metabolites in human plasma, urine and feces was conducted by using the LC-MS/MS method. The LC–MS/MS system consisted of the LC30AD liquid chromatographic system (Shimadzu, Kyoto, Japan) and Triple Quad 6500 mass spectrometer (AB Sciex, CA, United States). For the semi-quantitative profiling in circulation, the trapezoidal rule was used to yield the pooled samples that had the concentration proportional to the AUC (Hamilton et al., 1981; Hop et al., 1998) for each subject. For the relative quantification in urine and feces, sample pooling was conducted in proportion to the amount (volume or weight) of excreta collected in each sampling period (Penner et al., 2009). The proportion of 101BHG-D01 and each metabolite in these pooled samples was determined by the ratio of their peak area to the total peak area to represent their relative amounts.

Because of the extremely low concentration levels of 101BHG-D01 and M6 in the plasma samples collected from 24 to 96 h post-dosing, and to avoid unnecessary dilutions, the plasma samples ranged from 0 to 12 h post-dosing in the 600 and 900 μg dose cohorts were used to prepare the AUC pools for each subject (except for the placebo group). The urine and fecal samples collected up to 96 h post-dosing for each subject were mixed at the ratios according to all the collected sample volumes and weights, respectively.

The incubation, pre-dose and dose samples were analyzed sequentially. The ion pairs of 101BHG-D01 and the proposed metabolites were detected by using MRM with the same MS parameters. The ion pairs were chosen according to the MS/MS spectra of metabolite profiling in human liver microsomes. By comparing the retention time of each peak in XIC of the dosing samples with that of the incubation samples, the peaks of 101BHG-D01 and the metabolites in the dosing samples were identified. The blank samples were used as the negative controls.

2.8 Safety and tolerability assessments

During the study, all subjects remained in the clinical site under continuous observation. Safety signal monitoring included adverse events (AEs), serious adverse events (SAEs), physical examination, vital sign, pupillary measurement, laboratory examination (hematology, blood biochemistry, urinalysis, coagulation function) and ECG. AEs were graded using the Common Terminology Criteria for Adverse Events version 5.0 (CTCAE v5.0) (U.S. Department of Health and Human Services, 2017). Anticholinergic effects such as dry mouth, pupillary changes and tachycardia were specially focused. For the tolerability assessment, the next dose cohort would be tested when the investigators confirmed that the current dose was safe and well tolerated. In one dose cohort, if there was single drug-related SAE in the subjects receiving the study drug, the dose escalation was discontinued. If the drug-related AEs were reported as grade ≥2 (U.S. Department of Health and Human Services, 2017) in one-third or more of the subjects, the dose escalation was discontinued. If one-quarter or more of the subjects experienced the drug-related AEs of grade ≥3, or there were two same drug-related AEs of grade ≥3 (U.S. Department of Health and Human Services, 2017), the dose escalation was discontinued. When the dose escalation was discontinued, the former dose would be regarded as the maximum tolerated dose (MTD). After the study of 900 μg dose cohort was completed, the dose escalation was discontinued regardless of whether the subjects experienced the drug-related adverse events.

3 Results

3.1 Study population

A total of 250 Chinese volunteers were screened and 54 volunteers were enrolled in the study. The first subject was enrolled on 21 October 2019, and the last subject completed the follow-up on 17 May 2021. All the subjects completed the study according to the protocol. The baseline demographic data of the study population was summarized in Table 1.

3.2 Pharmacokinetic profiles

The detailed main pharmacokinetic parameters of 101BHG-D01 and M6 are presented in Table 2. The mean plasma concentration–time curves of 101BHG-D01 and M6 are shown in Figure 2. 101BHG-D01 was rapidly absorbed into plasma with the median time to reach the peak concentration about 5 min after single dose inhalation. 101BHG-D01 was eliminated slowly with the mean values of $t_{1/2z}$ about 30 h. M6, the main metabolite of 101BHG-D01, reached its peak concentration later than the parent drug, with the median time about 1.5–2 h. The mean $t_{1/2z}$ values of M6 about 7–8 h showed the metabolite eliminated more rapidly than the parent drug. The CLr values of 101BHG-D01 and M6 in the 600 μg dose

TABLE 1 Baseline demographic data of the study population.

Characteristic	20 μg	60 μg	150 μg	300 μg	600 μg	900 μg	Placebo
	(*n* = 4)	(*n* = 8)	(*n* = 8)	(*n* = 8)	(*n* = 8)	(*n* = 8)	(*n* = 10)
Sex, n							
Male/female	2/2	1/7	4/4	3/5	4/4	4/4	3/7
Age, years							
Mean (SD)	31.5 (2.38)	33.0 (5.95)	32.6 (2.62)	33.4 (6.97)	35.4 (5.90)	29.4 (7.48)	33.6 (4.27)
Min-Max	29–34	23–41	29–37	21–42	25–42	21–42	26–39
Height, cm							
Mean (SD)	163.25 (11.663)	162.45 (5.967)	167.31 (8.101)	166.61 (10.992)	164.30 (5.725)	165.31 (9.859)	163.48 (6.271)
Min-Max	150–173.3	155.1–172.4	157.1–181.5	150.4–188.4	152.6–169.6	154.5–179	156.6–172.6
Weight, kg							
Mean (SD)	68.300 (9.3453)	62.763 (7.8747)	61.719 (8.2330)	64.638 (11.6430)	62.606 (6.7663)	62.231 (9.2449)	64.290 (8.0377)
Min-Max	56.55–77.3	53–76.2	53.95–77.65	45.45–83.95	51.9–71	47.5–75.7	52.7–79.2
BMI, kg/m^2							
Mean (SD)	25.53 (0.750)	23.75 (2.282)	21.98 (1.326)	23.10 (1.838)	23.14 (1.354)	22.65 (1.493)	23.97 (1.584)
Min-Max	24.8–26.5	19.4–26.4	20–23.6	20.1–25.5	21.2–24.7	19.7–24.9	21–26.6

BMI, body mass index; SD, standard deviation; Max, maximum; Min, minimum.

TABLE 2 Main pharmacokinetic parameters of 101BHG-D01 and M6 after single inhaled doses of 101BHG-D01 in healthy Chinese subjects.

Pharmacokinetic parameters	101BHG-D01						M6	
	20 μg	60 μg	150 μg	300 μg	600 μg	900 μg	600 μg	900 μg
n	4	8	8	8	8	8	8	8
C_{max}, pg/mL	2.77 ± 1.64	13.83 ± 9.39	79.22 ± 76.98	181.1 ± 143.3	773.1 ± 317.8	594.8 ± 255.2	2.25 ± 0.75	1.46 ± 0.38
T_{max}, min	22.8 (15–30)	16.2 (5–30)	5 (5–5)	5 (5–5)	5 (5–5)	5 (5–5)	90 (30–240)	120 (120–240)
AUC_{0-t}, pg·h/mL	6.63 ± 7.70	96.69 ± 73.26	158.8 ± 130.6	423.4 ± 293.2	1884.0 ± 356.6	1337.8 ± 520.9	12.37 ± 7.87	5.79 ± 4.72
$AUC_{0-\infty}$, pg·h/mL	28.86[a]	150.9 ± 82.5	219.1 ± 151.0	494.4 ± 318.3	2039.7 ± 365.5	1491.1 ± 546.7	29.54 ± 7.80	NA
$t_{1/2z}$, h	8.81[a]	21.53 ± 5.36	36.62 ± 41.60	32.76 ± 14.11	29.24 ± 2.71	34.77 ± 5.08	7.55 ± 1.66	NA
CLr, mL/h	NA	NA	NA	NA	6821 ± 1525	8038 ± 1884	11799 ± 4512	NA
fe_u, %	NA	NA	NA	NA	2.36 ± 0.80	1.37 ± 0.69	0.05 ± 0.01	0.06 ± 0.04
fe_f, %	NA	NA	NA	NA	32.54 ± 11.30	29.85 ± 13.37	0.80 ± 0.27	0.31 ± 0.06

C_{max}, maximum concentration in plasma; T_{max}, time to maximum concentration; AUC_{0-t}, area under the concentration-time curve from time zero to the last measurable concentration; $AUC_{0-\infty}$, area under the concentration-time curve from time zero to infinity; $t_{1/2z}$, terminal phase half-life; CLr, renal clearance; fe_u%, the cumulative excretion rate in urine; fe_f%, the cumulative excretion rate in feces; NA, not applicable.

All values are expressed as mean ± SD, except for T_{max} values, which are expressed as median (range).

[a]In the 20 μg dose cohort, the $AUC_{0-\infty}$ value of only one subject could be calculated.

cohort were 6821 ± 1525 mL/h and 11799 ± 4512 mL/h, respectively. The maximum drug concentration and area under the plasma concentration-time curve of 101BHG-D01 increased with dose escalation in the range of 20 μg–600 μg. For the dose proportionality analysis, the 20 μg dose cohort was excluded due to the lack of the subjects whose significant PK parameters could be calculated. Based on the log-linearized power model, the β values of the C_{max}, AUC_{0-t} and $AUC_{0-\infty}$ over the dose range of 60–900 μg were 1.58, 1.355, 1.116, respectively. The 90% CIs of the C_{max}, AUC_{0-t} and $AUC_{0-\infty}$ were (1.306, 1.855), (1.01, 1.7), and (0.796, 1.435), respectively, which were not fully contained in the pre-defined CI criterion (0.918, 1.082). Hence, the linear pharmacokinetic characteristic of 101BHG-D01 was not observed.

After single inhaled dose of 600 and 900 μg of 101BHG-D01, its cumulative excretion rates in urine were 2.36% and 1.37%, and its cumulative excretion rates in feces over the time intervals of 0–96 h were 32.54% and 29.85%, respectively. These data

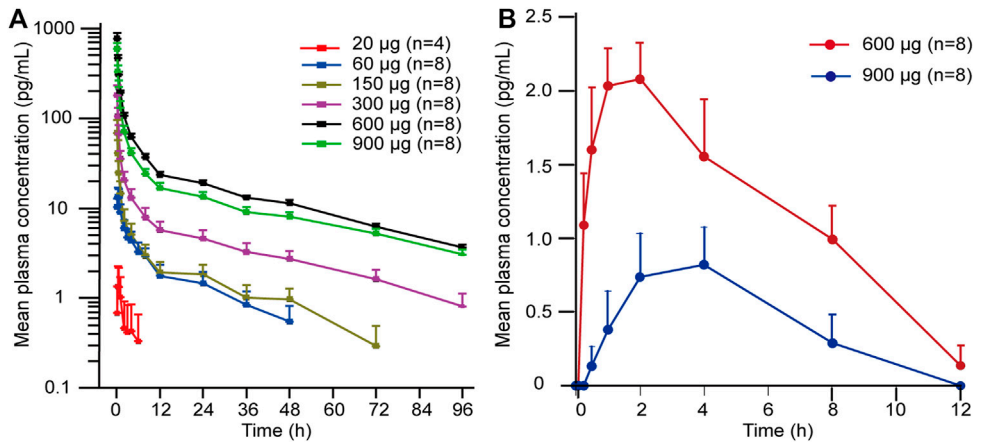

FIGURE 2
Mean plasma concentration-time curves of 101BHG-D01 and M6 after single inhaled doses of 101BHG-D01 inhalation aerosol in healthy Chinese subjects. **(A)** 101BHG-D01 (semi-logarithmic scale). **(B)** M6 (linear scale). Bars represent SDs. n, number of subjects.

suggested that fecal excretion might be the major excretion pathway of the unchanged 101BHG-D01. The total cumulative excretion rates in urine and feces of M6 over the time intervals of 0–96 h of 600 and 900 μg were 0.85% and 0.37%, respectively, which showed the amounts of this metabolite in urine and feces were low.

3.3 Metabolite profiling in human liver microsomes

101BHG-D01 and its 36 metabolites were identified in human liver microsomes by using HPLC-Q/TOF-MS method. According to the MS/MS information, the characteristic metabolic pathways involved hydroxylation, ketone formation and loss of phenyl group. As shown in Figure 1, we divided the structure of 101BHG-D01 into 2 parts, Part A and Part B, to characterize the structures of metabolites clearly. The detailed information, XIC, structures of the metabolites and the proposed metabolic pathways are shown in Table 3 and Figures 3,4.

3.3.1 Mass spectra analysis of parent drug

Before characterization of 101BHG-D01 metabolites, the chromatographic and mass spectroscopic behavior of the parent drug was investigated. The characteristic product ions of the parent drug were the substructural template for interpreting the structure of the metabolites.

101BHG-D01 was eluted at 16.8 min under the experimental condition. The accurate mass measurement gave the molecular ion at m/z 450.2985 with a theoretical elemental composition of $C_{29}H_{40}NO_3$ in the positive mode. The main fragment ions were observed at m/z 356.26 ($C_{23}H_{34}NO_2^+$), 328.23 ($C_{21}H_{30}NO_2^+$), 262.18 ($C_{16}H_{24}NO_2^+$), 168.14 ($C_{10}H_{18}NO^+$), and 124.11 ($C_8H_{14}NO^+$), respectively, *via* the cleavage of carbon-carbon bond and carbon-oxygen bond. The proposed fragmentation pathway and MS/MS spectrum of 101BHG-D01 are shown in Figure 5.

3.3.2 Identification of metabolites from 101BHG-D01

3.3.2.1 Mono-hydroxylation (M1 metabolites)

Metabolites M1-1-M1-7 (t_R = 14.38, 14.58, 14.96, 15.41, 15.55, 15.70 and 15.92 min, respectively) gave the same molecular ions $[M]^+$ at around m/z 466.295 ($C_{29}H_{40}NO_4$) which were 16 Da (O) more than that of 101BHG-D01. In the MS/MS spectra of M1-1-M1-5 and M1-7, the fragment ions at m/z 372.25 and m/z 344.22 were also 16 Da heavier than those of the parent drug at m/z 356.26 and 328.23, respectively, and the fragment ions at m/z 262.18, 168.14, 152.14 and 124.11 were the same as those generated by the parent drug. Accordingly, M1-1-M1-5 and M1-7 were determined as mono-hydroxylated metabolites and hydroxylation might occur at the cyclopentyl group or phenyl group in the part A. In the MS/MS spectra of M1-6, the typical fragment ions at m/z 278.18, which was 16 Da higher than that of 101BHG-D01 at 262.18, and m/z 328.23, 168.14, 152.14 and 124.11, which were the same as those generated by the parent drug, indicated that hydroxylation might occur at the phenyl group in the part B.

3.3.2.2 Mono-ketone formation (M2 metabolites)

Metabolites M2-1-M2-1 (t_R = 14.85 and 15.09 min) exhibited the same molecular ion $[M]^+$ at m/z 464.280 ($C_{29}H_{38}NO_4$) corresponding to the loss of a hydrogen molecule from the mono hydroxylated product of 101BHG-D01. Similar to the parent drug, the fragment ions at m/z 262.18, 168.14 and 124.11 were observed in their MS/MS spectra. The product

TABLE 3 Summary of 101BHG-D01 and its metabolites *in vitro* and *in vivo*.

Metabolite id	Metabolite description	Formula	m/z	Error (ppm)	t_R (min)	Relative amounts *in vitro* (%)[a]	Relative amounts *in vivo* (%)[a,b]		
							Plasma	Urine	Feces
M0	Parent	$C_{29}H_{40}NO_3$	450.3005	0.5	16.83	0.39	90.9 ± 3.2	73.4 ± 7.3	75.0 ± 9.3
M1-1	Hydroxylation	$C_{29}H_{40}NO_4$	466.2952	0.0	14.38	11.56			
M1-2	Hydroxylation	$C_{29}H_{40}NO_4$	466.2944	−1.7	14.58	6.07			
M1-3	Hydroxylation	$C_{29}H_{40}NO_4$	466.2949	−0.6	14.96	7.25			
M1-4	Hydroxylation	$C_{29}H_{40}NO_4$	466.2954	0.4	15.41	0.40	3.3 ± 1.6	3.1 ± 0.8	21.7 ± 8.9
M1-5	Hydroxylation	$C_{29}H_{40}NO_4$	466.2948	−0.9	15.55	0.12			
M1-6	Hydroxylation	$C_{29}H_{40}NO_4$	466.2947	−1.1	15.70	0.46			
M1-7	Hydroxylation	$C_{29}H_{40}NO_4$	466.2954	0.4	15.92	0.30			
M2-1	Ketone Formation	$C_{29}H_{38}NO_4$	464.2792	−0.6	14.85	1.59	-	0.4 ± 0.2	0.5 ± 0.2
M2-2	Ketone Formation	$C_{29}H_{38}NO_4$	464.2795	0.0	15.09	2.22			
M3-1	Di-Hydroxylation	$C_{29}H_{40}NO_5$	482.2893	−1.7	13.01	7.49			
M3-2	Di-Hydroxylation	$C_{29}H_{40}NO_5$	482.2894	−1.5	13.31	3.02			
M3-3	Di-Hydroxylation	$C_{29}H_{40}NO_5$	482.2896	−1.0	13.54	3.86			
M3-4	Di-Hydroxylation	$C_{29}H_{40}NO_5$	482.2901	0.0	13.74	4.33	-	2.4 ± 0.8	1.5 ± 0.6
M3-5	Di-Hydroxylation	$C_{29}H_{40}NO_5$	482.2899	−0.4	13.99	5.23			
M3-6	Di-Hydroxylation	$C_{29}H_{40}NO_5$	482.2902	0.2	14.50	1.07			
M3-7	Di-Hydroxylation	$C_{29}H_{40}NO_5$	482.2894	−1.5	14.71	2.65			
M3-8	Di-Hydroxylation	$C_{29}H_{40}NO_5$	482.2901	0.0	14.87	4.64			
M4-1	Hydroxylation + Ketone Formation	$C_{29}H_{38}NO_5$	480.2742	−0.4	13.56	3.63	-	1.7 ± 0.6	-
M4-2	Hydroxylation + Ketone Formation	$C_{29}H_{38}NO_5$	480.2742	−0.4	13.84	7.05			
M5-1	Tri-Hydroxylation	$C_{29}H_{40}NO_6$	498.2848	−0.6	12.51	0.62	-	-	-
M5-2	Tri-Hydroxylation	$C_{29}H_{40}NO_6$	498.2850	0.0	12.95	0.35			
M5-3	Tri-Hydroxylation	$C_{29}H_{40}NO_6$	498.2849	−0.2	13.22	0.20			
M5-4	Tri-Hydroxylation	$C_{29}H_{40}NO_6$	498.2849	−0.2	13.38	0.25			
M5-5	Tri-Hydroxylation	$C_{29}H_{40}NO_6$	498.2850	0.0	13.79	0.49			
M6	Loss of Phenyl group	$C_{23}H_{36}NO_3$	374.2686	−1.6	14.46	17.97	5.1 ± 2.0	8.1 ± 2.5	1.3 ± 0.6
M7-1	Loss of Phenyl group + Ketone Formation	$C_{23}H_{34}NO_4$	388.2480	−0.5	12.00	0.41			
M7-2	Loss of Phenyl group + Ketone Formation	$C_{23}H_{34}NO_4$	388.2478	−1.0	12.40	0.57			
M7-3	Loss of Phenyl group + Ketone Formation	$C_{23}H_{34}NO_4$	388.2481	−0.3	12.71	0.05	-	6.1 ± 3.0	-
M7-4	Loss of Phenyl group + Ketone Formation	$C_{23}H_{34}NO_4$	388.2485	0.8	12.97	0.08			
M8-1	Loss of Phenyl group + Hydroxylation	$C_{23}H_{36}NO_4$	390.2633	−1.5	11.49	1.42			
M8-2	Loss of Phenyl group + Hydroxylation	$C_{23}H_{36}NO_4$	390.2637	−0.5	11.84	0.57			
M8-3	Loss of Phenyl group + Hydroxylation	$C_{23}H_{36}NO_4$	390.2639	0.0	12.07	0.18			
M8-4	Loss of Phenyl group + Hydroxylation	$C_{23}H_{36}NO_4$	390.2637	−0.5	12.24	0.42	0.7 ± 1.0	5.0 ± 2.4	-
M8-5	Loss of Phenyl group + Hydroxylation	$C_{23}H_{36}NO_4$	390.2633	−1.5	12.40	1.38			
M8-6		$C_{23}H_{36}NO_4$	390.2637	−0.5	12.79	0.41			

(Continued on following page)

TABLE 3 (*Continued*) Summary of 101BHG-D01 and its metabolites *in vitro* and *in vivo*.

Metabolite id	Metabolite description	Formula	m/z	Error (ppm)	t_R (min)	Relative amounts *in vitro* (%)[a]	Relative amounts *in vivo* (%)[a,b]		
							Plasma	Urine	Feces
	Loss of Phenyl group + Hydroxylation								
M8-7	Loss of Phenyl group + Hydroxylation	$C_{23}H_{36}NO_4$	390.2637	−0.5	13.46	1.32			

[a]Relative amounts *in vitro* or *in vivo* (%) = peak area of 101BHG-D01, and each metabolite/total peak area in HLM, human plasma, urine or feces, respectively.
[b]The values of relative contents *in vivo* were mean ± SD.
HLM, human liver microsomes; t_R, retention time; -, not detected.

ion at m/z 342.21 indicated that ketone formation had occurred at the cyclopentyl group in the part A.

3.3.2.3 Di-hydroxylation (M3 metabolites)

Metabolites M3-1-M3-8 (t_R = 13.01, 13.31, 13.54, 13.74, 13.99, 14.50, 14.71 and 14.87 min, respectively) displayed the same molecular ions $[M]^+$ at around m/z 482.290 ($C_{29}H_{40}NO_5$). An increase of 32 Da in molecular weight compared to $[M]^+$ ion of the parent drug suggested that M3 metabolites were the di-hydroxylated metabolites. In the MS/MS spectra of M3-1, M3-6 and M3-7, the ions at m/z 372.25 and 344.22 originated from the fragment ions of 101BHG-D01 at m/z 356.26 and 328.23, respectively, corresponding to the mono-hydroxylation in the part A. While the ion at 278.17, which was 16 Da heavier than that of the parent drug at m/z 262.18, indicated that the other hydroxylation might occur at the phenyl group in the part B. The main fragment ions at 388.25 and 360.22 in the MS/MS spectra of M3-2-M3-4 and M3-8, which were 32 Da higher than those of the parent drug at m/z 356.26 and 328.23, showed di-hydroxylation occurred in the part A. In the spectrum of M3-5, the characteristic ions at m/z 380.22, 262.18 and 124.11 were observed. Among them, the product ion with m/z 380.22 was formed by the loss of the cyclopentane part from the molecular cation, which suggested that the two hydroxyl groups were located at the cyclopentyl group.

3.3.2.4 Hydroxylation and ketone formation (M4 metabolites)

Metabolite M4-1 and M4-2 (t_R = 13.56 and 13.84 min) were detected as molecular ions $[M]^+$ at m/z 480.274 ($C_{29}H_{38}NO_5$), which were 2 Da less than that of di-hydroxylated metabolites, indicating that they were the hydroxylated and ketone formed products of 101BHG-D01. The ketone formation occurred at cyclopentane because the key fragment ions were observed at m/z 370.24 and 342.21. The hydroxylation occurred at the phenyl group in the part B because the key fragment ion was observed at m/z 278.17.

3.3.2.5 Tri-hydroxylation (M5 metabolites)

Metabolites M5-1-M5-5 (t_R = 12.51, 12.95, 13.22, 13.38 and 13.79 min, respectively) showed the same molecular ions $[M]^+$ at around m/z 498.285 ($C_{29}H_{40}NO_6$), which indicated an addition of 48 Da compared with the molecular ion of the parent drug. In the MS/MS spectra of M5-1, M5-3, M5-4 and M5-5, the characteristic fragment ions at m/z 388.25 and 360.22, which were 32 Da (2O) higher than those of the parent drug at m/z 356.26 and 328.23, indicated two hydroxyl groups were located at the cyclopentyl group or phenyl group in the part A. The fragment ion at m/z 278.18, which was 16 Da heavier than that of the parent drug at m/z 262.18, suggested that one hydroxyl group was located at the phenyl group in the part B. In the MS/MS spectrum of M5-2, the main fragment ions at m/z 376.21, 262.14, 168.14 and 124.11 showed that tri-hydroxylation occurred at the cyclopentyl group or phenyl group in the part A.

3.3.2.6 Loss of phenyl group (M6 metabolite)

Metabolite M6 (t_R = 14.46 min) had a molecule ion $[M]^+$ at m/z 374.269($C_{23}H_{36}NO_3$), which was 76 Da lower than that of the parent drug, corresponding to the loss of phenyl group compared with parent drug. In the MS/MS spectrum, the characteristic fragment ion at m/z 186.15 was also 76 Da lower than that of 101BHG-D01 at m/z 262.18, which indicated the loss of phenyl group occurred in the part B.

3.3.2.7 Loss of phenyl group and ketone formation (M7 metabolites)

Metabolites M7-1-M7-4 (t_R = 12.00, 12.40, 12.71 and 12.97 min, respectively), with $[M]^+$ ions at around m/z 388.248 ($C_{23}H_{34}NO_4$), were 14 Da higher than that of M6 and the fragment ion at m/z 186.15 was similar to that of M6. Accordingly, M7 metabolites might be isomers of ketone formed product of M6 and ketone formation occurred at the cyclopentyl group in part A.

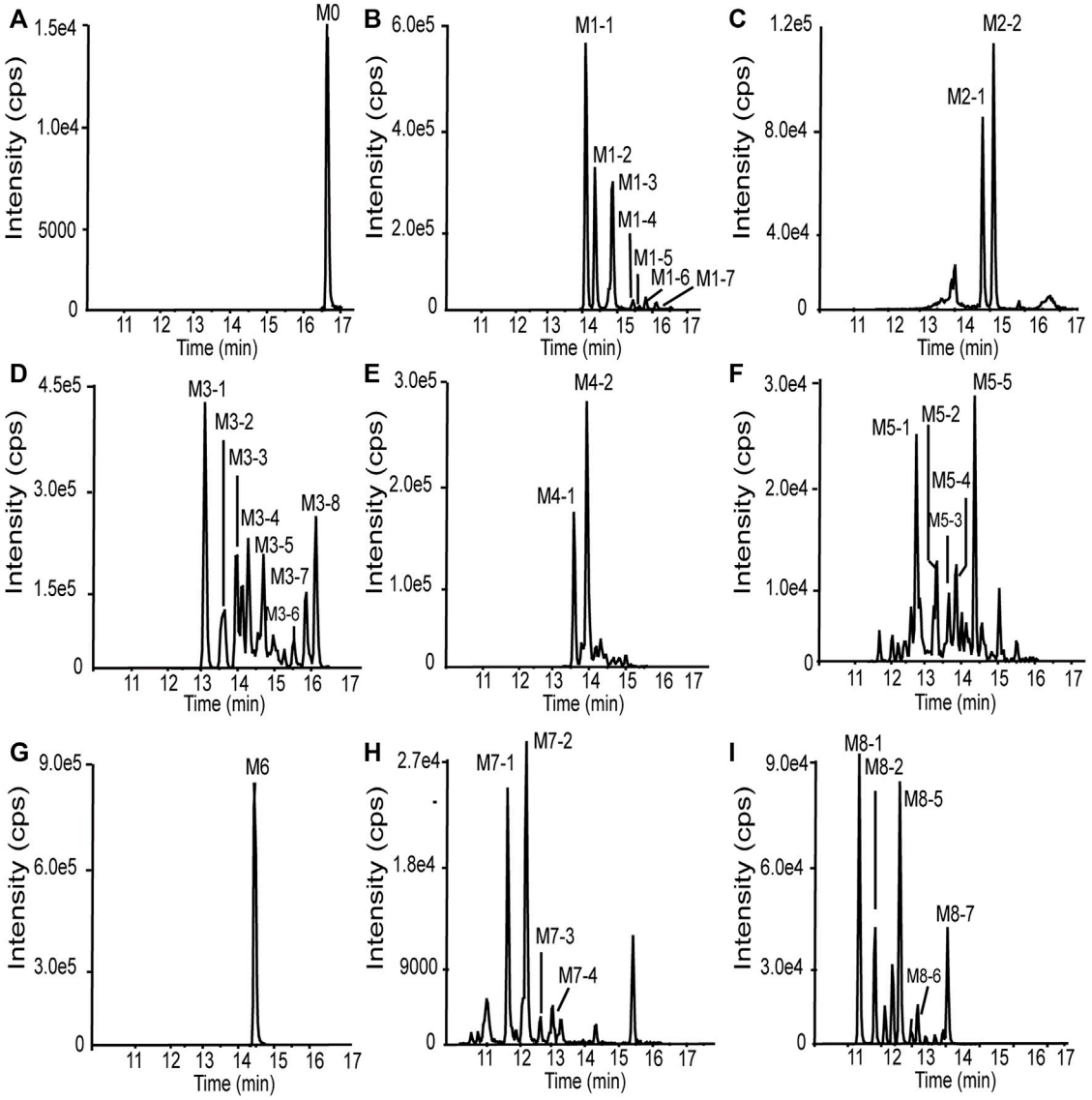

FIGURE 3
Extracted ion chromatograms of 101BHG-D01 and the metabolites in human liver microsomes. **(A)** M0 (101BHG-D01). **(B)** M1 metabolites. **(C)** M2 metabolites. **(D)** M3 metabolites. **(E)** M4 metabolites. **(F)** M5 metabolites. **(G)** M6 metabolite. **(H)** M7 metabolites. **(I)** M8 metabolites.

3.3.2.8 Loss of phenyl group and hydroxylation (M8 metabolites)

Metabolites M8-1-M8-8 (t_R = 11.49, 11.84, 12.07, 12.24, 12.40, 12.79 and 13.46 min, respectively) generated the molecular ions $[M]^+$ at around m/z 390.264 ($C_{23}H_{36}NO_4$), which were 16 Da more than that of M6. The key product ion at m/z 186.15 was detected in their MS/MS spectra, which was the same as that of M6. Accordingly, M8 was identified as the hydroxylated product of M6 and the hydroxyl group was located at the cyclopentyl group or phenyl group in the part A.

3.4 Relative quantification of 101BHG-D01 and metabolites in human plasma, urine and feces

Based on the result of metabolite profiling in human liver microsomes, 9 ion pairs were chosen. The metabolites detected in human plasma, urine and feces and their relative amounts are listed in Table 3. By comparing the retention time of each peak in XIC of the dosing samples with that of the incubation sample, the parent drug, M1 metabolites, M6 and M8 metabolites were found in the plasma samples. The parent drug, M1-M4 and M6-M8

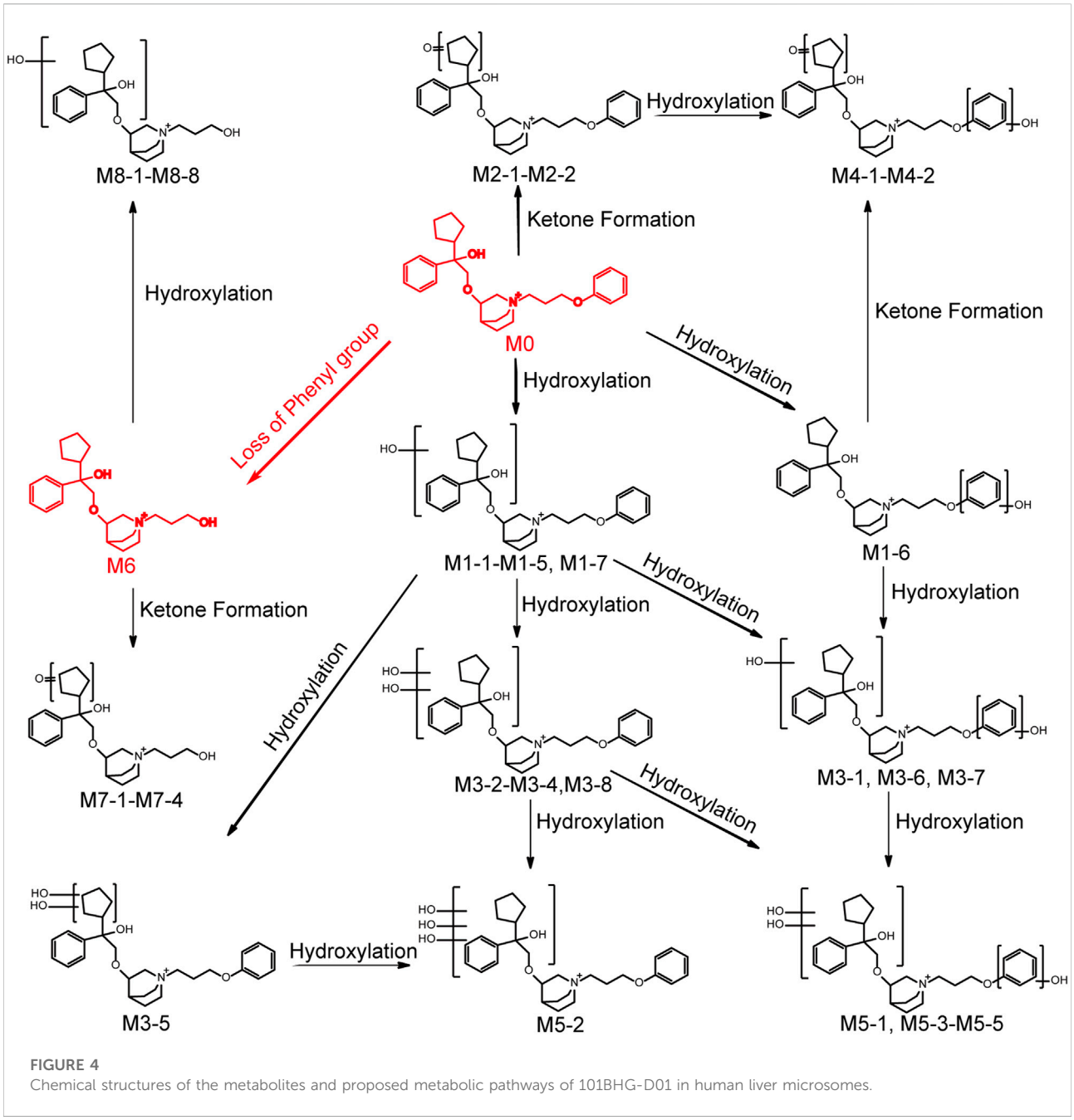

FIGURE 4
Chemical structures of the metabolites and proposed metabolic pathways of 101BHG-D01 in human liver microsomes.

metabolites were all detected in the urine samples. The parent drug, M1-M3 and M6 metabolites were found in the fecal samples. The proposed metabolic pathways of 101BHG-D01 *in vivo* mainly included loss of phenyl group and hydroxylation. The semi-quantification result in circulation showed 101BHG-D01 represented the main proportion of total drug-related exposure (90.9% ± 3.2% of the total peak area). The M1, M6 and M8 metabolites accounted for 3.3 ± 1.6%, 5.1 ± 2.0%, and 0.7 ± 1.0% of the total drug-related exposure, which showed that no peak ratio of any metabolite exceeded 10%.

3.5 Safety and tolerability

Overall, 25 subjects (46.3%) reported 46 AEs during the study. The details of AEs in subjects who received the study drug and placebo in the study are summarized in Supplementary Material. Among the 46 AEs, the 40 AEs (38.9%) were considered by the investigators as possibly related to the investigational drugs (101BHG-D01 inhalation and placebo) and reported as adverse drug reactions. The incidence of adverse drug reactions in the 101BHG-D01

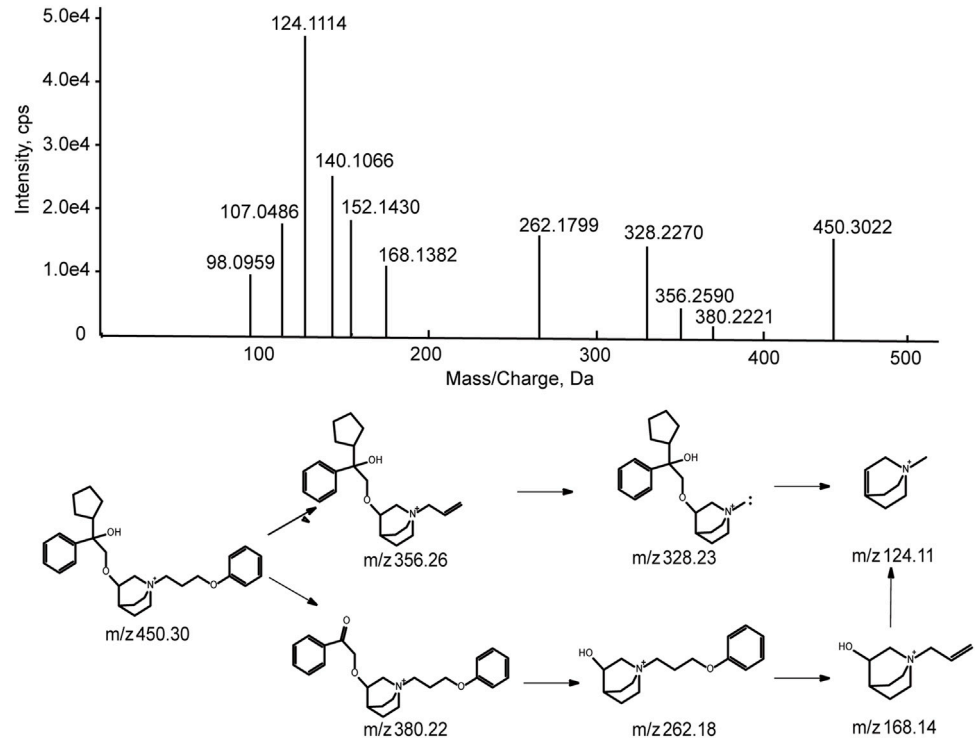

FIGURE 5
Accurate MS/MS spectra of 101BHG-D01 and its proposed fragmentation pathway.

inhalation treatment was lower than that in the placebo treatment (60%), and there was no obvious dose correlation. The most frequently adverse drug reactions were abnormal ECG and laboratory results, including: hyponatremia, hypertriglyceridemia, increased alanine aminotransferase, increased total bile acid, and sinus bradycardia. Oral ulcer and palpitation, which were considered to be related to the pharmacological effects of anticholinergics, had low incidence. All the adverse drug reactions were mild in intensity and reported as grade 1 (U.S. Department of Health and Human Services, 2017). The investigators confirmed that the adverse drug reactions had no clinical significance. No subject withdrew from the study due to the adverse events. No serious adverse reactions occurred. All events were resolved at the end of the trial. In general, 101BHG-D01 was safe and well tolerated in healthy subjects.

4 Discussion

This is the first clinical trial to investigate the pharmacokinetics, metabolite profiling, safety and tolerability of 101BHG-D01 delivered by MDI after single inhalation in Chinese healthy subjects. Meanwhile, according to the results of the metabolite profiling *in vitro*, the main metabolite of 101BHG-D01 was identified as M6, which corresponding to the loss of phenyl group compared with the parent drug. The pharmacokinetic profiles of M6 were also investigated. 101BHG-D01 was safe and well tolerated in this study.

In terms of the pharmacokinetic study, following single inhalation, 101BHG-D01 was rapidly absorbed into plasma and eliminated slowly. The T_{max} over the dose range was about 5 min, and the mean values of $t_{1/2z}$ were about 30 h. 101BHG-D01 inhalation aerosol is indicated for the treatment of COPD, which requires the study drug helps patients relieve the symptoms quickly. The immediate absorption showed 101BHG-D01 could reach its peak concentration in a few minutes, and implied 101BHG-D01 inhalation aerosol could exhibit its therapeutic effect rapidly after administration. The half-life of 101BHG-D01 is longer than that of bencycloquidium bromide (BCQB, about 15 h) (Luo et al., 2021), which indicates 101BHG-D01 has a higher affinity to the M receptors. BCQB is another M receptor antagonist. Its nasal spray has been approved by Chinese National Medical Products Administration (NMPA) and its inhalation aerosol is under the clinical trial. The long half-life of 101BHG-D01 suggests the frequency of clinical administration, and once-daily dosing can be explored in the

following dose exploration studies in COPD patients. These pharmacokinetic profiles are similar to the other anticholinergic bronchodilators (Cahn et al., 2013; Algorta et al., 2016; Sechaud et al., 2016). The systemic exposure to 101BHG-D01 after inhaled administration was low, when measured by C_{max} and AUC parameters. For the conventional oral drugs, after absorbed into the circulation, drugs are transported to the target organs by bloodstream. Contrary to the conventional oral drugs, after inhalation, 101BHG-D01 directed to its target organ lung, and then some of it was released from its target organ lung to blood, which resulted in its low systemic exposure. This characteristic might guarantee the safety of the study drug and minimize cardiovascular side effects resulted from the undesired binding with other muscarinic receptors in heart. M6 reached its peak concentration later than the parent drug and eliminated more rapidly than the parent drug. The C_{max} and AUC of 101BHG-D01 increased with dose escalation in the range of 20 to 600 μg, but the increasing rates were higher than the dose increasing rate. Compared with the 600 μg dose cohort, the significant increase of the systemic exposure to 101BHG-D01 in the 900 μg dose cohort was not observed. The C_{max} and AUC values of 101BHG-D01 increased out of proportion to the whole studied doses, which meant the linear pharmacokinetic characteristics of 101BHG-D01 was not observed. These results might be related to the large inter-individual variability of the C_{max} and AUC of 101BHG-D01.101BHG-D01 is a substrate for CYP2D6, and CYP2D6 is a drug-metabolizing enzyme with gene polymorphism. This characteristic might explain the large inter-subject variability of the PK parameters. Hence, the CYP2D6 genotyping in patients need to be considered in the Phase II and III studies. On the other hand, with the inhaled doses ascending, the binding sites of the M receptors might be saturated with the study drug, which might also result in that the C_{max} and AUC values of 101BHG-D01 increased out of proportion to the whole studied doses. The cumulative excretion rates of 101BHG-D01 and M6 in urine were low, which indicated that the renal excretion might not be a main elimination route for the study drug. This characteristic indicates that the treatment of COPD with 101BHG-D01 might reduce the risk of urinary retention. If the study drug is mainly excreted in urine, it would bind with the muscarinic M3 receptors in detrusor smooth muscle, cause the detrusor smooth muscle relaxation and increase the risk of urinary retention. Urinary retention is an adverse drug reaction of tiotropium, and this undesirable safety profile limits its clinical application in patients with urinary retention. Fecal excretion might be the major excretion pathway of 101BHG-D01. These data support the progression of 101BHG-D01 inhalation aerosol in the Phase II and III clinical study in patients with COPD.

The *in vitro* metabolic profiles of 101BHG-D01 and relative quantification of the parent drug and the metabolites *in vivo* were also thoroughly investigated using HPLC-Q/TOF-MS and LC-MS/MS method in this study. *In vitro*, 101BHG-D01 was incubated with human liver microsomes and 36 metabolites were identified. According to the unpublished data provided by Beijing Shuobai Pharmaceutical Technology Co., Ltd., compared with the metabolites identified in animal (mice, rat, beagle dog, and Macaca fascicularis) liver microsomes, there was no obvious difference from those identified in human liver microsomes, which demonstrated the nonclinical safety test has its reference value. Using the *in vitro* results as a reference, the relative contents of 101BHG-D01 and its metabolites in human plasma, urine and feces were calculated. The types and relative contents of the metabolites in plasma, urine and feces were different. The main characteristic metabolic biotransformation routes involved hydroxylation and loss of phenyl group. No major metabolite that exceeded 10% of total drug-related systemic exposure was observed in the single-dose escalation study. In the subsequent multiple-dose escalation study, the relative quantification of the parent drug and metabolites was also conducted in the multiple administration dose (MAD) samples. The results show that the types and relative contents of the metabolites in the MAD samples are similar with those in the single administration dose (SAD) samples. The safety testing of drug metabolites guidance for industry of FDA emphasizes human metabolites that present at greater than 10 percent of total drug-related exposure at steady state can raise a safety concern. The above results indicate that the additional safety and toxicity assessments of the major metabolites are not necessary at present.

5 Conclusion

In conclusion, the initial pharmacokinetics, metabolite profiling, safety and tolerability of 101BHG-D01 indicate that it is a good candidate for the treatment of COPD and enable further clinical development in subsequent studies in COPD patients.

Data availability statement

The original contributions presented in the study are included in the article/Supplementary Material, further inquiries can be directed to the corresponding authors.

Ethics statement

The studies involving human participants were reviewed and approved by Clinical Research Ethics Committee of China-Japan Friendship Hospital (Beijing, China). The patients/participants

provided their written informed consent to participate in this study.

Author contributions

HG wrote the manuscript. JL designed and conducted the study (as the Principal Investigator of this clinical trial). HG, MC, and GC (clinical sample collection and handling) conducted the study. HG, LD, and MC analyzed the data. XC, ZS, and LD reviewed and gave valuable comments on the manuscript. All authors read and approved the final manuscript.

Funding

This study was sponsored and funded by Beijing Shuobai Pharmaceutical Technology Co., Ltd.

Conflicts of interest

XC and ZS are employed by Beijing Shuobai Pharmaceutical Technology Co., Ltd. MC is employed by Nanjing Jiening Pharmaceutical Technology Co., Ltd. The authors declare that this study received funding from Beijing Shuobai Pharmaceutical Technology Co., Ltd.

The funder had the following involvement, the writing of this article and the decision to submit it for publication, in the study: Pharmacokinetics, metabolite profiling, safety, and tolerability of inhalation aerosol of 101BHG-D01, a novel, long-acting and selective muscarinic receptor antagonist, in healthy Chinese subjects.

Publisher's note

Supplementary material

The Supplementary material for this article can be found online at: https://www.frontiersin.org/articles/10.3389/fphar.2022.1064364/full#supplementary-material

References

Alfahad, A. J., Alzaydi, M. M., Aldossary, A. M., Alshehri, A. A., Almughem, F. A., Zaidan, N. M., et al. (2021). Current views in chronic obstructive pulmonary disease pathogenesis and management. *Saudi Pharm. J.* 29 (12), 1361–1373. doi:10.1016/j.jsps.2021.10.008

Algorta, J., Andrade, L., Medina, M., Kirkov, V., Arsova, S., Li, F., et al. (2016). Pharmacokinetic bioequivalence of two inhaled tiotropium bromide formulations in healthy volunteers. *Clin. Drug Investig.* 36 (9), 753–762. doi:10.1007/s40261-016-0441-8

Anzueto, A., and Kaplan, A. (2020). Dual bronchodilators in chronic obstructive pulmonary disease: Evidence from randomized controlled trials and real-world studies. *Respir. Med. X* X, 100016. doi:10.1016/j.yrmex.2020.100016

Barnes, P. J. (2000). The pharmacological properties of tiotropium. *Chest* 117 (2), 63S–66S. doi:10.1378/chest.117.2_suppl.63s

Cahn, A., Tal-Singer, R., Pouliquen, I. J., Mehta, R., Preece, A., Hardes, K., et al. (2013). Safety, tolerability, pharmacokinetics and pharmacodynamics of single and repeat inhaled doses of umeclidinium in healthy subjects: two randomized studies. *Clin. Drug Investig.* 33 (7), 477–488. doi:10.1007/s40261-013-0088-7

Calzetta, L., Coppola, A., Ritondo, B. L., Matino, M., Chetta, A., and Rogliani, P. (2021). The impact of muscarinic receptor antagonists on airway inflammation: A systematic review. *Int. J. Chron. Obstruct. Pulmon. Dis.* 16, 257–279. doi:10.2147/COPD.S285867

Chu, N. N., Huang, K., Que, L. L., Ding, Y., Gu, X. H., Zhang, L., et al. (2022). Safety, tolerability, and pharmacokinetic study of 101BHG-D01 nasal spray, a novel long-acting and selective cholinergic M receptor antagonist, in healthy Chinese volunteers: a randomized, double-blind, placebo-controlled, single-dose escalation, first-in-human study. *Eur. J. Drug Metab. Pharmacokinet.* 47 (4), 509–521. doi:10.1007/s13318-022-00769-6

da Silva, G., Feltrin, T. D., Pichini, F. D. S., Cielo, C. A., and Pasqualoto, A. S. (2022). Quality of life predictors in voice of individuals with chronic obstructive pulmonary disease. *J. Voice*. doi:10.1016/j.jvoice.2022.05.017

Donohue, J. F., van Noord, J. A., Bateman, E. D., Langley, S. J., Lee, A., Witek, T. J., Jr., et al. (2002). A 6-month, placebo-controlled study comparing lung function and health status changes in COPD patients treated with tiotropium or salmeterol. *Chest* 122 (1), 47–55. doi:10.1378/chest.122.1.47

Hamilton, R. A., Garnett, W. R., and Kline, B. J. (1981). Determination of mean valproic acid serum level by assay of a single pooled sample. *Clin. Pharmacol. Ther.* 29 (3), 408–413. doi:10.1038/clpt.1981.56

Hop, C. E. C. A., Wang, Z., Chen, Q., and Kwei, G. (1998). Plasma-pooling methods to increase throughput for *in vivo* pharmacokinetic screening. *J. Pharm. Sci.* 87 (7), 901–903. doi:10.1021/js970486q

Hummel, J., McKendrick, S., Brindley, C., and French, R. (2009). Exploratory assessment of dose proportionality: review of current approaches and proposal for a practical criterion. *Pharm. Stat.* 8 (1), 38–49. doi:10.1002/pst.326

Kabir, E. R., and Morshed, N. (2015). Different approaches in the treatment of obstructive pulmonary diseases. *Eur. J. Pharmacol.* 764, 306–317. doi:10.1016/j.ejphar.2015.07.030

Loke, Y. K., and Singh, S. (2013). Risk of acute urinary retention associated with inhaled anticholinergics in patients with chronic obstructive lung disease: systematic review. *Ther. Adv. Drug Saf.* 4 (1), 19–26. doi:10.1177/2042098612472928

Luo, Z., Hu, C., Pan, Y., Miao, J., Wang, Y., Ding, L., et al. (2021). Safety, tolerability and pharmacokinetics of bencycloquidium bromide, a novel inhaled anticholinergic bronchodilator, in healthy subjects: Results from phase I studies. *Eur. J. Pharm. Sci.* 157, 105646. doi:10.1016/j.ejps.2020.105646

Oba, Y., Zaza, T., and Thameem, Z. M. (2015). Safety, tolerability and risk benefit analysis of tiotropium in COPD. *Int. J. Chron. Obstruct. Pulmon. Dis.* 3, 575–584. doi:10.2147/copd.s3530

Penner, N., Klunk, L. J., and Prakash, C. (2009). Human radiolabeled mass balance studies: objectives, utilities and limitations. *Biopharm. Drug Dispos.* 30 (4), 185–203. doi:10.1002/bdd.661

Quinn, D., Barnes, C. N., Yates, W., Bourdet, D. L., Moran, E. J., Potgieter, P., et al. (2018). Pharmacodynamics, pharmacokinetics and safety of revefenacin (TD-4208), a long-acting muscarinic antagonist, in patients with chronic obstructive pulmonary disease (COPD): Results of two randomized, double-blind, phase 2 studies. *Pulm. Pharmacol. Ther.* 48, 71–79. doi:10.1016/j.pupt.2017.10.003

Rhee, C. K., Yoshisue, H., and Lad, R. (2019). Fixed-dose combinations of long-acting bronchodilators for the management of COPD: Global and asian perspectives. *Adv. Ther.* 36 (3), 495–519. doi:10.1007/s12325-019-0893-3

Sechaud, R., Machineni, S., Tillmann, H. C., Hara, H., Tan, X., Zhao, R., et al. (2016). Pharmacokinetics of glycopyrronium following repeated once-daily inhalation in healthy Chinese subjects. *Eur. J. Drug Metab. Pharmacokinet.* 41 (6), 723–731. doi:10.1007/s13318-015-0300-7

Tashkin, D. P., Celli, B., Senn, S., Burkhart, D., Halpin, D., Menjoge, S., et al. (2008). A 4-year trial of tiotropium in chronic obstructive pulmonary disease. *N. Engl. J. Med.* 359 (15), 1543–1554. doi:10.1056/NEJMoa0805800

U.S. Department of Health and Human Services (2017). *Common Terminology criteria for adverse events (CTCAE) version 5.0*. USA: U.S. Department of Health and Human Services, 27, 2017.

van Haarst, A., McGarvey, L., and Paglialunga, S. (2019). Review of drug development guidance to treat chronic obstructive pulmonary disease: US and EU perspectives. *Clin. Pharmacol. Ther.* 106 (6), 1222–1235. doi:10.1002/cpt.1540

Xu, S., Zhang, D., He, Q., Ma, C., Ye, S., Ge, L., et al. (2022). Efficacy of liuzijue qigong in patients with chronic obstructive pulmonary disease: A systematic review and meta-analysis. *Complement. Ther. Med.* 65, 102809. doi:10.1016/j.ctim.2022.102809

Yohannes, A. M., Connolly, M. J., and Hanania, N. A. (2013). Ten years of tiotropium: clinical impact and patient perspectives. *Int. J. Chron. Obstruct. Pulmon. Dis.* 8, 117–125. doi:10.2147/COPD.S28576

Zhang, W., Jiang, H., Jin, M., Wang, Q., Sun, Q., Du, Y., et al. (2018). UHPLC-Q-TOF-MS/MS based screening and identification of the metabolites *in vivo* after oral administration of betulin. *Fitoterapia* 127, 29–41. doi:10.1016/j.fitote.2018.04.010

frontiers | Frontiers in Pharmacology

TYPE Original Research
PUBLISHED 16 January 2023
DOI 10.3389/fphar.2023.1102244

OPEN ACCESS

EDITED BY
Stanislav Yanev,
Bulgarian Academy of Sciences (BAS), Bulgaria

REVIEWED BY
Xiangmeng Wu,
University of Arizona, United States
Jiaqi Mi,
Boehringer Ingelheim, Germany

*CORRESPONDENCE
Fen Yang,
yf7854@163.com

†These authors have contributed equally to this work and shared senior authorship

SPECIALTY SECTION
This article was submitted to Drug Metabolism and Transport, a section of the journal Frontiers in Pharmacology

RECEIVED 18 November 2022
ACCEPTED 04 January 2023
PUBLISHED 16 January 2023

CITATION
Li X, Bo Y, Yin H, Liu X, Li X and Yang F (2023), Population pharmacokinetic analysis of TQ-B3203 following intravenous administration of TQ-B3203 liposome injection in Chinese patients with advanced solid tumors.
Front. Pharmacol. 14:1102244.
doi: 10.3389/fphar.2023.1102244

Population pharmacokinetic analysis of TQ-B3203 following intravenous administration of TQ-B3203 liposome injection in Chinese patients with advanced solid tumors

Xiaoqing Li[1†], Yunhai Bo[1†], Han Yin[1], Xiaohong Liu[1], Xu Li[2] and Fen Yang[1*]

[1]Key laboratory of Carcinogenesis and Translational Research (Ministry of Education), National drug clinical trial center, Peking University Cancer Hospital & Institute, Beijing, China, [2]Chia Tai Tianqing Pharmaceutical Group Co Ltd, Nanjing, Jiangsu, China

Background: TQ-B3203 is a novel topoisomerase I inhibitor currently in development for the treatment of advanced solid tumors. Great differences in pharmacokinetic characteristics were found among individuals according to the phase I clinical trial following intravenous administration of TQ-B3203 liposome injection (TLI) in Chinese patients with advanced solid tumors. Thus, it is significant to establish a population pharmacokinetic model to find the key factors and recognize their effect on pharmacokinetic parameters in order to guide individualized administration.

Methods: Non-linear mixed effect models were developed using the plasma concentrations obtained from the phase I clinical trial by implementing the Phoenix NLME program. Covariates that may be related to pharmacokinetics were screened using stepwise methods. The final model was validated by goodness-of-fit plots, visual predictive check, non-parametric bootstrap and a test of normalized prediction distribution errors.

Results: A three-compartment model with first-order elimination was selected as the best structural model to describe TQ-B3203 disposition adequately. Direct bilirubin (DBIL) and body mass index (BMI) were the two most influential factors on clearance, while lean body weight (LBW) was considered to affect the apparent distribution volume of the central compartment. The population estimations of clearance and central volume were typical at 3.97 L/h and 4.81 L, respectively. Model-based simulations indicated that LBW had a great impact on C_{max}, BMI exerted a considerable influence on AUC_{0-t}, and the significance of DBIL on both AUC_{0-t} and C_{max} was similarly excellent.

Conclusion: The first robust population pharmacokinetic model of TQ-B3203 was successfully generated following intravenous administration of TLI in Chinese patients with advanced solid tumors. BMI, LBW and DBIL were significant covariates that affected the pharmacokinetics of TQ-B3203. This model could provide references for the dose regimen in the future study of TLI.

KEYWORDS

population pharmacokinetic model, camptothecin, TQ-B3203, model validation, model application

1 Introduction

Topoisomerase I, a critical intra-nuclear enzyme for DNA replication, has a higher activity and replication rate in most cancer cells. Camptothecin (CPT), extracted from traditional Chinese medicine prescriptions (Redinbo et al., 1998), is a topoisomerase I inhibitor that could combine topoisomerase I and DNA complex to form a stable ternary complex to prevent DNA reconnection, cause DNA damage, introduce G2/M phase arrest, and therefore lead to cancerous cell apoptosis (Hertzberg et al., 1989; Redinbo et al., 1998). CPT and its derivatives have played an essential role in the treatment of some solid tumors, including colorectal cancer, liver cancer, small-cell lung cancer and glioblastoma (Pommier, 2006; Selas et al., 2021).

Irinotecan, the most representative chemically modified CPT derivative, was created to avoid the poor water-solubility, low antineoplastic activity (Gottlieb and Luce, 1972) and many adverse reactions of CPT (Rozencweig et al., 1976). Although it has been clinically used in anticancer treatments for nearly 28 years after approval by the FDA, some obvious disadvantages still limit its application, such as short half-life and high toxicity (Herben et al., 1996; Chabot, 1997; Pommier, 2006). TQ-B3203 is a novel semisynthetic derivative of CPT with an aliphatic chain. It exhibited more vital pharmacodynamic activity than irinotecan in the tumor growth inhibition test of several cell types (Zhang et al., 2017) because it could accumulate more in cells to increase cytotoxicity due to its higher lipophilicity. Furthermore, TQ-B3203 liposome injection (TLI) was produced after TQ-B3203 was embedded in liposomes in order to acquire a significant reduction in toxicity and improvement of efficacy because liposomes, well-recognized drug delivery carriers, have the ability to prolong drug circulation time, passively accumulate in tumor tissues and increase drug exposure (Drummond et al., 1999; Yang et al., 2013). The formulation-related stability and the distribution *in vivo* were evaluated in the pre-clinical study (Supplementary Figure S1, S2 in Supplementary Material).

The narrow therapeutic window is a critical defect of cytotoxic anticancer drugs, thus their toxicity has a strong correlation with drug exposure, which depends on the pharmacokinetic characteristics. Therefore, it is necessary to find key factors leading to pharmacokinetic variability among patients (Ardizzoni et al., 1997). Population pharmacokinetic (PopPK) modeling is a standard method to identify the essential determinants of drug disposition by using the drug concentration and covariate information from subjects, such as demographics, clinical laboratory results and genetic characteristics. In previous PopPK studies of irinotecan, some covariates are considered to have significant effects on pharmacokinetic parameters, such as performance status and liver function on clearance (CL) and body weight on apparent distribution volume of the central compartment (V_1) (Klein et al., 2002; Mathijssen et al., 2002; Xie et al., 2002). As an analog of irinotecan, TQ-B3203 also showed great differences in pharmacokinetic characteristics among individuals according to the phase I clinical trial, so it is significant to find the potential covariates on pharmacokinetic parameters in order to guide individualized administration.

In this study, we aimed to develop a PopPK model of TQ-B3203. The influence of selected internal and external factors on pharmacokinetics was recognized and quantified to characterize the pharmacokinetic difference among individuals. Additionally, the effects of significant covariates on TQ-B3203 exposure in patients were also explored. This study will provide critical information for the future development and clinical application of TQ-B3203.

2 Methods

2.1 Clinical trial

This multi-center, dose-escalation phase I clinical study (Register No. NCT03447145) was conducted to assess the pharmacokinetic characteristics and safety of TQ-B3203 after TLI intravenous administration. This study was designed in accordance with the ethical principles described in the Declaration of Helsinki and approved by the Ethics Committee of Peking University Cancer Hospital. All patients signed informed consent prior to their enrollment in this study. The process of this phase I clinical study did not involve randomization, blinding and power analysis, and the attrition was recorded.

Demographic characteristics were collected from electronic medical records. Patients aged 18–80 years with clearly diagnosed advanced solid tumors were enrolled in this study. Other key inclusion criteria were as follows: body mass index (BMI) of 18.5–26 kg/m^2, Eastern Cooperative Oncology Group (ECOG) performance status of 0–1, life expectancy > 3 months, normal primary organ functions and >30 days recovery after receiving anti-tumor treatment or surgery.

Patients were not eligible if they have suffered from other malignant tumors within 5 years, have participated in other clinical trials within 4 weeks, have received other CPT analog therapy, and were in possession of neurological, circulatory and urinary diseases such as meningitis, pericardial effusion, coagulopathy or hypertension.

2.2 Drug administration and sampling

The novel anticancer drug TLI was provided by Nanjing Chia-tai Tianqing Pharmaceutical Group (Nanjing, China). Patients received TLI with dose levels ranging from 2 to 45 mg/m^2 by intravenous infusion for 90 min on days 1 (cycle 1) and 22 (cycle 2). Blood samples were collected at pre-dose, 45 and 90 min after the infusion start, and were obtained at .5, 1, 2, 4, 8, 12, 24, 48, 72 and 96 h after the end of the infusion. The whole blood samples were immediately centrifuged at 3,000 rpm for 10 min at 4°C and obtained plasma samples were stored at −80°C pending analysis.

2.3 Analytical methods

The plasma concentration of TQ-B3203 in this study was determined using a fully validated liquid chromatography-tandem mass spectrometry (LC-MS/MS) method with bis (p-nitrophenyl) phosphate (2 mol/L) used as the esterase inhibitor and TQ-B3203-d_8 used as the internal standard (the structures of TQ-B3203 and TQ-B3203-d_8 are shown in Supplementary Figure S3 in Supplementary Material), which has been reported in the previous study (Yang et al., 2021). The plasma samples were protein precipitated by methanol and the processed samples were chromatographed on an AQUITY BEH C8 column (50 × 2.1 mm, id 1.7 μm) with acetonitrile and water (.1% formic acid) as the mobile phase. Mass spectrometric analysis was performed on Waters Xevo TQS tandem mass spectrometer (Waters

10.3389/fphar.2023.1102244

TABLE 1 Baseline demographic and clinical characteristics[a].

Characteristic	Median (IQR)	Range
No. of patients	15	
Sex, male/female	10 (66.7%)/5 (33.3%)	
*UGT1A1*28*, TA (6)/TA (6); TA (6)/TA (7)	14 (93.3%)/1 (6.7%)	
*UGT1A1*6*, 211G/G; 211G/A	10 (66.7%)/5 (33.3%)	
Treatment episode	25	
No. of concentration	316	
Patient age, years (n = 25)	57 (44–65)	31–70
Height, cm (n = 25)	164 (160–173)	148–178
Weight, kg (n = 25)	64.0 (57.5–68.0)	47.9–80.0
Adj weight, kg (n = 25)	61.90 (55.55–70.57)	48.21–74.31
IBW, kg (n = 25)	60.50 (54.26–68.65)	45.81–73.18
LBW, kg (n = 25)	49.53 (38.36–55.45)	32.09–59.40
BF% (n = 25)	23.39 (20.94–33.01)	13.41–41.51
BMI, kg/m^2 (n = 25)	23.44 (21.05–24.91)	18.64–28.97
BSA, m^2 (n = 25)	1.678 (1.600–1.841)	1.420–1.938
CRE, μmol/L (n = 25)	60 (51–69)	38–204
CLcr, mg/dl (n = 25)	109.2 (83.64–120.0)	27.35–157.3
Adj CLcr, mg/dl (n = 25)	101.9 (83.64–113.9)	27.35–157.3
TBIL, μmol/L (n = 25)	9 (5.4–10.6)	2.9–25.8
DBIL, μmol/L (n = 25)	2.82 (2.3–4)	1.5–7.9
IBIL, μmol/L (n = 25)	6 (2.9–7.78)	.9–17.9
ALT, IU/L (n = 25)	11.3 (8–17)	3–24
AST, IU/L (n = 25)	16.7 (13.2–21)	11.2–29

[a]IQR, interquartile range; No. of patients, numbers of patients; No. of concentration, numbers of concentration; Adj weight, adjusted weight; IBW, ideal body weight; LBW, lean body weight; BF%, body fat percentage; BMI, body mass index; BSA, body surface area; CRE, serum creatinine; CLcr, endogenous creatinine clearance rate; Adj CLcr, adjusted endogenous creatinine clearance rate; TBIL, total bilirubin; DBIL, direct bilirubin; IBIL, indirect bilirubin; ALT, baseline alanine aminotransferase; AST, baseline aspartate transaminase.

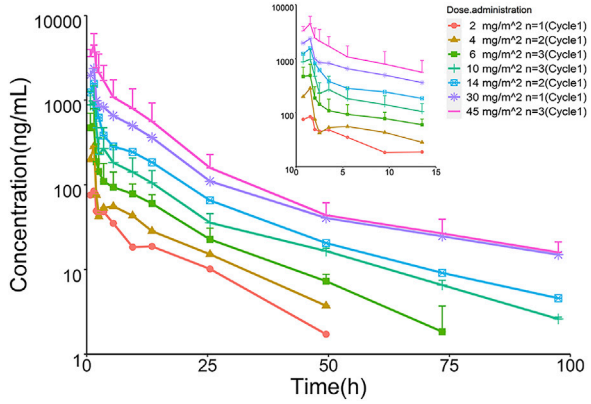

FIGURE 1
Semilogarithmic plots of mean concentration *versus* time of TQ-B3203.

Corp. Milford, MA, United States) equipped with an electrospray ionization source in positive mode (ESI+). The ESI source settings were as follows: Capillary voltage, 4.0 kV; Source temperature, 150°C; Desolvation temperature, 500°C; Cone gas flow, 150 L/h; Desolvation gas flow, 1000 L/h; Nebulizer gas pressure, 7 bar. Multiple reaction monitoring (MRM) transitions and related collision energy were m/z 949.5→393.1 (58 eV) for TQ-B3203 and m/z 957.4→398.0 (50 eV) for TQ-B3203-d_8. The linear range of TQ-B3203 was .5–500 ng/mL. Accuracy and precision were within the acceptable range of FDA bioanalytical assay validation criteria (e.g., ± 15%).

2.4 Pharmacokinetic study and statistical analyses

The pharmacokinetic parameters such as CL, the apparent volume of distribution (V_z), elimination half-life ($t_{1/2}$), the area under the plasma concentration-time curve from zero to the last time ($AUC_{0\text{-}t}$) and from zero to infinity ($AUC_{0\text{-}inf}$) were analyzed and calculated by the non-compartmental analysis (NCA) using the Phoenix (RRID:SCR_003163) WinNonlin (version 8.3, Pharsight Corporation, CA, United States), except that maximum observed plasma concentration (C_{max}) and time to C_{max} (T_{max}) were obtained directly from the observed concentration. The pharmacokinetic parameters (CL, V_z, $t_{1/2}$ and $AUC_{0\text{-}t}$) between cycles 1 and 2 were compared using paired t-tests, with significance denoted by $p < .05$.

2.5 PopPK modeling

The PopPK analysis of TQ-B3203 was performed using non-linear, mixed-effect modeling of Phoenix (RRID:SCR_003163) NLME (Version 8.3, Pharsight Corporation, CA, United States). R program

10.3389/fphar.2023.1102244

TABLE 2 Main pharmacokinetic parameters of TQ-B3203 calculated by NCA.

	Dose	AUC_{0-t}[a] (ng·h/mL)	AUC_{0-inf}[a] (ng·h/mL)	C_{max}[a] (ng/mL)	T_{max}[b] (h)	$t_{1/2}$[a] (h)	V_z[a] (L)	CL[a] (L/h)
cycle 1	2 (n = 1)	775	801	85	1.5	10.3	68.1	4.6
	4 (n = 2)	1,410	1,423	284	1.5 (1.5.1.5)	11.3	77.3	4.7
	6 (n = 3)	2705 (1,133)	2778 (1,121)	533 (236)	1.5 (.75.1.5)	16.4 (5.7)	90 (6.0)	4.0 (1.0)
	10 (n = 3)	5258 (1,679)	5326 (1,676)	1,044 (507)	1.5 (.75.1.5)	18.0 (.5)	87.4 (20.5)	3.4 (.7)
	14 (n = 2)	8584	8731	1,559	1.5 (1.5.1.5)	21.6	90	2.9
	30 (n = 1)	15882	16602	2357	1.5	33.3	133.8	2.8
	45 (n = 3)	26251 (11761)	27026 (11688)	4956 (787)	1.5 (.75.1.5)	34.3 (5.9)	148.7 (86.1)	2.9 (1.2)
cycle 2	4 (n = 2)	1,142	1,154	229	1.5	11.4	99.0	6.0
	6 (n = 3)	2366 (98)	2399 (102)	412 (126)	1.5 (.75.1.5)	17.5 (5.8)	111.6 (44)	4.4 (.3)
	10 (n = 3)	5493 (1,611)	5571 (1,608)	1,187 (687)	1.5 (.75.1.5)	17.9 (4.1)	81.2 (23.9)	3.1 (.5)
	14 (n = 1)	5901	5954	1,140	1.5	19.8	127.5	4.5
	30 (n = 1)	13040	13633	1,680	1.5	32.4	157.4	3.4

[a]The data are shown as mean (SD).
[b]T_{max} is shown as median (minimum, maximum).

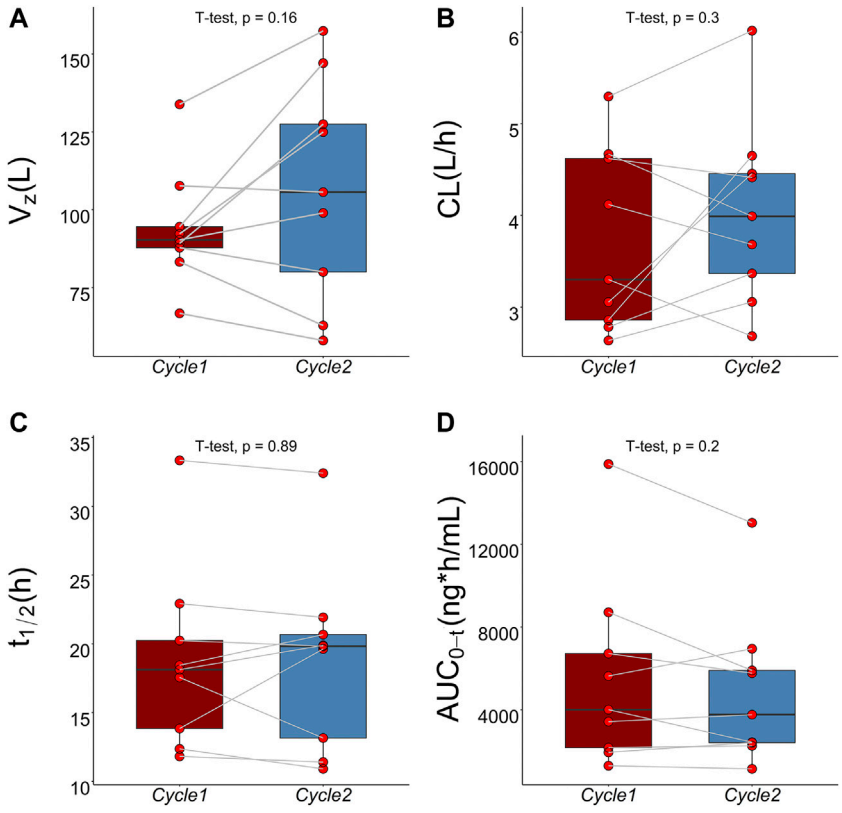

FIGURE 2
Comparison of pharmacokinetic parameters between cycle 1 and cycle 2 using paired *t*-test. **(A)** Comparison of V_z between cycle 1 and cycle 2, **(B)** Comparison of CL between cycle 1 and cycle 2, **(C)** Comparison of $t_{1/2}$ between cycle 1 and cycle 2, **(D)** Comparison of AUC_{0-t} between cycle 1 and cycle 2.

(Version 4.2.0, R Project for Statistical Computing, RRID:SCR_001905, http://www.r-project.org/) was used for statistical summaries and graphical analysis. The first-order conditional estimation-extended least-squares (FOCE-ELS) method built into the modeling program was applied for the estimation of pharmacokinetic parameters, covariate testing and model diagnostic.

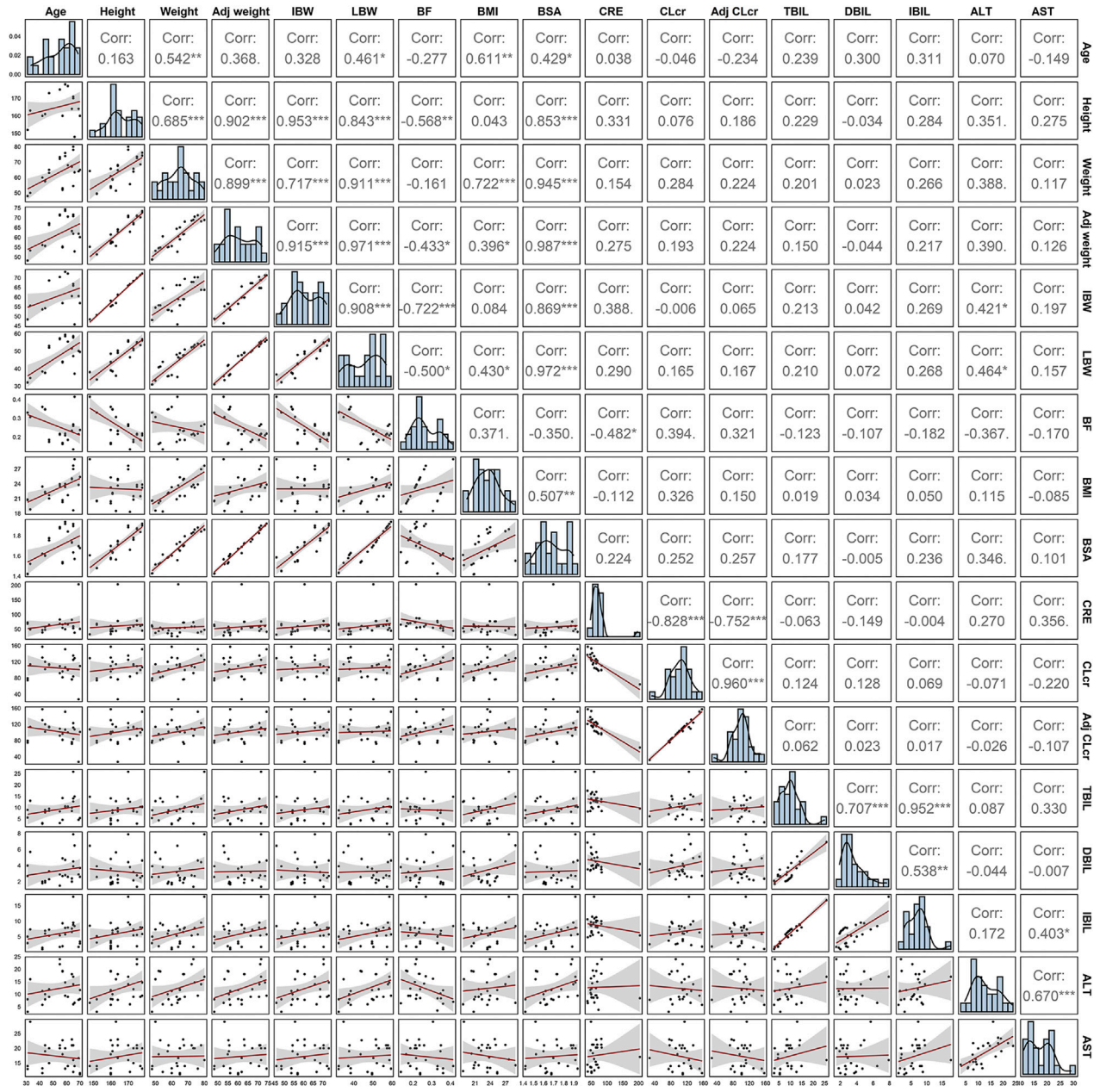

FIGURE 3
Spearman correlation analysis of continuous covariates.

2.5.1 Basic model

According to the semilogarithmic plots of individual TQ-B3203 plasma concentration-time, two- and three-compartment models with first-order elimination were tried to describe the dataset. Inter-individual variability (IIV, η, eta) was estimated by an exponential model, which was shown in Eq. 1:

$$\boldsymbol{P_{ij}} = \boldsymbol{\theta_i} * \boldsymbol{e^{\eta_{ij}}} \quad (1)$$

where P_{ij} represents the individual pharmacokinetic parameter estimation for *i*th parameter in *j*th individual, θ_i is the typical parameter estimation value for *i*th parameter and η_{ij} depicts the random variable for *i*th parameter in *j*th individual. Intra-individual variation, also known as residual variation (ε, epsilon), was tested by employing the additive, log-additive, proportional and power models. The distributions of η and ε were considered to follow a Gaussian distribution with mean of 0 and variance of ω^2 (omega) or σ^2 (sigma) as diagonal matrixes, respectively.

Inter-occasion variability (IOV) on the CL and the V_1 between Day 1 in cycles 1 (occasion 1) and 2 (occasion 2) was estimated in the basic model before the covariate selection. It was also included in the model as an exponential term (η_{IOV}) in Eq. 2 and Eq. 3 (Karlsson and Sheiner, 1993):

$$\boldsymbol{P_{ij}} = \boldsymbol{\theta_i} * \boldsymbol{e^{\eta_{ij}}} * \boldsymbol{e^{\eta_{IOV,1}}} \quad (2)$$

$$\boldsymbol{P_{ij}} = \boldsymbol{\theta_i} * \boldsymbol{e^{\eta_{ij}}} * \boldsymbol{e^{\eta_{IOV,2}}} \quad (3)$$

in which $\eta_{IOV,1}$ and $\eta_{IOV,2}$ are variabilities between occasions for the *i*th parameter in *j*th individual on occasion 1 and on occasion 2, respectively.

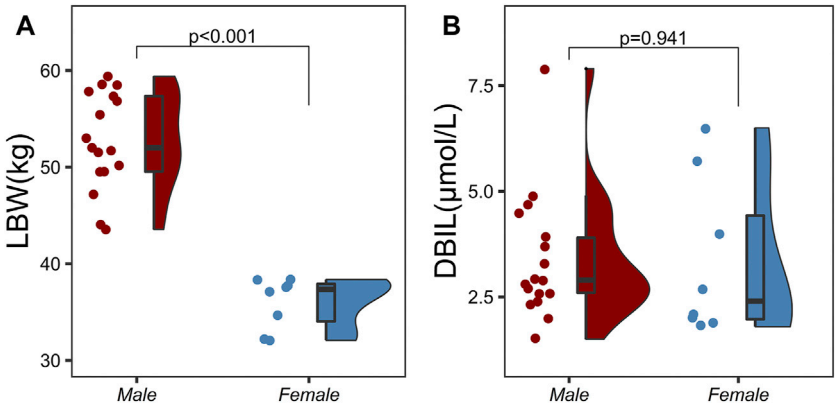

FIGURE 4
Correlation analysis between categorical variables and continuous variables using two independent samples *t*-test. **(A)** Correlation analysis between sex and lean body weight (LBW), **(B)** Correlation analysis between sex and direct bilirubin (DBIL).

TABLE 3 Results of the forward and backward stepwise procedure[a].

Step	Covariate screening	OFV	ΔOFV	p-value	Comments
1	None	160.054			Base model
Forward inclusion					
2	V_2-LBW	145.503	−14.551	<.001	
3	CL_2-DBIL/V_2-LBW	135.132	−10.371	<.01	
4	CL_2-DBIL-LBW/V_2-LBW	123.487	−11.645	<.001	
5	CL_2-DBIL-LBW/V_2-LBW/V_1-LBW	118.287	−5.2	<.05	
6	CL_2-DBIL-LBW/V_2-*UGT1A1*6*-LBW/V_1-LBW	111.601	−6.686	<.01	
7	CL-BMI/CL_2-DBIL-LBW/V_2- *UGT1A1*6*-LBW/V_1-LBW	104.794	−6.807	<.01	
8	CL-BMI-DBIL/CL_2-DBIL-LBW/V_2- *UGT1A1*6*-LBW/V_1-LBW	93.483	−11.311	<.001	Full model
Backward elimination					
9	CL-BMI-DBIL/CL_2-DBIL-LBW/V_2-LBW/V_1-LBW	97.753	4.27	>.01	Final model

[a]ΔOFV, the change of OFV.

The model superiority was determined by better visual inspection of the diagnostic plots and a smaller diagnostic index such as objective function (OFV), Akaike Information Criteria (AIC) and Bayesian information criteria (BIC). It was considered statistically significant that the OFV value (1 degree of freedom in χ2 distribution) was decreased by ≥ 3.84 points ($p < .05$).

2.5.2 Covariate analysis

Several covariates used for covariate analysis were directly obtained from the electronic medical records, such as age, height, weight, total bilirubin (TBIL), direct bilirubin (DBIL), indirect bilirubin (IBIL), baseline alanine aminotransferase (ALT), baseline aspartate transaminase (AST), sex, *UGT1A1*28* mutation type and *UGT1A1*6* mutation type. Other covariates were those from further calculated, including BMI, body surface area (BSA), lean body weight (LBW), body fat rate (BF%), endogenous creatinine clearance rate (CLcr), ideal body weight (IBW), adjusted weight and adjusted CLcr. BMI was calculated by the World Health Organization (WHO) admitted formula (Keys et al., 1972), and the BSA was obtained by applying Du Bios' formula (Du Bois and Du Bois, 1916). The LBW and BF% were considered as other covariates and added to the PopPK model because of the high lipid solubility of the drugs (Park et al., 2018). The Cockcroft-Gault formula (Eq. 4) was used to figure out the CLcr (Cockcroft and Gault, 1976). Additional covariates such as IBW (Eq. 5) (McCarron et al., 1974; Robinson et al., 1983), adjusted weight (Eq. 6) and adjusted CLcr (calculated by adjusted weight for BMI >25 kg/m^2) were introduced into the model (Winter et al., 2012).

For males:

$$CLcr\,(mg/dL) = \frac{(140 - age\,(years))^{*}weight\,(kg)^{*}88.4}{72^{*}serum\ creatinine\,(\mu mol/L)} \quad (4)$$

$$IBW\,(kg) = 50 + 2.3^{*}\left(\frac{height\,(cm)}{2.54} - 60\right) \quad (5)$$

$$adjusted\ weight\,(kg) = (weight\,(kg) - IBW\,(kg))^{*}0.4 + IBW\,(kg) \quad (6)$$

For females:

$$CLcr\,(mg/dL) = \frac{(140 - age\,(years))^{*}weight\,(kg)^{*}88.4}{72^{*}serum\ creatinine\,(\mu mol/L)}\ ^{*}0.85 \quad (4a)$$

$$IBW\,(kg) = 48.67 + 1.65^{*}\left(\frac{height\,(cm)}{2.54} - 60\right) \quad (5a)$$

$$adjusted\ weight\,(kg) = (weight\,(kg) - IBW\,(kg))^{*}0.4 + IBW\,(kg) \quad (6a)$$

TABLE 4 Pharmacokinetics parameter estimate in the final model and bootstrap results[a].

Parameters	Final model		Bootstrap	
	Estimate (%RSE)	95% CI	Median (%RSE)	95% CI
V_1 (L)	4.81 (8.47%)	4.01–5.61	4.83 (9.05%)	4.05–5.87
V_2 (L)	24.44 (5.94%)	21.58–27.30	24.69 (8.12%)	21.49–29.37
V_3 (L)	27.98 (6.69%)	24.30–31.66	27.81 (7.79%)	24.07–32.29
CL (L/h)	3.97 (4.85%)	3.59–4.35	3.96 (5.01%)	3.58–4.33
CL_2 (L/h)	1.95 (20.48%)	1.17–2.74	1.96 (23.87%)	1.28–3.13
CL_3 (L/h)	10.58 (11.28%)	8.23–12.92	10.45 (11.42%)	8.32–13.06
BMI on CL (L/h)	.78 (22.08%)	.44–1.12	.79 (39.13%)	.05–1.25
DBIL on CL (L/h)	−.24 (−36.01%)	−.42 to −.07	−.26 (−36.45%)	−.44 to −.09
DBIL on CL_2 (L/h)	−1.77 (−19.55%)	−2.46 to −1.09	−1.81 (−23.12%)	−2.68 to −1.04
LBW on CL_2 (L/h)	−2.55 (−27.03%)	−3.90 to −1.19	−2.53 (−31.22%)	−4.18 to −1.14
LBW on V_1 (L)	1.18 (37.01%)	.32–2.05	1.22 (44.96%)	.19–2.36
LBW on V_2 (L)	−1.41 (−19.49%)	−1.95 to −.87	−1.39 (−28.02%)	−1.92 to −.41
Inter-individual variability				
ω^2CL	.043 (36.00%)	.013–.073	.039 (39.06%)	.012–.071
ω^2V_3	.117 (29.88%)	.048–.185	.103 (35.64%)	.039–.185
ω^2CL_2	.573 (32.60%)	.203–.944	.529 (35.43%)	.173–.918
ω^2CL_3	.290 (32.50%)	.103–.477	.251 (34.40%)	.092–.424
Residual variability (σ)				
stdev0	.200 (10.30%)	.159–.240	.198 (10.43%)	.160–.239

[a]RSE, relative standard error; CI, confidence interval; ωCL, variance of inter-individual variability for CL; ωV_3, variance of inter-individual variability for V_3; ωCL_2, variance of inter-individual variability for CL_2; ωCL_3, variance of inter-individual variability for CL_3; stdev0, standard deviation.

The effect of continuous covariates was described by the power function after the normalization using the population median (Eq. 7), and the effect of categorical covariates was modeled using the exponential function (Eq. 8):

$$Effect_i = \left(\frac{Cov_{ij}}{Cov_{median}}\right)^{\theta_{covi}} \quad (7)$$

$$Effect_i = e^{Cov_{ij}*\theta_{covi}} \quad (8)$$

where $Effect_i$ is the multiplicative factor of the covariate i, Cov_{ij} is the continuous covariate value or categorical variable with the value of 0 or 1 for the covariate i in individual j, Cov_{median} is the median value of covariate, and θ_{covi} describe the fixed effect for covariate i.

However, not all the covariates mentioned above were applied to construct the final covariate model in order to avoid the presence of covariate collinearity. In the univariate screening process, when both two covariates had a significant impact on the same pharmacokinetic parameter and they were highly correlated ($r > .5$), such as CLcr and adjusted CLcr, only one of them was reserved in the model. The covariates that remained were selected or excluded utilizing forward and backward stepwise on the basis of the change of OFV value. If the decrease of OFV exceeded 3.84 points ($p < .05$, df = 1), the covariates could join the basic model in the forward inclusion process. Subsequently, backward elimination was employed to confirm the covariate selection. If the increase of OFV was less than 6.64 points ($p < .01$, df = 1), the covariates should be retained in the final PopPK model. Moreover, the correlation between IIV of pharmacokinetic parameters should be clarified to construct a covariance model.

2.6 Model validation

Goodness-of-fit (GOF) plots, visual predictive check (VPC), non-parametric bootstrap and test of normalized distribution errors (NPDE) were adopted to confirm the validity of the final model. The GOF plots evaluated the reliability of the final model, including drug concentration observations (DV) *versus* population predictions (PRED) or individual predictions (IPRED) and conditional weighted residuals (CWRES) *versus* time or PRED. VPC was performed by simulating 1,000 virtual data per time in the final model based on Monte Carlo simulation and the model predictions and DV at the 5th, 50th and 95th percentiles were compared. The bootstrap analysis was implemented to judge the robustness of the last model. During this analysis, the initial dataset was randomly resampled 1,000 times with replacement, and then the obtained 95% confidence intervals of pharmacokinetic parameters were compared with the typical value of parameters in the final model. NPDE values, which were supposed to obey standard normal distribution if the final model was effective, were acquired after the 1,000 times simulation of each subject observation.

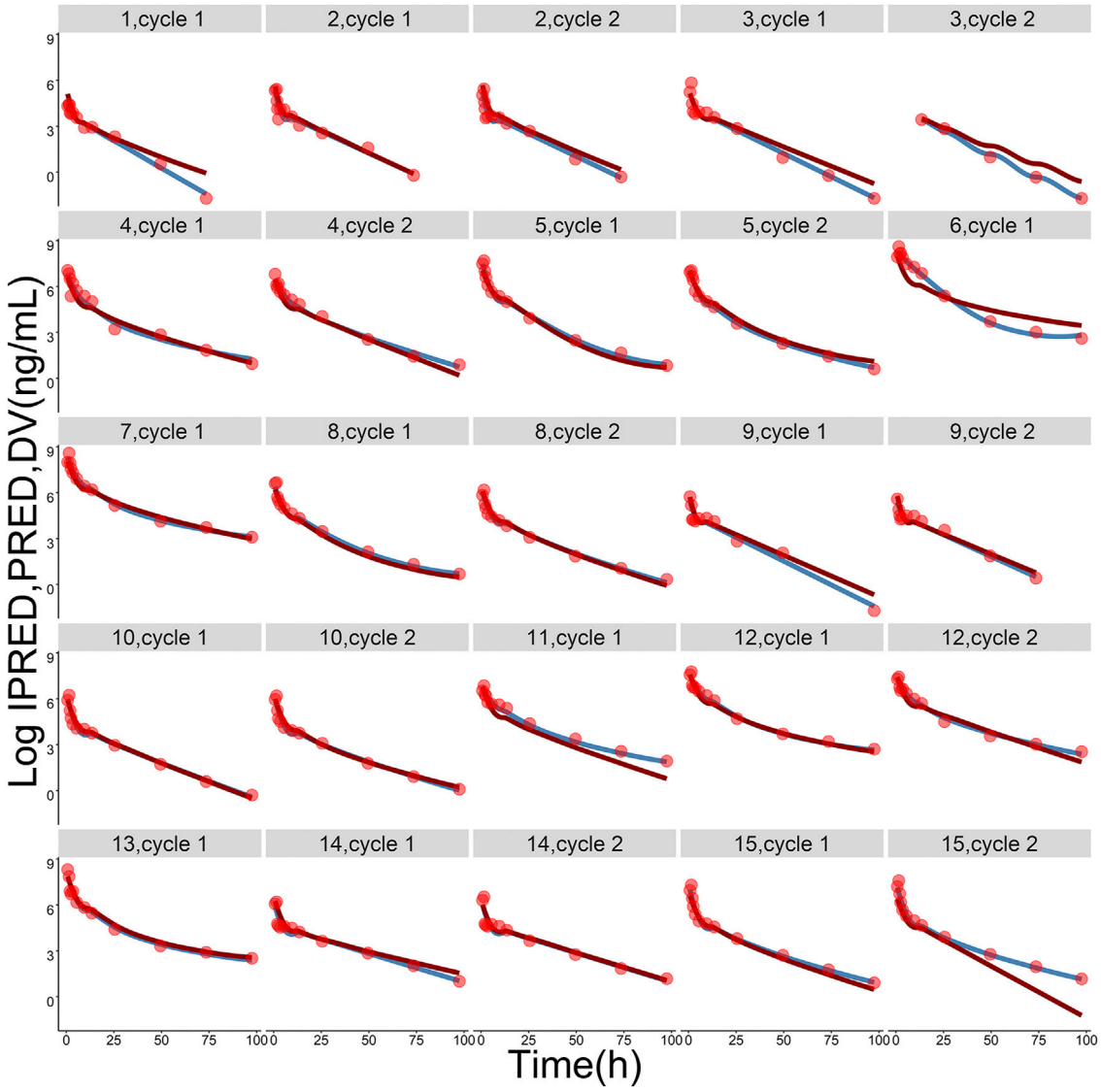

FIGURE 5
The logarithmic-transformed observations (log DV, red dots), logarithmic-transformed population predictions (log PRED, dark-red lines) and logarithmic-transformed individual predictions (log IPRED, steel-blue lines) from the final population pharmacokinetic model. The gray label on the top of each picture represents ID of each subject and treatment cycle.

2.7 Model application

This final PopPK model was used to predict TQ-B3203 exposure ($AUC_{0\text{-}t}$ and C_{max}), with the pharmacokinetic parameters counted by individual Bayes estimates. The sensitive plots were painted to clarify the effect of an identified covariate on the exposure parameters. Considering the occurrence of adverse effects, the single dose at 25 mg/m^2 level was finally chosen as a simulated dosing regimen in a representative population (with the median values of continuous covariates considered as the typical value). When the impact of one identified covariate was evaluated, the value of this covariate was regarded as the 5th or 95th percentiles of the population, with other covariates fixed to the typical value. The general exposure under the influence of covariates was compared with the exposure of the typical population.

3 Results

3.1 Clinical data summary

A total of 316 TQ-B3203 concentrations from 15 subjects with 25 episodes were used in the PopPK modeling. The demographic and clinical characteristics of baseline continuous and categorical covariates gathered from subjects are summarized in Table 1.

3.2 Pharmacokinetic analysis

The mean plasma TQ-B3203 concentration *versus* time semilogarithmic plot at different levels is displayed in Figure 1. The corresponding pharmacokinetic parameters are presented in Table 2. C_{max} always appears at the end of intravenous injection (1.5 h),

10.3389/fphar.2023.1102244

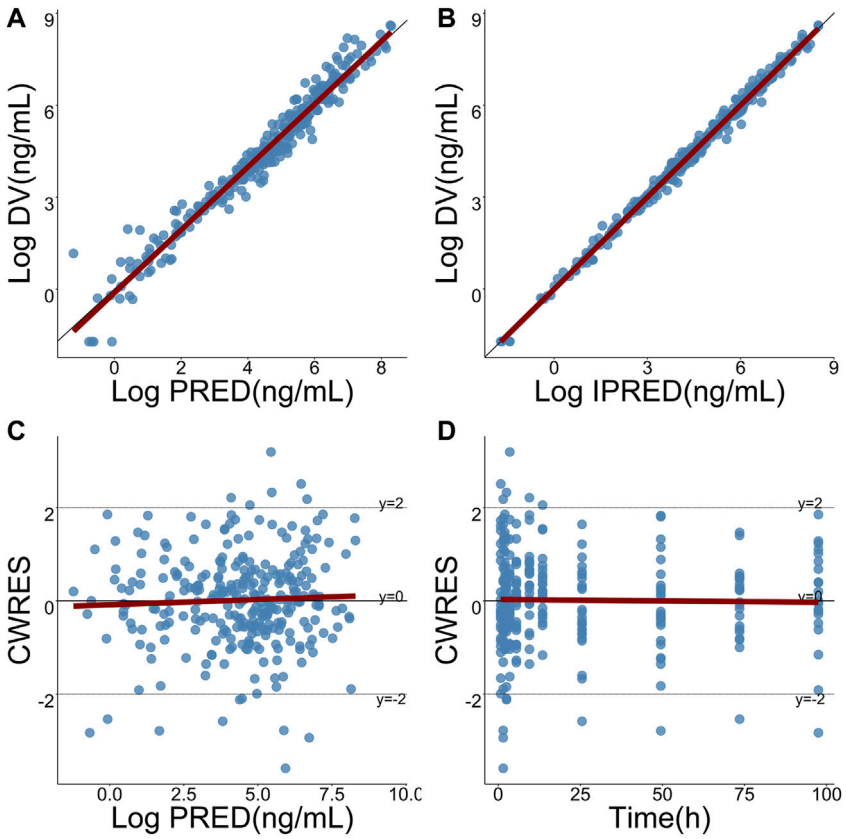

FIGURE 6
Goodness-of-fits plots for the final model. **(A)** Logarithmic-transformed observations (log DV) of TQ-B3203 *versus* logarithmic-transformed population predictions (log PRED), **(B)** Log DV *versus* logarithmic-transformed individual predictions (log IPRED), **(C)** Conditional weighted residual (CWRES) *versus* log PRED, **(D)** CWRES *versus* time. The dark-red lines represent linear regression.

followed by an obvious rapid elimination phase and a slow elimination phase. The half-life of TQ-B3203 is about 10–41 h (n = 15, median = 19.62, mean = 20). There is no significant difference in pharmacokinetic parameters between cycles 1 and 2 shown in Figure 2. Furthermore, an obvious accumulation of TQ-B3203 was not found in these dose groups.

3.3 PopPK model development

A three-compartment model with first-order elimination, which was parameterized as the V_1, the shallow peripheral volume of distribution (V_2), the deep peripheral volume of distribution (V_3), the CL and the inter-compartment clearance (CL_2 and CL_3), was selected as the best structural model to describe the pharmacokinetic profiles of TQ-B3203. The optimal model evaluation results were acquired in the selection of an exponential model to characterize the inter-individual variability and a log-additive model to describe intra-individual variability, so the pharmacokinetic parameters were estimated with the natural logarithm-transformed (log) plasma TQ-B3203 concentration data. IOV was not included in the model, because after the incorporation of IOV on CL and V_1, the log-additive error changed little from 22.4% to 21.4% and the fitting degree of the subsequent model was always poor in models, although there was a statistically significant decrease in OFV. Actually, there was no significant difference in pharmacokinetic parameters between cycles 1 and 2, so it could be considered that the cycle did not significantly affect the pharmacokinetic behavior of the TQ-B3203 *in vivo*. The distribution and correlation of continuous covariates are shown in Figure 3. The categorical covariate sex and continuous covariates such as LBW and DBIL were considered to have significant influences on the same pharmacokinetic parameters simultaneously, and the correlation between them required to be examined (shown in Figure 4). Two covariates with a correlation coefficient greater than .5 were refrained from containing in the covariate screening process simultaneously in order to avoid the covariate collinearity. So only adjusted CLcr, BMI, *UGT1A1*28* genotype, *UGT1A1*6* genotype, DBIL, ALT and LBW, both uncorrelated to each other, were utilized for covariate screening after the collinearity check. The results of forward and backward stepwise procedures are presented in detail in Table 3. The OFV significant decreases of adding BMI, DBIL and LBW to covariate models indicated that both three covariates had significant impacts on the pharmacokinetic parameters of TQ-B3203. The computational formulas of pharmacokinetic parameters V_1 and CL in the final model are shown as follows:

$$V_1\,(L) = 4.81 * \left(\frac{LBW}{49.53}\right)^{1.18} * e^{\eta V1} \tag{9}$$

$$CL\,(L/h) = 3.97 * \left(\frac{BMI}{23.44}\right)^{0.78} * \left(\frac{DBIL}{2.82}\right)^{-0.24} * e^{\eta CL} \tag{10}$$

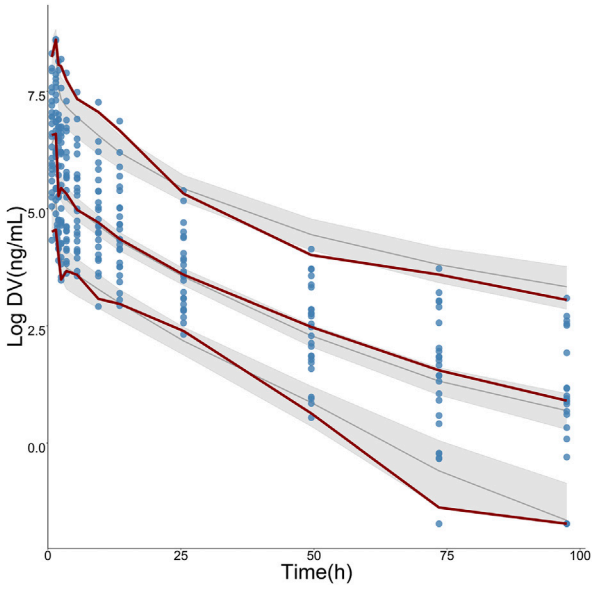

FIGURE 7
Visual predictive check (VPC) for logarithmic-transformed observations (log DV) of TQ-B3203. The steel-blue points represent log DV, while the dark-red dotted lines represent the 5th, 50th, and 95th percentiles of log DV. The solid black lines show the 5th, 50th, and 95th percentiles of simulated results, and the shaded regions represent the 95% confidence intervals for medians (solid black lines), respectively.

where 4.81 L and 3.97 L/h are typical values of V_1 and CL, respectively. The median values of significant covariates LBW, BMI and DBIL are 49.53 kg, 23.44 kg/m^2 and 2.82 μmol/L. The estimated correlation coefficients such as 1.18, .78 and −.24, represent the relationship between LBW and V_1, BMI and CL, DBIL and CL, respectively. The final PopPK parameters estimations are summarized in Table 4, which were obtained with satisfactory precision (RSE%<38%) and within the 95% confidence interval of bootstrap results.

3.4 Model validation

Pharmacokinetic curves of treatment episodes were predicted using the final model. The result, shown in Figure 5, indicated that the log IPRED profiles could almost entirely describe the log DV. The final model was evaluated by diagnostic plots shown in Figure 6, which suggested that the model was of good fit. The log DV *versus* log PRED or log IPRED was close-to-symmetrically distributed by the reference y = x, and the majority of CWRES *versus* log PRED or time were randomly distributed between −2 and +2 with no obvious bias. The VPC plots in Figure 7 indicated that the final model had excellent prediction performance because the vast majority of log DV were contained within the model-based simulated confidence intervals. All pharmacokinetic parameters estimations of the final model were included in the 95% confidence interval computed from the non-parametric bootstrap, listed in Table 4. As Figure 8 showed, the NPDE was considered a normal distribution and variance homogeneity, and the NPDE *versus* time or prediction had no apparent tendency to deviate from specified intervals. Furthermore, a statistical summary of the NPDE value distribution demonstrated that the mean did not significantly differ from 0 (Student's t-test, p = .591), variance had no remarkable difference from 1 (Fisher test, p = .265), and NPDE distribution was considered to be a standard normal distribution (Shapiro-Wilks test of normality, p = .539) so that the final model was appropriate to describe these observations. The results above indicated that the final model achieved the right qualifications for predicting and assessing pharmacokinetics in this group of patients.

3.5 Model application

The influence of significant covariates on TQ-B3203 predicted exposure (AUC_{0-t} and C_{max}) is presented in Figure 9. The percentage of AUC_{0-t} and C_{max} change was calculated compared with a simulated typical subject whose AUC_{0-t} and C_{max} were 9909.74 ng*h/mL and 1824.91 ng/mL, respectively. These 2 bar charts indicated that LBW had a great impact (14.44%) on C_{max} but little (2.19%) on AUC_{0-t}. On the contrary, BMI exerted a considerable influence (34.67%) on AUC_{0-t} but a small (7.28%) on C_{max}. The significance of DBIL on both AUC_{0-t} (36.76%) and C_{max} (31.54%) was similarly excellent.

4 Discussion

This research aimed to establish a PopPK model to find the potential covariates of inter-individual variation because highly variable pharmacokinetic characteristics of TQ-B3203 were observed in the phase I clinical trial. According to the results, a three-compartment model with first-order elimination was considered as the optimal structural model to characterize concentration data, in which the typical CL and V_1 were estimated as 3.97 L/h and 4.81 L, respectively. DBIL and BMI were the two most influential factors on CL, and LBW was considered to affect V_1 following the stepwise covariate modeling process. Furthermore, LBW was found to be related to V_2 as well as CL_2, and CL_2 was also influenced by DBIL.

In the previous PopPK analysis of irinotecan, the SN38 (a metabolite of irinotecan) concentration was also included to build a combined model, because irinotecan is a prodrug and SN38 showed a 300–1,000 times higher activity than irinotecan (Berg et al., 2015; Adiwijaya et al., 2017; Oyaga-Iriarte et al., 2019; Brendel et al., 2021; Liu et al., 2022). In this study, although TQ-B3203 also could be metabolized to produce SN38, the conversion ratio was very low (<5%), and TQ-B3203 mainly existed in the form of the prototype *in vivo*. It is reasonable that only the TQ-B3203 concentration was used in the modeling procedure.

BMI is the most extensively used indicator of judging whether an individual is thin, overweight or obese. Generally, the bigger the BMI value is, the fatter the person is, and the increasing BMI value or obesity will cause slow distribution, prolonged half-life and relatively decreased CL of lipophilic drugs due to its high tendency to distribute in adipose tissue (Powis et al., 1987). However, obesity could also boost phase I and phase II metabolism procedures, thus resulting in increased drug CL (Abernethy et al., 1983; Morgan and Bray, 1994; Marik and Varon, 1998; Brill et al., 2012). In this study, BMI was positively correlated with CL, which was consistent with other fat-soluble drugs, such as tigecycline and dilmapimod (Xie et al., 2017; Yang and Dumitrescu, 2017).

LBW could quantify the variation of renal and hepatic CL for individuals and provide the basis for the conceptual transformation of

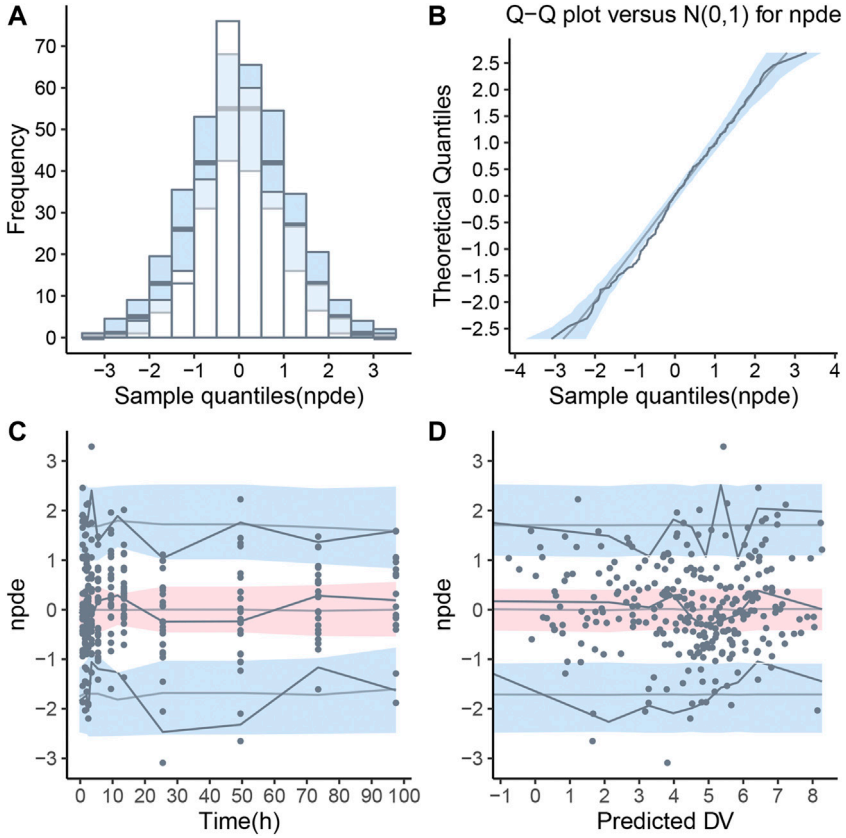

FIGURE 8
Normalized prediction distribution error (NPDE) for final population pharmacokinetic model. **(A)** Histogram of NPDE distribution with the density of the theoretical standard normal distribution (semi-transparent blue fields), **(B)** Quantile-quantile plot of NPDE against expected standard normal distribution (semi-transparent blue fields), **(C)** Scatterplot of NPDE *versus* time, **(D)** Scatterplot of NPDE *versus* population predictions (PRED). These two scatterplots showed the observations as blue dots, the median observations as solid red lines, the 5th and 95th percentiles of observations as solid blue lines, and 95% confidence intervals of relevant forecast percentiles as the red or blue fields.

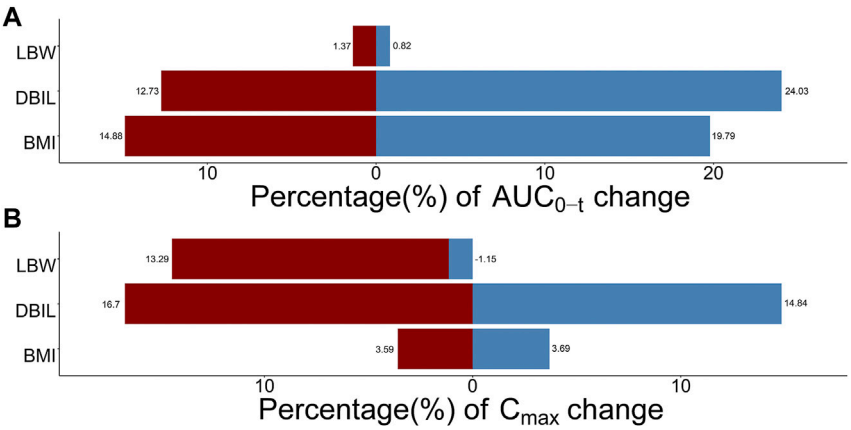

FIGURE 9
Sensitive analysis plots comparing the influence of covariates on TQ-B3203 exposure (AUC_{0-t} and C_{max}). **(A)** The effect of covariates on AUC_{0-t}, **(B)** The effect of covariates on C_{max}. The percentage of change is calculated compared with a simulated typical population whose AUC_{0-t} is 9909.74 ng*h/mL and C_{max} is 1824.91 ng/mL.

the relationship between body components and CL (Han et al., 2007). Although the relationship between LBW and CL was theoretically strong, it was not found in this study, which may be due to insufficient samples (Morgan and Bray, 1994). In the present model, LBW was the only significant covariate for V_1 and larger LBW was associated with greater V_1.

In the preclinical study, TQ-B3203 was found to be excreted into feces through bile in the form of the prototype. The impaired bile excretion function will lead to the increase of DBIL level and the decrease of TQ-B3203 CL, so DBIL was negatively correlated with TQ-B3203 CL, which could be identified in this study. In addition, other liver function-related indicators such as TBIL, IBIL, ALT and AST were all considered to be included in this covariate analysis at first. After the univariate screening process, only DBIL and ALT were retained in the final covariate selection to avoid covariate collinearity, but we did not find evidence of ALT as a significant covariate on CL.

As a study to establish a PopPK model of a novel antitumor agent using the data obtained from early clinical trials, there is a defect that is not neglected. Due to the limited number of subjects in the dose-escalating stage of the phase I clinical trial, the range of covariates provided by the population was narrow, so the extrapolation of research results was restricted. However, the intensive sampling points of every subject could offer detailed preliminary data on the pharmacokinetics of advanced solid tumor patients. This could make up for the defect of a small number of subjects to some extent and improve the significance of our model. This study is the first PopPK analysis of TQ-B3203, more extensive research is needed to take place to identify clinically relevant covariates of TQ-B3203 pharmacokinetics. The significant covariates obtained in this study, such as LBW, BMI and DBIL, suggested that weight and liver function related covariates may be the important factors affecting the pharmacokinetics of TQ-B3203, which could provide references for subsequent studies.

5 Conclusion

The first robust PopPK model of TQ-B3203 was successfully generated following intravenous administration of TLI in Chinese patients with advanced solid tumors. BMI, LBW, and DBIL were significant covariates that affected the pharmacokinetics of TQ-B3203. The final model was applied to predict the influence of significant covariates on drug exposure. In a word, this PopPK model could provide the references for the dose regimen in the future study of TLI.

Data availability statement

The original contributions presented in the study are included in the article/Supplementary Materials, further inquiries can be directed to the corresponding author.

Ethics statement

The studies involving human participants were reviewed and approved by Ethics Committee of Peking University Cancer Hospital. The patients/participants provided their written informed consent to participate in this study.

Author contributions

XQL and YB: Acquisition, analysis, or interpretation of data, drafting of the manuscript, review of the manuscript. HY, XHL, and XUL: Acquisition, analysis, or interpretation of data, review of the manuscript. FY: Study design, analysis, or interpretation of data, drafting of the manuscript, review of the manuscript, funding acquisition.

Funding

This work was supported by National Natural Science Foundation of China (Nos. 82073817 and 81602655) and Science Foundation of Peking University Cancer Hospital (No.2021-3).

Conflict of interest

Author XL is employed by Chia Tai Tianqing Pharmaceutical Group CO., Ltd.

The remaining authors declare that the research was conducted in the absence of any commercial or financial relationships that could be construed as a potential conflict of interest.

Publisher's note

Supplementary Material

The Supplementary Material for this article can be found online at: https://www.frontiersin.org/articles/10.3389/fphar.2023.1102244/full#supplementary-material

References

Abernethy, D. R., Greenblatt, D. J., Divoll, M., and Shader, R. I. (1983). Enhanced glucuronide conjugation of drugs in obesity: Studies of lorazepam, oxazepam, and acetaminophen. *J. Laboratory Clin. Med.* 101 (6), 873–880.

Adiwijaya, B. S., Kim, J., Lang, I., Csoszi, T., Cubillo, A., Chen, J. S., et al. (2017). Population pharmacokinetics of liposomal irinotecan in patients with cancer. *Clin. Pharmacol. Ther.* 102 (6), 997–1005. doi:10.1002/cpt.720

Ardizzoni, A., Hansen, H., Dombernowsky, P., Gamucci, T., Kaplan, S., Postmus, P., et al. (1997). Topotecan, a new active drug in the second-line treatment of small-cell lung cancer: A phase II study in patients with refractory and sensitive disease. The European organization for research and treatment of cancer early clinical studies group and new drug development office, and the lung cancer cooperative group. *J. Clin. Oncol.* 15 (5), 2090–2096. doi:10.1200/JCO.1997.15.5.2090

Berg, A. K., Buckner, J. C., Galanis, E., Jaeckle, K. A., Ames, M. M., and Reid, J. M. (2015). Quantification of the impact of enzyme-inducing antiepileptic drugs on irinotecan pharmacokinetics and SN-38 exposure. *J. Clin. Pharmacol.* 55 (11), 1303–1312. doi:10.1002/jcph.543

Brendel, K., Bekaii-Saab, T., Boland, P. M., Dayyani, F., Dean, A., Macarulla, T., et al. (2021). Population pharmacokinetics of liposomal irinotecan in patients with cancer and

exposure-safety analyses in patients with metastatic pancreatic cancer. *CPT Pharmacometrics Syst. Pharmacol.* 10 (12), 1550–1563. doi:10.1002/psp4.12725

Brill, M. J., Diepstraten, J., van Rongen, A., van Kralingen, S., van den Anker, J. N., and Knibbe, C. A. (2012). Impact of obesity on drug metabolism and elimination in adults and children. *Clin. Pharmacokinet.* 51 (5), 277–304. doi:10.2165/11599410-000000000-00000

Chabot, G. G. (1997). Clinical pharmacokinetics of irinotecan. *Clin. Pharmacokinet.* 33 (4), 245–259. doi:10.2165/00003088-199733040-00001

Cockcroft, D. W., and Gault, M. H. (1976). Prediction of creatinine clearance from serum creatinine. *Nephron* 16 (1), 31–41. doi:10.1159/000180580

Drummond, D. C., Meyer, O., Hong, K., Kirpotin, D. B., and Papahadjopoulos, D. (1999). Optimizing liposomes for delivery of chemotherapeutic agents to solid tumors. *Pharmacol. Rev.* 51 (4), 691–743.

Du Bois, D., and Du Bois, E. F. (1916). A formula to estimate the approximate surface area if height and weight be known. *Arch. Intern. Med. XVII*, 863–871. doi:10.1001/archinte.1916.00080130010002

Gottlieb, J. A., and Luce, J. K. (1972). Treatment of malignant melanoma with camptothecin (NSC-100880). *Cancer Chemother. Rep.* 56 (1), 103–105.

Han, P. Y., Duffull, S. B., Kirkpatrick, C. M., and Green, B. (2007). Dosing in obesity: A simple solution to a big problem. *Clin. Pharmacol. Ther.* 82 (5), 505–508. doi:10.1038/sj.clpt.6100381

Herben, V. M. M., ten Bokkel Huinink, W. W., and Beijnen, J. H. (1996). Clinical pharmacokinetics of topotecan. *Clin. Pharmacokinet.* 31 (2), 85–102. doi:10.2165/00003088-199631020-00001

Hertzberg, R. P., Caranfa, M. J., and Hecht, S. M. (1989). On the mechanism of topoisomerase I inhibition by camptothecin: Evidence for binding to an enzyme-DNA complex. *Biochemistry* 28 (11), 4629–4638. doi:10.1021/bi00437a018

Karlsson, M. O., and Sheiner, L. B. (1993). The importance of modeling interoccasion variability in population pharmacokinetic analyses. *J. Pharmacokinet. Biopharm.* 21 (6), 735–750. doi:10.1007/bf01113502

Keys, A., Fidanza, F., Karvonen, M. J., Kimura, N., and Taylor, H. L. (1972). Indices of relative weight and obesity. *J. Chronic Dis.* 25 (6), 329–343. doi:10.1016/0021-9681(72)90027-6

Klein, C. E., Gupta, E., Reid, J. M., Atherton, P. J., Sloan, J. A., Pitot, H. C., et al. (2002). Population pharmacokinetic model for irinotecan and two of its metabolites, SN-38 and SN-38 glucuronide. *Clin. Pharmacol. Ther.* 72 (6), 638–647. doi:10.1067/mcp.2002.129502

Liu, Z., Martin, J. H., Liauw, W., McLachlan, S. A., Link, E., Matera, A., et al. (2022). Evaluation of pharmacogenomics and hepatic nuclear imaging-related covariates by population pharmacokinetic models of irinotecan and its metabolites. *Eur. J. Clin. Pharmacol.* 78 (1), 53–64. doi:10.1007/s00228-021-03206-w

Marik, P., and Varon, J. (1998). The obese patient in the ICU. *Chest* 113 (2), 492–498. doi:10.1378/chest.113.2.492

Mathijssen, R. H., Verweij, J., de Jonge, M. J., Nooter, K., Stoter, G., and Sparreboom, A. (2002). Impact of body-size measures on irinotecan clearance: Alternative dosing recommendations. *J. Clin. Oncol.* 20 (1), 81–87. doi:10.1200/JCO.2002.20.1.81

McCarron, M. M., Devine, B. J. J. D. I., and Pharmacy, C. (1974). Clinical pharmacy: Case studies: Case number 25 gentamicin therapy. *Drug Intell. Clin. Pharm.* 8 (11), 650–655. doi:10.1177/106002807400801104

Morgan, D. J., and Bray, K. M. (1994). Lean body mass as a predictor of drug dosage. Implications for drug therapy. *Clin. Pharmacokinet.* 26 (4), 292–307. doi:10.2165/00003088-199426040-00005

Oyaga-Iriarte, E., Insausti, A., Sayar, O., and Aldaz, A. (2019). Population pharmacokinetic model of irinotecan and its metabolites in patients with metastatic colorectal cancer. *Eur. J. Clin. Pharmacol.* 75 (4), 529–542. doi:10.1007/s00228-018-02609-6

Park, J. H., Choi, S. M., Park, J. H., Lee, K. H., Yun, H. J., Lee, E. K., et al. (2018). Population pharmacokinetic analysis of propofol in underweight patients under general anaesthesia. *Br. J. Anaesth.* 121 (3), 559–566. doi:10.1016/j.bja.2018.04.045

Pommier, Y. (2006). Topoisomerase I inhibitors: Camptothecins and beyond. *Nat. Rev. Cancer* 6 (10), 789–802. doi:10.1038/nrc1977

Powis, G., Reece, P., Ahmann, D. L., and Ingle, J. N. (1987). Effect of body weight on the pharmacokinetics of cyclophosphamide in breast cancer patients. *Cancer Chemother. Pharmacol.* 20 (3), 219–222. doi:10.1007/BF00570489

Redinbo, M. R., Stewart, L., Kuhn, P., Champoux, J. J., and Hol, W. G. (1998). Crystal structures of human topoisomerase I in covalent and noncovalent complexes with DNA. *Science* 279 (5356), 1504–1513. doi:10.1126/science.279.5356.1504

Robinson, J. D., Lupkiewicz, S. M., Palenik, L., Lopez, L. M., and Ariet, M. (1983). Determination of ideal body weight for drug dosage calculations. *Am. J. Hosp. Pharm.* 40 (6), 1016–1019. doi:10.1093/ajhp/40.6.1016

Rozencweig, M., Slavik, M., Muggia, F. M., and Carter, S. K. (1976). Overview of early and investigational chemotherapeutic agents in solid tumors. *Med. Pediatr. Oncol.* 2 (4), 417–432. doi:10.1002/mpo.2950020408

Selas, A., Martin-Encinas, E., Fuertes, M., Masdeu, C., Rubiales, G., Palacios, F., et al. (2021). A patent review of topoisomerase I inhibitors (2016-present). *Expert Opin. Ther. Pat.* 31 (6), 473–508. doi:10.1080/13543776.2021.1879051

Winter, M. A., Guhr, K. N., and Berg, G. M. (2012). Impact of various body weights and serum creatinine concentrations on the bias and accuracy of the Cockcroft-Gault equation. *Pharmacotherapy* 32 (7), 604–612. doi:10.1002/j.1875-9114.2012.01098.x

Xie, J., Roberts, J. A., Alobaid, A. S., Roger, C., Wang, Y., Yang, Q., et al. (2017). Population pharmacokinetics of tigecycline in critically ill patients with severe infections. *Antimicrob. Agents Chemother.* 61 (8), 003455–e417. doi:10.1128/AAC.00345-17

Xie, R., Mathijssen, R. H., Sparreboom, A., Verweij, J., and Karlsson, M. O. (2002). Clinical pharmacokinetics of irinotecan and its metabolites: A population analysis. *J. Clin. Oncol.* 20 (15), 3293–3301. doi:10.1200/JCO.2002.11.073

Yang, F., Wang, H., Liu, M., Hu, P., and Jiang, J. (2013). Determination of free and total vincristine in human plasma after intravenous administration of vincristine sulfate liposome injection using ultra-high performance liquid chromatography tandem mass spectrometry. *J. Chromatogr. A* 1275, 61–69. doi:10.1016/j.chroma.2012.12.026

Yang, F., Zhou, J., Bo, Y., Yin, H., Liu, X. H., and Li, J. (2021). A validated UHPLC-MS/MS method for determination of TQ-B3203 in human plasma and its application to a pharmacokinetic study in Chinese patients with advanced solid tumor. *J. Sep. Sci.* 44 (5), 945–953. doi:10.1002/jssc.202001023

Yang, S., and Dumitrescu, T. P. (2017). Population pharmacokinetics and pharmacodynamics modelling of dilmapimod in severe trauma subjects at risk for acute respiratory distress syndrome. *Drugs R. D.* 17 (1), 145–158. doi:10.1007/s40268-016-0161-9

Zhang, X., Cao, M., Xing, J., Liu, F., Dong, P., Tian, X., et al. (2017). TQ-B3203, a potent proliferation inhibitor derived from camptothecin. *Med. Chem. Res.* 26 (12), 3395–3406. doi:10.1007/s00044-017-2032-5

frontiers | Frontiers in Pharmacology

TYPE Original Research
PUBLISHED 16 January 2023
DOI 10.3389/fphar.2022.1104735

OPEN ACCESS

EDITED BY
Yurong Lai,
FAAPS, Gilead , United States

REVIEWED BY
Huang Kai,
Wuxi People's Hospital Affiliated to Nanjing Medical University, China
Cyprian Onyeji,
University of Nigeria, Nigeria
Oluseye Bolaji,
Obafemi Awolowo University, Nigeria

*CORRESPONDENCE
Babu L. Tekwani,
btekwani@southernresearch.org
Larry A. Walker,
lwalker@olemiss.edu

SPECIALTY SECTION
This article was submitted to Drug Metabolism and Transport, a section of the journal Frontiers in Pharmacology

RECEIVED 22 November 2022
ACCEPTED 30 December 2022
PUBLISHED 16 January 2023

CITATION
Khan W, Wang Y-H, Chaurasiya ND, Nanayakkara NPD, Bandara Herath HM, Harrison KA, Dale G, Stanford DA, Dahl EP, McChesney JD, Gul W, ElSohly MA, Jollow D, Tekwani BL and Walker LA (2023), Comparative metabolism and tolerability of racemic primaquine and its enantiomers in human volunteers during 7-day administration.
Front. Pharmacol. 13:1104735.
doi: 10.3389/fphar.2022.1104735

Comparative metabolism and tolerability of racemic primaquine and its enantiomers in human volunteers during 7-day administration

Washim Khan[1], Yan-Hong Wang[1], Narayan D. Chaurasiya[2], N. P. Dhammika Nanayakkara[1], H. M. Bandara Herath[1], Kerri A. Harrison[1], Gray Dale[1], Donald A. Stanford[1], Eric P. Dahl[1], James D. McChesney[3], Waseem Gul[4], Mahmoud A. ElSohly[1,4,5], David Jollow[6], Babu L. Tekwani[2]* and Larry A. Walker[1]*

[1]National Center for Natural Products Research, The University of Mississippi, University, MS, United States, [2]Department of Infectious Diseases, Division of Drug Discovery, Southern Research Institute, Birmingham, AL, United States, [3]Ironstone Separations Inc., Etta, MS, United States, [4]ElSohly Laboratories Inc., Oxford, MS, United States, [5]Pharmaceutics and Drug Delivery, School of Pharmacy, The University of Mississippi, University, MS, United States, [6]Professor Emeritus, Department Cell and Molecular Pharmacology and Experimental Therapeutics, Medical University of South Carolina, Charleston, SC, United States

Primaquine (PQ) is an 8-aminoquinoline antimalarial, active against dormant *Plasmodium vivax* hypnozoites and *P. falciparum* mature gametocytes. PQ is currently used for *P. vivax* radical cure and prevention of malaria transmission. PQ is a racemic drug and since the metabolism and pharmacology of PQ's enantiomers have been shown to be divergent, the objectives of this study were to evaluate the comparative tolerability and metabolism of PQ with respect to its two enantiomers in human volunteers in a 7 days' treatment schedule. Fifteen subjects with normal glucose-6-phosphate dehydrogenase (G6PDn) completed four arms, receiving each of the treatments, once daily for 7 days, in a crossover fashion, with a 7–14 days washout period in between: *R*-(−) enantiomer (RPQ) 22.5 mg; *S*-(+) enantiomer (SPQ) 22.5 mg; racemic PQ (RSPQ) 45 mg, and placebo. Volunteers were monitored for any adverse events (AEs) during the study period. PQ and metabolites were quantified in plasma and red blood cells (RBCs) by UHPLC-UV-MS/MS. Plasma PQ was significantly higher in SPQ treatment group than for RPQ. Carboxy-primaquine, a major plasma metabolite, was much higher in the RPQ treated group than SPQ; primaquine carbamoyl glucuronide, another major plasma metabolite, was derived only from SPQ. The ortho-quinone metabolites were also detected and showed differences for the two enantiomers in a similar pattern to the parent drugs. Both enantiomers and racemic PQ were well tolerated in G6PDn subjects with the 7 days regimen; three subjects showed mild AEs which did not require any intervention or discontinuation of the drug. The most consistent changes in G6PDn subjects were a gradual increase in methemoglobin and bilirubin, but these were not clinically important. However, the bilirubin increase suggests mild progressive damage to a small fraction of red cells. PQ enantiomers were also individually administered to two G6PD deficient (G6PDd) subjects, one heterozygous female and one hemizygous male. These G6PDd subjects showed similar results with the two enantiomers, but the responses in the hemizygous male were more pronounced. These studies suggest that

although the metabolism profiles of individual PQ enantiomers are markedly different, they did not show significant differences in the safety and tolerability in G6PDn subjects.

KEYWORDS

primaquine, enantiomers, racemate, metabolism, clinical pharmacokinetics, safety

1 Introduction

Globally, the number of malaria deaths has dropped by 63% over the past 15 years as a result of improved access to medications and insecticide-treated bed nets (WHO, 2021). As a result of this accomplishment, more challenging objectives have been set, including a vision from the WHO to eradicate malaria within the next 15 years by reducing morbidity and mortality by 90%. This battle will require a robust arsenal of effective antimalarial drugs, as pressures of drug resistance continually undermine the public health effectiveness. In addition, the proportion of malaria cases attributable to the *Plasmodium vivax* parasite is growing in many parts of the world, and this presents additional challenges because of the difficulty in eradicating the dormant hypnozoites in the liver. At present, only the 8-aminoquinoline drug class is effective for these forms of the parasite, which are also formed with *P. ovale*. Though several treatments are available for the asexual blood stages of malaria, still primaquine (PQ) and tafenoquine (TQ) are the only choices for the liver hypnozoites (Baird and Rieckmann, 2003; Baird, 2018). PQ has a broad spectrum of activity against most *Plasmodium* species, also showing efficacy against the late-stage gametocytes in blood.

Although the 8-aminoquinolines are generally very well tolerated, there is a major limitation in their potential to cause hemolysis in patients with glucose-6- phosphate dehydrogenase (G6PD) deficiency (Bancone and Chu, 2021). G6PD deficiency is the most common enzyme deficiency worldwide and is prominent in many malaria-endemic regions (Nkhoma et al., 2009). In these patients, the oxidative stress caused by metabolites of PQ and TQ can cause red cell damage, leading to their removal from the circulation.

Since its introduction in the early 1950s, PQ has been used as a racemic mixture of (*S*)- and (*R*)-enantiomers. Previous studies from our laboratory and others indicate that the stereochemistry of PQ significantly affects the efficacy, metabolism, and toxicity in animal models (Nanayakkara et al., 2014; Saunders et al., 2014; Fasinu et al., 2016). The stereochemistry of other 8-aminoquinolines (as exemplified for NPC1161) demonstrated a significant impact on efficacy and toxicity (Tekwani and Walker, 2006; Nanayakkara et al., 2008). In a mouse model of infection, SPQ showed both increased activity and higher toxicity than RPQ (Nanayakkara et al., 2014). In the Rhesus monkey models the efficacy of both enantiomers was similar (Schmidt et al., 1977; Saunders et al., 2014), but RPQ showed greater hepatotoxicity compared to SPQ or racemate (Schmidt et al., 1977).

In the first study to look at this question in human volunteers, we observed that after the administration of racemic PQ, the two enantiomers are indeed sharply distinct in their primary metabolic pathways and pharmacokinetic profile (Tekwani et al., 2015). The RPQ appears to account for the vast majority of circulating carboxyprimaquine (cPQ), derived from oxidation of the terminal primary amine by monoamine oxidases. Recently we confirmed and extended these studies in healthy, G6PD normal volunteers, by administering the individual enantiomers separately (single oral dose) and comparing their pharmacokinetics and metabolism, along with the racemic version in a crossover fashion. Two major metabolites, cPQ and PQ-N-carbamoyl glucuronide (PQ-N-CG), were profiled in plasma. cPQ was the predominant plasma metabolite with the (*R*)-enantiomer, many fold higher than the parent drug, but PQ-N-CG was not detected. In contrast, for the (*S*)-enantiomer, PQ-N-CG was the major plasma metabolite, while very low levels of cPQ were seen (Khan et al., 2022a). Both enantiomers and the racemate were well tolerated at single doses of 22.5 mg and 45 mg for enantiomers and racemate, respectively.

Typically, the observed hemolytic toxicity of PQ in G6PD deficient subjects is observed only after a few days of administration. Presumably, this is because of the time required to generate sufficient oxidative stress by metabolite redox cycling, secondary intracellular damage and external membrane signaling, and the kinetics of splenic sequestration. Based on the divergent metabolism of PQ enantiomers in humans, and the differential safety profiles in animal studies, the present study explored the safety, tolerability, and metabolism of the individual enantiomers along with racemic PQ, administered with daily dosing for 7 days. 7 days' dosing of PQ has been suggested to be effective in preventing malaria relapse in people with *P. vivax* (Milligan et al., 2020). The studies were conducted in healthy G6PD normal (G6PDn) volunteers during 7 days administration. We were also able to explore these parameters with multiple doses in two subjects with G6PD deficiency (G6PDd).

2 Methodology

2.1 Chemicals, reagents, and study materials

For analysis, HPLC grade solvents, e.g., methanol, acetonitrile, and formic acid (FA), were purchased from Thermo Scientific (Rockford, IL, United States). Water used for analysis was purified using Millipore Synergy® UV Ultrapure Water Purification System (EMD Millipore Corporation, MA, United States). Reference standards, primaquine diphosphate was purchased from Sigma (St Louis, MO, United States). Different metabolites of PQ and internal standards were synthesized at the National Center for Natural Products Research, University of Mississippi. Synthesis of reference standards have been described in the previous article; primaquine-5,6-orthoquinone (POQ) (Potter et al., 2015), carboxyprimaquine-5,7-orthoquinone (cPOQ) (Khan et al., 2021), PQ-N-CG (Fasinu et al., 2016), cPQ (McChesney and Sarangan, 1984), 4-methylprimaquine-5,6-orthoquinone (4-MePOQ), and deuterated primaquine (d3-PQ) (Khan et al., 2022b). The racemic PQ, PQ enantiomers and placebo capsules used for the clinical study were prepared with complete characterization, purity, and stability, by ElSohly Laboratories, Inc (ELI), Oxford, MS. Each capsule contained the desired specific amount of PQ base as the diphosphate salt. Structure of all analytes are shown in Figure 1.

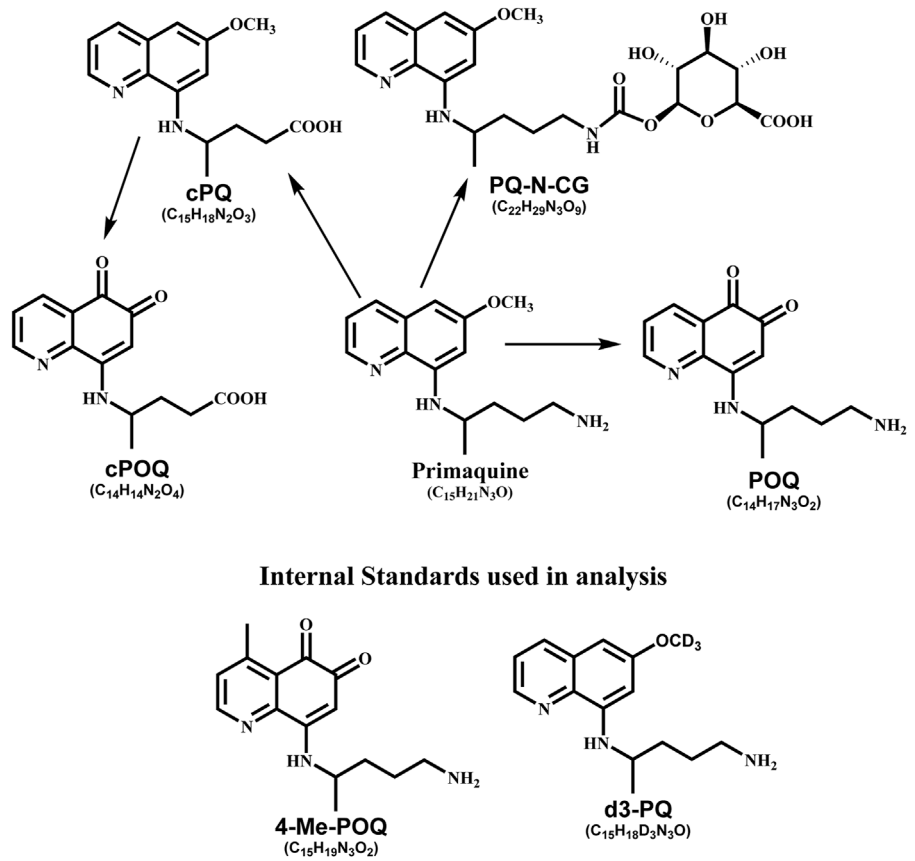

FIGURE 1
Chemical structure of analyte used in this study.

2.2 Clinical study

2.2.1 Study design, ethics, and participants

This study was conducted at the National Center for Natural Products Research, University of Mississippi, MS, United States, in accordance with the ethical principles under protocols approved by the Division of Research Integrity and Compliance-Institutional Review Board, Office of Research and Sponsored Programs, University of Mississippi (IRB# 18–075) and by the Human Research Protection Office of the United States Army Medical Research and Development Command. The ClinicalTrials.gov Identifiers for these studies are NCT03934450 and NCT04073953. A signed written consent was obtained from each individual who participated in this study. Normal healthy adults aged 18–65 years were screened. Screening included history, physical exam, vital signs, electrocardiogram, and blood sampling for baseline hematology, clinical chemistry panel, and G6PD activity. Participants in these trials were healthy, non-smokers, and ranging in age from 20 to 26 years old, with an average body weight of 68 and 80 kg for females and males, respectively. Additionally, eligible female subjects were required not to be pregnant, or breastfeeding, or expected to conceive during the study, or lactating, or of childbearing potential. Volunteers with liver, kidney, hematological, cardiac, and autoimmune disorders were excluded.

Clinical pharmacokinetic studies in G6PDn subjects were single-blinded, placebo-controlled crossover studies conducted at the National Center for Natural Products Research, University of Mississippi, United States of America. Dose selection was based on the clear safety and tolerability from our previous single dose study using SPQ, RPQ, and RSPQ (Khan et al., 2022a) and also from previous clinical studies with racemic PQ (Bancone and Chu, 2021). The study in G6PDn volunteers consisted of four arms. Each subject participated in all four arms, with appropriate washout. The first arm involved the administration of 45 mg of RSPQ once daily for 7 days, followed by at least a 1 week washout; arm two involved administration of 22.5 mg of RPQ every day for 7 days, followed by at least a 1 week washout period; arm three involved administration of placebo every day for 7 days, followed by at least a 1 week washout; and arm four involved administration of 22.5 mg of SPQ every day for 7 days. For power considerations, we used the approach of Kang et al. (2005). Because the key question is whether a reliable clinically important difference in the hematological liability exists (to warrant field trials of the single enantiomer). Assuming we could establish an 80% difference between the two enantiomers in terms of the hematological effects, even allowing an inter-subject variability of 80%, 18 subjects would equate to a power level of 0.8 (α = 0.05) (Kang et al., 2005). Thus 18 subjects were enrolled for the study. But only 15 subjects completed all four arms, with complete PQ and metabolite data.

After a light breakfast, one of the PQ doses (RPQ, SPQ, or RSPQ) or placebo was administered to volunteers divided into different groups. Dosing was once daily on days 0–6, for seven consecutive

TABLE 1 Subject demographics and baseline clinical characteristics that participated in study.

Parameters	Total	Gender	
		Male	Female
G6PD normal	15	11	04
African/Afr. American	01	01	01
Caucasian	10	06	04
Asian	04	04	00
Age (Mean, SD)		22, 1.9	
Age range		20–26	
G6PD deficient	02	01	01
African/Afr. American	02	01	01
Age		42	23

doses. In this study, blood samples (10 mL) were collected by direct venipuncture on day zero pre-dose, on day three pre-dose and at 1 hour post-dose, on day five pre-dose and at 1 hour post dose, and on day seven, 24 h after the last dose. Within 1 h of blood sample collection, it was centrifuged at 15294 *g* for 10 min at 4°C, plasma and blood cells were separated. Packed red cells were washed with cold phosphate buffered saline (PBS), centrifuged, and supernatant discarded. White buffy coat as WBC found in between the layer of RBCs and PBS, were also collected for future studies. The separated plasma and RBC pellets were aliquoted and preserved at −80°C for studies.

Only two volunteers with G6PDd conditions were enrolled in two arms of the multidose pharmacokinetic study of PQ enantiomers. Volunteers were enrolled to receive 15 mg of SPQ every day for 5 days, followed by 2 weeks washout period, then 15 mg of RPQ every day for 4 days. Blood samples were collected at pre-dose and 2 h after oral administration of PQ on days 0, 1, 2, 3, and 4.

2.2.2 Determination of G6PD enzyme activity and biochemical parameters

G6PD status was assessed in each subject by screening prior to enrollment. Hematological and biochemical parameters, including G6PD activity and liver enzyme were assessed by certified clinical laboratory methods by LabCorp (Memphis, TN). For that, blood samples were collected in a different specified vacutainer tube containing with and or without EDTA. Blood samples were sent on the same day of collection. For the determination of G6PD activity, the method biochemical, spectrophotometric method based on the formation of NADPH as estimated by monitoring UV absorbance of the sample at 340 nm.

2.2.3 Adverse events and safety monitoring

Safety was evaluated during the study by monitoring of vital signs (blood pressure, pulse, respiratory rate, oxygen saturation and body temperature), and by recording any adverse events (AEs) at sampling times, and at follow-up visits after study completion. Analysis of biochemical safety and hematological parameters was performed by LabCorp (Memphis, TN). All available data from human volunteers who received either test drug and or placebo, were included in the summaries of the safety data.

2.3 Bioanalytical assay for quantification of PQ and its metabolites in plasma and RBCs

All the stored plasma and RBCs samples were thawed in ice and processed to quantify analytes. PQ, cPQ, and PQ-N-CG by a validated ultra-high performance liquid chromatography coupled with Xevo G2-S QToF mass spectrometer (UHPLC-MSMS) (Waters Corp., Milford, MA, United States) (Khan et al., 2022a). As the levels of POQ and cPOQ in plasma were very low, and QToF was not sensitive enough, these two analytes were quantified using Xevo TQ-S triple quadrupole mass spectrometer (UHPLC-TQ-MS, Waters Corp., Milford, MA, United States). The method for quantification of these two analytes was validated as per USFDA guidelines (USFDA, 2018). The method for extraction and analysis of POQ and cPOQ in red blood cells (RBCs) was previously described (Khan et al., 2021). Analysis was carried out using gradient elution and detected by electrospray ionization (ESI) in positive mode. Chromatographic separation was performed using a reversed-phase column (Acquity UPLC HSS T3, 1.8 µm, 2.1 × 100 mm, Waters, United States) set at 35°C. The mobile phase consisted of solvent A (water with 0.05% formic acid) and solvent B (acetonitrile with 0.05% formic acid, v/v). For the analysis of plasma, gradient elution was started with 95% A (0 min), a linear gradient from 95% to 55% A (0–9 min), later up to 0% A (9–10 min). For analysis of RBCs, the gradient elution was started with 15% B at the beginning and increased to 55% B at 3.5 min. To detect analytes, ionization was achieved using electrospray ionization (ESI) operated in positive-ion mode (M + H). The MS/MS transition for POQ, cPOQ, PQ, cPQ, PQ-N-CG, 4-MePOQ and d3-PQ were 260.1 > 175.0, 275.2 > 175.0, 260.1 > 175.1, 275.1 > 175.1, 480.2 > 243.1, 274.2 > 189.0, and 263.2 > 178.1, respectively. All data collected in centroid mode were acquired using MassLynx™ NT 4.1 software. Accurate mass tolerance of molecular ion and major fragments was limited to 5 ppm, while minor fragments of parent ions were tolerated up to 10 ppm.

Blood samples for PQ and its metabolite analysis were drawn at baseline, then on days 3 and 5 pre-dose and at 1 h post-dose, and then on day 7 at 24 h after the last dose. These were analyzed as described above, and the relative plasma exposure of the different enantiomers and racemate were compared, along with the major metabolites.

2.4 Statistical analysis

Statistical analysis was performed using the GraphPad prism software version 22.0 (SPSS Inc., Chicago, IL, United States). All data, including PK and biochemical parameters, were summarized using descriptive statistics. Values are expressed as the mean ± SEM for all parameters.

3 Results

3.1 Safety, tolerability and biochemical profiling assessment of G6PDn subjects

Eighteen G6PDn subjects were enrolled and 15 completed all four arms, receiving RPQ, SPQ, RSPQ, and placebo, separately, in crossover fashion. In each cycle, subjects received one dose of PQ

TABLE 2 Adverse events in G6PDn and G6PDd subjects during 7 days oral administration of PQ and its enantiomers.

Parameters	No. Of subjects	Adverse event	Drug-related?	Comments
G6PDn				
Hematological	1/15	• Elevated MetHgB • Dyspnea on exertion • Headache	Yes	Exaggerated MetHgB response to all forms of PQ, symptomatic with RPQ
Liver enzyme markers	2/15	• Increase in AST and ALT	No	• One consumed alcohol during SPQ arm • One subject during placebo arm; found on followup to have history of gallbladder trouble
G6PDd				
Hematological	1/2	• Bilirubin increase above preset stop criterion	Yes	Indicative of excess oxidative damage to red cells due to G6PD deficiency

Note: All subjects were monitored during the study period and on followup by the study physician until symptoms and signs normalized.

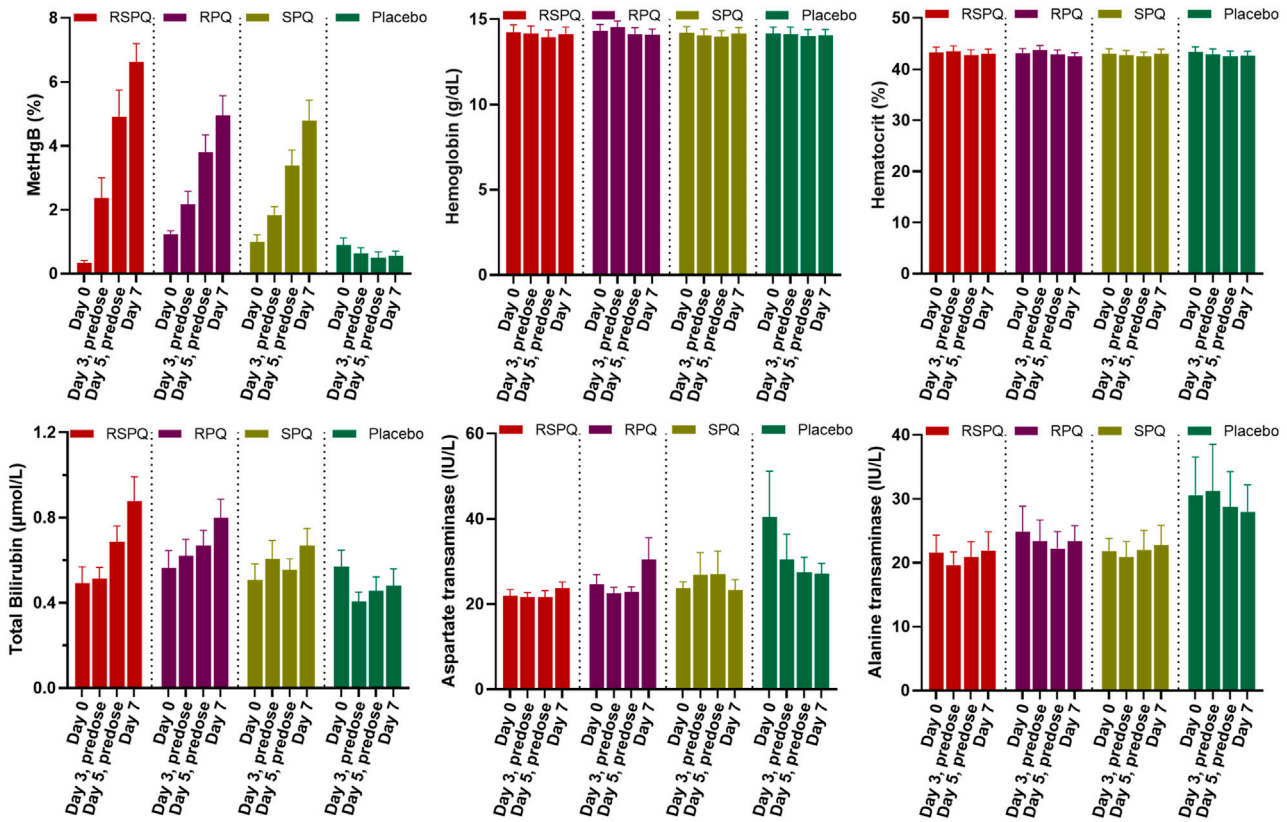

FIGURE 2
Biochemical and hematological parameters in G6PDn subjects during 7 days daily oral administration of PQ and its individual enantiomers. Bar graphs are presented as mean with SEM (*N* = 15).

daily for 7 days. In between each cycle, subjects were given at least a 1 week washout period. The baseline demographic and clinical characteristics of the clinical study subjects of both categories are shown in Table 1. The mean age and body weight (±SEM) of G6PDn subjects were 22.0 ± 0.4 years and 168 ± 7 lb, respectively. No changes in BP, pulse, respiratory rate, oxygen saturation, body temperature and weight were observed. The most consistent findings in the G6PDn subjects were elevations in methemoglobin and very small increases in bilirubin, but neither resulted in clinical symptoms, nor required discontinuation of drug.

No serious adverse events (AEs) or withdrawals due to AEs were observed in G6PDn subjects. The adverse events and their incidence are tabulated in Table 2. Three subjects reported mild AEs. None of these three required withdrawal from the study. Two of the events, in the judgment of the study director and physician, were likely unrelated to the drug treatment. These two showed transient mild elevations in aspartate transaminase (AST) and alanine transaminase (ALT) levels, likely attributable to acute alcohol consumption in one subject (during the SPQ arm) and one with a latent past history of gallbladder trouble (increased AST/ALT during placebo arm). The third subject—who had

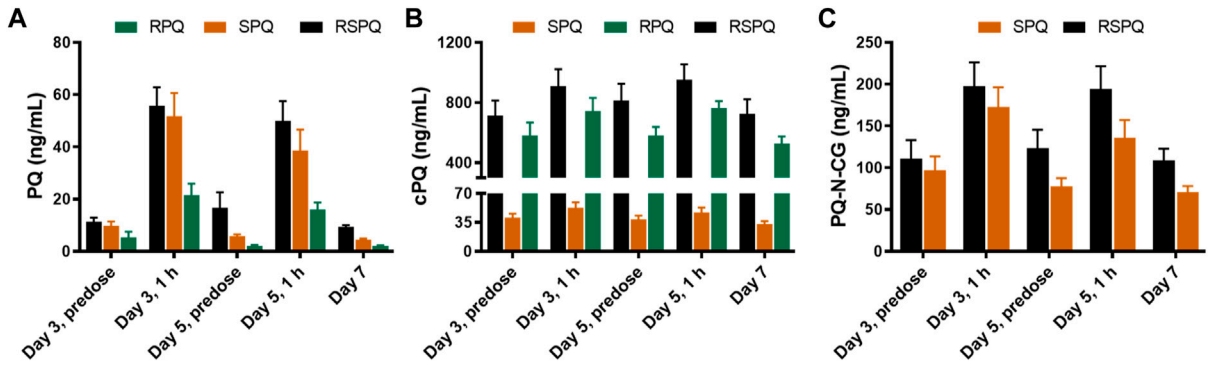

FIGURE 3
Concentrations of PQ **(A)** and its metabolites **(B,C)** in plasma of G6PDn subjects after oral administration of PQ enantiomers or racemate for 7 days. Bar graphs are presented as mean with SEM (N = 15).

the most prominent methemoglobin response, developed some dyspnea on exertion and mild cyanosis the evening after the 7th dose of RPQ. The subject was seen in the clinic the following day, and dyspnea had resolved, and the subject was monitored for several days until methemoglobin returned to normal. This reaction did appear to be drug-related; though the subject did not report any exertional dyspnea with SPQ or RSPQ, methemoglobinemia increased prominently during each of these drug arms. This subject was followed by the study nurse and physician until symptoms dissipated (by the next day) and MetHgb returned to normal over several days. She was also examined by a local primary care physician, but no medical intervention was required. This subject was cleared by the physicians to continue in the study.

In G6PDn subjects, biochemical parameters were not significantly affected except for methemoglobin (MetHgB) and total bilirubin (Figure 2). Significant increases (p < .0001) in methemoglobin (MetHgB) from the baseline were seen in subjects receiving PQ enantiomers (at 22.5 mg), although the maximum values averaged about 5% of HgB, and were not associated with clinical symptoms. The increases in MetHgB were not different with the two enantiomers. Subjects receiving racemic primaquine (45 mg) showed a somewhat higher increase in MetHgB, but still only reached a mean of 7% HgB. During placebo administration, MetHgB did not change. From the baseline level, bilirubin progressively increased during daily PQ administration, but these increases were very modest and still under the normal clinical laboratory limits. There were no differences between the enantiomers, and RSPQ showed somewhat higher MetHgB response than the individual enantiomers. In this study, parameters for kidney, liver, and hematological profiles were also analyzed, and no significant changes were observed (Supplementary Tables S1, S2). Findings for vital signs are also tabulated in Supplementary Table S3.

3.2 PQ and its metabolite profiling in G6PDn subjects

During daily PQ administration for 7 days (days 0–6), blood samples were taken on day zero pre-dose, on day three pre-dose and at 1 h post-dose, on day five pre-dose and at 1 h post-dose, and on day seven, 24 h after the last dose. The plasma concentrations of PQ on days 3 and 5 were very low at pre-dose, consistent with our prior study (Khan et al., 2022a) and those of others (Mihaly et al., 1984), and increased 1 h after oral administration (Figure 3). Two major metabolites of PQ (Figure 3A), cPQ (Figure 3B) and PQ-N-CG (Figure 3C), were measured in plasma at these time intervals. When in the SPQ arm, the subjects showed high concentrations of PQ and low concentrations of cPQ; the reverse situation; low PQ and high cPQ was seen during the RPQ arm. When the racemic mixture RSPQ was administered, both PQ and cPQ were high, reflecting the contribution of each enantiomer. Although the dose of RSPQ was the sum of the individual enantiomers, levels of PQ and cPQ were not doubled, presumably reflecting at least in part, a higher apparent volume of distribution (Vd) for RPQ as compared to SPQ in mice (Fasinu et al., 2022), monkeys (Saunders et al., 2014) and humans (Khan et al., 2022a), and also an expected much lower Vd for cPQ as compared to PQ (Baker et al., 1984).

PQ-N-CG, which is formed through direct N-glucuronide conjugation of PQ, was observed only after SPQ administration. Though PQ-N-CG was not detected after RPQ administration, subjects that received RSPQ showed consistently higher plasma levels than those receiving SPQ (Figure 3C).

POQ and cPOQ are the orthoquinones of PQ and cPQ, respectively, formed secondarily to hepatic metabolism, and are believed to reflect the redox-active metabolite pathway for PQ. These two metabolites were measured in plasma and RBCs (Figure 4). POQ was detected in both plasma (Figure 4Ai) and red cells (Figure 4Bi) in the general range of 4–10 ng/ml with an approximate equal distribution between plasma and cells.

POQ levels in plasma were higher in RSPQ and SPQ than in RPQ arm samples as expected due to their higher levels of PQ. cPOQ was found at higher concentrations in plasma (range 30–60 ng/ml) and red cells (range 10–20 ng/ml) in subjects that received RPQ or RSPQ. This is consistent with the higher levels of cPQ in these subjects. Of interest, the concentration of cPOQ in plasma (Figure 4Aii) was notably higher than POQ in all arms of the study; whether this results from enhanced formation or slower elimination of cPOQ is unknown. Similarly, the concentration of cPOQ in RBC (Figure 4Bii) was markedly higher (ca. two-fold) than POQ in all arms, implying that cPQ may contribute more to the oxidant stress within red cells than PQ. Overall, RBC exposure to orthoquinone metabolites showed different profiles depending on which PQ

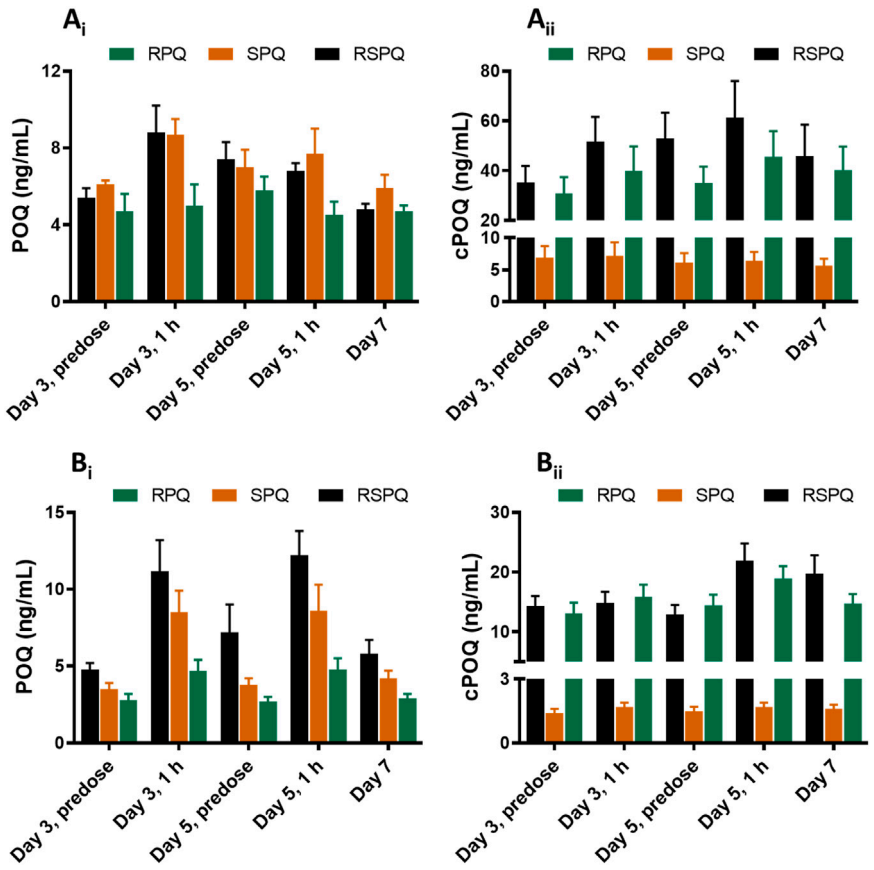

FIGURE 4
Concentrations of ortho-quinone metabolites of PQ in plasma **(Ai and Aii)** and RBCs **(B_i and B_{ii})** of G6PDn subjects during oral administration of PQ enantiomers or racemate for 7 days. Bar graphs are presented as mean with SEM (N = 15).

enantiomer is dosed, but both enantiomers contribute to the potential for hemolytic injury.

3.3 Findings in G6PDd subjects

We were able to enroll two healthy human volunteers with G6PDd in a pilot investigation for 5 days of dosing with the individual PQ enantiomers. One subject was a heterozygous female (A-variant with G6PD activity of 7.4 units/gram of hemoglobin), who received RPQ at a dose of 15 mg daily for 5 days, and after a 2 week washout, received SPQ at the same dose. The other subject was a hemizygous male (A-variant with G6PD activity of 1.2 units/gram of hemoglobin), who was also enrolled to receive both enantiomers. However, this subject (TS212) could not complete the 5 days of dosing with either SPQ or RPQ, since his bilirubin level was significantly increased, and dosing was discontinued after the third dose. Both G6PDd subjects showed progressive significant increase in bilirubin levels with both enantiomers (Figure 5); this was especially more prominent in the hemizygous subject, and reached the stop criterion for discontinuation of dosing after the third dose. Except for lactate dehydrogenase, no other biochemical parameters were changed (Supplementary Tables S4, S5).

The G6PDd subjects were closely monitored after dosing, and blood samples were collected at pre-dose and 2 h after administration on days 0, 1, 2, and 3, and then on day 4 (24 h after the last dose). In plasma, PQ, cPQ, PQ-N-CG, and cPOQ were quantified. Like G6PDn subjects, G6PDd subjects also showed a similar pattern of plasma exposure for PQ, cPQ, and PQ-N-CG (Figure 6). Again, PQ exposure in plasma was found to be somewhat higher with SPQ than RPQ, and RPQ showed around 37-fold higher exposure for cPQ than SPQ. POQ could be detected but not quantified in RBCs of G6PDd subjects, likely because of the lower PQ dose. But cPOQ was detectable in plasma and RBCs after RPQ administration (Figure 7A, B), respectively.

4 Discussion

The differential pharmacokinetic, metabolism and pharmacologic profiles of individual enantiomers of PQ is now well established, as evidenced in *in vitro* human hepatocytes and also in animals (Fasinu et al., 2014; 2016; 2022; Saunders et al., 2014; Chaurasiya et al., 2021). A recent study from our group also demonstrated highly enantioselective PK and metabolism profiles in subjects treated with single dose of individual PQ enantiomers (Khan et al., 2022a). Since recent clinical studies have suggested the use of a 7 days regimen of PQ for *P. vivax* radical cure (Taylor et al.,

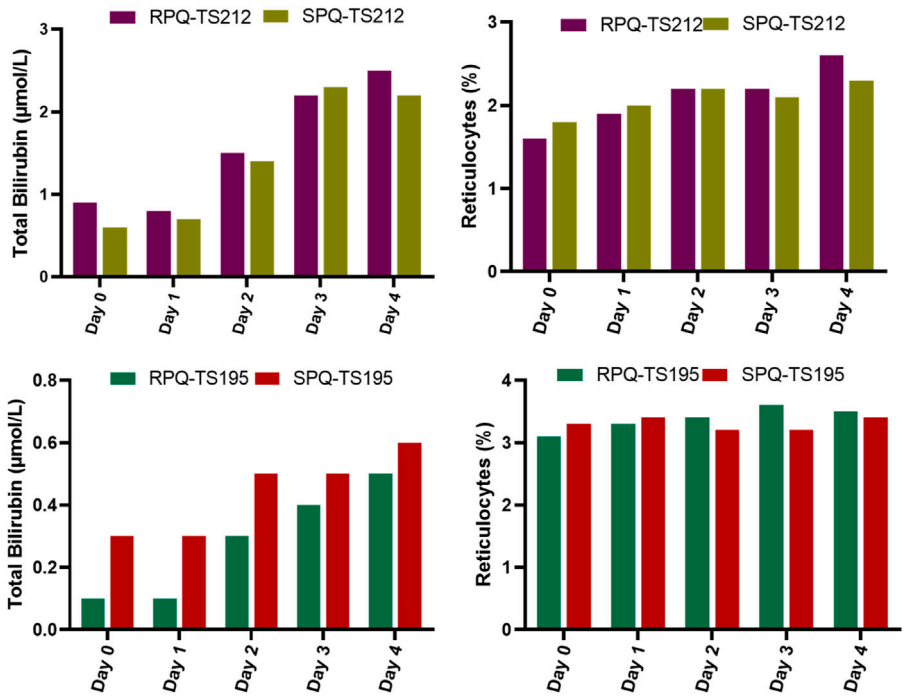

FIGURE 5
Biochemical and hematological parameters in G6PDd subjects during daily oral administration of the individual enantiomers of PQ.

2019; Milligan et al., 2020), the current study was undertaken to assess the metabolism of the individual enantiomers of PQ—RPQ and SPQ—and to gauge their general and hematological tolerability in relation to metabolite formation. The rationale for the study was based on the following observations.

4.1 PQ metabolism pathways

Although the 8-aminoquinoline class of antimalarials has an unique place in malaria chemotherapy, their optimal employment is limited due to safety concerns in individuals with G6PDd (Clyde, 1981; Baird and Rieckmann, 2003). It is established that this liability in G6PDd is due to the enhanced sensitivity of their red cells to oxidative stressors. In the case of PQ, this has long been attributed to redox active metabolites (Allahyari et al., 1984; Bowman et al., 2004; Ganesan et al., 2009; 2012), though the precise nature of the metabolites and their pathways/locations *in vivo* were for many years uncertain (Strother et al., 1984; Marcsisin et al., 2016; Flaherty et al., 2022). cPQ is well known as a major circulating metabolite, likely formed by the actions of monoamine oxidases (Nicholl et al., 1987; Fasinu et al., 2016). cPQ is not redox active. Other pathways are also now well established, including the hydroxylation of PQ by cytochrome P450 (CYP) pathways, observed using isolated enzyme systems, liver microsomes, and in intact human hepatocytes (Avula et al., 2013; Jin et al., 2014; Ariffin et al., 2019). Among these CYPs, CYP 2D6 accomplishes the formation of at least four different metabolites *via* hydroxylation of the PQ ring at 2-, 3-, four- and five- positions (Pybus et al., 2012; Fasinu et al., 2014; Potter et al., 2015). This CYP 2D6 activity has been shown to be an important determinant of the altered metabolism of PQ in animals (Pybus et al., 2013) and humans (Potter et al., 2015), and poor CYP 2D6 metabolizer phenotypes show a reduced anti-relapse efficacy of PQ (Bennett et al., 2013). These hydroxylated metabolites have proven difficult to detect in plasma, whether by virtue of instability, compartmentalization within tissues, or rapid conjugation and excretion (Mihaly et al., 1984).

Several studies have now shown that 5-OH-PQ is exceedingly unstable, rapidly oxidizing to its quinone-imine, then to 5,6-dihydroxy-PQ, and finally to the 5,6-orthoquinone (POQ) (Camarda et al., 2019; Fasinu et al., 2019). Even the more stable POQ is not typically observed in plasma, though it is detected readily in urine (Spring et al., 2019).

Recently, our group also reported that POQ can be formed directly from PQ on incubation with human red cells, presumably *via* heme- or hemoglobin-dependent formation of oxygen free radicals (Fasinu et al., 2019); the qualitative importance of this *in situ* generation of oxidants vis-a-vis that derived from hepatic metabolism is yet to be determined. We have also observed that cPQ can also give rise to an ortho-quinone type metabolite (cPOQ), presumably by analogous metabolic routes, but this does not appear to be accomplished by CYP 2D6 (Khan et al., 2021). The relative contributions of POQ and cPOQ to red cell oxidant stress and subsequent injury in humans is clearly of interest to resolution of the importance of the two enantiomers in the clinical use of PQ.

4.2 Stereochemistry and pharmacodynamics and metabolism of PQ

PQ is a racemic mixture of (*R*) and (*S*) enantiomers, and our prior studies have shown vastly different metabolism of the two enantiomers,

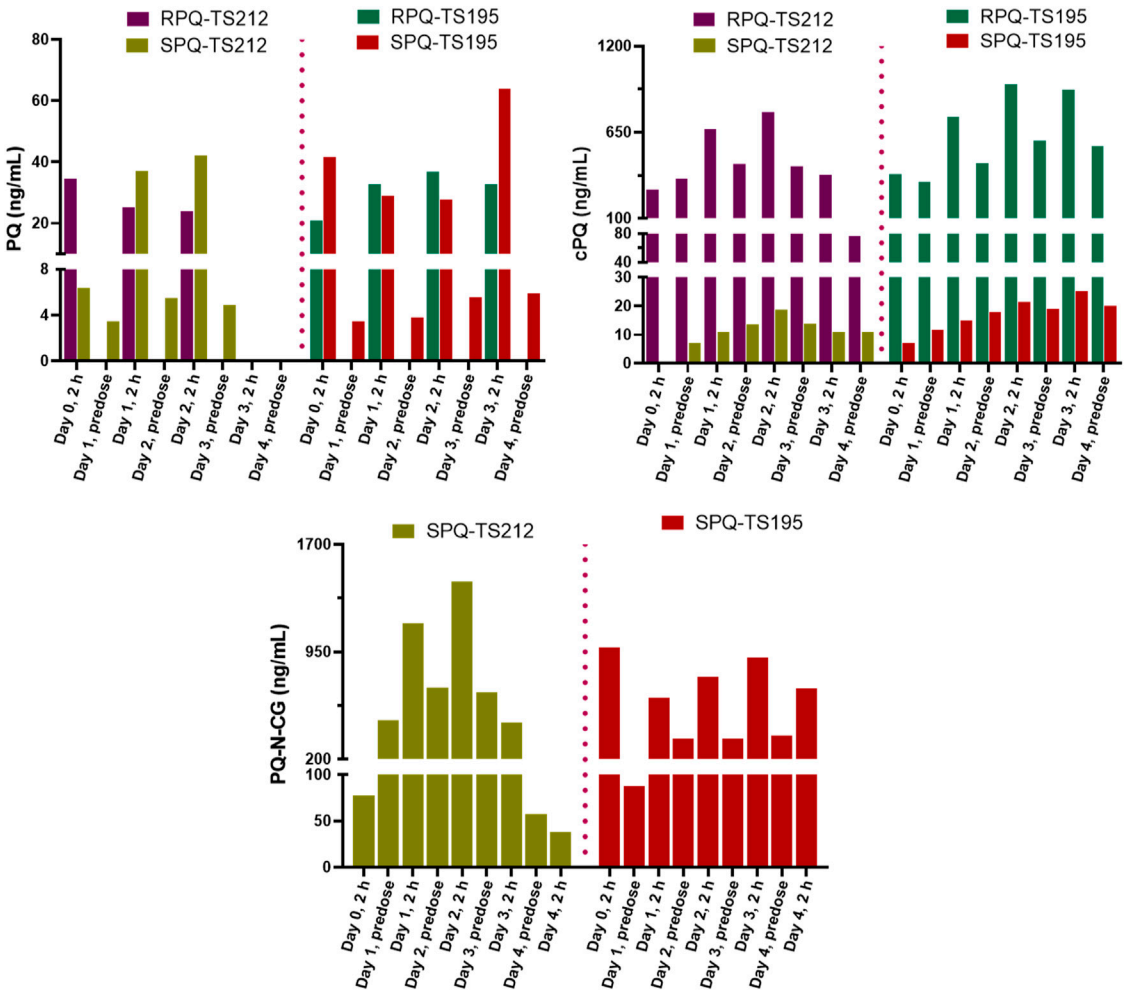

FIGURE 6
Concentrations of PQ and its metabolite in plasma of G6PDd subjects during daily oral administration of the individual enantiomers of PQ.

whether with *in vitro* drug metabolizing enzymes (Pybus et al., 2012; Fasinu et al., 2014; 2016), in animal models (Baker and McChesney, 1988; Saunders et al., 2014), or in humans (Tekwani et al., 2015; Khan et al., 2022a). RPQ is much more significantly converted *via* the MAO pathway to cPQ, the major PQ metabolite in human plasma. PQ-N-CG has been recently identified as a PQ metabolite in plasma, notably after administration of SPQ (Khan et al., 2022a). The formation of the hydroxylated products of PQ also showed quite distinct patterns with the two enantiomers, though both RPQ and SPQ gave rise to all of the reported ring-hydroxylated species (Fasinu et al., 2016). Several reported animal studies have shown dramatic differences in the toxicity of PQ enantiomers, including their hematological effects, with SPQ showing greater systemic toxicity than RPQ in mice (Schmidt et al., 1977), but lower hepatotoxicity in primates (Schmidt et al., 1977; Saunders et al., 2014); however, hematological effects of SPQ were more pronounced than RPQ's effects in both species (Nanayakkara et al., 2014; Saunders et al., 2014); this is in spite of an equivalent radical curative efficacy of the two enantiomers in primates (Schmidt et al., 1977; Saunders et al., 2014).

A critical question that arises, then, for the safe use of PQ in humans with G6PDd is whether the differential metabolic profile of enantiomers will translate to a better therapeutic index. Toward answering that question, we undertook to assess the tolerability and metabolism of the RPQ and SPQ, first in G6PDn human volunteers receiving a single dose (Khan et al., 2022a). SPQ showed higher plasma exposure of PQ as compared to RPQ. cPQ was the predominant plasma metabolite with RPQ administration, many folds higher than the parent drug, but PQ-N-CG was not detected. In contrast, for SPQ, PQ-N-CG was the major plasma metabolite, while much lower levels of cPQ were seen (Khan et al., 2022a). POQ and cPOQ were also identified in the RBCs of subjects receiving single doses (Khan et al., 2021). However, in this study using single doses, there were no identifiable tolerability issues, so we could not distinguish any safety advantage. Typically, the hematological toxicity of PQ in G6PDd subjects appear after a few days dosing.

4.3 The current study

In the current study we aimed to check the comparative tolerability of racemic PQ and its individual enantiomers in G6PDn subjects, and profile the plasma and RBCs for parent and

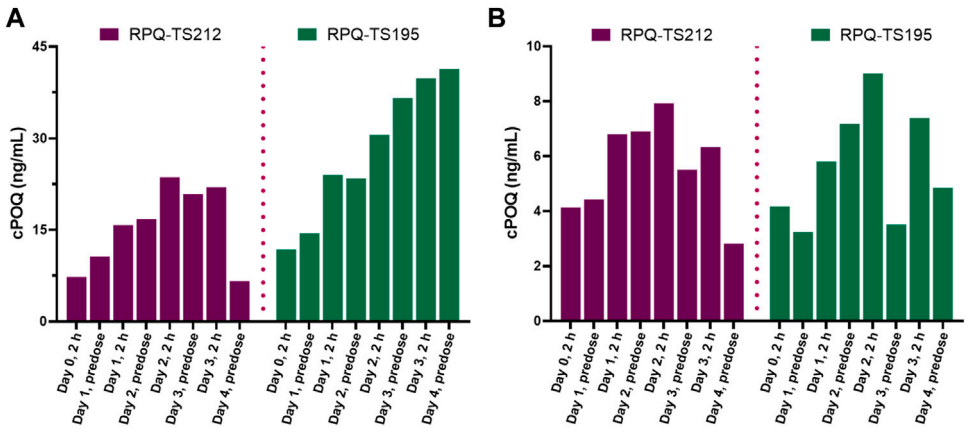

FIGURE 7
Concentrations of the cPQ metabolite cPOQ in plasma **(A)** and RBCs **(B)** of G6PDd subjects during daily oral administration of the individual enantiomers of PQ.

metabolites during oral administration once daily for seven consecutive days. Two G6PDd individuals also received PQ enantiomers for a 5 day course.

4.4 PQ metabolism in G6PDn

With respect to metabolism, as observed in our single dose study (Khan et al., 2022a), plasma exposure to parent drug was significantly higher for SPQ treated groups than for RPQ, and RSPQ behaved in an additive fashion. Plasma cPQ levels were much higher after RPQ administration than SPQ, likely reflecting the greater vulnerability of RPQ to metabolism by monoamine oxidases (Chaurasiya et al., 2021). This presumably also accounts for the reduced exposure to the parent drug after RPQ administration. Of note, cPQ concentrations were sustained in the blood over the 24 h daily dosing interval, such that it was still very high when subsequent doses were administered. Consistent with this prolonged exposure, higher and sustained levels of cPOQ were observed in plasma and RBC, as compared with POQ, raising the possibility that cPQ may contribute more to the overall oxidant stress and haemolytic activity seen clinically than PQ does directly. If so, and if the two enantiomers show similar redox cycling within the red cell, it would follow that the RPQ enantiomer would contribute more to the hemotoxicity of the parent drug than the SPQ enantiomer, with implications for difference in therapeutic index. Conversely, if the sustained higher levels of cPOQ in red cells is due to lesser capacity to redox cycle, and hence lesser production of active oxygen species, RPQ may have carry less potential for haemolytic injury.

In addition, SPQ is cleared by metabolism to PQ-N-CG *via* a phase II conjugation pathway. N-carbamoylation and glucuronidation of amines is relatively uncommon, but not unknown (Obach et al., 2006). The analogous metabolite of RPQ was not observed in this study or in our previous single dose study (Khan et al., 2022a). The contribution of this metabolite to the therapeutic efficacy of primaquine is not known, but a possible role implies an additional further differentiation in the therapeutic index of the two enantiomers.

Collectively, these considerations further emphasize the relevance of the stereoselective metabolism of primaquine in the clinical use of this drug.

The orthoquinone metabolite of PQ, derived from 5-hydroxylation (POQ) was observed only at very low concentrations in circulation after PQ administration. Further, POQ concentrations in red cells after SPQ administration were higher than after RPQ, and RSPQ showed an additive response. In other words, POQ in red cells appeared to fluctuate in a manner reflecting PQ plasma concentrations.

Our findings with respect to PQ metabolism in the two G6PDd subjects (one heterozygous female, one hemizygous male) did not show any clear differences from the G6PDn subjects with respect to the metabolic clearance of the enantiomers. These data further support the concept that the greater susceptibility of G6PDd individuals to hemolytic anemia after PQ lies in the lesser protective ability of their red cells and not in enhanced production of oxidant metabolites.

Even though the POQ in RBCs after SPQ is somewhat higher than after RPQ, the latter gives rise to substantially higher amounts of cPOQ in both plasma and RBCs. Although POQ has long been assumed to reflect the redox active pathways for efficacy and toxicity of PQ, any contribution of cPOQ in this respect has not been anticipated.

4.5 Tolerability/safety

Both PQ enantiomers were well tolerated in G6PDn individuals with 7 day dosing at 22.5 mg (or with 45 mg of RSPQ). The primary findings of interest here were the progressive elevations of methemoglobin (MetHgB) and total bilirubin observed. MetHgB is formed on oxidation of hemoglobin when the ferrous ion is converted to ferric (Rifkind et al., 2015). Methemoglobinemia is one of the hallmark effects of PQ with multiple days dosing. However, methemoglobinemia, *per se*, is rarely of serious clinical significance with PQ administration (Carmona-Fonseca et al., 2009). A rise in MetHgB was observed in most of our subjects, and there was no difference between the two enantiomers. RSPQ tended to show a higher response, as the dose was double that with the racemate, but in only one subject—the most sensitive responder—was a clinical impact observed. This subject showed some transient exertional dyspnea on the RSPQ arm that required discontinuation of dosing after the 5th dose. However, this subject responded to each drug form—RPQ, SPQ and RSPQ with the most robust MetHgB rise of any subject—to above

10% of HgB with each enantiomer and with the racemate. This subject did not show any other hematological or biochemical abnormalities on study endpoints, but displayed an elevated thyroid stimulating hormone (TSH). All other subjects exhibited minimal to modest responses with a gradual rise in MetHgB to an average of 4%–5% of HgB. Our findings are thus consistent with earlier reports that methemoglobinemia is generally not a limiting concern with PQ administration, in that many subjects experience mild increases, with no obvious impact on hemolysis (Carmona-Fonseca et al., 2009).

This study was not designed to address gender differences—nor was it sufficiently powered for such. However, safety parameters and profiles of PQ and metabolites were considered to assess any obvious distinctions. In terms of safety, there did not appear to be anything thing clinically significant. The mean MetHgB response in females is somewhat greater than in males after RSPQ administration, but this seems largely influenced by the one female subject mentioned earlier with an exaggerated response. We did find a significantly increased POQ content in red cells in female subjects, as compared to males. These data are depicted in the supplemental files (Supplementary Figures S1, S2). The significance of this—if any—is unknown, but may be a subject for exploration as further field studies with PQ are pursued.

A somewhat unexpected finding of this study was the sensitivity of the total bilirubin responses in G6PDn subjects. Though the changes were still well below the clinical upper limits of normal and did not approach clinical significance in terms of patient safety, the gradual increase with daily dosing was observed consistently. Placebo administration did not result in any increase in bilirubin. In one subject with severe G6PDd deficiency, the rise in bilirubin was much exaggerated, even with a lower dose (15 mg daily) of either of the enantiomers, such that the preset safety limits were exceeded, and dosing had to be discontinued after 3 days with both RPQ and SPQ. The heterozygous female subject showed enhanced responses to the G6PDn individuals in terms of bilirubin. The increase in total bilirubin after PQ or its enantiomers were confirmed to be due to indirect bilirubin (unconjugated), and thus likely derived from red cell destruction, rather than liver injury. This suggests that a minor fraction of red cells—perhaps the oldest fraction in circulation, which display the cumulative oxidative insults of normal cell aging—are impacted by the addition of the oxidative stress of the PQ metabolites. Early studies of PQ sensitivity suggested that even in G6PDn subjects, subclinical responses in various endpoints can be observed, likely due to a minor fraction of aging red cells with lower G6PD and other glycolytic enzymes (Powell and Degowin, 1965). The changes in bilirubin were not significantly different between RPQ and SPQ, though there was a slight tendency toward a greater RPQ response. Our studies suggest that bilirubin might serve as a better hemolysis-relevant marker in G6PDn individuals as compared to methemoglobin.

5 Conclusion

Studies herein indicate that a course of seven daily doses of racemic primaquine (45 mg) or its individual enantiomers (at 22.5 mg), are very well tolerated in G6PDn individuals, with no apparent differences in safety of the enantiomers, in spite of widely divergent exposure to the parent drug and key metabolites. Gradual increases in methemoglobin and bilirubin were consistently observed with both enantiomers and racemate. The bilirubin response in a single hemizygous G6PDd male was much exaggerated, and required discontinuation with both enantiomers.

Data availability statement

The original contributions presented in the study are included in the article/supplementary material, further inquiries can be directed to the corresponding authors.

Ethics statement

The studies involving human participants were reviewed and approved by the Division of Research Integrity and Compliance of The University of Mississippi and the Human Research Protection Office of the United States Army Medical Research and Development Command. The participants provided their written informed consent to participate in this study.

Author contributions

LW, BT, JM and DJ, NN contributed to the conceptual development of the project; LW, BT designed the study; WK, Y-HW, NN and HH prepared standards and developed and executed analytical methods; MAE, and WG prepared test articles, conducted regulatory support studies and documentation; LW, KH, DS and GD, ED, NC developed local compliance protocols and carried out the study; LW, BT, JM and DJ, NN, WK, Y-HW and ME contributed to interpretation and analysis of data; WK, Y-HW and LW prepared the initial draft; all authors contributed to the final version of the manuscript.

Funding

This study was supported by the US Army Medical Research & Materiel Command Award (No. W81XWH-15-1-0704 and W81XWH-18-2-0029) to the University of Mississippi (LW, NN and BT). BT is also supported by NIAID grant (1R01AI130134-01A1) (PI-Peter A Zimmerman CWRU).

Conflict of interest

JM was employed by Ironstone Separations Inc. WG and ME were employed by ElSohly Laboratories, Inc. Neither these commercial entities nor these authors have any financial interest in the drugs tested or study outcome.

The remaining authors declare that the research was conducted in the absence of any commercial or financial relationships that could be construed as a potential conflict of interest.

Publisher's note

All claims expressed in this article are solely those of the authors and do not necessarily represent those of their affiliated

organizations, or those of the publisher, the editors and the reviewers. Any product that may be evaluated in this article, or claim that may be made by its manufacturer, is not guaranteed or endorsed by the publisher.

Supplementary Material

The Supplementary Material for this article can be found online at: https://www.frontiersin.org/articles/10.3389/fphar.2022.1104735/full#supplementary-material

References

Allahyari, R., Strother, A., Fraser, I. M., and Verbiscar, A. J. (1984). Synthesis of certain hydroxy analogues of the antimalarial drug primaquine and their *in vitro* methemoglobin-producing and glutathione-depleting activity in human erythrocytes. *J. Med. Chem.* 27, 407–410. doi:10.1021/jm00369a031

Ariffin, N. M., Islahudin, F., Kumolosasi, E., and Makmor-Bakry, M. (2019). Effects of MAO-A and CYP450 on primaquine metabolism in healthy volunteers. *Parasitol. Res.* 118, 1011–1018. doi:10.1007/s00436-019-06210-3

Avula, B., Tekwani, B. L., Chaurasiya, N. D., Nanayakkara, N. D., Wang, Y.-H., Khan, S. I., et al. (2013). Profiling primaquine metabolites in primary human hepatocytes using UHPLC-QTOF-MS with ^{13}C stable isotope labeling. *J. Mass Spectrom.* 48, 276–285. doi:10.1002/jms.3122

Baird, J. K., and Rieckmann, K. H. (2003). Can primaquine therapy for *vivax* malaria be improved? *Trends Parasitol.* 19, 115–120. doi:10.1016/S1471-4922(03)00005-9

Baird, J. K. (2018). Tafenoquine for travelers' malaria: Evidence, rationale and recommendations. *J. Travel Med.* 25, tay110–13. doi:10.1093/jtm/tay110

Baker, J. K., Bedford, J. A., Clark, A. M., and McChesney, J. D. (1984). Metabolism and distribution of primaquine in Monkeys. *Pharm. Res. Off. J. Am. Assoc. Pharm. Sci.* 1, 98–100. doi:10.1023/A:1016363600790

Baker, J. K., and McChesney, J. D. (1988). Differential metabolism of the enantiomers of primaquine. *J. Pharm. Sci.* 77, 380–382. doi:10.1002/jps.2600770503

Bancone, G., and Chu, C. S. (2021). G6PD variants and haemolytic sensitivity to primaquine and other drugs. *Front. Pharmacol.* 12, 638885–638913. doi:10.3389/fphar.2021.638885

Bennett, J. W., Pybus, B. S., Yadava, A., Tosh, D., Sousa, J. C., McCarthy, W. F., et al. (2013). Primaquine failure and cytochrome P-450 2D6 in *Plasmodium vivax* malaria. *N. Engl. J. Med.* 369, 1381–1382. doi:10.1056/NEJMc1301936

Bowman, Z. S., Oatis, J. E., Whelan, J. L., Jollow, D. J., and McMillan, D. C. (2004). Primaquine-induced hemolytic anemia: Susceptibility of normal versus glutathione-depleted rat erythrocytes to 5-hydroxyprimaquine. *J. Pharmacol. Exp. Ther.* 309, 79–85. doi:10.1124/jpet.103.062984

Camarda, G., Jirawatcharadech, P., Priestley, R. S., Saif, A., March, S., Wong, M. H. L., et al. (2019). Antimalarial activity of primaquine operates via a two-step biochemical relay. *Nat. Commun.* 10, 3226. doi:10.1038/s41467-019-11239-0

Carmona-Fonseca, J., Alvarez, G., and Maestre, A. (2009). Methemoglobinemia and adverse events in *Plasmodium vivax* malaria patients associated with high doses of primaquine treatment. *Am. J. Trop. Med. Hyg.* 80, 188–193. doi:10.4269/ajtmh.2009.80.188

Chaurasiya, N. D., Liu, H., Doerksen, R. J., Dhammika Nanayakkara, N. P., Walker, L. A., and Tekwani, B. L. (2021). Enantioselective interactions of anti-infective 8-aminoquinoline therapeutics with human monoamine oxidases A and B. *Pharmaceuticals* 14, 398. doi:10.3390/ph14050398

Clyde, D. F. (1981). Clinical problems associated with the use of primaquine as a tissue schizontocidal and gametocytocidal drug. *Bull. World Health Organ.* 59, 391–395.

Fasinu, P. S., Avula, B., Tekwani, B. L., Dhammika Nanayakkara, N. P., Wang, Y. H., Bandara Herath, H. M. T., et al. (2016). Differential kinetic profiles and metabolism of primaquine enantiomers by human hepatocytes. *Malar. J.* 15, 224. doi:10.1186/s12936-016-1270-1

Fasinu, P. S., Chaurasiya, N. D., Dhammika Nanayakkara, N. P., Wang, Y. -H., Bandara Herath, H. M. T., Avula, B., et al. (2022). Comparative pharmacokinetics and tissue distribution of primaquine enantiomers in mice. *Malar. J.* 21, 33–15. doi:10.1186/s12936-022-04054-4

Fasinu, P. S., Nanayakkara, N. P. D., Wang, Y. H., Chaurasiya, N. D., Herath, H. M. B., McChesney, J. D., et al. (2019). Formation primaquine-5, 6-orthoquinone, the putative active and toxic metabolite of primaquine via direct oxidation in human erythrocytes. *Malar. J.* 18, 30–38. doi:10.1186/s12936-019-2658-5

Fasinu, P. S., Tekwani, B. L., Nanayakkara, N. P. D., Avula, B., Herath, H. M. T. B., Wang, Y. H., et al. (2014). Enantioselective metabolism of primaquine by human CYP2D6. *Malar. J.* 13, 507. doi:10.1186/1475-2875-13-507

Flaherty, S., Strauch, P., Maktabi, M., Pybus, B. S., Reichard, G., Walker, L. A., et al. (2022). Mechanisms of 8-aminoquinoline induced haemolytic toxicity in a G6PDd humanized mouse model. *J. Cell. Mol. Med.* 26, 3675–3686. doi:10.1111/jcmm.17362

Ganesan, S., Chaurasiya, N. D., Sahu, R., Walker, L. A., and Tekwani, B. L. (2012). Understanding the mechanisms for metabolism-linked hemolytic toxicity of primaquine against glucose 6-phosphate dehydrogenase deficient human erythrocytes: Evaluation of eryptotic pathway. *Toxicology* 294, 54–60. doi:10.1016/j.tox.2012.01.015

Ganesan, S., Tekwani, B. L., Sahu, R., Tripathi, L. M., and Walker, L. A. (2009). Cytochrome P450-dependent toxic effects of primaquine on human erythrocytes. *Toxicol. Appl. Pharmacol.* 241, 14–22. doi:10.1016/j.taap.2009.07.012

Jin, X., Pybus, B. S., Marcsisin, S. R., Logan, T., Luong, T. L., Sousa, J., et al. (2014). An LC-MS based study of the metabolic profile of primaquine, an 8-aminoquinoline antiparasitic drug, with an *in vitro* primary human hepatocyte culture model. *Eur. J. Drug Metab. Pharmacokinet.* 39, 139–146. doi:10.1007/s13318-013-0139-8

Kang, D., Schwartz, J. B., and Verotta, D. (2005). Sample size computations for PK/PD population models. *J. Pharmacokinet. Pharmacodyn.* 32, 685–701. doi:10.1007/s10928-005-0078-3

Khan, W., Wang, Y.-H., Chaurasiya, N. D., Nanayakkara, Npd., Herath, H. M. B., Harrison, K. A., et al. (2022a). Comparative single dose pharmacokinetics and metabolism of racemic primaquine and its enantiomers in human volunteers. *Drug Metab. Pharmacokinet.* 45, 100463. doi:10.1016/j.dmpk.2022.100463

Khan, W., Wang, Y.-H., Dhammika Nanayakkara, N. P., Bandara Herath, M. T. H., Chaurasiya, N. D., Tekwani, B. L., et al. (2022b). Quantitative analysis of primaquine and its metabolites in human urine using liquid chromatography coupled with tandem mass spectrometry. *J. Chromatogr. B* 1213, 123517. doi:10.1016/j.jchromb.2022.123517

Khan, W., Wang, Y. H., Nanayakkara, N. P. D., Herath, H. M. T. B., Catchings, Z., Khan, S., et al. (2021). Quantitative determination of primaquine-5, 6-ortho-quinone and carboxyprimaquine-5, 6-ortho-quinone in human erythrocytes by UHPLC-MS/MS. *J. Chromatogr. B Anal. Technol. Biomed. Life Sci.* 1163, 122510. doi:10.1016/j.jchromb.2020.122510

Marcsisin, S. R., Reichard, G., and Pybus, B. S. (2016). Primaquine pharmacology in the context of CYP 2D6 pharmacogenomics: Current state of the art. *Pharmacol. Ther.* 161, 1–10. doi:10.1016/j.pharmthera.2016.03.011

McChesney, J. D., and Sarangan, S. (1984). Synthesis of 8-(3-Carboxy-l-methyl-propylammo)-6-methoxyquinoline: A newly characterized primaquine metabolite. *Pharm. Res.* 1, 96–98. doi:10.1023/A:1016311616719

Mihaly, G., Ward, S., Edwards, G., Orme, M., and Breckenridge, A. (1984). Pharmacokinetics of primaquine in man: Identification of the carboxylic acid derivative as a major plasma metabolite. *Br. J. Clin. Pharmacol.* 17, 441–446. doi:10.1111/j.1365-2125.1984.tb02369.x

Milligan, R., Daher, A., Villanueva, G., Bergman, H., and Graves, P. M. (2020). Primaquine alternative dosing schedules for preventing malaria relapse in people with *Plasmodium vivax*. *Cochrane Database Syst. Rev.* 8, CD012656. doi:10.1002/14651858.CD012656.pub3

Nanayakkara, N. P. D., Ager, A. L., Bartlett, M. S., Yardley, V., Croft, S. L., Khan, I. A., et al. (2008). Antiparasitic activities and toxicities of individual enantiomers of the 8-aminoquinoline 8-[(4-amino-1-methylbutyl)amino]-6-methoxy-4-methyl-5-[3, 4-dichlorophenoxy]quinoline succinate. *Antimicrob. Agents Chemother.* 52, 2130–2137. doi:10.1128/AAC.00645-07

Nanayakkara, N. P. D., Tekwani, B. L., Herath, H. M. T. B., Sahu, R., Gettayacamin, M., Tungtaeng, A., et al. (2014). Scalable preparation and differential pharmacologic and toxicologic profiles of primaquine enantiomers. *Antimicrob. Agents Chemother.* 58, 4737–4744. doi:10.1128/AAC.02674-13

Nicholl, D. D., Edwards, G., Ward, S. A., Orme, M. L. E., and Breckenridge, A. M. (1987). The disposition of primaquine in the isolated perfused rat liver. Stereoselective formation of the carboxylic acid metabolite. *Biochem. Pharmacol.* 36, 3365–3369. doi:10.1016/0006-2952(87)90312-1

Nkhoma, E. T., Poole, C., Vannappagari, V., Hall, S. A., and Beutler, E. (2009). The global prevalence of glucose-6-phosphate dehydrogenase deficiency: A systematic review and meta-analysis. *Blood Cells. Mol. Dis.* 42, 267–278. doi:10.1016/j.bcmd.2008.12.005

Obach, R. S., Reed-Hagen, A. E., Krueger, S. S., Obach, B. J., O'Connell, T. N., Zandi, K. S., et al. (2006). Metabolism and disposition of vareniciline, a selective α4β2 acetyl choline receptor partial agonist, *in vivo* and *in vitro*. *Drug Metab. Dispos.* 34, 121. doi:10.1124/dmd.105.006767

Potter, B. M. J., Xie, L. H., Vuong, C., Zhang, J., Zhang, P., Duan, D., et al. (2015). Differential CYP 2D6 metabolism alters primaquine pharmacokinetics. *Antimicrob. Agents Chemother.* 59, 2380–2387. doi:10.1128/aac.00015-15

Powell, R. D., and Degowin, R. L. (1965). Relationship between activity of pyruvate. *Nature* 205, 507. doi:10.1038/205507a0

Pybus, B. S., Marcsisin, S. R., Jin, X., Deye, G., Sousa, J. C., Li, Q., et al. (2013). The metabolism of primaquine to its active metabolite is dependent on CYP 2D6. *Malar. J.* 12, 212. doi:10.1186/1475-2875-12-212

Pybus, B. S., Sousa, J. C., Jin, X., Ferguson, J. A., Christian, R. E., Barnhart, R., et al. (2012). CYP450 phenotyping and accurate mass identification of metabolites of the 8-aminoquinoline, anti-malarial drug primaquine. *Malar. J.* 11, 259. doi:10.1186/1475-2875-11-259

Rifkind, J. M., Mohanty, J. G., and Nagababu, E. (2015). The pathophysiology of extracellular hemoglobin associated with enhanced oxidative reactions. *Front. Physiol.* 6, 500–507. doi:10.3389/fphys.2014.00500

Saunders, D., Vanachayangkul, P., Imerbsin, R., Khemawoot, P., Siripokasupkul, R., Tekwani, B. L., et al. (2014). Pharmacokinetics and pharmacodynamics of (+)-Primaquine and (−)-Primaquine enantiomers in Rhesus macaques (*Macaca mulatta*). *Antimicrob. Agents Chemother.* 58, 7283–7291. doi:10.1128/aac.02576-13

Schmidt, L. H., Alexander, S., Allen, L., and Rasco, J. (1977). Comparison of the curative antimalarial activities and toxicities of primaquine and its d and l isomers. *Antimicrob. Agents Chemother.* 12, 51–60. doi:10.1128/AAC.12.1.51

Spring, M. D., Sousa, J. C., Li, Q., Darko, C. A., Morrison, M. N., Marcsisin, S. R., et al. (2019). Determination of Cytochrome P450 Isoenzyme 2D6 (CYP2D6) Genotypes and pharmacogenomic impact on primaquine metabolism in an active-duty US Military population. *J. Infect. Dis.* 220, 1761–1770. doi:10.1093/infdis/jiz386

Strother, A., Allahyari, R., Buchholz, J., Fraser, I. M., and Tilton, B. E. (1984). *In vitro* metabolism of the antimalarial agent primaquine by mouse liver enzymes and identification of a methemoglobin-forming metabolite. *Drug Metab. Dispos.* 12, 35.

Taylor, W. R. J., Thriemer, K., von Seidlein, L., Yuentrakul, P., Assawariyathipat, T., Assefa, A., et al. (2019). Short-course primaquine for the radical cure of *Plasmodium vivax* malaria: A multicentre, randomised, placebo-controlled non-inferiority trial. *Lancet* 394, 929–938. doi:10.1016/S0140-6736(19)31285-1

Tekwani, B. L., Avula, B., Sahu, R., Chaurasiya, N. D., Khan, S. I., Jain, S., et al. (2015). Enantioselective pharmacokinetics of Primaquine in healthy human volunteers. *Drug Metab. Dispos.* 43, 571–577. doi:10.1124/dmd.114.061127

Tekwani, B. L., and Walker, L. A. (2006). 8-Aminoquinolines: Future role as antiprotozoal drugs. *Curr. Opin. Infect. Dis.* 19, 623–631. doi:10.1097/QCO.0b013e328010b848

USFDA (2018). Office of clinical pharmacology in the center for drug evaluation and research and the center for veterinary medicine at the food and drug administration: Bioanalytical method validation: Guidance for industry. *Asian J. Pharm. Analysis* 5, 219. doi:10.5958/2231-5675.2015.00035.6

WHO (2021). Briefing kit global messaging: World malaria report 2021. Available at: https://cdn.who.int/media/docs/default-source/malaria/world-malaria-reports/world-malaria-report-2021-global-briefing-kit-eng.pdf?sfvrsn=8e5e915_23&download=true.

frontiers | Frontiers in Pharmacology

TYPE Clinical Trial
PUBLISHED 13 March 2023
DOI 10.3389/fphar.2023.1083464

OPEN ACCESS

EDITED BY
Stanislav Yanev,
Bulgarian Academy of Sciences (BAS), Bulgaria

REVIEWED BY
Linling Que,
Wuxi People's Hospital, China
Chunjiang Wang,
Third Xiangya Hospital, Central South University, China

*CORRESPONDENCE
Na Sun,
17709875898@163.com
Guangjun Fan,
17709875899@163.com

†These authors have contributed equally to this work

SPECIALTY SECTION
This article was submitted to Drug Metabolism and Transport, a section of the journal Frontiers in Pharmacology

RECEIVED 29 October 2022
ACCEPTED 28 February 2023
PUBLISHED 13 March 2023

CITATION
Luo X, Wang S, Li D, Wen J, Sun N and Fan G (2023), Population pharmacokinetics of tigecycline in critically ill patients.
Front. Pharmacol. 14:1083464.
doi: 10.3389/fphar.2023.1083464

Population pharmacokinetics of tigecycline in critically ill patients

Xiangru Luo†, Shiyi Wang†, Dong Li, Jun Wen, Na Sun* and Guangjun Fan*

Department of Pharmacy, The Second Affiliated Hospital of Dalian Medical University, Dalian, China

Objective: In critically ill patients, the change of pathophysiological status may affect the pharmacokinetic (PK) process of drugs. The purpose of this study was to develop a PK model for tigecycline in critically ill patients, identify the factors influencing the PK and optimiz dosing regimens.

Method: The concentration of tigecycline was measured LC-MS/MS. We established population PK model with the non-linear mixed effect model and optimized the dosing regimens by Monte Carlo simulation.

Result: A total of 143 blood samples from 54 patients were adequately described by a one-compartment linear model with first-order elimination. In the covariate screening analysis, the APACHEII score and age as significant covariates. The population-typical values of CL and Vd in the final model were 11.30 ± 3.54 L/h and 105.00 ± 4.47 L, respectively. The PTA value of the standard dose regimen (100 mg loading dose followed by a 50 mg maintenance dose at q12 h) was 40.96% with an MIC of 2 mg/L in patients with HAP, the ideal effect can be achieved by increasing the dosage. No dose adjustment was needed for *Klebsiella pneumoniae* for AUC0−24/MIC targets of 4.5 and 6.96, and the three dose regimens almost all reached 90%. A target AUC0−24/MIC of ≥17.9 reached 100% in patients with cSSSI in the three tigecycline dose regimens, considering MIC ≤ 0.25 mg/L.

Conclusion: The final model indicated that APACHEII score and age could affect the Cl and Vd of tigecycline, respectively. The standard dose regimen of tigecycline was often not able to obtain satisfactory therapeutic effects for critically ill patients. For patients with HAP and cIAI caused by one of three pathogens, the efficacy rate can be improved by increasing the dose, but for cSSSI infections caused by *Acinetobacter baumannii* and *K. pneumoniae*, it is recommended to change the drug or use a combination of drugs.

KEYWORDS

critically ill patients, population pharmacokinetics, tigecycline, Monte Carlo simulation, dosage regimen

1 Introduction

Tigecycline is a new type of glycylcycline antibiotic that inhibits bacterial protein synthesis by binding to the 30S subunit of ribosome to prevent aminoacylated tRNA molecules from entering the A-site of the ribosome. It has a wide antibacterial spectrum and has shown good antibacterial activity against common pathogens and drug-resistant bacteria, including multidrug-resistant and extensively drug-resistant pathogens. It is therefore also considered as an anti-infective drug for critically ill patients in the intensive care unit (ICU), although pharmacokinetics (PK) data for this group are scarce (Kim et al., 2016; Xie et al., 2017; Papadimitriou-Olivgeris et al., 2018).

The Food and Drug Administration (FDA) approved it for the treatment of complicated skin and soft tissue infection (cSSSI), complex abdominal cavity infection (cIAI) and community acquired bacterial pneumonia (Yaghoubi et al., 2022). It is also widely used to treat hospital-acquired pneumonia (HAP), urinary tract infection, blood flow infection and other diseases (De Pascale et al., 2014; Wang et al., 2017; Ben Mabrouk et al., 2021). The FDA issued a black-box warning that tigecycline can increase the mortality risk, but the reason for the high mortality rate has not yet been determined (Dixit et al., 2014; Jean et al., 2016).

Clinical studies have characterized the PK properties of tigecycline by its high rate of binding with plasma proteins (71%–89%) and atypical non-linear protein binding. Tigecycline has a large distribution volume in its steady state of about 500–700 L (7–9 L/kg), suggesting that its distribution volume in the tissue exceeds that in plasma. Tigecycline is also not widely metabolized in the body (Muralidharan et al., 2005; Pai, 2014). The main excretory pathway is bile secretion of the tigecycline prototype and its metabolites, and the secondary pathway is glycosylation and renal excretion of the tigecycline prototype (Yamashita et al., 2014).

In critically ill patients, pathophysiological changes may affect drug PK, thus affecting the required dose (Blot et al., 2014; Borsuk-De Moor et al., 2018; Broeker et al., 2018). PK changes in patients with severe illness include changes in the clearance (CL) rate caused by increased cardiac output or organ failure, and changes in distribution volume (Vd) caused by increased vascular permeability or changes in protein binding (Bastida et al., 2022). The status of patients will change according to disease development. The use of a standard dose of antibacterial drugs in ICU patients may lead to insufficient concentrations of the target drugs, which will lead to insufficient antibacterial activity and negatively impact outcomes (Montravers et al., 2014; Ibrahim et al., 2018). Therefore, it is necessary to quantify the relationship between patient covariates and pharmacokinetic parameters so as to achieve individualized administration. It is therefore necessary to quantify the relationship between patient covariates and PK parameters so as to achieve individualized administration. Early pharmacodynamics (PD) studies found that the ratio of the area under the 24 h curve to the pathogen MIC (AUC_{0-24}/MIC) was the optimal pharmacokinetics/pharmacodynamics (PK/PD) target for tigecycline, but the specific target differed depending on the type of infection (Koomanachai et al., 2009). Previous studies found that the AUC_{0-24}/MIC breakpoints were 17.9 for cSSSI, 6.96 for cIAI and 4.5 for HAP (Van Wart et al., 2006; Passarell et al., 2008; Kuti et al., 2019). However, the dose required to achieve these goals in ICU patients has not been investigated in detail.

The purpose of this study was to collect the blood concentration data and clinical information of patients treated in the ICU of a tertiary hospital, establish a PK model for tigecycline in ICU patients, determine the relationship between patient characteristics and PK parameters and evaluate the treatment effect of three infections under different drug regimens, so as to propose dose adjustment and provide a basis for promoting rational clinical drug use.

2 Materials and methods

2.1 Research population

This study retrospectively collected the information of 54 patients with severe illness from who used tigecycline to fight infection at the Second Affiliated Hospital of Dalian Medical University. The sample collection time was from December 2017 to July 2018. All patients were treated with a standard regimen of tigecycline (100 mg loading dose, 50 mg maintenance dose, q12 h). Inclusion criteria of patients were as follows: (1) received tigecycline intravenous infusion for more than 3 days, (2) male or female and aged ≥18 years, (3) clinically confirmed or suspected infection caused by G^+ and G^- bacteria and (4) the blood concentration of tigecycline had been monitored. The exclusion criteria were (1) tigecycline was used for prevention, (2) the plasma concentration of tigecycline was not monitored during the treatment, (3) death occurred within 24 h of using tigecycline, (4) pregnancy, (5) known allergy to tigecycline or (6) incomplete clinical data. This research was approved by the Ethics Committee of the Second Affiliated Hospital of Dalian Medical University (2019 no. 049).

2.2 Clinical data

The baseline characteristics of patients were obtained from the electronic clinical records of the hospital. The information collected included 1). basic characteristics of patients (e.g., sex, age, weight); 2). laboratory test indicators (e.g., white blood cells, albumin, alanine aminotransferase, aspartate transaminase, blood creatinine); 3). certain types of infection and associated diseases; and 4). adverse reactions possibly caused by drugs such as hepatotoxicity, nephrotoxicity and anaphylaxis.

2.3 Blood sample collection and concentration determination

When the blood concentration of tigecycline reached a steady state after application, blood samples were collected by collecting residual blood, which would not cause secondary injury to patients. The sampling points were before administration and 1, 2, and 4 h after administration. The blood samples were centrifuged at 1.295×10^5 g (TGL-16M desktop high-speed centrifuge, Shanghai Anting Scientific Instrument Factory) for 8 min to separate the supernatant and then stored in a refrigerator at −80°C for testing. The plasma concentration of tigecycline was determined using the liquid chromatography–mass spectrometry method established by our research group. The method was stable and reliable according to validation of its specificity, precision, accuracy, recovery and stability. Tigecycline had a strongly linear relationship over the concentration range of 1–2000 ng/mL (R^2 = 0.9907), the minimum detection limit was 10 ng/mL, and the relative standard deviations of intra- and interday precisions were 4.15% and 2.74%, respectively.

2.4 PK modelling

The plasma concentration data of tigecycline were fitted using a non-linear mixed-effects model (NONMEM 7.3.0, ICON Development Solutions, Hanover, Maryland, United States), and the PK parameters were estimated. The first-order interaction condition estimation (FOCE-I) method was used to estimate parameters, and the fixed effect parameters were CL and Vd. The modelling process included 1). preparing data files, 2). establishing a basic model, 3). establishing a statistical model, 4). establishing a covariate model, and 5). evaluating and verifying the models. Demographic data and biological indicators (including age, weight, AST, and albumin) were included as covariates in the model for testing. The covariates with objective function value (OFV) values that decreased by more than 3.84 ($p < 0.05$, df = 1) were retained by using the forward inclusion method. All of the covariates that had been retained were then eliminated one by one using the reverse elimination method. The covariates with OFV values that changed by more than 6.64 ($p < 0.01$, df = 1) were retained. Finally, the full regression model is obtained.

2.5 Model evaluation

The accuracy and applicability of the final model were evaluated by determining goodness of fit (GOF), which mostly focused on the GOF of observation concentration-population prediction concentration (PRED) and observation concentration individual prediction concentration (IPRE) scatter plots, PRED-conditional weight residuals (CWRES) and time-vs.-CWRES scatter plots. Ideally, these values should be evenly distributed on the Y = *X*-axis, with closeness to the axis indicating a more-accurate model fit. If the model fits well, CWRES should be symmetrically distributed on both sides of the Y = 0 reference line, most of which were within −2 and +2 and did not show obvious change trends with time. Bootstrapping, visual predictive check (VPC) and normal predictive distribution errors (NPDEs) could also be used to further verify the accuracy and predictability of the model.

2.6 Dose simulation

We used Monte Carlo simulation to assess the attainment of three AUC_{0-24}/MIC targets that were derived from different types of infections (≥17.9 for cSSSI, ≥6.96 for cIAI and ≥4.5 for HAP) according to MIC distributions from european committee on antimicrobial susceptibility testing (EUCAST). Three different dose regimens were simulated: 1). 100 mg loading dose followed by a 50 mg maintenance dose at q12h, 2). 100 mg loading dose followed by a 75 mg maintenance dose at q12 h and 3). 200 mg loading dose followed by a 100 mg maintenance dose at q12 h. The simulation was performed 5,000 times with 95% confidence intervals (CIs) calculated to obtain the probability of target attainment (PTA) value, and the cumulative fraction of response (CFR) was then calculated. The treatment was considered effective if PTA was ≥90%. AUC_{0-24} was calculated as the ratio of the total tigecycline dose within 24 h to the total CL of the individual.

2.7 Data analysis

SPSS (version 22.0) software was used for descriptive statistical analyses, and the data were expressed as means and standard deviations or medians and quartiles. NONMEM (version 7.3.0) software was used for PPK analysis, and R (version 3.4.0) software and GraphPad Prism (version 8.0) were used for mapping.

3 Result

3.1 Demographic data

The study included 54 infected patients, and 143 blood drug concentrations were measured. The median age of patients was 72.0 years (57.5–80.3 years), and they comprised 30 males and 24 females. The median observed concentration was 444.0 ng/mL (222.3–716.6 ng/mL). Table 1 lists the basic clinical data of the patients.

3.2 Population pharmacokinetic analysis

A one-compartment linear model fully described the concentration–time process of tigecycline. The index model was the best for both the interindividual variation and residual variation models. In the covariate screening analysis, the Acute Physiology and Chronic Health Evaluation II score (APACHEII) was found to have a significant impact on the CL of tigecycline, and age had a significant impact on the Vd. The population-typical values of CL and Vd in the final model were 11.30 L/h and 105.00 L, respectively. The model was described as follows:

$$\mathrm{CL}\left(\frac{\mathrm{L}}{\mathrm{h}}\right) = (11.30 - 0.14 \times \mathrm{APACHE\ II\ score}) \times e^{0.065} \quad (1)$$

$$\mathrm{V\,(L)} = [105.00 \times (1 - 0.0059 \times \mathrm{AGE})] \times e^{0.160} \quad (2)$$

The GOF indicated that the observed concentration vs. PRED and IPRE data were evenly distributed on both sides of the Y = *X*-axis in the final model, with good consistency. The CWRES distribution was symmetric and most of the values fell within −2 and +2, and there were no values outside of −4 and +4 (Figure 1). The model was verified using the bootstrap method. This was performed 500 times, and 442 iterations were successful (88.4% robustness rate). The estimated parameters of the final model were close to the median values obtained through bootstrapping, the relative deviation was small and all values fell within the 95% CI. The established model was relatively stable (Table 2). In the final model, only the APACHEII score was supported as a linear covariate of tigecycline CL. After APACHEII score was added, the predicted and corrected VPC and NPDE had good GOF and excellent prediction performance (Figures 2, 3).

3.3 Dose simulation

3.3.1 MIC distribution

The distribution of strains are listed in Table 3, including 34,389 strains of *Acinetobacter* baumannii, 79,232 of *Klebsiella pneumoniae* and 108,666 of *Escherichia coli*.

10.3389/fphar.2023.1083464

TABLE 1 Demographic characteristics and clinical data of ICU patients.

Demographic characteristics	Number of patients or median value (IQR)
Male/female	30 vs. 24
Age (years)	72.0 (57.5–80.3)
Weight (kg)	68.0 (58.3–70.0)
ALT (U/L)	29.09 (18.70–63.73)
AST (U/L)	33.37 (21.80–77.15)
ALP(U/L)	89.30 (62.60–136.1)
TB (mmol/L)	16.22 (9.88–24.08)
Scr(μmol/L)	77.49 (53.98–121.7)
BUN(mmol/L)	9.30 (5.99–13.18)
ALB (g/L)	27.91 (25.58–32.50)
APACHE II	22.50 (16.50–27.00)
Na^+(mmol/L)	137.0 (133.9–141.6)
Antifungal therapy	28
Number of modeling	54
Sample size	143
Observed concentration (ng/mL)	444.0 (222.3–716.6)

ALT, alanine aminotransferase; AST, aspartate aminotransferase; ALP, alkaline phosphatase; TB, total bilirubin; APACHE II, Acute physiology and chronic health evaluation II score; ALB, albumin.

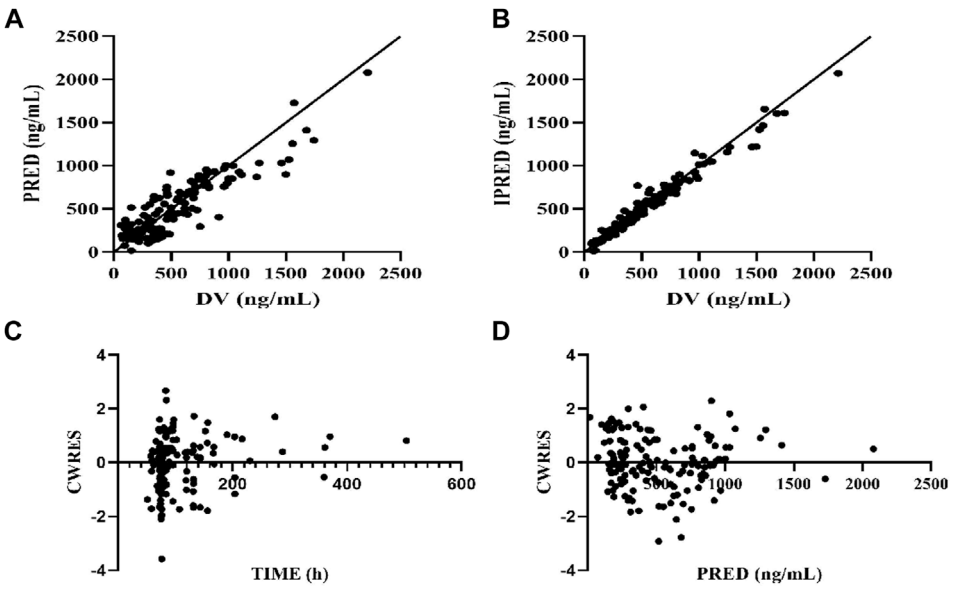

FIGURE 1
Diagnostic plot of final population pharmacokinetic model. **(A)** Scatter plot of observed values-population predicted values, **(B)** Scatter plot of observed values-individual predicted values, **(C)** Scatter plot of conditional weighted residuals—time since initial dose, **(D)** Scatter plot of conditional weighted residuals-predicted values of the population. The solid line is reference line.

TABLE 2 PK parameters and bootstrap results of final model.

Parameter	Value	Bootstrap		Relative bias(%)
		Median	95%CI	
Theta1	11.30	10.90	8.75–13.40	3.54
Theta2	105.00	100.30	54.7–160.0	4.47
Theta3	0.14	0.13	0.03–0.21	7.14
Theta4	0.0059	0.0049	0.0033–0.0079	16.94
Omega1	0.065	0.060	0.021–0.106	7.69
Omega2	0.160	0.153	0.018–0.0483	4.37
Sigma1	0.0316	0.0314	0.0063–0.048	0.63

CI, confidence interval; Theta1, population typical value of clearance; Theta2, Population typical value of distribution volume; Theta3, population typical value of APACHE II-CL; Theta4, population typical value of AGE-V; Omega1, interindividual variability of clearance; Omega2, interindividual variability of distribution volume; Sigma1, residual variability.

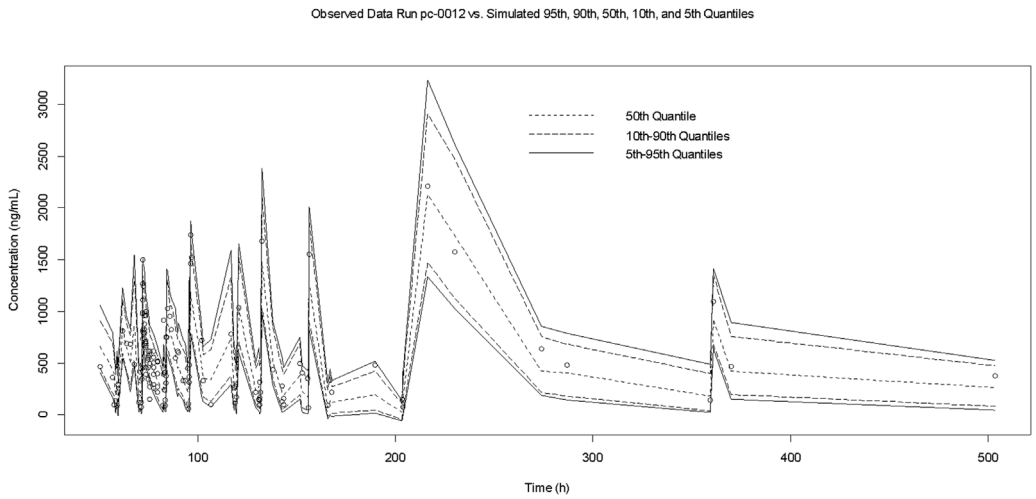

FIGURE 2
VPC graph of the final popPK mode.

3.3.2 PTA of tigecyclinee in different dosing regimens

PTA *versus* MIC profiles that corresponded to Monte Carlo simulations of different dose regimens for three PK/PD targets (AUC_{0-24}/MIC ≥4.5, ≥6.96, and ≥17.9) are represented in Table 4; Figure 4. The results indicated that considering a target AUC_{0-24}/MIC of ≥4.5, more than 90% of the patients with HAP would be successfully treated for bacteria in all three dose regimens with MIC ≤1 mg/L. The PTA value of the standard dose regimen (100 mg loading dose followed by a 50 mg maintenance dose at q12 h) was 40.96% with an MIC of 2 mg/L in patients with HAP; the ideal effect can be achieved by increasing the dosage. Considering a target AUC_{0-24}/MIC of ≥6.96, the three dose regimens could be used to treat bacteria with MIC ≤1 mg/L in patients with cIAI. Regarding an MIC of 2 mg/L, only a higher maintenance dose of 100 mg at q12 h reached the ideal efficacy, and the other two regimens were not applicable. Finally, a target AUC_{0-24}/MIC of ≥17.9 reached 100% in patients with cSSSI in the three tigecycline dose regimens, considering MIC ≤0.25 mg/L.

3.3.3 CFR of tigecyclinee for different pathogens under 3 dosing regimens

Monte Carlo simulation results indicated that for HAP, cIAI, and cSSSI infections caused by *A. baumannii*, the efficacy was poor when a standard dosage was used. When the maintenance dose was 100 mg, the CFRs of patients with HAP and cIAI were 96.11% and 93.97%, respectively, suggesting that increased doses should be considered in this group. No dose adjustment was needed for *K. pneumoniae* for AUC_{0-24}/MIC targets of 4.5 and 6.96, and the three dose regimens almost all reached 90%. However, the efficacy of the three dose regimens was poor for patients with cSSSI, and it is necessary to consider the combination of drugs or different drugs to improve the effective rate. For the infections caused by *E. coli*, the CFR of the three

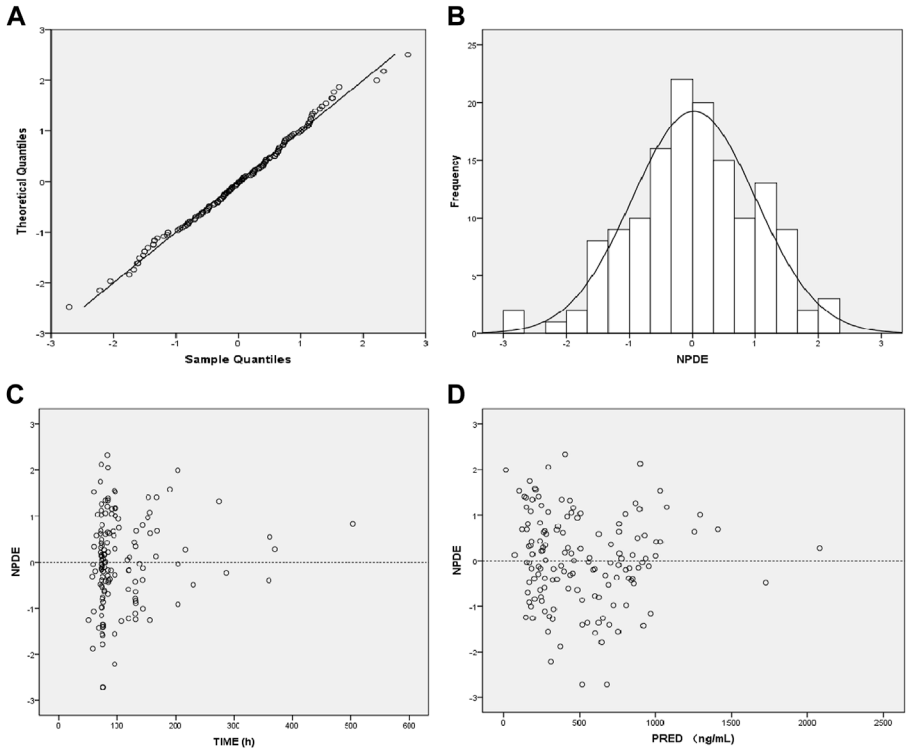

FIGURE 3
Diagnostic plot of the normalized prediction distribution error (NPDE) of the final model. **(A)** Q-Q plot of NPDE, **(B)** distribution histogram of NPDE, **(C)** Scatter plot of NPDE-TIME, **(D)** Scatter plot of NPDE-Population Predicted Values.

TABLE 3 MIC distribution of tigecycline about three pathogens.

MIC (mg/L)	*Acinetobacter baumannii*		*Klebsiella pneumoniae*		*Escherichia coli*	
	Number of strains	Percentage (%)	Number of strains	Percentage (%)	Number of strains	Percentage (%)
0.06	2,153	6.26	300	0.38	17,910	16.48
0.125	5,370	15.62	3,130	3.95	46,735	43.01
0.25	6,025	17.52	21,790	27.50	30,621	28.18
0.5	7,078	20.58	31,110	39.26	9,804	9.02
1	7,622	22.16	13,484	17.02	2,725	2.51
2	4,106	11.94	6,081	7.67	825	0.76
4	1,683	4.89	2,872	3.62	40	0.04
8	352	1.02	465	0.59	6	0.01
total	34,389	100	79,232	100	108,666	100

MIC, minimal inhibitory concentration.

dose regimens were all higher than 90%, indicating that tigecycline is more sensitive to infections caused by *E. coli* (Figure 5).

4 Discussion

Clinical efficacy and safety are the gold standard in antibiotic evaluations, and PK and PD play increasingly important roles in antibiotic selection. Understanding PK and PD is necessary for the formulation of drug delivery schemes, which can optimize tigecycline treatment to the maximum extent and reduce antibiotic resistance.

Most patients had pulmonary infections and multiple associated syndromes in this study. Considering that the PK characteristics of tigecycline may be affected by different disease states, various possible covariates (e.g., sex, age, weight, department distribution, liver function index, kidney function index, APACHEII score, course of

TABLE 4 PTA values of three tigecycline dosing regimens at different MIC.

Infection types	Dosage regimen	AUC_{0-24} (mg·h/L)	PK/PD target (AUC_{0-24}/MIC)	PTA(%)							
				0.06	0.125	0.25	0.5	1	2	4	8
HAP	100/50 mg, q12 h	8.85	>4.50	100	100	100	100	100	40.96	0	0
	100/75 mg, q12 h	13.27	>4.50	100	100	100	100	100	100	0.07	0
	200/100 mg, q12 h	17.70	>4.50	100	100	100	100	100	100	41.48	0
cIAI	100/50 mg, q12 h	8.85	>6.96	100	100	100	100	99.07	0	0	0
	100/75 mg, q12 h	13.27	>6.96	100	100	100	100	100	30.29	0	0
	200/100 mg, q12 h	17.70	>6.96	100	100	100	100	100	99.02	0	0
cSSSI	100/50 mg, q12 h	8.85	>17.90	100	100	100	42.18	0	0	0	0
	100/75 mg, q12 h	13.27	>17.90	100	100	100	100	0.1	0	0	0
	200/100 mg, q12 h	17.70	>17.90	100	100	100	100	41.48	0	0	0

AUC_{0-24}/MIC, ratio of the 24-h area under the curve to the MIC; PK/PD, Pharmacokinetics/pharmacodynamics; PTA, probability of target attainment; HAP, hospital acquired pneumonia; cIAI, complicated intra-abdominal infections; cSSSI, complicated skin and skin-structure infections.

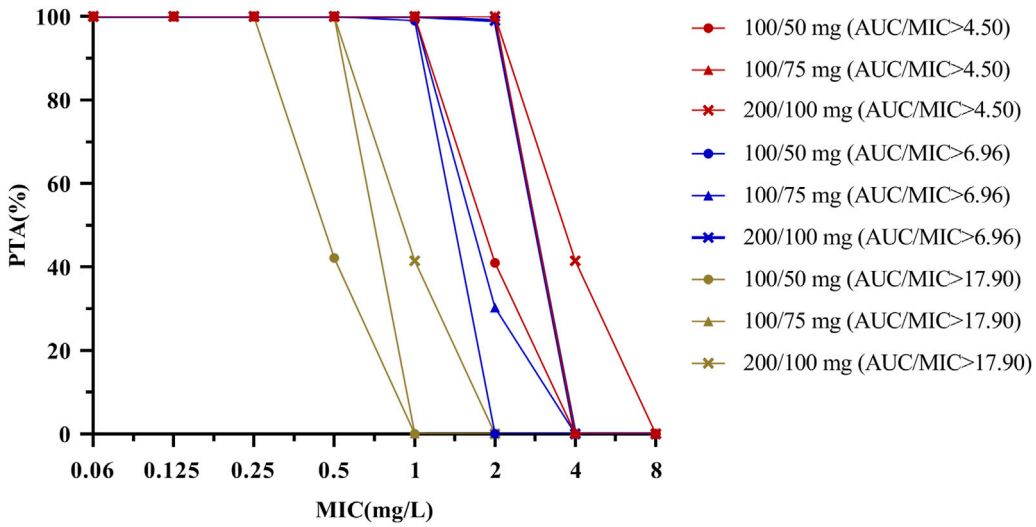

FIGURE 4
PTA by MIC for simulations of different dosing regimens of tigecycline for a PK/PD target of AUC_{0-24}/MIC ≥ 4.5, 6.96 and 17.9. The PK/PD target is achieved when the probability of target attainment (PTA) is 90% coverage. PK parameter uncertainty (see Table 2) should be considered when using this figure.

treatment, combination of hepatotoxic drugs, and combination of antifungal treatment) were considered for selection. The preliminary screening results indicate that many possible covariates proposed in advance had no significant impact on the fixed-effect parameters in this study. In this study, the final PPK model indicates that APACHEII score and age will affect the CL and apparent Vd, respectively, of tigecycline in patients with severe illness. It was speculated that APACHEII score may be related to the special pathophysiological conditions of patients, while age to the drug distribution in patients, and liver and kidney functions. Our study was consistent with that of Xie et al. (2017), and there was no correlation between patient weight and tigecycline CL. Previous studies found that age, BMI, AST, and CLcr affect tigecycline CL and weight affects Vd in ICU patients (Borsuk-De Moor et al., 2018; Broeker et al., 2018; Zhou et al., 2021). However, the influence of weight on PK parameters was not observed in this study, which may be related to the small sample size of our study population and the age distribution of the enrolled population (the median age was 72 years, and the overall distribution was relatively concentrated). Because CL can be easily transformed into AUC, our model combined with the PK/PD target of tigecycline can provide accurate individualized treatment plans for clinical practice.

Tigecycline is a time-dependent antibacterial agent with a long post-antibiotic effect, and its PK/PD parameter is AUC/MIC. Some scholars

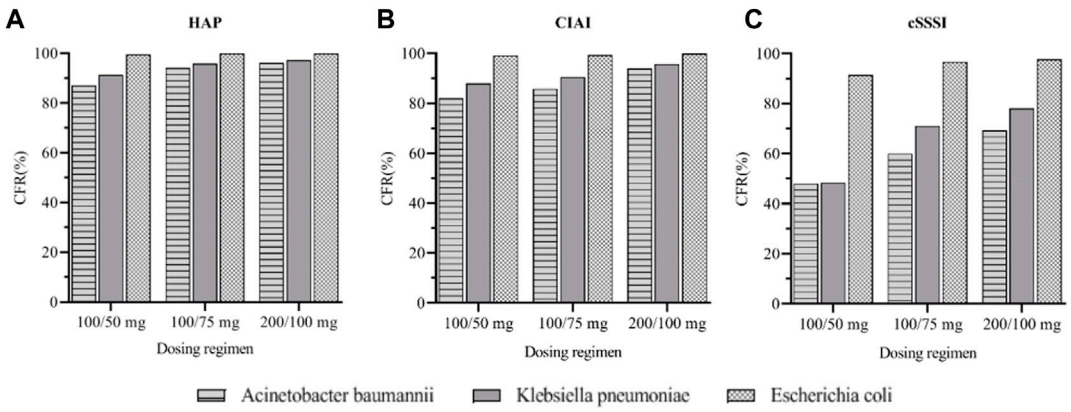

FIGURE 5
Cumulative fraction of response (CFR) of three tigecycline dosages regimens in different sites of infection. **(A)**: CFR for three Gram-negative bacteria under different dosages regimens of HAP **(B)**: CFR for three Gram-negative bacteria under different dosages regimens of cIAI **(C)**: CFR for three Gram-negative bacteria under different dosages regimens of cSSSI.

believe that increased bacterial MIC and insufficient clinical tigecycline dosages are the main reasons for its poor clinical treatment effects. Our study therefore also evaluated the compliance of three PK/PD targets for different dose regimens. The results indicated that the PTA and CFR increased as the tigecycline dose increased and the MIC decreased. For patients with cSSSI caused by *A. baumannii* and *K. pneumoniae*, the CFRs of all dose regimens were less than 90%, so it is recommended to use a different drug or to use multiple drugs in combination. A meta-analysis found that for patients with severe blood flow infection, tigecycline combination therapy had lower mortality and more advantages than single drug therapy (Wang et al., 2017). For patients with HAP or cIAI caused by *A. baumannii* or *K. pneumoniae*, the tigecycline dosage needs to be increased to achieve the ideal therapeutic effect. Our study found that when treating multidrug-resistant bacterial infections, high-dose tigecycline had higher clinical efficiency, lower mortality and lower safety, which was consistent with the findings of Falagas et al. (2014). The clinical increase in tigecycline dosage is mostly limited by adverse drug reactions. Some studies have found that the gastrointestinal adverse reactions of tigecycline are related to eating. The single dose that patients can tolerate after eating can be increased from 100 mg to 200 mg (Kasbekar, 2006). It is worth noting that the PTA of tigecycline in the routine recommended dose regimen is less than 90% with an MIC of 2 mg/L, which may be related to the PK distribution characteristics of tigecycline in different parts of the human body and the physiological differences of the population.

The final model indicated that APACHEII score could affect the CL of tigecycline, which was still the advantage of this study. However, there were also some limitations: 1). the small number of patients enrolled and the large number of covariates included in the study led to more-stringent exclusion criteria, and so our final model may not fully represent all conditions of ICU patients, and 2). this study had a retrospective design and the sampling points of plasma concentration measurements were relatively sparse, which may not necessarily correspond to the concentration at the target site. We therefore intend to conduct a prospective study with intensive sampling to address the limitations in the current study.

5 Conclusion

In the PPK model of tigecycline established in this study, APACHEII score and age affected the CL and Vd of tigecycline, respectively. The evaluation and validation indicated a good fit to the data and an excellent prediction performance. The standard dose regimen of tigecycline (100 mg loading dose followed by a 50 mg maintenance dose at q12 h) was often not able to obtain satisfactory therapeutic effects for critically ill patients. For patients with HAP and cIAI caused by one of three pathogens, the efficacy rate can be improved by increasing the dose. This study provides a basis for the adjustment of the therapeutic dose of tigecycline for patients with severe nosocomial infection to ensure the antibacterial effect of tigecycline and reduce potential adverse drug reactions and drug resistance in the future.

Data availability statement

The raw data supporting the conclusion of this article will be made available by the authors, without undue reservation.

Ethics statement

The studies involving human participants were reviewed and approved by the Ethics Committee of the Second Affiliated Hospital of Dalian Medical University (2019 No. 049). The patients/participants provided their written informed consent to participate in this study.

Author contributions

GF and NS had full access to all of the data in the study and take responsibility for the integrity of the data and the accuracy of the

data analysis. Concept and design: XL and DL. Acquisition, analysis, or interpretation of data: XL, SW, and JW. Drafting of the manuscript: XL and DL. Critical revision of the manuscript for important intellectual content: XL and SW. Statistical analysis: XL, SW, DL, and JW. Obtained funding: GF and NS. Supervision: GF. All authors contributed to the article and approved the submitted version.

Conflict of interest

The authors declare that the research was conducted in the absence of any commercial or financial relationships that could be construed as a potential conflict of interest.

Publisher's note

Supplementary material

The Supplementary Material for this article can be found online at: https://www.frontiersin.org/articles/10.3389/fphar.2023.1083464/full#supplementary-material

References

Bastida, C., Hernández-Tejero, M., Cariqueo, M., Aziz, F., Fortuna, V., Sanz, M., et al. (2022). Tigecycline population pharmacokinetics in critically ill patients with decompensated cirrhosis and severe infections. *J. Antimicrob. Chemother.* 77 (5), 1365–1371. doi:10.1093/jac/dkac036

Ben Mabrouk, A., Ben Brahim, H., Kooli, I., Marrakchi, W., Aouam, A., Loussaief, C., et al. (2021). Off label uses of tigecycline. *Ann. Pharm. Fr.* 79 (3), 244–254. doi:10.1016/j.pharma.2020.10.010

Blot, S. I., Pea, F., and Lipman, J. (2014). The effect of pathophysiology on pharmacokinetics in the critically ill patient--concepts appraised by the example of antimicrobial agents. *Adv. Drug Deliv. Rev.* 77, 3–11. doi:10.1016/j.addr.2014.07.006

Borsuk-De Moor, A., Rypulak, E., Potręć, B., Piwowarczyk, P., Borys, M., Sysiak, J., et al. (2018). Population pharmacokinetics of high-dose tigecycline in patients with sepsis or septic shock. *Antimicrob. Agents Chemother.* 62 (4), 022733-e23.17. doi:10.1128/aac.02273-17

Broeker, A., Wicha, S. G., Dorn, C., Kratzer, A., Schleibinger, M., Kees, F., et al. (2018). Tigecycline in critically ill patients on continuous renal replacement therapy: A population pharmacokinetic study. *Crit. Care* 22 (1), 341. doi:10.1186/s13054-018-2278-4

De Pascale, G., Montini, L., Pennisi, M., Bernini, V., Maviglia, R., Bello, G., et al. (2014). High dose tigecycline in critically ill patients with severe infections due to multidrug-resistant bacteria. *Crit. Care* 18 (3), R90. doi:10.1186/cc13858

Dixit, D., Madduri, R. P., and Sharma, R. (2014). The role of tigecycline in the treatment of infections in light of the new black box warning. *Expert Rev. Anti Infect. Ther.* 12 (4), 397–400. doi:10.1586/14787210.2014.894882

Falagas, M. E., Vardakas, K. Z., Tsiveriotis, K. P., Triarides, N. A., and Tansarli, G. S. (2014). Effectiveness and safety of high-dose tigecycline-containing regimens for the treatment of severe bacterial infections. *Int. J. Antimicrob. Agents* 44 (1), 1–7. doi:10.1016/j.ijantimicag.2014.01.006

Ibrahim, M. M., Abuelmatty, A. M., Mohamed, G. H., Nasr, M. A., Hussein, A. K., Ebaed, M. E. D., et al. (2018). Best tigecycline dosing for treatment of infections caused by multidrug-resistant pathogens in critically ill patients with different body weights. *Drug Des. Devel Ther.* 12, 4171–4179. doi:10.2147/dddt.S181834

Jean, S. S., Hsieh, T. C., Hsu, C. W., Lee, W. S., Bai, K. J., and Lam, C. (2016). Comparison of the clinical efficacy between tigecycline plus extended-infusion imipenem and sulbactam plus imipenem against ventilator-associated pneumonia with pneumonic extensively drug-resistant Acinetobacter baumannii bacteremia, and correlation of clinical efficacy with *in vitro* synergy tests. *J. Microbiol. Immunol. Infect.* 49 (6), 924–933. doi:10.1016/j.jmii.2015.06.009

Kasbekar, N. (2006). Tigecycline: A new glycylcycline antimicrobial agent. *Am. J. Health Syst. Pharm.* 63 (13), 1235–1243. doi:10.2146/ajhp050487

Kim, W. Y., Moon, J. Y., Huh, J. W., Choi, S. H., Lim, C. M., Koh, Y., et al. (2016). Comparable efficacy of tigecycline versus colistin therapy for multidrug-resistant and extensively drug-resistant acinetobacter baumannii pneumonia in critically ill patients. *PLoS One* 11 (3), e0150642. doi:10.1371/journal.pone.0150642

Koomanachai, P., Kim, A., and Nicolau, D. P. (2009). Pharmacodynamic evaluation of tigecycline against Acinetobacter baumannii in a murine pneumonia model. *J. Antimicrob. Chemother.* 63 (5), 982–987. doi:10.1093/jac/dkp056

Kuti, J. L., Kim, A., Cloutier, D. J., and Nicolau, D. P. (2019). Evaluation of plazomicin, tigecycline, and meropenem pharmacodynamic exposure against carbapenem-resistant enterobacteriaceae in patients with bloodstream infection or hospital-acquired/ventilator-associated pneumonia from the CARE study (ACHN-490-007). *Infect. Dis. Ther.* 8 (3), 383–396. doi:10.1007/s40121-019-0251-4

Montravers, P., Dupont, H., Bedos, J. P., and Bret, P. (2014). Tigecycline use in critically ill patients: A multicentre prospective observational study in the intensive care setting. *Intensive Care Med.* 40 (7), 988–997. doi:10.1007/s00134-014-3323-7

Muralidharan, G., Micalizzi, M., Speth, J., Raible, D., and Troy, S. (2005). Pharmacokinetics of tigecycline after single and multiple doses in healthy subjects. *Antimicrob. Agents Chemother.* 49 (1), 220–229. doi:10.1128/aac.49.1.220-229.2005

Pai, M. P. (2014). Serum and urine pharmacokinetics of tigecycline in obese class III and normal weight adults. *J. Antimicrob. Chemother.* 69 (1), 190–199. doi:10.1093/jac/dkt299

Papadimitriou-Olivgeris, M., Bartzavali, C., Spyropoulou, A., Lambropoulou, A., Sioulas, N., Vamvakopoulou, S., et al. (2018). Molecular epidemiology and risk factors for colistin- or tigecycline-resistant carbapenemase-producing *Klebsiella pneumoniae* bloodstream infection in critically ill patients during a 7-year period. *Diagn Microbiol. Infect. Dis.* 92 (3), 235–240. doi:10.1016/j.diagmicrobio.2018.06.001

Passarell, J. A., Meagher, A. K., Liolios, K., Cirincione, B. B., Van Wart, S. A., Babinchak, T., et al. (2008). Exposure-response analyses of tigecycline efficacy in patients with complicated intra-abdominal infections. *Antimicrob. Agents Chemother.* 52 (1), 204–210. doi:10.1128/aac.00813-07

Van Wart, S. A., Owen, J. S., Ludwig, E. A., Meagher, A. K., Korth-Bradley, J. M., and Cirincione, B. B. (2006). Population pharmacokinetics of tigecycline in patients with complicated intra-abdominal or skin and skin structure infections. *Antimicrob. Agents Chemother.* 50 (11), 3701–3707. doi:10.1128/aac.01636-05

Wang, J., Pan, Y., Shen, J., and Xu, Y. (2017). The efficacy and safety of tigecycline for the treatment of bloodstream infections: A systematic review and meta-analysis. *Ann. Clin. Microbiol. Antimicrob.* 16 (1), 24. doi:10.1186/s12941-017-0199-8

Xie, J., Roberts, J. A., Alobaid, A. S., Roger, C., Wang, Y., Yang, Q., et al. (2017). Population pharmacokinetics of tigecycline in critically ill patients with severe infections. *Antimicrob. Agents Chemother.* 61 (8), 003455-e417. doi:10.1128/aac.00345-17

Yaghoubi, S., Zekiy, A. O., Krutova, M., Gholami, M., Kouhsari, E., Sholeh, M., et al. (2022). Tigecycline antibacterial activity, clinical effectiveness, and mechanisms and epidemiology of resistance: Narrative review. *Eur. J. Clin. Microbiol. Infect. Dis.* 41 (7), 1003–1022. doi:10.1007/s10096-020-04121-1

Yamashita, N., Matschke, K., Gandhi, A., and Korth-Bradley, J. (2014). Tigecycline pharmacokinetics, tolerability, safety, and effect on intestinal microflora in healthy Japanese male subjects. *J. Clin. Pharmacol.* 54 (5), 513–519. doi:10.1002/jcph.236

Zhou, Y., Xu, P., Li, H., Wang, F., Yan, H., Liang, W., et al. (2021). Population pharmacokinetics and exposure-response analysis of tigecycline in patients with hospital-acquired pneumonia. *Br. J. Clin. Pharmacol.* 87 (7), 2838–2846. doi:10.1111/bcp.14692

frontiers | Frontiers in Pharmacology

TYPE Original Research
PUBLISHED 31 March 2023
DOI 10.3389/fphar.2023.1116073

OPEN ACCESS

EDITED BY
Zhihao Liu,
Dalian Medical University, China

REVIEWED BY
Yukuang Guo,
Takeda Oncology, United States
Huang Kai,
Wuxi People's Hospital Affiliated to Nanjing Medical University, China

*CORRESPONDENCE
Dafang Zhong,
dfzhong@simm.ac.cn
Xingxing Diao,
xxdiao@simm.ac.cn
Liyan Miao,
miaolysuzhou@163.com

†These authors have contributed equally to this work

SPECIALTY SECTION
This article was submitted to Drug Metabolism and Transport, a section of the journal Frontiers in Pharmacology

RECEIVED 05 December 2022
ACCEPTED 23 March 2023
PUBLISHED 31 March 2023

CITATION
Zhang H, Yan S, Zhan Y, Ma S, Bian Y, Li S, Tian J, Li G, Zhong D, Diao X and Miao L (2023), A mass balance study of [^{14}C] SHR6390 (dalpiciclib), a selective and potent CDK4/6 inhibitor in humans. *Front. Pharmacol.* 14:1116073. doi: 10.3389/fphar.2023.1116073

A mass balance study of [^{14}C] SHR6390 (dalpiciclib), a selective and potent CDK4/6 inhibitor in humans

Hua Zhang[1,2†], Shu Yan[3†], Yan Zhan[3], Sheng Ma[1,2], Yicong Bian[1,2], Shaorong Li[4], Junjun Tian[3], Guangze Li[4], Dafang Zhong[3*], Xingxing Diao[3*] and Liyan Miao[1,2*]

[1]Department of Clinical Pharmacology, The First Affiliated Hospital of Soochow University, Suzhou, China, [2]Institute for Interdisciplinary Drug Research and Translational Sciences, Soochow University, Suzhou, China, [3]Shanghai Institute of Materia Medica, Chinese Academy of Sciences, Shanghai, China, [4]Jiangsu Hengrui Medicine Co., Ltd., Lianyungang, Jiangsu, China

SHR6390 (dalpiciclib) is a selective and effective cyclin-dependent kinase (CDK) 4/6 inhibitor and an effective cancer therapeutic agent. On 31 December 2021, the new drug application was approved by National Medical Product Administration (NMPA). The metabolism, mass balance, and pharmacokinetics of SHR6390 in 6 healthy Chinese male subjects after a single oral dose of 150 mg [^{14}C]SHR6390 (150 μCi) in this research. The *Tmax* of SHR6390 was 3.00 h. In plasma, the $t_{1/2}$ of SHR6390 and its relative components was approximately 17.50 h. The radioactivity B/P (blood-to-plasma) AUC_{0-t} ratio was 1.81, indicating the preferential distribution of drug-related substances in blood cells. At 312 h after administration, the average cumulative excretion of radioactivity was 94.63% of the dose, including 22.69% in urine and 71.93% in stool. Thirteen metabolites were identified. In plasma, because of the low level of radioactivity, only SHR6390 was detected in pooled $AUC_{0-24\ h}$ plasma. Stool SHR6390 was the main component in urine and stool. Five metabolites were identified in urine, and 12 metabolites were identified in stool. Overall, faecal clearance is the main method of excretion.

KEYWORDS

SHR6390, [^{14}C]SHR6390, radioactivity, drug metabolism, CDK, pharmacokinetics

1 Introduction

The disorder of cell division, which leads to abnormal cell proliferation, is one of the key signs of cancer. In cancer treatment, the target of blocking cell division is a very important research goal. Cell cycle usually refers to the stage in which cells pass through a predetermined number of stages under the control of a complex network of regulators (Hartwell et al., 1974). The cell cycle consists of several different stages (Malumbres and Barbacid, 2001). The initiation of cell cycle requires the induction of cyclin and cyclin dependent kinases (CDKs) expression through growth factors, estrogen and other mitogenic stimuli (de Dueñas et al., 2018). Breast cancer is associated with the imbalance of D-cyclin dependent kinase 4/6-retinoblastoma (cyclin D-CDK4/6-retinoblastoma) pathway (Arnold and Papanikolaou, 2005; Cancer Genome Atlas Network, 2012; Witkiewicz and Knudsen, 2014). Class D cyclins (D1, D2 and D3) are regulators of CDK4 and CDK6 kinases, and together form active complexes (Weinberg, 1995). Among them, CDK4/6 manages the

process of cell cycle through reversible binding with cyclin D1. At the early stage of G1, active CDK4 and CDK6 phosphorylate retinoblastoma (RB) protein (a tumor inhibitor), leading to partial release of E2F transcription factor, and then promoting the transcription of downstream genes required to enter S phase through G1 restriction point (Morgan, 1997; Lundberg and Weinberg, 1998). P16 is an endogenous CDK4 inhibitor, which plays a role in reducing cell cycle and is often expressed as loss in malignant tumors (Bartkova et al., 1996). A key feature of tumorigenesis is the uncontrolled proliferation of cells, which is due to the disorder of cell cycle regulation. Therefore, cyclin D1-CDK4/6-RB pathway is a good target for anticancer drugs (Long et al., 2019).

First-generation CDK inhibitors are non-selective universal CDK blockers with limited antitumour activity and obvious toxicity (Shapiro, 2006). More recently, in the treatment of metastatic breast cancer, selective small molecule CDK4/6 inhibitors have also become increasingly effective, such as palbociclib, ribociclib and abemaciclib, which have been developed in metastatic luminal breast cancer (Cadoo et al., 2014). Three CDK4/6 inhibitors, Palbicilib, Ribocib and Abemacilib, which were previously marketed. The chemical structures of Palbicilib and ribocib are similar and have good selectivity. Abemachilib is different from them in structure. Its structure can inhibit other kinases, such as CDK9 (Gelbert et al., 2014). In addition, these CDK4/6 inhibitors show differences in terms of toxicity, so they correspond to different administration schemes. Palbociclib and ribociclib induce bone marrow suppression, which is usually administered for 1 week to restore the neutrophil count in patients, whereas abemaciclib is dosed continuously and elicits fatigue and diarrhoea as more relevant dose-limiting toxicities (Asghar et al., 2015).

SHR6390 (dalpiciclib) is a selective and effective cyclin-dependent kinase (CDK) 4/6 inhibitor and an effective cancer therapeutic agent. On 31 December 2021, the new drug application was approved by NMPA (National Medical Product Administration). SHR6390 exhibited potent antiproliferative activity against a wide range of human RB-positive tumor cells, and exclusively induced G1 arrest as well as cellular senescence, with a concomitant reduction in the levels of Ser780-phosphorylated RB protein. Although many research results on SHR6390 have been published, there are still many problems of concern that have not been solved or disclosed (Wang et al., 2017; Long et al., 2019; Chen et al., 2020; Zhang et al., 2021). To date, there are no data to evaluate its overall metabolism in humans. It is very important to understand the metabolism of SHR6390 through radioactive substances so as to evaluate its safety in the future (Robison and Jacobs, 2009; Penner et al., 2012; Prakash et al., 2019). This research can also help guide the clinical evaluation of SHR6390 in the future and help to select the appropriate dose. The use of radioactive tracers in pharmacokinetic studies enables us to better understand the excretion pathway and metabolism of drugs (Murai et al., 2014; Lappin, 2015; Meng et al., 2019; Yamada et al., 2019; Tian et al., 2021; Zheng et al., 2021). Therefore, in this study, the pharmacokinetics, biotransformation pathway and mass balance of [^{14}C]SHR6390 in humans were investigated.

2 Materials and methods

2.1 Chemicals and reagents

SHR6390 (purity 99.50%) was provided by Jiangsu Hengrui Medicine Co., Ltd. (Lianyungang, China). [^{14}C]SHR6390 (150 μCi, purity 98.62%) and SHR6390 (150 mg) were dissolved in 5% carboxymethylcellulose sodium (CMC-Na, purchased from Aladdin, Shanghai, China) and stored at approximately −20°C. For other reagent information, please refer to another article in our group (Zheng et al., 2021).

2.2 Instruments

High-resolution mass spectrometry (HR-MS) and HR-MS^2 acquisition are currently widely used in the field of metabolite identification, while background subtraction and mass loss filtering techniques have promoted the development of metabolite identification (Zhang et al., 2008; Zhang et al., 2009; Ming Yao et al., 2020). In this study, data are collected through the XCalibur and Laura systems. A Vanquish Ultra High Performance Liquid Chromatography (UHPLC) system was used to carry out detection with a Q Executive Plus mass spectrometer (Thermo, MA, United States). The system setting are shown in Table 1. The mass spectrum data were analysed using Compound Discoverer software (Themo).

2.3 Design, subjects and sample collection

The clinical trial (No. CTR20230830) was an open-label, single-center, single-dose trial conducted at the First Affiliated Hospital of Soochow University (Suzhou, China). This study was conducted in accordance with the ethical principles required by the Helsinki Declaration and approved by the Hospital Ethics Committee (2020. No.151). Six healthy Chinese male subjects were recruited between 18 and 45 years old with a body mass index between 19 and 26 kg/m^2. All subjects signed a written ICF (informed consent form) before the start of the study. Plasma samples were collected from pre-dose to 144 h after dose. Urine and stool samples were collected pre-dose to 312 h after dose administration. The standards of subject out were the following three criteria: The cumulative excretion radioactivity exceeded 80% of the dose radioactivity; the radioactivity excreted was less than 1% of the radioactivity administration over a 24 h period on two consecutive days; and the measured radioactivity in the collected plasma was 3 times lower than that of the pre-dose (Bian et al., 2021). Fasting for at least 10 h and then water deprivation for 1 h, each subject was given a single oral dose of 150 mg [^{14}C]SHR6390 (150 μCi) suspension. Rinse the dosing bottle with warm water and give it to the subjects. The total volume of drug preparation and lotion did not exceed 240 mL. After taking the medicine, the subjects fasted for 4 h and refrained from water for 1 h after dosing. Twenty millilitres of whole blood was collected before administration and 2, 6, 10, 24 and 48 h after administration. In 20 mL of whole blood, 1.6 mL was used for the test, and 0.4 mL was placed in the backup tube. Centrifuge (3,500 rpm, 5 min, 4°C) 10 mL of whole blood to produce plasma. The volume of plasma in one of the two tubes was 3.2 mL, and the remaining plasma was put into the backup tube. The

TABLE 1 UHPLC-HRMS setting.

UHPLC condition		
Colume	ACQUITY UPLC HSS T3 (100 mm × 2.1 mm, 1.8 μm, Waters, United States)	
Phase A	5 mM ammonium acetate aqueous solution	
Phase B	Acetonitrile	
UV detection	254 nm	
Gradient elution	time (min)	B (%)
	0	10
	2	10
	24	30
	26	95
	28.8	95
	28.9	10
	35	10
MS condition		
Source	ESI	
Mode	Positive	
Scan range	100–1,000 Da	
Sheath gas	45 L/min	
Aux gas	10 L/min	
Capillary temperature	320°C	
Capillary voltage	3.5 kV	

remaining 8 mL whole blood was centrifuged (3,500 rpm, 5 min, 4°C) to produce plasma for metabolic study. Meanwhile, 10 mL whole blood was collected at 0.5, 1, 3, 4, 8, 72, 96, 120, and 144 h. The plasma required for detection is obtained by whole blood centrifugation. In addition to collecting urine samples before administration and 0–4 h, 4–8 h, 8–12 h and 12–24 h after administration, urine samples will be collected every 24 h in the following collection periods. Collection of fecal samples, except before administration, shall be conducted at 24-h intervals after administration. Plasma samples were stored at −80°C, and urine and stool samples were stored at −20°C until analysis.

2.4 Radioactivity

The radioactivity of urine and plasma was detected by liquid scintillation counter (LSC) (Tri-Carb 3110 TR, PerkinElmer, MA, United States). Two times the weight of acetonitrile-water (1:1, *v*: *v*) was added to the stool and homogenized. Blood and stool homogenate were weighed and burned in a biological oxidizer (OX-501, Harvey, NY, United States). Then, the CO_2 with 14C labled was trapped in the liquid scintillation cocktail (RDC, NJ, United States) and detected by LSC.

2.5 Radioprofiling

2.5.1 Recovery

The total extraction recovery was 119%, 84.69% and 116.64% in plasma, urine and feces, respectively. The colume recovery was 92.21%, 100.14%, 99.13% in plasma, urine and feces, respectively. The recovery improved the method of extraction and LC-MS was suitable.

2.5.2 Plasma

According to the AUC principle, the plasma of 6 subjects from 0–24 h was pooled (Hop et al., 1998). The plasma sample (15 mL) after pooled was added 15 mL methanol and 15 mL acetonitrile and centrifugation (3,500 rpm, 10 min, 4°C). Extract the centrifuged solid with 7.5 mL water and 22.5 mL methanol acetonitrile (50:50, *v*: *v*). The first two extracted supernatants were combined and concentrated. The concentration of the substance is at 200 μL Acetonitrile water (20: 80, *v*: *v*) was dissolved again and centrifuged again (3,600 rpm, 10 min, 4°C). Part of the supernatant was injected into the UHPLC-FC (Fraction collector) system (Thermo). The eluent from the UHPLC was collected into the Deepwell LumaPlate 96 (PerkinElmer) at the rate of 10 s per well within minutes. The total collection time is

TABLE 2 Pharmacokinetic parameters of total radioactivity and SHR6390 in plasma after a single oral administration of [^{14}C]SHR6390 to healthy volunteers [mean (s.d.)].

Parameter	Unit	^{14}C plasma	SHR6390
C_{max}	ng eq./mL	167 (19.1)	42.9 (10.4)
AUC_{last}	ng eq./mL*h	1,670 (668)	1,150 (198)
AUC_{inf}	ng eq./mL*h	3,930 (1,250)	1,250 (206)
$t_{1/2}$	h	17.50 (7.92)	43.5 (7.77)
T_{max}	h	3.17 (1.83)	3.00 (1.79)

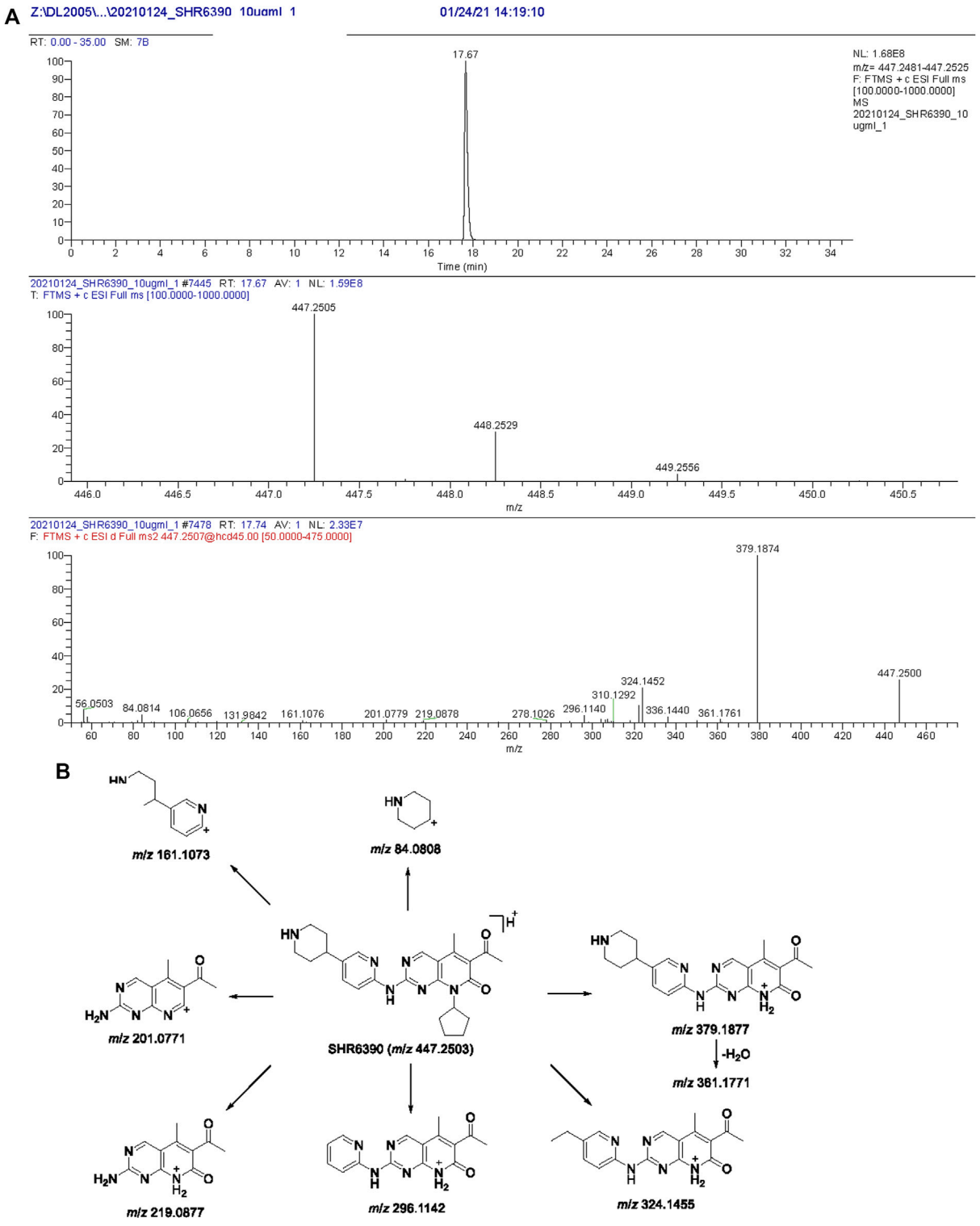

FIGURE 1
Extracted ion chromatograms, product ion spectra **(A)** and proposed fragmentation patterns of SHR6390 **(B)**.

35 min. The plates were dried by Integrated SpeedVac (Thermo), and the radiation value of each well were detected by a microplate reader (Sense Beta Hidex, Finland). Data were reconstructed to radio-chromatogram by Laura software (Lablogic, United Kingdom) to give the radio profiling of plasma.

2.5.3 Urine

According to the principle of equal volume, the urine samples of 6 subjects from 0 to 120 h were merged. The combined samples were centrifuged, concentrated by N_2 and dissolved in a 200 μL mixture of 40 mL acetonitrile and 160 mL-water, and 120 μL was injected into

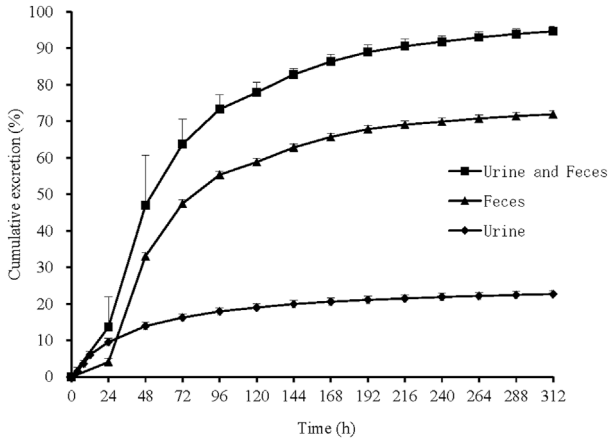

FIGURE 2
Mean cumulative excretion of total radioactivity in urine and feces following a single oral administration of [^{14}C]SHR6390. Each point represents the mean ± S.D. of six subjects.

the UHPLC-FC system (Thermo). Other operation steps are the same as those of plasma.

2.5.4 Stool

According to the principle of equal proportion weight, the fecal homogenates of 6 subjects from 0 to 168 h were combined. Add 6 mL methanol acetonitrile (50:50, v: v) to the combined fecal homogenate (2 g) sample. The mixture was then whirled (1 min) and centrifuged6 (3,500 rpm, 10 min, 4°C). Transfer the supernatant into a clean tube, and then extract the extracted solid again with 2 mL water and 2 mL methanol and 2 mL acetonitrile. The two supernatants were combined, concentrated by N_2 at 25°C and dissolved in acetonitrile-water (20: 80, v: v) of 200 μL, and 60 μL was injected into the UHPLC-FC system (Thermo). Other operation steps are the same as those of plasma.

2.6 Metabolite identification

The MS signal of the metabolites were obtained through UHPLC-HRMS, and the metabolic pathway of the metabolite was speculated. Through the MSMS spectrum obtained, the structure of the metabolite was identified by comparing the mass spectrum fragment with the mass spectrum fragment produced by the parent compound.

2.7 Pharmacokinetic analysis

The application software Phoenix WinNonlin (Version 7.0; Pharsight Corporation, Mountain View, CA) used a non-compartment model to calculate the parameters related to drug metabolism in this experiment. The related pharmacokinetic parameters for radioactivity are summarized in Table 2. By measuring the concentration of radioactive drugs in urine and stool, calculate the radioactive excretion rate (dose percentage) of each sample collected.

3 Result

3.1 HR-MS analysis of SHR6390

Chromatographic and HR-MS fragmentation of SHR6390 was studied. The structural analysis of metabolites is based on the structural analysis of the parent drug. SHR6390, $C_{25}H_{30}O_2N_6{\cdot}C_2H_6O_4S$, with $[M + H]^+$ at *m/z* 447.2503 eluted at 17.67 min and showed product ions at *m/z* 84.0808, 161.1073, 201.0771, 219.0877, 296.1142, 324.1455, 361.1771 and 379.1877 (Figures 1A, B). The base peak ion at *m/z* 379.1877 was generated by N-C cleavage of cyclopentane; further neutralization of H_2O and C_3H_5N led to *m/z* 361.1771 and 324.1455, respectively. Based on the peak ion, *m/z* 379.1877 underwent further N-C cleavages, generating *m/z* 219.0877 and 201.0771.

3.2 Pharmacokinetics

The radioactivity concentration-time profiles, the C_{max} of radioactivity was 166 ng eq./mL. The mean AUC_{last} value was 1,670 ng eq./mL*h. The mean T_{max} and $t_{1/2}$ were approximately 3.17 and 17.50 h, respectively. The radioactivity blood-to-plasma AUC_{inf} ratio (BPAR) of was 1.81. For SHR6390 in plasma, the mean C_{max} value of radioactivity was 42.9 ng/mL, and the mean AUC_{last} value was 1,150 ng/mL h. The mean AUC_{inf} values were 1,250 ng eq./mL*h. The mean T_{max} and $t_{1/2}$ were approximately 3.00 and 43.5 h, respectively.

3.3 Mass balance

In 6 healthy Chinese male subjects after an oral dose of 150 mg [^{14}C]SHR6390 (150 μCi), the recovery of total radioactivity was 94.63% (range 92.85%–96.34%). Stool excretion was the predominant route of elimination, accounting for 71.93% of the administered dose, while the mean urinary excretion was 22.69%. The total recovery in urine and stool in radioactive, 312 h after dosing was 94.63% (Figure 2).

3.4 Quantitative metabolite profiling

Radio-chromatograms of each matrix are shown in Figure 3. Table 3 summarizes some characteristics of 13 metabolites, from which the structure identification of metabolites can also be confirmed. The naming rule of metabolites is 'M + molecular weight.

3.4.1 Plasma

In AUC-pooled 0–24 h plasma, only SHR6390 was detected (Figure 3). The main reason was that the radioactivity in plasma was too low, and the signals of metabolites could not be distinguished from the background signal.

3.4.2 Urine

In the 0–120 h pooled urine sample, a total of 6 radio-chromatographic peaks were identified, and the major peak was the parent SHR6390 (Figure 3), accounting for 14.11% of the dose.

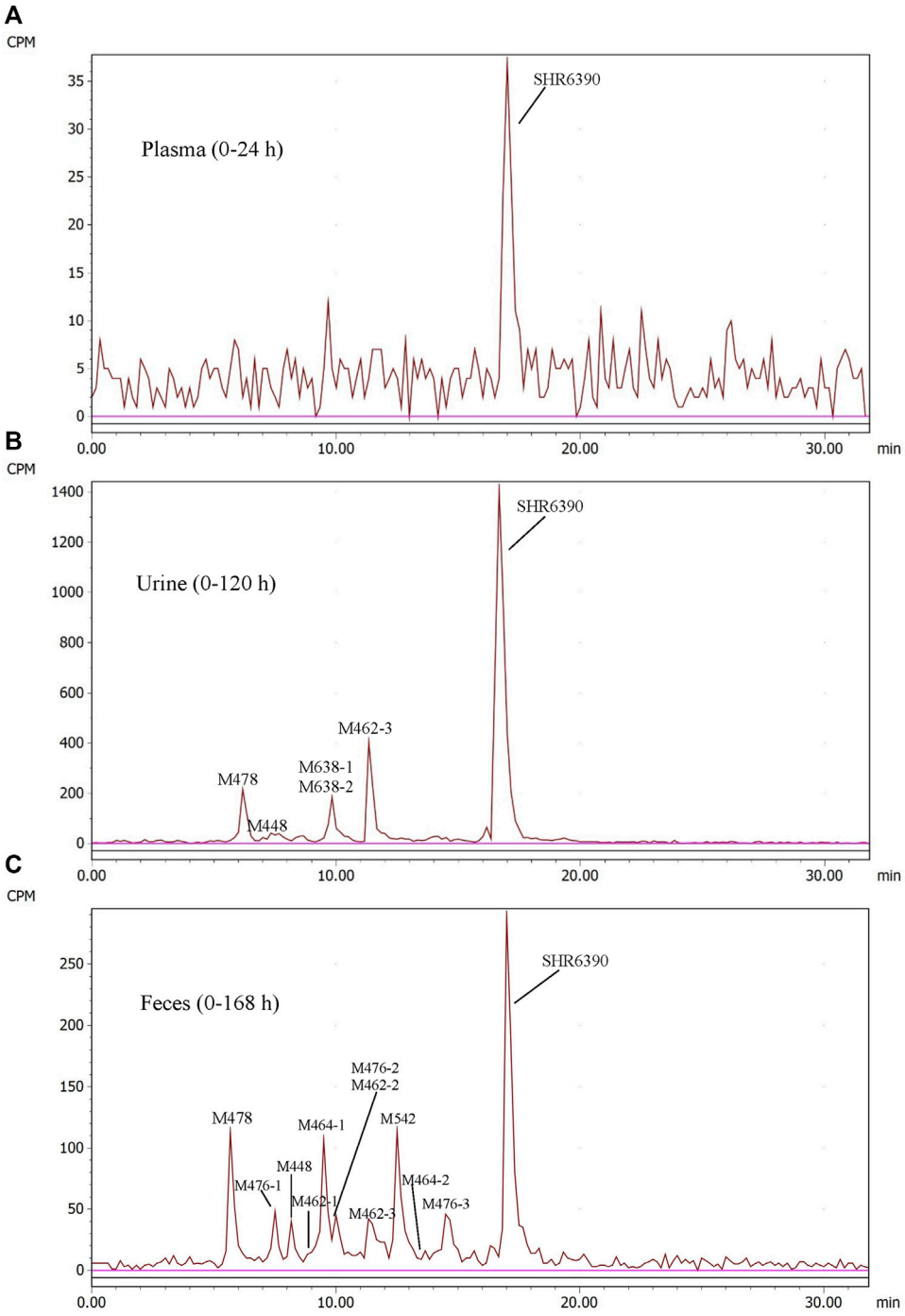

FIGURE 3
Representative radio-chromatograms of metabolites in human plasma (0–24 h) **(A)**, urine (0–120 h) **(B)**, and feces (0–168 h) **(C)** following oral administration of 150 mg [^{14}C]SHR6390 (150 μCi).

Five metabolites were assigned as M478, M448, M638-1/M638-2 (coeluting) and M462-3, accounting for 1.53%, 0.63%, 1.55% and 2.95% of the dose, respectively.

M462-3: The signal of MS showed that the elemental change of M462-3 might be an oxygen atom more than SHR6390. The main fragment ions were *m/z* 120.0808, 217.0720, 294.0984, 322.1293, 334.1299, 377.1721 and 395.1826. Comparing the ion fragments with those of the parent, the structure of M464-1 was deduced, as shown in Figures 4A, B.

M478: The signal of MS showed that the elemental change of M478 might be di-oxidation of parent SHR6390. The main fragment ions were *m/z* 178.1339, 223.1553, 349.1770, 365.1721, 393.1670 and 411.1775. Comparing the ion fragments with those of the parent, the structure of M464-1 was deduced, as shown in Figures 4C, D.

TABLE 3 Information on SHR6390 metabolites detected in human plasma, urine, and stool.

ID	Metabolic pathway	Formula	Retention time (min)	$[M + H]^+$ (determined)	Mass error (ppm)	Fragment ions
SHR6390	Parent	$C_{25}H_{30}O_2N_6$	16.67–17.00	447.2510	1.7	379.1847, 324.1452, 296.1140, 219.0878, 201.0779, 161.1076
M478	2[O]	$C_{25}H_{30}O_4N_6$	5.20–6.00	479.2410	1.8	411.1775, 393.1670,365.1721, 349.1770, 223.1552, 178.1339
M476-1	2[O]+[-2H]	$C_{25}H_{28}O_4N_6$	7.53	477.2254	2.0	409.1617, 365.1720, 310.1296, 282.1354, 205.0731, 161.1074
M448	$[-CH_2]$+[O]	$C_{24}H_{28}O_3N_6$	7.33–8.20	449.2312	3.6	363.1561, 337.1768, 308.1144, 282.1346, 161.1072
M462-1	[O]	$C_{25}H_{30}O_3N_6$	8.87	463.2471	4.1	379.1875, 324.1453, 296.1141, 201.0771, 161.1078
M464-1	[O]+[2H]	$C_{25}H_{32}O_3N_6$	9.53	465.2621	2.8	379.1875, 324.1451, 296.1144, 161.1078
M638-1	[O]+[GluA]	$C_{31}H_{38}O_9N_6$	9.83	639.2781	1.3	463.2460, 395.1830, 377.1721, 294.0976, 217.0718, 161.1075
M638-2	[O]+[GluA]	$C_{31}H_{38}O_9N_6$		639.2780	1.1	463.2457, 395.1827, 294.0999, 203.1290, 84.0816
M462-2	[O]	$C_{25}H_{30}O_3N_6$	10.03	463.2465	2.8	379.1874, 324.1458, 296.1136, 120.0810, 86.0971
M476-2	2[O]+[-2H]	$C_{25}H_{28}O_4N_6$		477.2255	2.2	409.1615, 365.1721, 310.1299, 282.1349, 205.0722, 161.1073
M462-3	[O]	$C_{25}H_{30}O_3N_6$	11.33-11.37	463.2467	3.3	395.1824, 377.1719, 322.1293, 294.0984, 217.0726, 120.0811
M542	[O]+$[SO_3]$	$C_{25}H_{30}O_6N_6S$	12.53	543.2034	2.5	463.2452, 395.1829, 377.1718, 322.1296, 294.0986, 217.0718
M464-2	[O]+[-2H]	$C_{25}H_{32}O_3N_6$	13.87	465.2624	3.3	379.1876, 324.1459, 296.1145, 219.0884, 136.0757, 120.0810
M476-3	2[O]+[-2H]	$C_{25}H_{28}O_4N_6$	14.53	477.2264	3.4	393.1670, 322.1299, 120.0808

In addition, M448 and two mono-oxidation and phase II glucuronide acid conjugates (M638-1 and M638-2) were also detected as minor metabolites in urine.

3.4.3 Stool

Parent SHR6390 and 12 metabolites were identified in the pooled 0–168 h fecal samples (Figure 3). Among them, SHR6390 was the predominant component (16%), and three abundant metabolites, M478, M464-1 and M542, accounted for 7.16%, 7.07% and 9.03% of the dose, respectively.

M464-1: The signal of MS showed that the elemental change of M478 was di-oxidation of parent SHR6390. The main product ions were *m/z* 161.1073, 296.1142, 324.1455 and 379.1877,397.1983. Comparing the ion fragments with those of the parent, the structure of M464-1 was deduced, as shown in Figures 4E, F.

M478: The details are shown in the urine section above.

M542: The signal of MS showed that the elemental change of M542 might be mono-oxidation and sulfation of the parent SHR6390. The main product ions were *m/z* 217.0720, 294.0986, 322.1299, 377.1717, 395.1926 and 463.2452. Comparing the ion fragments with those of the parent, the structure of M464-1 was deduced, as shown in Figures 4G, H.

In addition, M448, M462-1, M462-2, M462-3, M464-2, M476-1, M476-2 and M476-3 were also identified in stool as minor metabolites.

4 Discussion

This study reported the mass balance study of [^{14}C]SHR6390 in human. After oral administration, 94.63% of the dosed radioactivity was recovered in urine and stool by 312 h post-dose, which indicated complete excretion, with 22.69% in urine and 71.93% in stool.

Based on high radioactivity recovery in sample extraction, the metabolite profiles were evaluated. A total of 13 metabolites were identified, and unchanged SHR6390 was the major metabolite in three matrix following an oral administration of [^{14}C]SHR6390. In plasma, because of the low level of radioactivity, only SHR6390 was detected in pooled $AUC_{0\text{-}24h}$ plasma. In urine and stool, SHR6390 was the major component; 5 and 12 metabolites were identified, respectively.

The proposed biotransformation pathway based on findings from the present metabolism study is shown in Figure 5. The major metabolic pathways might be oxidation, glucuronidation and sulfation. As shown in Figure 5, the most susceptible metabolic spot of SHR6390 is the methyl on pyridyl pyrimidine and methyl of the acetyl group. The product ions at *m/z* 322.1293 and 294.0986 were used as diagnostic ions to determine the location of metabolism by summarizing the MS^2 spectra of SHR6390 and the available reference standards for the main metabolites. This rule applies in most cases, with occasional exceptions.

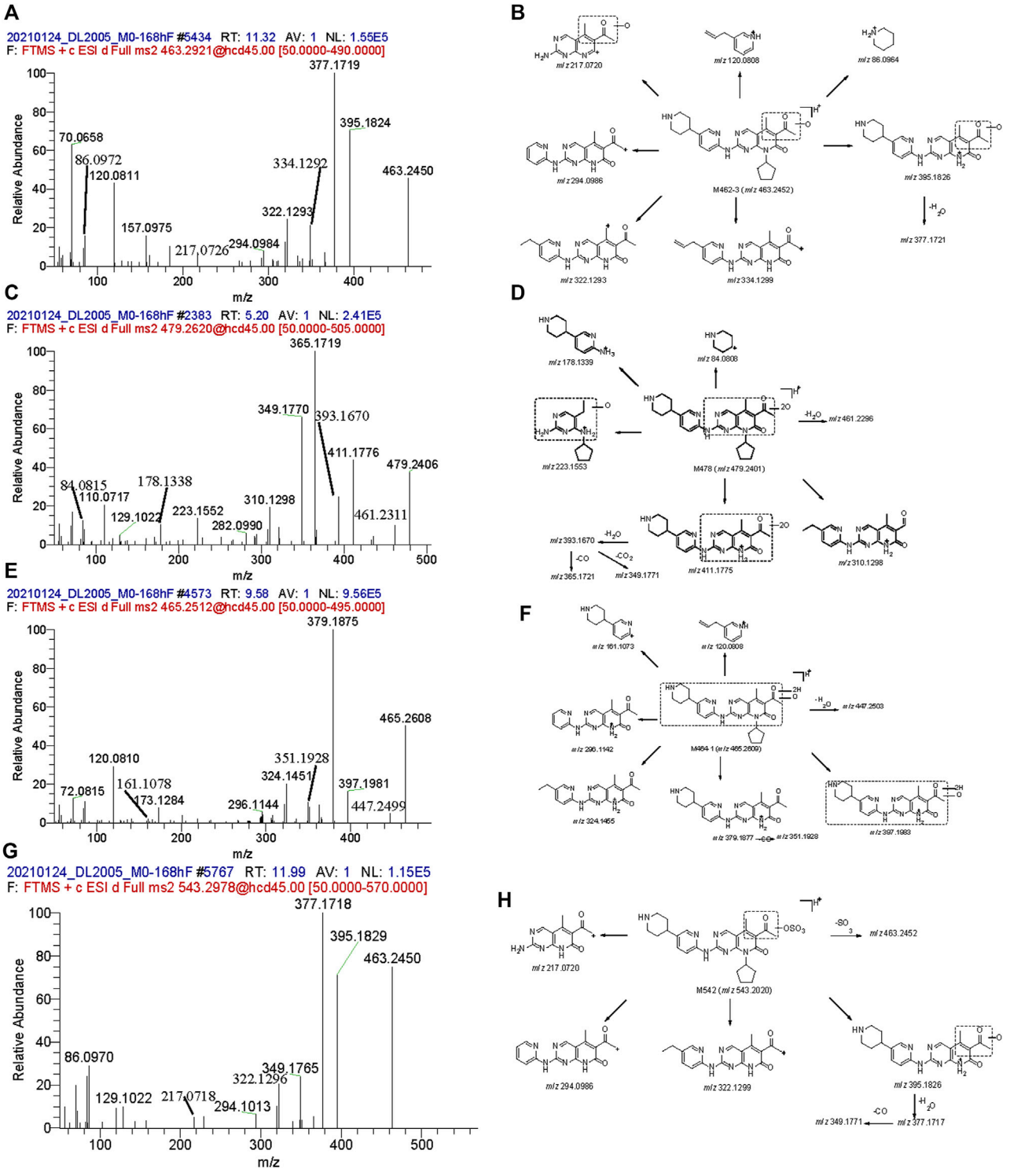

FIGURE 4
Mass spectra and the proposed fragmentation profiles of metabolites: M462-3 **(A, B)**, M478 **(C, D)**, M464-1 **(E, F)**, and M542 **(G, H)** in ESI (+).

In plasma, for the radioactivity concentration-time profiles, the mean C_{max} value of radioactivity was 166 ng eq/mL, and the mean AUC_{last} value was 1,670 ng eq./mL h. The mean T_{max} and $t_{1/2}$ were approximately 3.17 and 17.50 h, respectively. The blood-to-plasma AUC_{inf} ratio (BPAR) of the radioactivity was 1.81. For the observed blood-to-plasma ratio, it should be detected and identification the metabolites in blood to determine a more complete metabolic profiling. For SHR6390 in plasma, the mean Cmax value of radioactivity was 42.9 ng/mL, and the mean AUC_{0-t} value was 1,150 ng/mL h. The

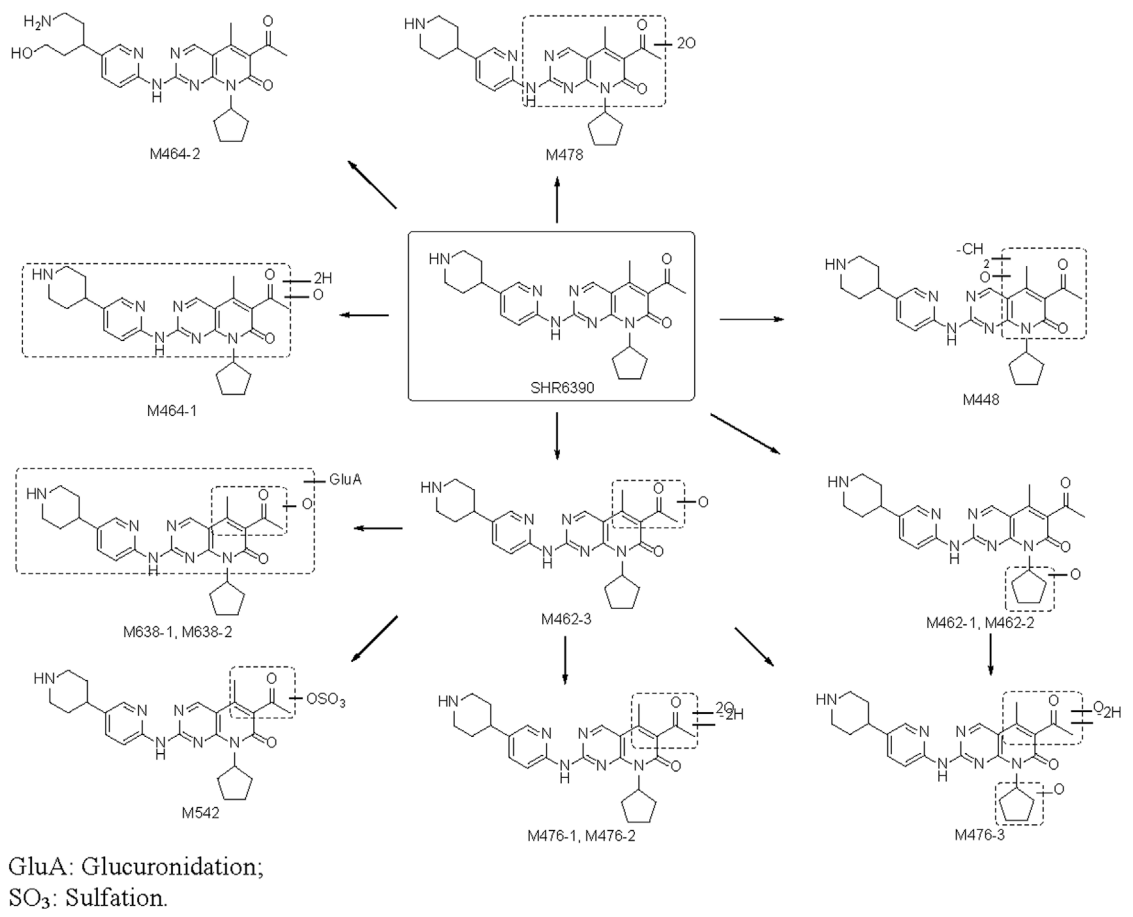

FIGURE 5
Metabolic pathway of SHR6390 in healthy Chinese male subjects.

mean $AUC_{0\text{-inf}}$ value was 1,250 ng/mL h. The mean T_{max} and $t_{1/2}$ were approximately 3.00 and 43.5 h, respectively.

Ribociclib was a medicine with similar structure. Concentrations of total radioactivity in blood and plasma were measured by AMS. The radioactivity mean $t_{1/2}$ in plasma of ribociclib were was 293 h. The mean C_{max} value of radioactivity was 1,140 ng eq/mL. The mean $AUC_{0\text{-inf}}$ value was 37,200 ng eq/mL*h (Alexander et al., 2020). The C_{max} and $AUC_{0\text{-inf}}$ of SHR6390 was lower. SHR6390 may have better activity. The differences in data do not fully explain the superiority of drugs, and may also be caused by differences in detection methods.

In conclusion, this study shows that after a single oral administration of [^{14}C] SHR6390, 94.63% of the dose was recovered in urine and feces, of which 22.69% was recovered in urine and 71.93% in feces. The characterization of SHR6390 pharmacokinetics, mass balance and metabolism is helpful to guide our understanding of SHR6290 metabolism and elimination pathway. In plasma, for the low level of radioactivity, only SHR6390 was detected in pooled $AUC_{0-24\ h}$ plasma. In urine and stool, SHR6390 was the major component; 5 and 12 metabolites were identified, respectively. Overall, faecal elimination played a significant role.

Data availability statement

The original contributions presented in the study are included in the article/supplementary material, further inquiries can be directed to the corresponding authors.

Ethics statement

The studies involving human participants were reviewed and approved by Ethics Committee of the First Affiliated Hospital of Soochow University. The patients/participants provided their written informed consent to participate in this study.

Author contributions

SY, JT, and YZ were responsible for the sample analysis; HZ, SY, LM, and XD were responsible for this manuscript; LM, XD, DZ, HZ, SY, SM, and GL designed the clinical study scheme and recruited volunteers; Jiangsu Hengrui Medicine Co., Ltd. offered the test drug and financial support.

Funding

This study was funded by Jiangsu Hengrui Pharmaceutical Co., Ltd. (Limited Company), and part of the funding was from the National Natural Science Foundation of China (81903701). This work was also supported by the national key new drug creation project (2017ZX09304-021), Suzhou Key Laboratory of Clinical Research and Personalized Medicine (SZS201719) and the special research fund of Wu Jieping Medical Foundation of Clinical Pharmacy Branch of Chinese Medical Association (320.6750.19090-50).

Conflict of interest

Authors SL and GL were employed by Jiangsu Hengrui Medicine Co., Ltd.

The remaining authors declare that the research was conducted in the absence of any commercial or financial relationships that could be construed as a potential conflict of interest.

Publisher's note

References

Alexander, D. J., Hilmar, S., Cyrille, M., Yi, J., Hubert, B., Ulrike, G., et al. (2020). An integrated assessment of the ADME properties of the CDK4/6 Inhibitor ribociclib utilizing preclinical *in vitro*, *in vivo*, and human ADME data. *Pharmacol. Res. Perspec* 8 (3), e00599. doi:10.1002/prp2.599

Arnold, A., and Papanikolaou, A. (2005). Cyclin D1 in breast cancer pathogenesis. *J. Clin. Oncol.* 23, 4215–4224. doi:10.1200/jco.2005.05.064

Asghar, U., Witkiewicz, A. K., Turner, N. C., and Knudsen, E. S. (2015). The history and future of targeting cyclin-dependent kinases in cancer therapy. *Nat. Rev. Drug Discov.* 14, 130–146. doi:10.1038/nrd4504

Bartkova, J., Lukas, J., Guldberg, P., Alsner, J., Kirkin, A. F., Zeuthen, J., et al. (1996). The p16-cyclin D/Cdk4-pRb pathway as a functional unit frequently altered in melanoma pathogenesis. *Cancer Res.* 56, 5475–5483.

Bian, Y., Zhang, H., Ma, S., Jiao, Y., Yan, P., Liu, X., et al. (2021). Mass balance, pharmacokinetics and pharmacodynamics of intravenous HSK3486, a novel anaesthetic, administered to healthy subjects. *Br. J. Clin. Pharmacol.* 87, 93–105. doi:10.1111/bcp.14363

Cadoo, K. A., Gucalp, A., and Traina, T. A. (2014). Palbociclib: An evidence-based review of its potential in the treatment of breast cancer. *Breast cancer (Dove Med. Press)* 6, 123–133. doi:10.2147/bctt.S46725

Cancer Genome Atlas Network (2012). Comprehensive molecular portraits of human breast tumours. *Nature* 490, 61–70. doi:10.1038/nature11412

Chen, Z., Xu, Y., Gong, J., Kou, F., Zhang, M., Tian, T., et al. (2020). Pyrotinib combined with CDK4/6 inhibitor in HER2-positive metastatic gastric cancer: A promising strategy from avatar mouse to patients. *Clin. Transl. Med.* 10, e148. doi:10.1002/ctm2.148

de Dueñas, E. M., Gavila-Gregori, J., Olmos-Antón, S., Santaballa-Bertrán, A., Lluch-Hernández, A., Espinal-Domínguez, E. J., et al. (2018). Preclinical and clinical development of palbociclib and future perspectives. *Clin. Transl. Oncol.* 20, 1136–1144. doi:10.1007/s12094-018-1850-3

Gelbert, L. M., Cai, S., Lin, X., Sanchez-Martinez, C., Del Prado, M., Lallena, M. J., et al. (2014). Preclinical characterization of the CDK4/6 inhibitor LY2835219: *In-vivo* cell cycle-dependent/independent anti-tumor activities alone/in combination with gemcitabine. *Invest. New Drugs* 32, 825–837. doi:10.1007/s10637-014-0120-7

Hartwell, L. H., Culotti, J., Pringle, J. R., and Reid, B. J. (1974). Genetic control of the cell division cycle in yeast. *Science* 183, 46–51. doi:10.1126/science.183.4120.46

Hop, C. E., Wang, Z., Chen, Q., and Kwei, G. (1998). Plasma-pooling methods to increase throughput for *in vivo* pharmacokinetic screening. *J. Pharm. Sci.* 87, 901–903. doi:10.1021/js970486q

Lappin, G. (2015). A historical perspective on radioisotopic tracers in metabolism and biochemistry. *Bioanalysis* 7, 531–540. doi:10.4155/bio.14.286

Long, F., He, Y., Fu, H., Li, Y., Bao, X., Wang, Q., et al. (2019). Preclinical characterization of SHR6390, a novel CDK 4/6 inhibitor, *in vitro* and in human tumor xenograft models. *Cancer Sci.* 110, 1420–1430. doi:10.1111/cas.13957

Lundberg, A. S., and Weinberg, R. A. (1998). Functional inactivation of the retinoblastoma protein requires sequential modification by at least two distinct cyclin-cdk complexes. *Mol. Cell. Biol.* 18, 753–761. doi:10.1128/mcb.18.2.753

Malumbres, M., and Barbacid, M. (2001). To cycle or not to cycle: A critical decision in cancer. *Nat. Rev. Cancer* 1, 222–231. doi:10.1038/35106065

Meng, J., Liu, X. Y., Ma, S., Zhang, H., Yu, S. D., Zhang, Y. F., et al. (2019). Metabolism and disposition of pyrotinib in healthy male volunteers: Covalent binding with human plasma protein. *Acta Pharmacol. Sin.* 40, 980–988. doi:10.1038/s41401-018-0176-6

Ming Yao, T. C., Duchoslav, E., Ma, L., Guo, X., Zhu, M., and Zhu, M. (2020). Software-aided detection and structural characterization of cyclic peptide metabolites in biological matrix by high-resolution mass spectrometry. *J. Pharm. Analysis* 10, 240–246. doi:10.1016/j.jpha.2020.05.012

Morgan, D. O. (1997). Cyclin-dependent kinases: Engines, clocks, and microprocessors. *Annu. Rev. Cell. Dev. Biol.* 13, 261–291. doi:10.1146/annurev.cellbio.13.1.261

Murai, T., Takakusa, H., Nakai, D., Kamiyama, E., Taira, T., Kimura, T., et al. (2014). Metabolism and disposition of [(14)C]tivantinib after oral administration to humans, dogs and rats. *Xenobiotica* 44, 996–1008. doi:10.3109/00498254.2014.926572

Penner, N., Xu, L., and Prakash, C. (2012). Radiolabeled absorption, distribution, metabolism, and excretion studies in drug development: Why, when, and how? *Chem. Res. Toxicol.* 25, 513–531. doi:10.1021/tx300050f

Prakash, C., Fan, B., Altaf, S., Agresta, S., Liu, H., and Yang, H. (2019). Pharmacokinetics, absorption, metabolism, and excretion of [(14)C]ivosidenib (AG-120) in healthy male subjects. *Cancer Chemother. Pharmacol.* 83, 837–848. doi:10.1007/s00280-019-03793-7

Robison, T. W., and Jacobs, A. (2009). Metabolites in safety testing. *Bioanalysis* 1, 1193–1200. doi:10.4155/bio.09.98

Shapiro, G. I. (2006). Cyclin-dependent kinase pathways as targets for cancer treatment. *J. Clin. Oncol.* 24, 1770–1783. doi:10.1200/jco.2005.03.7689

Tian, J., Lei, P., He, Y., Zhang, N., Ge, X., Luo, L., et al. (2021). Absorption, distribution, metabolism, and excretion of [14C]NBP (3-n-butylphthalide) in rats. *J. Chromatogr. B* 1181, 122915. doi:10.1016/j.jchromb.2021.122915

Wang, J., Li, Q., Yuan, J., Wang, J., Chen, Z., Liu, Z., et al. (2017). CDK4/6 inhibitor-SHR6390 exerts potent antitumor activity in esophageal squamous cell carcinoma by inhibiting phosphorylated Rb and inducing G1 cell cycle arrest. *J. Transl. Med.* 15, 127. doi:10.1186/s12967-017-1231-7

Weinberg, R. A. (1995). The retinoblastoma protein and cell cycle control. *Cell.* 81, 323–330. doi:10.1016/0092-8674(95)90385-2

Witkiewicz, A. K., and Knudsen, E. S. (2014). Retinoblastoma tumor suppressor pathway in breast cancer: Prognosis, precision medicine, and therapeutic interventions. *Breast Cancer Res.* 16, 207. doi:10.1186/bcr3652

Yamada, M., Mendell, J., Takakusa, H., Shimizu, T., and Ando, O. (2019). Pharmacokinetics, metabolism, and excretion of [(14)C]esaxerenone, a novel mineralocorticoid receptor blocker in humans. *Drug Metab. Dispos.* 47, 340–349. doi:10.1124/dmd.118.084897

Zhang, H., Ma, L., He, K., and Zhu, M. (2008). An algorithm for thorough background subtraction from high-resolution LC/MS data: Application to the detection of troglitazone metabolites in rat plasma, bile, and urine. *J. Mass Spectrom.* 43, 1191–1200. doi:10.1002/jms.1432

Zhang, H., Zhang, D., Ray, K., and Zhu, M. (2009). Mass defect filter technique and its applications to drug metabolite identification by high-resolution mass spectrometry. *J. Mass Spectrom.* 44, 999–1016. doi:10.1002/jms.1610

Zhang, P., Xu, B., Gui, L., Wang, W., Xiu, M., Zhang, X., et al. (2021). A phase 1 study of dalpiciclib, a cyclin-dependent kinase 4/6 inhibitor in Chinese patients with advanced breast cancer. *Biomark. Res.* 9, 24. doi:10.1186/s40364-021-00271-2

Zheng, Y. D., Zhang, H., Zhan, Y., Bian, Y. C., Ma, S., Gan, H. X., et al. (2021). Pharmacokinetics, mass balance, and metabolism of [(14)C]vicagrel, a novel irreversible P2Y(12) inhibitor in humans. *Acta Pharmacol. Sin.* 42, 1535–1546. doi:10.1038/s41401-020-00547-7

Frontiers in Pharmacology

Explores the interactions between chemicals and living beings

The most cited journal in its field, which advances access to pharmacological discoveries to prevent and treat human disease.

Discover the latest Research Topics

See more →

Frontiers

Avenue du Tribunal-Fédéral 34
1005 Lausanne, Switzerland
frontiersin.org

Contact us

+41 (0)21 510 17 00
frontiersin.org/about/contact